2017

The effect of intestinal inflammation and enteric nervous system deregulation in the pathogenesis of Parkinsonian syndrome

Shivani Ghaisas
Iowa State University

The effect of intestinal inflammation and enteric nervous system deregulation in the pathogenesis of Parkinsonian syndrome.

by

Shivani Ghaisas

A dissertation submitted to the graduate faculty

in partial fulfillment of the requirements for the degree of

DOCTOR OF PHILOSOPHY

Major: Immunobiology

Program of Study Committee:

Anumantha Kanthasamy, Major Professor

Arthi Kanthasamy

Julie Kuhlman

Michael Wannemuehler

Jesse Hostetter

Iowa State University

Ames, Iowa

2017

To my parents Sulabha Ghate-Ghaisas and Vishwas Ghaisas

TABLE OF CONTENTS

ABSTRACT

Increasing evidence from epidemiological studies, retrospective studies, clinical observations as well as pre-clinical *in vitro* and *in vivo* data suggest that Parkinson's disease (PD) involves both the enteric (ENS) and central nervous system. Notably, along with anosmia, intestinal dysfunction is one of the most common prodromal symptoms, which can emerge even decades before PD diagnosis. To understand how intestinal inflammation affects the enteric nervous system in the context of PD, we conducted studies involving multiple mouse models including: a transgenic model of PD (MitoPark), a model of chronic exposure to the environmental toxin manganese (Mn) as well as the dextran sodium sulfate (DSS) model of colitis. Many neurological diseases, including PD, are gradually being recognized as multi-faceted maladies involving genetic predisposition and environmental triggers.

Mn exposure has been implicated in environmentally-linked PD as evidenced by epidemiological studies done on humans exposed to Mn during mining, welding, and dry battery manufacturing. With the prevalence of high Mn content in the groundwater in many regions of the US, we investigated the effect of chronic low-dose exposure to Mn on the GI tract. We found that oral administration of Mn does affect the mouse ENS. In particular, Mn accumulation in enteric glial cells (EGC) induces mitochondrial dysfunction and ultimately cell death. In an *in vivo* model of chronic Mn exposure, we observed that even a low dose of Mn was sufficient to decrease gastrointestinal (GI) motility, alter the gut microbiome population as well as GI metabolism. MitoPark mice, which mimic the adult-onset and progressive nature of PD, showed mild intestinal inflammation and spatial differences in GI motility. Curiously, when compared to their wild-type littermate controls, these mice have

higher motility in the small intestine but lower in the large intestine. Moreover, exposure to an environmental toxin potentiated cell death of EGC in the colon with 12-week-old MitoParks having increased levels of the pro-apoptotic protein bax compared to non-exposed MitoParks. In older MitoPark mice, the ENS showed presence of inflammation with increased expression of pro-inflammatory factors, including inducible nitric oxide (iNOS) and tumor necrosis factor alpha (TNFα).

We also found similar results in mice afflicted with DSS-induced colitis. These mice showed intestinal inflammation as well as immune cell infiltrations. Intriguingly, the lumbosacral region of the spinal cord and the *substantia nigra* region in the brain of DSS mice also showed higher pro-inflammatory (TNFα, iNOS and IL-1β) transcripts.

Taken together, our data suggest that intestinal inflammation, caused either by a genetic predisposition or exposure to environmental toxins can induce neurochemical changes in the ENS, and consequently CNS changes, via the gut-brain axis.

CHAPTER 1

GENERAL INTRODUCTION

Dissertation Organization

The alternative format was chosen for this thesis and consists of manuscripts that have been published, or are being prepared for submission. The dissertation contains a general introduction, three research papers and a conclusions/future directions section that briefly discusses the overall findings from all chapters. The references for each manuscript chapter are listed at the end of that specific section. References pertaining to the background and literature review as well as those used in general conclusion section are listed at the end of the dissertation. The introduction section under Chapter I provides a brief background and overview of Parkinson's disease (PD). In the Literature review-I section, authors discuss and summarize current literature implicating the effect of environmental toxins on the gut microbiome and subsequently the gut-brain axis. The Literature Review-II section published in *Pharmacology & Therapeutics* covers current evidence implicating intestinal inflammation in the pathogenesis of various neurological disorders including PD and pertains to Chapters II and III.

Chapter II explores how chronic exposure to a low-dose toxin can lead to intestinal inflammation. Particularly, it explores the role of Mn toxicity in changing gastrointestinal physiology and enteric glial functioning. Chapter III pertains to the characterization of gastrointestinal motility symptoms in the MitoPark mouse model of PD. Chapter IV studies intestinal inflammation potentiates neuroinflammation in the mid-brain providing evidence

of involvement of the gut-brain axis via spinal nerves. Chapters II, III and IV are in the process of being submitted for publication.

This dissertation also contains an appendix section. Appendix I is a paper that was published in *Nanomedicine: Nanotechnology, Biology and Medicine* evaluating the efficacy of polyanhydride nanoparticles as a platform for delivery of the antioxidant MitoApocynin to neurons.

This dissertation contains the experimental data and results obtained by the author during his Ph.D. study under the supervision of his major professor Dr. Anumantha G. Kanthasamy at Iowa State University, Department of Biomedical Sciences.

BACKGROUND

Parkinson's disease

Originally described in Ayurveda as "Kampavata" (Kampa = shaking; vata = affliction), Parkinson's disease (PD) was later described as the "shaking palsy" in AD 175 by the physician Galen. The disease received considerable interest as a medical condition in 1817 after Dr. James Parkinson's publication titled, "An essay on the Shaking Palsy". Since then and following an increasingly ageing world population, research in the area of PD has gained much importance. PD is the second most common neurodegenerative disorder after Alzheimer's disease (AD) and is the most common movement disorder in people over the age of 65. It affects approximately 1% of individuals older than 65 years and is characterized by resting tremor, stiffness (rigidity), slow and decreased movement (bradykinesia), and gait and/or postural instability (Hirtz et al., 2007; Shulman et al., 2011). By the time the symptoms are manifested, more than 60% of the dopaminergic neurons have already been

lost, along with 80% of striatal dopamine (Dauer and Przedborski, 2003). The cardinal pathological feature of this disease is a progressive degeneration of neuromelanin-containing dopaminergic neurons in the substantia nigra pars compacta (SNpc) along with the development of eosinophilic cytoplasmic inclusions termed Lewy bodies and Lewy neurites (Dickson et al., 2009). While aging appears to be the greatest risk for the development of PD, pathogenesis of the disease is still incompletely understood and remains to be elucidated. Various genes have been implicated to PD and can account for about 10% of the PD cases, however a majority of PD cases are more likely caused by a complex interplay of genetic and environmental factors. Recent epidemiological and clinical studies have suggested potential environmental risk factors for PD. These include: repeated head injury, heavy metal exposure, exposure to pesticides, dinking well water, farming etc (Ascherio and Schwarzschild, 2016).

Non-motor symptoms of PD

Till date, diagnosis of PD rests on assessment of a battery of neurological and motor tests. However, data from retrospective studies have implicated that PD has a broader impact of the nervous system. NMS appear throughout the course of PD, some developing before motor symptoms are even recognized. During the asymptomatic phase of the disease, patients develop non-motor deficits in cognition, behavioral/neuropsychiatric changes, autonomic nervous system, gastrointestinal problems, olfactory impairment and sleep disturbances. Importantly, most non-motor symptoms (NMS) show little or no response to dopamine replacement and contribute substantially to overall disability, especially late in disease. It has been hypothesized that there may be early involvement of autonomic neurons in the spinal cord, heart, gastrointestinal and genitourinary tracts and may explain the presence of α-

synuclein aggregates found in the gastrointestinal tissue of post-mortem PD cases (Grinberg et al., 2010). Constipation is one of the most common complaints among PD patients and prolonged gastrointestinal transit time is seen in 40-80% of patients. Anosmia – loss of olfactory sense or discrimination - is one of the most common and early indicators seen in more that 90% of PD cases and increases as the disease advances (Cersosimo and Benarroch, 2008; Katzenschlager et al., 2004). Other commonly observed symptoms include sleep dysfunction that occur in 60–98% of patients, depression which occurs in 40% cases and decreased visuospatial, attentional and executive processing (Garcia-Ruiz et al., 2014). Most non-motor symptoms vary in different patients. Many patients experience some symptoms and not others, and even the pace at which the disease worsens varies on an individual basis. However these symptoms are thought to be seen when nigro-striatal degeneration begins to occur and by the time the disease is diagnosed based on motor symptoms, about 70% dopaminergic neurons are lost rendering most medications mainly symptomatic treatments. Thus it is necessary to develop sensitive tests in order to accurately determine early PD stages and thus improve a PD patient's quality of life.

Manganese neurotoxicity

In trace amounts, manganese (Mn) is an essential metal found in all body tissues, as it is fundamental for many ubiquitous enzymatic reactions, including synthesis of amino acids, lipids, proteins, and carbohydrates. It also plays a key nutritional role in bone formation, fat and carbohydrate metabolism, blood sugar regulation, and calcium absorption in the body (Bowman et al., 2011). Primary route of Mn exposure in humans is through diet, as it is present in whole grains, rice, nuts, tea, leafy green vegetables and manganese-containing nutritional supplements. However, occupational exposure to Mn can cause a

neurodegenerative disorder known as “manganism”, characterized by severe neurological deficits that often resemble the involuntary extrapyrimydal symptoms associated with PD. Major anthropogenic sources of Mn include the use of methylcyclopentadienyl manganese tricarbonyl (MMT) as an antiknock gasoline additive, Mn in fertilizers, in paint and cosmetics known as manganese violet (Farina et al., 2013). The other major sources of Mn include municipal wastewater discharges, welding, mining and mineral processing, emissions from alloy, steel, and iron production, combustion of fossil fuel and dry-cell manufacturing.

Ulcerative colitis

Ulcerative colitis (UC) is a chronic condition characterized by sudden, acute flares of intestinal inflammation. Particularly, this disease primarily affects the distal colon and rectum (Lakhan and Kirchgessner, 2010). Prolonged occurrence of this disease leads to ulceration on the intestinal lining and tissue damage occurring even at the sub-mucosa and deeper tissue. While the cause of UC is not known, it is thought that genetic predisposition to a hyperactive immune system or failure to regulate pro-inflammatory cytokine generation in response to gut bacteria or a virus might be the culprit (Brower, 2004).

Literature Review I

Environmental toxins, enteric glia and intestinal inflammation: implications on progressive neurodegeneration

Introduction

The nervous system comprising the central (CNS) and peripheral nervous systems (PNS) innervates all organs and is one of the first to develop in a growing fetus. With this network of nerves present in every body part, there is a bi-directional communication between the CNS and the rest of the body. Hence, changes in various organ systems directly reflect in biochemical changes in particular regions of the CNS. For example, the hypothalamic-pituitary axis (HPA) plays a role in satiety and feeding behavior. In long-term diabetic patients who have autonomic neural imbalance, a hyperactive HPA axis with abnormal secretion of cortisol has been observed (Chiodini et al., 2007). Since cortisol is one of the glucocorticoids involved in satiety regulation, a disturbance in normal secretion of this important hormone can lead to hypo- or hyperphagia. In fact, much research conducted in the fields of type-2 diabetes and obesity have found that the CNS in conjunction with the autonomic nervous system plays a major role in the chronicity of these metabolic disorders

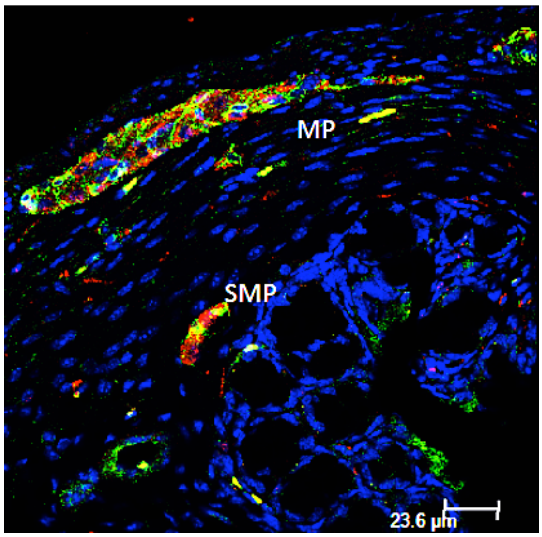

Figure 1: 60x image of mouse ileum showing enteric neurons (PGP9.5, red) and enteric glial cells (GFAP, green). The ENS is present in two distinct layers- Myenteric plexus (MP) and the submucosal plexus.

(Anderson et al., 2016; Miranda et al., 2016; Rosmond, 2003; Rosmond et al., 1998). However, not only does diabetes induce an abnormal HPA functioning, it also affects the enteric nervous system (ENS) disturbing intestinal motility (Yamamoto et al., 2008).

The ENS is a part of the PNS and is present throughout the length of the gastrointestinal (GI) tract. Unlike the CNS, which is a concerted mass of neurons and glial cells, the ENS is present in discrete layers of the gut and consists of i) myenteric (Auerbach's) plexus that is present in between the longitudinal and circular muscles and ii) sub-mucosal (Meissner's and Henle) plexus that is present beneath the mucosal layer (Figure 1). Their location has functional relevance with the myenteric plexus mainly regulating GI smooth muscle contractions while the sub-mucosal plexus controls GI blood flow and intestinal absorption at the villi (Domoto et al., 1990; Hens et al., 2001). Besides neurons, the ENS also constitutes the enteric glial cells (EGCs). These cells were once thought to primarily provide a structural framework to the enteric neurons but have since emerged as key players in GI physiology (Gulbransen and Sharkey, 2012; Neunlist et al., 2014). Unlike enteric neurons that are mainly restricted to the two plexi, EGCs are present across all layers of the gut even extending into the mucosal villi (Neunlist et al., 2007). These cells act as mediators between enteric neurons and other non-neuronal cells.

The gut encompasses about 100 million neurons with functionally distinct populations having individual neurochemical signatures (Benarroch, 2007). Along with interstitial cells of Cajal (also called the pacemaker of the gut) and excitable smooth muscle cells, the ENS is able to induce spontaneous contractions of the GI tract even in the absence of CNS input (Rao and Gershon, 2016). However, under normal physiological conditions, the there is a two-way signaling – through the vagus, pelvic, celiac, superior and inferior mesenteric

nerves- between the ENS and the CNS. Hence, perturbations in either region can lead to altered communication and thus physiological dysfunctions in the body.

Neurological disorders and associated gastrointestinal disturbances

GI dysfunction is a surprisingly common occurrence in many neurological disorders. We now know that patients suffering from Parkinson's (PD), dementia with lewy bodies (DLB) and autism have GI dysfunction in the early phase of the disorder. This phenomenon is predominantly observed in PD patients with 25-77% patients diagnosed as constipated while 30% DLB patients show gastrointestinal disturbances (Knudsen et al., 2017; Mishima et al., 2017; Stubendorff et al., 2012). While these symptoms have long been documented, the relation between altered CNS and/or PNS and GI dysfunction has gained much attention only in the past decade. In 2003 and 2006 Braak and colleagues showed that aggregated α-synuclein, a histological hallmark of PD, is observed in the ENS and CNS of post-mortem PD patients. Importantly, it appeared that aggregated α-synuclein- positive neurons were mainly detected in the olfactory bulb or ENS in early stage patients advancing to the brain stem, caudate nucleus, substantia nigra and finally the frontal cortex as the disease progressed (Braak et al., 2006; Braak et al., 2003). This evidence - although not universally accepted – certainly gave credence to the idea that since the nasal passage and gut are continuously exposed to environmental toxins and xenobiotics that can be inhaled or ingested, this prolonged exposure could cause oxidative stress and low-grade inflammation in the GI tract. The constant presence of oxidative stress and inflammation can lead to mitochondrial dysfunction in neurons, an exaggerated response by the resident immune cells as well as generation of pro-inflammatory cytokines and chemokines thus leading to

misfolding of proteins such as the natively unfolded α-synuclein. A variety of transgenic and toxin-based animal models of PD have shown varying degrees of deregulation in intestinal motility and aggregated protein inclusions in the ENS (Anderson et al., 2007; Greene et al., 2009; Kuo et al., 2010; Toti and Travagli, 2014). However, the degree of dysfunction and pathology differ when compared to post-mortem histopathological analysis of PD patients. A major limiting factor of animal models is that neither toxin models (where a healthy animal is given a high or chronic dose of the toxin to induce desired disease) nor transgenic models (where the enteric neurons are genetically programmed to undergo dysfunction) can really recapitulate the complex etiology of PD. Unlike the results observed in animal models of PD, retrospective studies have shown that the prodromal phase of PD- where GI dysfunction is first observed – shows negligible loss of enteric neurons. Even at the advanced stages of this disease, the percentage of dying enteric neurons is minimal compared to 80% dopaminergic cell death observed in the CNS. To explain this observation, Engelender and Isacson postulated an alternative theory wherein they speculated that the CNS and ENS had different thresholds to insult mainly due to a larger functioning reserve and redundant signaling pathways between the dopaminergic neurons in the brain as compared to the dopaminergic neurons in the gut (Engelender and Isacson, 2017). While this idea is novel and can explain disease onset and progression; the molecular and biochemical signatures that cause such distinct thresholds between enteric and mid-brain dopaminergic neurons needs to be elucidated.

Along with PD, other synucleinopathies such as multiple system atrophy (MSA) and dementia with lewy bodies (DLB) have also shown intestinal inflammation in concurrence with CNS dysfunction. Immunohistochemistry of the sigmoid colon mucosa of a small

cohort of MSA patients showed disrupted tight junction protein indicating a "leaky" intestinal barrier compared to healthy control subjects (Engen et al., 2017). The study also revealed intestinal inflammation and a shift in the gut microbial profile that produces more pro-inflammatory factors compared to the healthy cohort. These observations give credence to the notion that intestinal inflammation and a dysfunctional motility are closely associated with degenerating neurons in the CNS and PNS. In the case of DLB, lewy bodies containing protease-resistant α-synuclein is seen at early stages in the ENS and olfactory bulb similar to the lewy body progression seen in many PD patients. While no study to our knowledge has shown intestinal inflammation or altered motility in DLB patients, nonetheless, given the similar disease pathology and progression with PD, it is possible that DLB patients also suffer from ENS associated GI dysfunctions.

In the case of autism spectrum disorder (ASD)- mild, acute or chronic inflammation of the colon, rectum, small intestine and stomach as well as increased intestinal permeability is a common outcome (de Magistris et al., 2010; Fiorentino et al., 2016). Such children display cognitive deficits, fixed behaviors, and impairments in social skills. The relation between altered intestinal permeability or "leaky gut" and cognitive or social impairments has been shown through various studies where ASD children had increased free amino acids and short chain fatty acids (SCFAs) in the feces (De Angelis et al., 2015). Notably, glutamate – a non-essential amino acid that also functions as an inhibitory neurotransmitter – was found at substantially higher amounts in ASD children compared to healthy controls (Adams et al., 2011; De Angelis et al., 2015; Shimmura et al., 2011). Excess glutamate can lead to alterations in neuronal signaling and even apoptosis. Children with ASD also have lower amounts of SCFAs in general with the notable exception of propionic acid and acetic acid

that are found in larger amounts compared to healthy controls (De Angelis et al., 2013). Intraventricular infusions of propionic acid in rats have shown ASD-like behavioral abnormalities (MacFabe et al., 2011; Thomas et al., 2010). These rats also showed significantly altered acylcarnitine and various phospholipid species in the brain suggesting a role played by intestinal metabolites in modifying brain lipid profiles leading to neurological impairment (Thomas et al., 2010). Similarly, rodents exposed to valproic acid during prenatal development also showed ASD-like behavioral characteristics as well as intestinal inflammation (Roullet et al., 2013). This enteric inflammation was associated with higher levels of the neurotransmitter serotonin (5-HT) in the intestine. Notably, hyperseretonemia (elevated blood serotonin levels) is observed in 30% of children with ASD indicating that elevated 5-HT in the intestine might be a potential biomarker in concurrence with behavioral tests (Gabriele et al., 2014). Interestingly, children with autism might also suffer from zinc deficiency and a Cu/Zn imbalance compared to healthy age-matched children. Particularly, zinc deficiency between 0-3 years of age positively correlated with higher incidence of ASD (Pfaender and Grabrucker, 2014; Yasuda et al., 2011). While the exact mechanisms are not fully understood, nonetheless zinc is known to increase villous height and improve mucosal defense against enteric pathogens as well as play a role in memory and cognition in the brain (Caine et al., 2009; Tyszka-Czochara et al., 2014). In parallel to increased intestinal permeability observed in such patients, an altered blood-brain barrier (BBB) as well as neuroinflammation is also observed (Fiorentino et al., 2016). For more information related to intestinal inflammation and CNS dysfunction please refer to Rao and Gershon (2016) and Ghaisas *et al* (Ghaisas et al., 2016; Rao and Gershon, 2016).

Role of the ENS following intestinal inflammation

Clinical and histopathological observations have implicated the role of the ENS in intestinal inflammation. For example, hypertrophy or hyperplasia of myenteric ganglion cells are observed in Crohn's disease (CD) while neurotransmitter deregulation, particularly 5-HT is observed in inflammatory bowel disease (IBD) (Geboes and Collins, 1998; Manocha and Khan, 2012). Since the gut is made of different layers each with distinct functions with the ENS coordinating these functions, it is necessary to understand the interactions between the enteric neurons/glia with other cells during intestinal inflammation.

Role of Enteric Glia in intestinal inflammation

As the "phenotypical equivalents" of astrocytes in the CNS, EGCs form an important part of the ENS (Capoccia et al., 2015). Recently, these cells were classified into different groups based on their morphology and function (Gulbransen and Sharkey, 2012); however despite morphological distinctions, much of the functions overlap. Similar to astrocytes and Schwann cells, EGCs remain in close contact with enteric neurons, ensheathing them albeit incompletely, allowing the neurons to make contact with other cell types such as surveilling immune cells and interstitial cells of Cajal (Figure 2) (Gabella, 1972). As mentioned before, EGCs also extend in the villi and are present directly beneath the epithelial cells that line the villi (Figure 3).

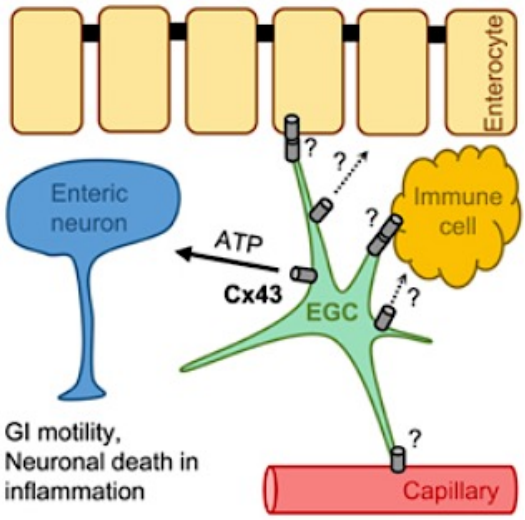

Figure 2: Enteric glia communicate with other cells in the gastrointestinal tract.

Unlike astrocytic end-feet that wrap around endothelial cells and form a unit of the BBB, EGCs do not ensheath epithelial cells but regulate the tight junctions mainly via paracrine pathways (Savidge et al., 2007b).

Various toxin and transgenic animal studies have highlighted the importance of EGCs in maintaining the epithelial barrier as well as in increasing intestinal permeability. For example, EGC knockout mice as well as mice administered the gliotoxin fluorocitrate both develop intestinal inflammation and a highly compromised intestinal permeability (Savidge et al., 2007a) while patients with slow-transit constipation showed massive loss of EGCs in both the small and large intestines (Bassotti et al., 2006). The glial s-nitrosoglutathione (GSNO), a molecule mainly produced by EGCs, is critically involved in maintaining tight

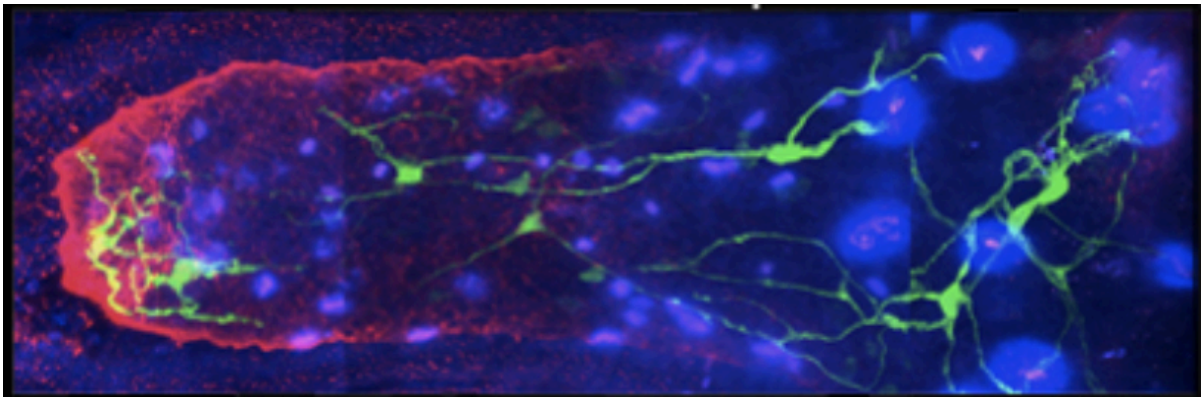

Figure 3: Enteric glia extending from the submucosa into the villi.

junction proteins and epithelial f-actin. Similarly, glia derived neurotrophic factor (GDNF) that helps enterocyte development while TGF-β and 15-deoxy-(12,14)-prostaglandin J2 produced by EGCs are other important factors involved in maintaining epithelial tight junctions (Bach-Ngohou et al., 2010; von Boyen et al., 2011). Thus EGCs control epithelial cell proliferation and maturation by regulating transcription factors associated with cell-

matrix, cell-cell adhesion, lipid and protein metabolism as well as cell survival (Van Landeghem et al., 2009).

During inflammation, upon sensing bacterial products like LPS as well as advanced glycation/oxidation products, aggregated proteins etc these cells highly express Toll-like receptor 4 (TLR4) as well as RAGE (receptor for advanced glycation end products). Increased expression of these receptors renders the cells "reactive". Patients with ulcerative colitis (UC), have a higher expression of EGCs and GDNF in the large intestine compared to healthy controls (von Boyen et al., 2011). Higher GDNF expression in the intestine is a protective mechanism as GDNF not only confers protection on enterocytes but also promotes survival of the EGCs themselves (Steinkamp et al., 2012). Notably, the EGCs have increased S100-β immunoreactivity as well as increased nitric oxide production via RAGE signaling (Cirillo et al., 2009). However, following GI inflammation, EGCs as well as mucosal immune cells release pro-inflammatory factors including TNFα, IL-1β and iNOS (Turco et al., 2014). These factors re-arrange junctional adhesion proteins increasing intestinal permeability.

The idea that the CNS can –in part- control EGC functions came from an interesting study conducted by Langness and colleagues (Langness et al., 2017). Selective ablation of EGC by topical application of Benzalkonium chloride followed by ischemia-reperfusion injury resulted in increased intestinal permeability, inflammation and immune cell recruitment. This disease state was reduced to a certain extent with vagal nerve stimulation. However in the presence of EGCs + vagal nerve stimulation, mice had much lower permeability, inflammation and immune cell invasion in the intestine. This study showed that the EGCs in

tandem with inputs from the vagus nerve (that arises from the brain stem) are able to control intestinal inflammation.

Role of Enteric Neurons in intestinal inflammation

Since the 1970s when Gabella first observed neuroglial junctions in the ENS; several histological and electrophysiology studies have shown the enteric neurons and glia routinely communicate with one another. While enteric glial hyperplasia is commonly observed in patients with IBD, what is also commonly observed is enteric neuronal cell death. In 2014, McClain *et al* reported that connexin-43 hemichannels mediate neuro-glia crosstalk via purinergic signaling (McClain et al., 2014). Using a mouse model of IBD, they found that increased nitric oxide production activated connexin-43 channels in EGCs thus releasing ATP. This ATP continually drives intracellular [Ca^{+2}] response in adjacent enteric neurons leading to neuronal death (Brown et al., 2016). In a similar study, Gulbransen *et al* observed that activating P2X7 receptors and pannexin-1 channels lead to Asc and caspase activation concluding in enteric neuronal death (Gulbransen et al., 2012). Inhibition of either P2X7 receptors or pannexin-1 channels prevented the onset of inflammation. Dying neurons release caspases, products of partial nitration and oxidation as well as pro-inflammatory cytokines and chemokines. These stimulate intraepithelial lymphocytes to migrate and envelope the dead neurons (Tornblom et al., 2002).

Sensory neurons are enabled to detect molecular signals and environmental cues both from luminal contents as well as the intestinal tissue. They are also able to detect pathogenic bacteria, bacterial toxins, metabolites and cell components and communicate these findings to the patrolling immune cells (Lai et al., 2017). Studies have shown how chemical irritants

activate sensory neurons resulting in vasodilation and immune influx (Geppetti et al., 2008). Hence acute application of dextran sodium sulfate (DSS) or 2,4,6 trinitrobenzenesulfonic acid (TNBS), induces hyperexcitability in the sensory neurons that persists for weeks even after the insult is removed inducing visceral hypersensitivity in the area of inflammation (Abdrakhmanova et al., 2012). There have been conflicting reports regarding the pro- or anti-inflammatory role of sensory neuron activation (Engel et al., 2012; Ghia et al., 2006; McCafferty et al., 1997; Okayama et al., 2004; Reinshagen et al., 1996). However direct

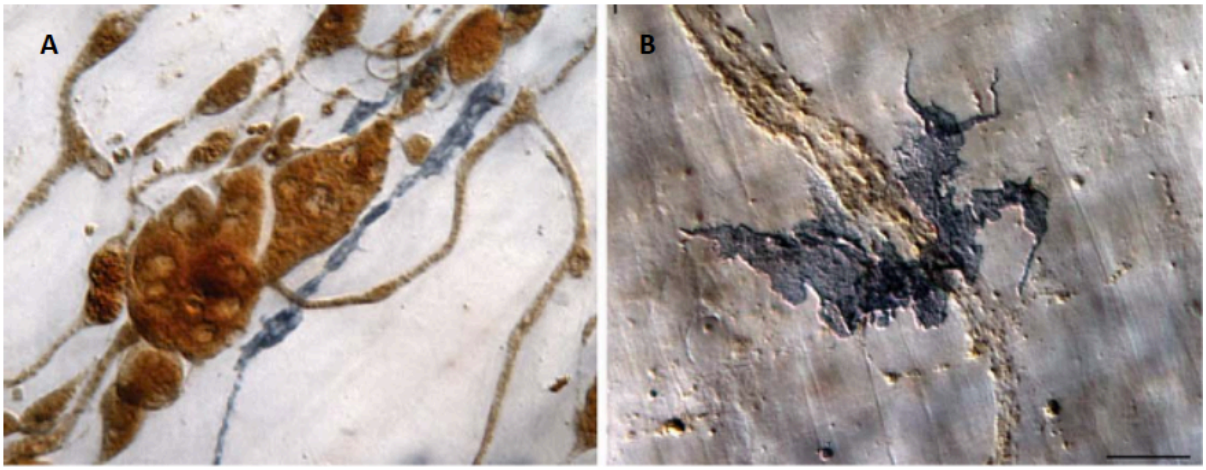

Figure 4: (A) Dense a-synuclein staining observed in the myenteric plexus of aged Fisher rats (brown) with macrophages (dark blue) seen nearby. (B) Macrophages surrounding enteric neurons possibly due to presence of aggregated a-synuclein.

comparison between studies is not possible due to the different treatment schedules and toxin dosage. Even following natural ageing, there are changes in GI physiology with a shift in the immune population from an anti-inflammatory state to a pro-inflammatory state (Becker et al., 2017). This means that even low-grade inflammation or a mild acute toxic insult would lead to an exaggerated response by the mucosal immune cells leading to a loss in enteric neurons and delayed transit time. So how is an “ageing” gut different from a young, healthy GI tract? By histological observations, the GI tract of an older individual (≥ 65 years of age) has fewer enteric neurons compared to the GI tract of a young and healthy individual (16-25

years) (Wade and Cowen, 2004). A summary of the changes in myenteric neuronal numbers with age has been tabulated in a review by Saffery (Saffrey, 2013). Based on a number of histological observations made in both animal models as well as humans, the general consensus is that as we age, the number of neurons (mainly myenteric neurons were observed) decrease with the largest reduction seen in the large intestine i.e the colon followed by the ileum, jejunum and least in the stomach and esophagus. It is hypothesized that the aged ENS has a lower threshold for ROS-induced oxidative damage. Coupled with the shift in immune cells from an anti- to pro-inflammatory status, it is easy to understand why neuronal cell death would occur as an individual gets older. Ageing is associated with decreased autophagy; consequently these enteric neurons accumulate products of incomplete lysosomal digestion as well as aggregated and protease resistant proteins (Abalo et al., 2007; Phillips and Powley, 2007; Phillips et al., 2009). Phillips *et al* observed that the small intestine of aged rats expressed greater aggregated α-synuclein mainly in the enteric neurons (Phillips et al., 2013). In many instances, activated macrophages (indicated by MHCII surface expression normally not seen in resident macrophages) were found in close contact with neurons exhibiting dense α-synuclein staining (Figure 4a). However, upon ingesting aggregated synuclein, most activated macrophages lost their morphological integrity and were unable to clear the aggregated proteins (Figure 4b). If the aggregate proteins are not efficiently lysed either during lysosomal degradation or by phagocytosing immune cells, they contribute to oxidative stress and a pro-inflammatory state in the vicinity. A few studies have showed the direct spread of aggregated α-synuclein and prion protein from the gut to the brain through the vagus or glossopharyngeal nerve (Breid et al., 2016; Holmqvist et al., 2014; McBride et al., 2001). Together these observations give credence to the idea that a disruption

in protein quality control leads to the formation of toxic cellular aggregates; if these aggregates are not solubilized, they can travel from the gut to the brain via the spinal cord nerves leading to development of protein aggregation and neuroinflammation in the CNS. Unlike sub-granular zone and sub-ventricular regions of the brain where neurogenesis occurs even in aged individuals (albeit at a much slower rate than in healthy young brains), neurogenesis has not been demonstrated in the aged gut. This could mean that the enteric neurons are more susceptible to age-related loss compared to the neurons in the CNS. This premise ties back to the "threshold theory" mentioned previously in this review where the authors Engelender and Isacson postulated that even a small loss of enteric neuronal numbers during the early stages of PD can lead to decreased gut motility and other GI disorders compared to a more than 80% loss of neurons in the substantia nigra pars compacta when the disease is actually detected based on motor symptoms (Engelender and Isacson, 2017).

Influence of ingested toxins and xenobiotics on the ENS: consequences on the GI physiology and CNS

It is a well-accepted theory that neurological disorders such as AD, PD, MSA as well as ASD are the result of genetic predisposition and exposure to environmental triggers. Multiple sub-acute exposures or a chronic exposure to water and food pollutants such as heavy metals, pesticides, herbicides, neurotoxins, as well as maternal smoking have been linked to progressive neurological and associated motor impairment (Belbasis et al., 2015; Bellou et al., 2016; Killin et al., 2016; Modabbernia et al., 2017; Yan et al., 2016). Besides the skin, which is the largest organ exposed to the environment, the GI and nasal tracts are also continuously exposed to environmental factors including toxins and xenobiotics. Pan-

Montojo and others have shown that the environmental toxin rotenone acts locally on the enteric neurons and triggers release of α-synuclein via exosomes (Pan-Montojo et al., 2012). Indeed, many animal studies of pesticide exposure have shown that these chemicals - that are mainly mitochondrial complex I inhibitors- selectively target enteric neurons causing mitochondrial dysfunction and ultimately apoptosis (Greene et al., 2009; Zhu et al., 2012). Loss of enteric neurons disrupts the intricate circuitry between the ENS and other cells leading to dysmotility, increased permeability and finally intestinal inflammation. With the vagus nerve innervating most of the GI tract, changes in GI physiology and motility are conveyed to its dorsal nucleus located in the medulla. As mentioned before, this innervation also provides a physical link where in theory- aggregated proteins can travel from the gut to the brain stem or vice versa. Studies with higher rotenone exposure than the Pan-Montojo study have shown neurochemical and behavioral deficits in the brain of exposed rats (Cannon et al., 2009; Sherer et al., 2003). Till date, no study has shown conclusive evidence of just how ingested neurotoxins cause neurological deficits but it is thought that the absorbed neurotoxins cause damage to the ENS thereby deregulating gut motility and increasing intestinal inflammation. These inflammatory signals are passed via the blood and across the BBB to the CNS. Alternatively the vagus nerve can convey information regarding changes in the gut to the brain stem via signaling pathways that have yet to be elucidated.

Heavy metals and metal mixtures from industrial effluents can contaminate water bodies. While few studies have dealt with the effect of metals on human GI physiology, a majority of our knowledge on GI metal toxicity comes from research in aquatic animals. A review by DeForest comprehensively states that fish given metal-rich food develop intestinal dysmotility and impacted abdomens (DeForest and Meyer, 2015). Enterocytes lining the

intestine are equipped with a variety of metal ion transporters such as divalent metal transporter-1, ferroportin, ZIP8, SLC30A10 etc to regulate the influx and efflux of metals. Metals such as copper, iron, manganese, magnesium, zinc, selenium etc are required in trace amounts for normal cellular functioning. However in the presence of chronic exposure (through drinking water or food containing high amounts of divalent/trivalent metal species) the membrane channels and receptors involved in maintaining metal homeostasis become overburdened and hence non-functional. A deregulated metal homeostasis may lead to bioaccumulation of redox-active metals culminating in free-radical formation and mitochondrial dysfunction. For example, chronic mercury exposure in humans has been linked to GI ulcers, fluid accumulation in the intestines as well as diarrhea (McGinnis, 2001; Zahir et al., 2005). The fluid accumulation following mercury exposure is caused in part by a down regulation of the group of water channels- aquaporins (AQP) especially AQP3, 4 and 7. With the recent revelation of elevated levels of lead in drinking water at various locations in the US and associated GI and neurological problems, the issue of heavy metal poisoning and its effect on the gut-brain axis is gaining considerable attention. In the case of chronic lead exposure especially through drinking water, stomach cramps, changes in gut motility and nutrient absorption have been observed (Begovic et al., 2008; Mongolu and Sharp, 2013). Particularly, diet deficient in iron, zinc or calcium can lead to lead or cadmium poisoning. This occurs because following iron deficiency, there is increased influx of cadmium or lead via the divalent metal transporter that is possibly compensating for the lack of iron (Goyer, 1996). Cadmium can also induce the enterocytes to become more permeable as indicated by an *in-vitro* model of cadmium exposure on human enterocytes that revealed

reduced transepithelial electrical resistance and subsequently increased permeability (Breton et al., 2016).

Another target of toxin or xenobiotic exposure is the gut microbiome. It is now well known that the gut microbiome is instrumental in brain and GI tract development (Ghaisas et al., 2016). Moreover specific microbial communities can detoxify the food we ingest thus preventing in their absorption and helping eliminate these toxic compounds. A study conducted by Maurice and others have shown that toxicants and host-targeted drugs alter microbial gene expression especially those related to xenobiotic metabolism (Maurice et al., 2013). This change in bacteria gene expression can (depending upon the bacterial species) either lead to detoxification and removal of the toxins from the body or conversion of non-toxic compounds into potential toxins. Long-term exposure to such toxins can significantly alter the bacterial population influencing the growth of pathogenic, "inflammatory" bacteria over other species leading to an altered GI functioning. For example, Glyphosphate is an active component of many herbicides while chlorpyrifos is a pesticide widely used. Exposure to either of these compounds either through contact or food consumption (that it was applied to) can lead to decrease in beneficial bacteria such as *Enterococcus faecalis, Bacillus badius* and probiotic bacteria such as *Bifidobacterium* and *Lactobacillus sp*. with an increase or no change in pathogenic species of *Salmonella* and *Clostridium* (Joly et al., 2013; Shehata et al., 2013). Similarly, chronic exposure to even low doses of the heavy metal arsenic lead to a reduction in the population of Firmicutes in mice with concurrent alterations in bacterial metabolites such as indole derivatives, isoflavones, fatty acids etc (Lu et al., 2014). Increased presence of *Clostridium*, *Salmonella* sp. or adherent invasive *Escherichia coli* can lead to increased permeability and translocation of gut bacteria from the lumen into the deeper

intestinal tissue. This translocation activates surveilling immune cells that mount a response to the bacterial cell wall components especially on gram-negative bacteria that have lipopolysaccharide. Activated macrophages and dendritic cells recruit circulating monocytes to the site of invasion leading to an abundance of activated monocytes that produce pro-inflammatory cytokines and chemokines. But how does activation of immune cells present in the GI tract lead to neuroinflammation in the CNS?

Changes in CNS following intestinal inflammation

Following intestinal or systemic inflammation both pro-inflammatory (to activate and recruit immune cells and remove the agent of inflammation) and anti-inflammatory factors (wound healing, cell re-proliferation etc.) are produced by immune and non-immune cells. Extensive evidence links molecules associated with inflammatory conditions, including cytokines, reactive oxygen species, matrix metalloproteases, and mediators of angiogenesis, with BBB disruption (Wardill et al., 2016). For instance many children with ASD display not only intestinal inflammation with associated dysmotility but also presence of activated monocytes and perivascular macrophages in the cerebellum (Vargas et al., 2005). CSF and brain parenchyma showed a higher levels of macrophage chemoattractant protein 1 (MCP-1), which is a potent recruiter of monocytes and macrophages to the site of expression. Monocytes are a subset of circulating white blood cells that can further differentiate into macrophages and dendritic cells. They mediate host antimicrobial and innate immune defense and are implicated in systemic and various organ-specific diseases. Remarkably, these cells have the ability to mobilize and traffic to the area of inflammation and further differentiate depending on the inflammatory stimuli. Despite the presence of microglia that

are the innate immune cells in the brain and spinal cord, these immune cells are known to recruit monocytes in to the brain in response to TNFα produced during peripheral inflammation (D'Mello et al., 2009). In another instance, chronic IBD or IBS patients usually display "sickness behavior" including increased anxiety and depression. The prevalence of cytokines such as IL-1β, IL-6 and TNFα during peripheral inflammation is thought to activate the HPA resulting in a depressive mental condition (Figure 5) (Dantzer et al., 2008; Dunn, 2006).

Curiously, most neurological disorders including AD and PD show inflammation and immune cell activation in areas closely situated to circumventricular organs (CVOs). CVOs are situated adjacent to brain ventricles and are characterized by extensive vasculature and a porous blood brain barrier (BBB). These areas receive chemical inputs from the bloodstream and relay these inputs to hypothalamus, medulla oblongata and endocrine hypothalamus-pituitary axis. In doing so, they maintain body fluid homeostasis and cardiovascular regulation, and play an important role in the generation of central acute immune and febrile responses. The importance of CVOs as possible primary sites of immune invasion came from a variety of studies investigating pathogen or peripheral immune invasion following parasitic or bacterial infection. In 1988 Schultzburg and colleagues showed that lab rats infected with *Trypanosoma brucei* showed early invasion of the parasite in areas of the brain lacking BBB such as the CVOs while Schulz and Engelhardt found that CVOs are a site for the entry of immune cells into the CNS and CSF and consequently are involved in the inflammatory process in the CNS during experimental autoimmune encephalitis (Schultzberg et al., 1988; Schulz and Engelhardt, 2005). Interestingly, disease-associated prion protein (PrP^d) deposition is found in the CVOs as well as gut-associated lymphoid tissue in preclinical

sheep with scrapie (Siso et al., 2010). However it is unknown if the entry of this pathogen is via the innervating nerves or via blood-CVO route. A summary of events observed in the CNS following peripheral inflammation is given in Table 1.

Conclusions

Over the years, our understanding of various neurological disorders such as PD, AD, MSA and ASD to name a few has expanded from documentation of brain regions primarily involved in disease pathogenesis to identification of the biochemical and molecular pathways that initiate and propagate these diseases. Strikingly, most of these diseases also display altered GI physiology. Common regulatory mechanisms must exist in the development and maintenance of a healthy GI tract, immune system and brain since a deregulation in this triad commonly results in the symptoms observed in these diseases. Gut microbiome also play an important part in the normal development of the nervous, enteric and immune systems. Hence focus has now shifted to the role played by the microbiome-gut-brain axis in neurodegeneration. He need of the hour is to delineate the specific roles played by each system in this triad and the signaling pathways involved following genetic predisposition or toxin exposure in order to devise effective therapeutic interventions.

REFERENCES

1. Chiodini, I., et al., *Cortisol secretion in patients with type 2 diabetes: relationship with chronic complications.* Diabetes Care, 2007. **30**(1): p. 83-8.
2. Rosmond, R., *Stress induced disturbances of the HPA axis: a pathway to Type 2 diabetes?* Med Sci Monit, 2003. **9**(2): p. RA35-9.

3. Rosmond, R., M.F. Dallman, and P. Bjorntorp, *Stress-related cortisol secretion in men: relationships with abdominal obesity and endocrine, metabolic and hemodynamic abnormalities.* J Clin Endocrinol Metab, 1998. **83**(6): p. 1853-9.

4. Miranda, R.A., et al., *HPA axis and vagus nervous function are involved in impaired insulin secretion of MSG-obese rats.* J Endocrinol, 2016. **230**(1): p. 27-38.

5. Anderson, A.J., et al., *Metformin Increases Cortisol Regeneration by 11betaHSD1 in Obese Men With and Without Type 2 Diabetes Mellitus.* J Clin Endocrinol Metab, 2016. **101**(10): p. 3787-3793.

6. Yamamoto, T., et al., *Disturbed gastrointestinal motility and decreased interstitial cells of Cajal in diabetic db/db mice.* J Gastroenterol Hepatol, 2008. **23**(4): p. 660-7.

7. Hens, J., et al., *Morphological and neurochemical identification of enteric neurones with mucosal projections in the human small intestine.* J Neurochem, 2001. **76**(2): p. 464-71.

8. Domoto, T., et al., *An in vitro study of the projections of enteric vasoactive intestinal polypeptide-immunoreactive neurons in the human colon.* Gastroenterology, 1990. **98**(4): p. 819-27.

9. Gulbransen, B.D. and K.A. Sharkey, *Novel functional roles for enteric glia in the gastrointestinal tract.* Nat Rev Gastroenterol Hepatol, 2012. **9**(11): p. 625-32.

10. Neunlist, M., et al., *Enteric glial cells: recent developments and future directions.* Gastroenterology, 2014. **147**(6): p. 1230-7.

11. Neunlist, M., et al., *Enteric glia inhibit intestinal epithelial cell proliferation partly through a TGF-beta1-dependent pathway.* Am J Physiol Gastrointest Liver Physiol, 2007. **292**(1): p. G231-41.

12. Benarroch, E.E., *Enteric nervous system: functional organization and neurologic implications.* Neurology, 2007. **69**(20): p. 1953-7.

13. Rao, M. and M.D. Gershon, *The bowel and beyond: the enteric nervous system in neurological disorders.* Nat Rev Gastroenterol Hepatol, 2016. **13**(9): p. 517-28.

14. Knudsen, K., et al., *Objective Colonic Dysfunction is Far more Prevalent than Subjective Constipation in Parkinson's Disease: A Colon Transit and Volume Study.* J Parkinsons Dis, 2017.

15. Mishima, T., et al., *The Prevalence of Constipation and Irritable Bowel Syndrome in Parkinson's Disease Patients According to Rome III Diagnostic Criteria.* J Parkinsons Dis, 2017.

16. Stubendorff, K., et al., *The impact of autonomic dysfunction on survival in patients with dementia with Lewy bodies and Parkinson's disease with dementia.* PLoS One, 2012. **7**(10): p. e45451.

17. Braak, H., et al., *Staging of brain pathology related to sporadic Parkinson's disease.* Neurobiol Aging, 2003. **24**(2): p. 197-211.

18. Braak, H., et al., *Gastric alpha-synuclein immunoreactive inclusions in Meissner's and Auerbach's plexuses in cases staged for Parkinson's disease-related brain pathology.* Neurosci Lett, 2006. **396**(1): p. 67-72.

19. Anderson, G., et al., *Loss of enteric dopaminergic neurons and associated changes in colon motility in an MPTP mouse model of Parkinson's disease.* Exp Neurol, 2007. **207**(1): p. 4-12.

20. Greene, J.G., A.R. Noorian, and S. Srinivasan, *Delayed gastric emptying and enteric nervous system dysfunction in the rotenone model of Parkinson's disease.* Exp Neurol, 2009. **218**(1): p. 154-61.

21. Kuo, Y.M., et al., *Extensive enteric nervous system abnormalities in mice transgenic for artificial chromosomes containing Parkinson disease-associated alpha-synuclein gene mutations precede central nervous system changes.* Hum Mol Genet, 2010. **19**(9): p. 1633-50.

22. Toti, L. and R.A. Travagli, *Gastric dysregulation induced by microinjection of 6-OHDA in the substantia nigra pars compacta of rats is determined by alterations in the brain-gut axis.* Am J Physiol Gastrointest Liver Physiol, 2014. **307**(10): p. G1013-23.

23. Engelender, S. and O. Isacson, *The Threshold Theory for Parkinson's Disease.* Trends Neurosci, 2017. **40**(1): p. 4-14.

24. Engen, P.A., et al., *The Potential Role of Gut-Derived Inflammation in Multiple System Atrophy.* J Parkinsons Dis, 2017.

25. de Magistris, L., et al., *Alterations of the intestinal barrier in patients with autism spectrum disorders and in their first-degree relatives.* J Pediatr Gastroenterol Nutr, 2010. **51**(4): p. 418-24.

26. Fiorentino, M., et al., *Blood-brain barrier and intestinal epithelial barrier alterations in autism spectrum disorders.* Mol Autism, 2016. **7**: p. 49.

27. De Angelis, M., et al., *Autism spectrum disorders and intestinal microbiota.* Gut Microbes, 2015. **6**(3): p. 207-13.

28. Adams, J.B., et al., *Gastrointestinal flora and gastrointestinal status in children with autism--comparisons to typical children and correlation with autism severity.* BMC Gastroenterol, 2011. **11**: p. 22.

29. Shimmura, C., et al., *Alteration of plasma glutamate and glutamine levels in children with high-functioning autism.* PLoS One, 2011. **6**(10): p. e25340.

30. De Angelis, M., et al., *Fecal microbiota and metabolome of children with autism and pervasive developmental disorder not otherwise specified.* PLoS One, 2013. **8**(10): p. e76993.

31. Thomas, R.H., et al., *Altered brain phospholipid and acylcarnitine profiles in propionic acid infused rodents: further development of a potential model of autism spectrum disorders.* J Neurochem, 2010. **113**(2): p. 515-29.

32. MacFabe, D.F., et al., *Effects of the enteric bacterial metabolic product propionic acid on object-directed behavior, social behavior, cognition, and neuroinflammation in adolescent rats: Relevance to autism spectrum disorder.* Behav Brain Res, 2011. **217**(1): p. 47-54.

33. Roullet, F.I., J.K. Lai, and J.A. Foster, *In utero exposure to valproic acid and autism--a current review of clinical and animal studies.* Neurotoxicol Teratol, 2013. **36**: p. 47-56.

34. Gabriele, S., R. Sacco, and A.M. Persico, *Blood serotonin levels in autism spectrum disorder: a systematic review and meta-analysis.* Eur Neuropsychopharmacol, 2014. **24**(6): p. 919-29.

35. Pfaender, S. and A.M. Grabrucker, *Characterization of biometal profiles in neurological disorders.* Metallomics, 2014. **6**(5): p. 960-77.

36. Yasuda, H., et al., *Infantile zinc deficiency: association with autism spectrum disorders.* Sci Rep, 2011. **1**: p. 129.

37. Tyszka-Czochara, M., et al., *The role of zinc in the pathogenesis and treatment of central nervous system (CNS) diseases. Implications of zinc homeostasis for proper CNS function.* Acta Pol Pharm, 2014. **71**(3): p. 369-77.

38. Caine, W.R., et al., *Supplementation of diets for gestating sows with zinc amino acid complex and gastric intubation of suckling pigs with zinc-methionine on mineral status, intestinal morphology and bacterial translocation in lipopolysaccharide-challenged early-weaned pigs.* Res Vet Sci, 2009. **86**(3): p. 453-62.

39. Ghaisas, S., J. Maher, and A. Kanthasamy, *Gut microbiome in health and disease: Linking the microbiome-gut-brain axis and environmental factors in the pathogenesis of systemic and neurodegenerative diseases.* Pharmacol Ther, 2016. **158**: p. 52-62.

40. Geboes, K. and S. Collins, *Structural abnormalities of the nervous system in Crohn's disease and ulcerative colitis.* Neurogastroenterol Motil, 1998. **10**(3): p. 189-202.

41. Manocha, M. and W.I. Khan, *Serotonin and GI Disorders: An Update on Clinical and Experimental Studies.* Clin Transl Gastroenterol, 2012. **3**: p. e13.

42. Capoccia, E., et al., *Enteric glia: A new player in inflammatory bowel diseases.* Int J Immunopathol Pharmacol, 2015. **28**(4): p. 443-51.

43. Gabella, G., *Fine structure of the myenteric plexus in the guinea-pig ileum.* J Anat, 1972. **111**(Pt 1): p. 69-97.

44. Savidge, T.C., M.V. Sofroniew, and M. Neunlist, *Starring roles for astroglia in barrier pathologies of gut and brain.* Lab Invest, 2007. **87**(8): p. 731-6.

45. Savidge, T.C., et al., *Enteric glia regulate intestinal barrier function and inflammation via release of S-nitrosoglutathione.* Gastroenterology, 2007. **132**(4): p. 1344-58.

46. Bassotti, G., et al., *Enteric neuropathology of the terminal ileum in patients with intractable slow-transit constipation.* Hum Pathol, 2006. **37**(10): p. 1252-8.

47. von Boyen, G.B., et al., *Distribution of enteric glia and GDNF during gut inflammation.* BMC Gastroenterol, 2011. **11**: p. 3.

48. Bach-Ngohou, K., et al., *Enteric glia modulate epithelial cell proliferation and differentiation through 15-deoxy-12,14-prostaglandin J2.* J Physiol, 2010. **588**(Pt 14): p. 2533-44.

49. Van Landeghem, L., et al., *Regulation of intestinal epithelial cells transcriptome by enteric glial cells: impact on intestinal epithelial barrier functions.* BMC Genomics, 2009. **10**: p. 507.

50. Steinkamp, M., et al., *GDNF protects enteric glia from apoptosis: evidence for an autocrine loop.* BMC Gastroenterol, 2012. **12**: p. 6.

51. Cirillo, C., et al., *Increased mucosal nitric oxide production in ulcerative colitis is mediated in part by the enteroglial-derived S100B protein.* Neurogastroenterol Motil, 2009. **21**(11): p. 1209-e112.

52. Turco, F., et al., *Enteroglial-derived S100B protein integrates bacteria-induced Toll-like receptor signalling in human enteric glial cells.* Gut, 2014. **63**(1): p. 105-15.

53. Langness, S., et al., *Enteric glia cells are critical to limiting the intestinal inflammatory response after injury.* Am J Physiol Gastrointest Liver Physiol, 2017. **312**(3): p. G274-G282.

54. McClain, J.L., et al., *Ca2+ responses in enteric glia are mediated by connexin-43 hemichannels and modulate colonic transit in mice.* Gastroenterology, 2014. **146**(2): p. 497-507 e1.

55. Brown, I.A., et al., *Enteric glia mediate neuron death in colitis through purinergic pathways that require connexin-43 and nitric oxide.* Cell Mol Gastroenterol Hepatol, 2016. **2**(1): p. 77-91.

56. Gulbransen, B.D., et al., *Activation of neuronal P2X7 receptor-pannexin-1 mediates death of enteric neurons during colitis.* Nat Med, 2012. **18**(4): p. 600-4.

57. Tornblom, H., et al., *Full-thickness biopsy of the jejunum reveals inflammation and enteric neuropathy in irritable bowel syndrome.* Gastroenterology, 2002. **123**(6): p. 1972-9.

58. Lai, N.Y., K. Mills, and I.M. Chiu, *Sensory neuron regulation of gastrointestinal inflammation and bacterial host defence.* J Intern Med, 2017.

59. Geppetti, P., et al., *The concept of neurogenic inflammation.* BJU Int, 2008. **101 Suppl 3**: p. 2-6.

60. Abdrakhmanova, G.R., et al., *Nicotine suppresses hyperexcitability of colonic sensory neurons and visceral hypersensivity in mouse model of colonic inflammation.* Am J Physiol Gastrointest Liver Physiol, 2012. **302**(7): p. G740-7.

61. Ghia, J.E., et al., *The vagus nerve: a tonic inhibitory influence associated with inflammatory bowel disease in a murine model.* Gastroenterology, 2006. **131**(4): p. 1122-30.

62. Okayama, M., et al., *Protective effect of lafutidine, a novel histamine H2-receptor antagonist, on dextran sulfate sodium-induced colonic inflammation through capsaicin-sensitive afferent neurons in rats.* Dig Dis Sci, 2004. **49**(10): p. 1696-704.

63. Reinshagen, M., et al., *Action of sensory neurons in an experimental at colitis model of injury and repair.* Am J Physiol, 1996. **270**(1 Pt 1): p. G79-86.

64. McCafferty, D.M., J.L. Wallace, and K.A. Sharkey, *Effects of chemical sympathectomy and sensory nerve ablation on experimental colitis in the rat.* Am J Physiol, 1997. **272**(2 Pt 1): p. G272-80.

65. Engel, M.A., et al., *The proximodistal aggravation of colitis depends on substance P released from TRPV1-expressing sensory neurons.* J Gastroenterol, 2012. **47**(3): p. 256-65.

66. Becker, L., et al., *Age-dependent shift in macrophage polarisation causes inflammation-mediated degeneration of enteric nervous system.* Gut, 2017.

67. Wade, P.R. and T. Cowen, *Neurodegeneration: a key factor in the ageing gut.* Neurogastroenterol Motil, 2004. **16 Suppl 1**: p. 19-23.

68. Saffrey, M.J., *Cellular changes in the enteric nervous system during ageing.* Dev Biol, 2013. **382**(1): p. 344-55.

69. Abalo, R., et al., *Age-related changes in the gastrointestinal tract: a functional and immunohistochemical study in guinea-pig ileum.* Life Sci, 2007. **80**(26): p. 2436-45.

70. Phillips, R.J. and T.L. Powley, *Innervation of the gastrointestinal tract: patterns of aging.* Auton Neurosci, 2007. **136**(1-2): p. 1-19.

71. Phillips, R.J., et al., *Alpha-synuclein immunopositive aggregates in the myenteric plexus of the aging Fischer 344 rat.* Exp Neurol, 2009. **220**(1): p. 109-19.

72. Phillips, R.J., C.N. Billingsley, and T.L. Powley, *Macrophages are unsuccessful in clearing aggregated alpha-synuclein from the gastrointestinal tract of healthy aged Fischer 344 rats.* Anat Rec (Hoboken), 2013. **296**(4): p. 654-69.

73. Breid, S., et al., *Neuroinvasion of alpha-Synuclein Prionoids after Intraperitoneal and Intraglossal Inoculation.* J Virol, 2016. **90**(20): p. 9182-93.

74. Holmqvist, S., et al., *Direct evidence of Parkinson pathology spread from the gastrointestinal tract to the brain in rats.* Acta Neuropathol, 2014. **128**(6): p. 805-20.

75. McBride, P.A., et al., *Early spread of scrapie from the gastrointestinal tract to the central nervous system involves autonomic fibers of the splanchnic and vagus nerves.* J Virol, 2001. **75**(19): p. 9320-7.

76. Bellou, V., et al., *Environmental risk factors and Parkinson's disease: An umbrella review of meta-analyses.* Parkinsonism Relat Disord, 2016. **23**: p. 1-9.

77. Belbasis, L., et al., *Environmental risk factors and multiple sclerosis: an umbrella review of systematic reviews and meta-analyses.* Lancet Neurol, 2015. **14**(3): p. 263-73.

78. Killin, L.O., et al., *Environmental risk factors for dementia: a systematic review.* BMC Geriatr, 2016. **16**(1): p. 175.

79. Yan, D., et al., *Pesticide exposure and risk of Alzheimer's disease: a systematic review and meta-analysis.* Sci Rep, 2016. **6**: p. 32222.

80. Modabbernia, A., E. Velthorst, and A. Reichenberg, *Environmental risk factors for autism: an evidence-based review of systematic reviews and meta-analyses.* Mol Autism, 2017. **8**: p. 13.

81. Pan-Montojo, F., et al., *Environmental toxins trigger PD-like progression via increased alpha-synuclein release from enteric neurons in mice.* Sci Rep, 2012. **2**: p. 898.

82. Zhu, H.C., et al., *Gastrointestinal dysfunction in a Parkinson's disease rat model and the changes of dopaminergic, nitric oxidergic, and cholinergic neurotransmitters in myenteric plexus.* J Mol Neurosci, 2012. **47**(1): p. 15-25.

83. Cannon, J.R., et al., *A highly reproducible rotenone model of Parkinson's disease.* Neurobiol Dis, 2009. **34**(2): p. 279-90.

84. Sherer, T.B., et al., *Subcutaneous rotenone exposure causes highly selective dopaminergic degeneration and alpha-synuclein aggregation.* Exp Neurol, 2003. **179**(1): p. 9-16.

85. DeForest, D.K. and J.S. Meyer, *Critical Review: Toxicity of Dietborne Metals to Aquatic Organisms.* Critical Reviews in Environmental Science and Technology 2015. **45**(11): p. 1176-1241

86. McGinnis, W.R., *Mercury and autistic gut disease.* Environ Health Perspect, 2001. **109**(7): p. A303-4.

87. Zahir, F., et al., *Low dose mercury toxicity and human health.* Environ Toxicol Pharmacol, 2005. **20**(2): p. 351-60.

88. Begovic, V., et al., *Extreme gastric dilation caused by chronic lead poisoning: a case report.* World J Gastroenterol, 2008. **14**(16): p. 2599-601.

89. Mongolu, S. and P. Sharp, *Acute abdominal pain and constipation due to lead poisoning.* Acute Med, 2013. **12**(4): p. 224-6.

90. Goyer, R.A., *Results of lead research: prenatal exposure and neurological consequences.* Environ Health Perspect, 1996. **104**(10): p. 1050-4.

91. Breton, J., et al., *Does oral exposure to cadmium and lead mediate susceptibility to colitis? The dark-and-bright sides of heavy metals in gut ecology.* Sci Rep, 2016. **6**: p. 19200.

92. Maurice, C.F., H.J. Haiser, and P.J. Turnbaugh, *Xenobiotics shape the physiology and gene expression of the active human gut microbiome.* Cell, 2013. **152**(1-2): p. 39-50.

93. Shehata, A.A., et al., *The effect of glyphosate on potential pathogens and beneficial members of poultry microbiota in vitro.* Curr Microbiol, 2013. **66**(4): p. 350-8.

94. Joly, C., et al., *Impact of chronic exposure to low doses of chlorpyrifos on the intestinal microbiota in the Simulator of the Human Intestinal Microbial*

Ecosystem (SHIME) and in the rat. Environ Sci Pollut Res Int, 2013. **20**(5): p. 2726-34.

95. Lu, K., et al., *Arsenic exposure perturbs the gut microbiome and its metabolic profile in mice: an integrated metagenomics and metabolomics analysis.* Environ Health Perspect, 2014. **122**(3): p. 284-91.

96. Wardill, H.R., et al., *Cytokine-mediated blood brain barrier disruption as a conduit for cancer/chemotherapy-associated neurotoxicity and cognitive dysfunction.* Int J Cancer, 2016. **139**(12): p. 2635-2645.

97. Vargas, D.L., et al., *Neuroglial activation and neuroinflammation in the brain of patients with autism.* Ann Neurol, 2005. **57**(1): p. 67-81.

98. D'Mello, C., T. Le, and M.G. Swain, *Cerebral microglia recruit monocytes into the brain in response to tumor necrosis factoralpha signaling during peripheral organ inflammation.* J Neurosci, 2009. **29**(7): p. 2089-102.

99. Dunn, A.J., *Effects of cytokines and infections on brain neurochemistry.* Clin Neurosci Res, 2006. **6**(1-2): p. 52-68.

100. Dantzer, R., et al., *From inflammation to sickness and depression: when the immune system subjugates the brain.* Nat Rev Neurosci, 2008. **9**(1): p. 46-56.

101. Schultzberg, M., et al., *Spread of Trypanosoma brucei to the nervous system: early attack on circumventricular organs and sensory ganglia.* J Neurosci Res, 1988. **21**(1): p. 56-61.

102. Schulz, M. and B. Engelhardt, *The circumventricular organs participate in the immunopathogenesis of experimental autoimmune encephalomyelitis.* Cerebrospinal Fluid Res, 2005. **2**: p. 8.

103. Siso, S., L. Gonzalez, and M. Jeffrey, *Neuroinvasion in prion diseases: the roles of ascending neural infection and blood dissemination.* Interdiscip Perspect Infect Dis, 2010. **2010**: p. 747892.

Literature review II

Gut microbiome in health and disease: linking the microbiome-gut-brain axis and environmental factors in the pathogenesis of systemic and neurodegenerative diseases

Manuscript published in Pharmacology & Therapeutics

Shivani Ghaisas, Joshua Maher, Anumantha Kanthasamy[‡]

Parkinson's Disorder Research Laboratory, Iowa Center for Advanced Neurotoxicology, Department of Biomedical Sciences, Iowa State University, Ames, Iowa 50011, USA

[‡]To whom correspondence should be addressed:

Dept. of Biomedical Sciences,

2062 College of Veterinary Medicine Building,

Iowa State University,

Ames, IA 50011.

Tel: 515-294-2516;

Email: akanthas@iastate.edu

1. Abstract

The gut microbiome comprises the collective genome of the trillions of microorganisms residing in our gastrointestinal ecosystem. The interaction between the host and its gut microbiome is a complex relationship whose manipulation could prove critical to preventing or treating not only various gut disorders, like irritable bowel syndrome (IBS) and ulcerative colitis (UC), but also central nervous system (CNS) disorders, such as Alzheimer's and Parkinson's diseases. The purpose of this review is to summarize what is known about the gut microbiome, how it is connected to the development of disease and to identify the bacterial and biochemical targets that should be the focus of future research. Understanding the mechanisms behind the activity and proliferation of the gut microbiome will provide us new insights that may pave the way for novel therapeutic strategies.

Keyword: microbiome-gut-brain axis, Parkinson's disease, gut microbiota, neurological diseases, Autism, manganese, metals, environmental factors, neurotoxicity

2. Introduction

Among the many microbial communities colonizing the human body, the gut microbiome is emerging as a major player influencing the health status of the host. The composition of the gut microbiome is established early during the host's development and can undergo a myriad of changes throughout a lifetime. The complex interaction between host physiology and the gut microbiome is a topic of research that is still in its infancy. Yet broadening our understanding of this interaction could lead to beneficial therapeutic strategies for improving human health. Although we are only in the beginning stages of

defining the biomarkers, bacterial species, and diets necessary to manipulate and study the human microbiome, we can appreciate the potential implications this research has on the future of medicine. The objective of this review is to summarize current findings linking host gut microbiome and health and to identify future directions necessary for unraveling the gut microbiome's role in the pathogenesis of chronic metabolic and central nervous system diseases.

3. The Gut Microbiome

The gut microbiome comprises the collective genome of roughly 100 trillion microorganisms residing in the gastrointestinal tract (Tsai and Coyle, 2009). The gene repertoire of our gut bacteria contains 150 times more unique genes than the human genome (Qin et al., 2010).

The fetal gastrointestinal tract (GIT) is sterile prior to birth with microbial colonization first occurring at delivery (Morelli, 2008). In vaginally delivered infants, the GIT is primarily colonized by bifidobacteria as well as lactobacilli, *Bacteroides*, *Proteobacteria* and *Actinobacteria*. In contrast, infants delivered via cesarean section have more *Escherichia coli* (*E. coli*) as well as *Clostridia*, especially *C. difficile,* and fewer *Bacteroides* and bifidobacteria (Penders et al., 2006). Similarly, breast-fed infants showed a higher abundance of bifidobacteria, whereas in formula-fed infants, bifidobacteria and *Bacteroides* as well as *Clostridia* and Staphylococci were found in equal numbers (Harmsen et al., 2000). Conversely, other groups have shown an abundance of *Bifidobacterium*, *Actinomyces*, and *Haemophilus* in breast-fed babies while formula-fed babies had an abundance of Firmicutes and Bacteroidetes in their gut (Yatsunenko et al., 2012). This

discrepancy in estimating the gut microbiome population is possibly due to differences in the techniques used to sample and analyze the data. However, despite these discrepancies, most studies emphasize that both the type of diet and mode of delivery can preferentially promote certain bacterial communities over others. While the mechanism remains unclear, it is known that the earliest gut microbiota primarily consists of bacteria that can metabolize the lactose absorbed from breast milk or infant formulas made from cow's milk. However, with the introduction of solid food, the gut becomes dominated by bacterial species associated with carbohydrate, protein and fat utilization as well as vitamin synthesis (Koenig et al., 2011). The host also selectively favors particular bacterial species in different regions of the gut. For example, butyrate-synthesizing bacteria such as the Firmicutes are present in higher proportions in the colon and are less well represented in the upper small intestine. This is beneficial and quite necessary since short chain fatty acids like butyrate are the main source of energy for colonic epithelial cells (Hooper et al., 2002; Roediger, 1980; Wong et al., 2006).

Not surprisingly, the interaction between an organism and its gut microbes is not unidirectional but involves feedback with the host environment affecting the gut microbiotic composition and the colonized bacteria, influencing host development. Following bacterial colonization, certain physiological changes have been observed in the gut, including increased production of neurotransmitters such as serotonin (5-HT) and γ-aminobutyric acid (GABA) as well as the expression of various cytokines. These changes are integral to gut homeostasis and to programming of the hypothalamic-pituitary-adrenal (HPA) axis, which plays an important role in stress responses (Diaz Heijtz et al., 2011; Sudo et al., 2004). As shown in Figure 1, early colonization of certain enterotypes can have a long-lasting influence

on the health status of the host. For example, infants with a higher prevalence of *Bifidobacterium* and *Collinsella* at age 6 months showed lower adiposity at 18 months (Dogra et al., 2015). In another study, overweight subjects exhibited decreased numbers of Bifidobacter*ia* and the *Bacteroides* (Santacruz et al., 2010). The gut microbiome composition throughout a host's lifespan is not static, but measuring these changes proves difficult due to confounding changes in diet, environment, and disease state throughout life. As previously stated, numerous studies have studied gut microbiome composition early in life, yet much fewer studies have reported gut microbiome changes in middle-aged and elderly subjects. Shifts from *Bifidobacterium* to *Clostridia* and Bacteriodetes occur as the host develops from a newborn into an adult (Yatsunenko et al., 2012). Decreases in *Faecalibacterium prauznitzii* and its anti-inflammatory relatives occur as young adults mature to become elderly or even centenarians (Biagi et al., 2010). However, determining to what extent such changes reflect normal development and maturation versus dietary/environmental changes or pathological deficiencies will require further study.

3.1 The Gut Microbiome and Health

It was initially thought that gut microbes were mainly commensals whose only benefit was controlling the population of pathogenic bacteria. We now know that these symbionts play important roles in aiding digestion, in the production of essential metabolites and in the development of the immune system (Walker and Lawley, 2013). Gut bacteria play a pivotal role in immune modulation and development of the nervous system and are the main source of vitamin K, and to a lesser extent the vitamin B complex (Kelly et al., 2007; Littman and Pamer, 2011; Resta, 2009). Indeed, germ-free rats require a higher intake of exogenous sources of vitamins K, B12 and B6 compared to their conventional counterparts

(Gustafsson, 1959; Sumi et al., 1977; Wostmann, 1981). Recognition of the importance of the gut microbiota in infant development has been greatly aided by the development of gnotobiotic animal models. Germ-free rodents fed sterile chow, identical in all other respects to that consumed by their conventional mates, showed decreased basal metabolic rate, increased cholesterol in liver and blood as well as structural and functional differences in the enteric nervous system (ENS) (Danielsson and Gustafsson, 1959; Dupont et al., 1965; Wostmann et al., 1966). Furthermore, systemic T- and B-cell deficiencies in these animals are thought to result from the lack of exposure of the naïve immune cells to microbial products generally found in animals with normal intestinal microbiota (Falk et al., 1998; Mazmanian et al., 2005; Szeri et al., 1976).

Other studies have shown that seemingly abrupt and chaotic shifts in the gut microbiota correspond to changes in the host's environment, diet and genetic predisposition. Dysbiosis of the gut microbiome has been implicated in numerous disorders, ranging from intestinal diseases, such as colorectal cancer and inflammatory bowel disease (IBD), to more systemic diseases such as diabetes, metabolic syndrome and atopy (Walker and Lawley, 2013). The gut microbiome also influences various Type-2 Diabetes (T2D)-related complications (Fig. 2), including diabetic retinopathy, kidney toxicity, atherosclerosis, hypertension, diabetic foot ulcers, and cystic fibrosis (Zhang and Zhang, 2013). Recent research has also linked microbial dysbiosis to neurological disorders, such as Parkinson's and Alzheimer's diseases, multiple sclerosis and autism. The CNS connects with the gut *via* sympathetic and parasympathetic nerves. However, the importance of these connections had not been studied in depth until the past decade. Villaran and co-workers reported that peripheral inflammation in the form of dextran sodium sulfate (DSS)-induced colitis can

aggravate LPS-induced neuroinflammation and neurodegeneration (Villaran et al., 2010) as shown by increased mRNA transcripts of TNFα, iNOS and IL-6 in the midbrain. Interestingly, even rats with colitis alone (no midbrain injection of LPS) showed increased mRNA transcripts of TNFα, iNOS and IL-6 in the midbrain. Other studies have also shown that recurring systemic infections can increase the probability of developing multiple sclerosis, Alzheimer's or Parkinson's disease (Serres et al., 2009; Tilvis et al., 2004). A concise summary of the changes seen in the gut and CNS in various diseases is shown in Figure 3.

3.2 Systemic Diseases and Gut Microbiome Dysbiosis

Multi-disciplinary studies incorporating advances in next generation sequencing (NGS), have revealed that various systemic diseases, such as arthritis, atherosclerosis, IBD, as well as diabetes and obesity, show significant changes not only in the composition of the resident gut microbiota but also in the host's gut homeostasis and metabolic processes (Musso et al., 2011; Scher et al., 2015; Vieira et al., 2015; Yamashita et al., 2015). In essence, the gut microbiota influence and even facilitate various metabolic processes such as regulating xenobiotic metabolism and energy production. As discussed later in this review, diet and environment play an important part in maintaining gut bacterial populations. Perturbations in this ecosystem can have negative and prolonged effects on host physiology. While there are many such systemic disorders that show an inherent gut microbiota dysbiosis, we summarize two common and well-studied diseases- ulcerative colitis and type-2 diabetes.

3.2.1 Ulcerative colitis

Ulcerative colitis (UC) is a type of IBD characterized by chronic inflammation and sores (ulcers) along the lining of the large intestine and rectum. In addition, neuroplastic changes in the ENS are observed in UC, including degeneration of ganglion cells and nerve hyperplasia (Vasina et al., 2006). UC results from a combination of host genetic risk factors, environment, and alterations in gut microbiome composition. Dysbiosis in the gut microbiome of UC patients is characterized by a lower proportion of Firmicutes and a higher percentage of Gammaproteobacteria, sulfate-reducing Deltaproteobacteria, Actinobacteria and Proteobacteria compared to that of healthy hosts (Lepage et al., 2011; Sokol et al., 2007; Sokol et al., 2009). In general, Gram-negative bacteria populations tend to increase, while those of Gram-positive bacteria tend to decrease. Increases in Gram-negative bacteria like *E.coli* may lead to increased Lipopolysaccharide (LPS) translocation in the gut and consequently to a chronic state of low-grade inflammation as seen in UC. In addition to changes in the composition of the gut microbiome in IBD patients, gene expression for amino acid metabolism and biosynthesis are greatly downregulated while the expression of lysine, histidine, and arginine transport genes is upregulated. Expression in UC patients of transport and metabolism genes for the antioxidant glutathione (a tripeptide synthesized by bacterial species) also increases, thus possibly revealing the mechanism by which the gut microbiome responds to inflammatory oxidative stress (Gardiner et al., 1993; Morgan et al., 2012). Besides UC, gut microbiome dysbiosis also occurs in other forms of IBD where it causes vast changes in gut microbiome metabolic function and microbiotic reaction to the inflammatory response. Neither the extent to which dysbiosis alters GI microbiome function

nor the specific consequences of such changes in gut microbiome composition are fully understood, and both require further metabolic and genetic study.

3.2.2 Diabetes

T2D is a chronic metabolic disorder wherein the body either does not produce enough insulin or cannot effectively metabolize glucose despite insulin production. Assessing the gut microbiome of healthy and T2D-diagnosed individuals showed that Betaproteobacteria were present in higher proportions in T2D individuals (Larsen et al., 2010). This difference correlated more with increased glucose plasma levels than with body mass indices (BMI), suggesting that this species might be involved in glucose metabolism (Larsen et al., 2010).

Although research linking PD to diabetes is still in its infancy, preliminary studies suggest that individuals with T2D have a higher incidence of PD than do non-T2D individuals (Hu et al., 2007; Schernhammer et al., 2011; Sun et al., 2012). During a 9-year study, diabetic patients in Taiwan had a significantly increased risk of developing PD in both sexes and most age groups. Although the mechanistic link between T2D and PD is not known, chronic inflammation and oxidative stress are also linked in the risk of PD. Furthermore, insulin plays a role in regulating central dopaminergic signaling, and thus insulin dysregulation in T2D patients may contribute to nigro-striatal dopaminergic dysfunction. Peroxisome proliferator-activated receptor gamma coactivator 1-alpha (PGC-1α) is an important gene involved in mitochondrial biogenesis, regulating energy homeostasis relative to environmental stimuli (Knusel et al., 1990; Puigserver and Spiegelman, 2003; Wu et al., 1999). PGC-1α and its downstream targets are downregulated in both PD and T2D patients (Mootha et al., 2003; Zheng et al., 2010). Recently, it has been found that the zinc finger protein Parkin Interacting Substrate (PARIS) binds to the insulin

response sequences in the PGC-1α promoter. This interaction represses the expression of PGC-1α and Nuclear Respiratory Factor-1 (NRF-1) genes in dopaminergic neurons leading to their loss (Shin et al., 2011). Thus, both T2D and PD share common pathophysiological mechanisms including oxidative stress, inflammation and mitochondrial dysfunction.

Since individuals with T2D run an increased risk of developing PD, we need to better understand the effect of anti-diabetic drugs on PD. A patient's risk of developing PD increases 2.2 fold when diagnosed with T2D, but that risk is lowered to only 1.3 fold with oral anti-hyperglycemic agent (OAA) therapy, suggesting that OAAs could also protect against neurodegenerative diseases like Parkinson's (Wahlqvist et al., 2012). Metformin is an oral anti-hyperglycemic agent prescribed to treat T2D and metabolic syndrome (Knowler et al., 2002). It is a well-tolerated drug that has been extensively used for decades, and thus, testing the drug's efficacy against neurodegenerative diseases seems promising. Metformin's mechanism of action was originally reported to involve activating AMPK through inhibition of mitochondrial respiration (El-Mir et al., 2000; Owen et al., 2000). However, recent evidence indicates that the metformin induced AMPK activation occurs independent of mitochondrial respiration (Bergheim et al., 2006). We found that metformin does not inhibit mitochondrial respiration in neuronal cells at therapeutic concentrations. Recent evidence suggests that altering the gut microbiome to favor *Akkermansia muciniphila*, a newly discovered mucin-degrading bacterium, in mice fed a high-fat diet (HFD) may contribute to the anti-diabetic effects of metformin (Shin et al., 2014). Treatment with *A. muciniphila* can reverse HFD-induced metabolic disorders such as adipose tissue inflammation, weight gain, and insulin resistance (Everard et al., 2013). Metformin also affects host levels of methionine and folate, two nutrients essential to human health yet not produced *de novo,* but

instead are synthesized by certain gut microbes. Folates are B-vitamins involved in the biosynthesis of purines and pyrimidines as well as the biotransformation of amino acids within the host. Interestingly, deficiencies in B-12 vitamins, and folate specifically, have been implicated in Alzheimer's disease patients (Lahiri and Maloney, 2010). Methionine is a sulfur-containing amino acid that occurs in proteins with proposed antioxidant activity (Levine et al., 1996). Folate and methionine are just two examples of possible gut byproducts that influence bacterial and host metabolism and the development of CNS disease.

3.3 Central Nervous System Disorders and Gut Microbes

Although not well understood, the gut microbiome could have a significant influence on behavior and psychosis. Adult mice that had been separated as neonates from their mother for a protracted time showed elevated levels of basal and stress-evoked adrenocorticotropic hormone (ACTH) and corticotropic releasing hormone (CRH). This response was inversely related to the age of the mice at the time of maternal separation (Schmidt et al., 2002), thus development of the HPA axis may have a maturation window influenced and regulated to some extent by the gut microbial composition. Sudo and colleagues showed that germ-free (GF) BALB/c mice had significantly higher levels of plasma corticosterone and ACTH compared to specific pathogen-free (SPF) mice in response to restraint stress (Sudo et al., 2004). This response was tempered by the presence of *Bifidobacterium infantis,* which is known to be present in the neonate gut. In a highly intuitive experiment, they showed that gnotobiotic BALB/c mice colonized with enteropathogenic *Escherichia coli* (EPEC) developed an exaggerated response to stress, much higher than what the GF mice had shown. However, another set of mice colonized with the mutant EPEC strain ΔTir, did not display a heightened HPA response to stress. ΔTir bacteria lack the intimin receptor, thus preventing

microbial adherence and internalization in the intestinal tissue. This study showed that early colonization by intestinal bacteria regulates the development of the HPA axis. Colonization with commensal bacteria that are known to produce pro-health micronutrients is essential because neurodevelopment is impaired if pathogenic bacteria colonize the gastrointestinal tract.

3.3.1 Neurodevelopmental disorders:

Autism spectrum disorder (ASD)

Human studies have shown that gut problems in early childhood might contribute to autism development. Various disorders, such as Attention Deficit Hyperactive Disorder (ADHD) and Autism Spectrum Disorder (ASD) share behavioral abnormalities in sociability, communication, and/or compulsive activity (Hsiao et al., 2013). An abnormal HPA response and altered microbial and metabolic profiles have been implicated in these disorders (Kaneko et al., 1993; King et al., 1998; Ming et al., 2012). Ming and colleagues showed altered amino acid metabolism and increased oxidative stress in ASD children relative to age-matched controls (Ming, Stein et al. 2012). A sub-group of ASD children with a history of gastrointestinal perturbations had an altered microbial profile compared to controls. The ASD group showed decreased levels of both 5-amino-valerate, which is thought to act as a weak GABA agonist, and 3-(3-hydroxyphenyl) propionic acid, an antioxidant.

ASD children usually have a higher abundance of Proteobacteria and Bacteroidetes and a lower abundance of the Firmicutes and bifidobacteria when compared to healthy controls (Finegold et al., 2010; Finegold et al., 2012; Mezzelani et al., 2014). Interestingly, of the many classes of bacteria that constitute the Firmicutes, one class in particular, the Clostridia*,* is shown to be present in higher numbers in autistic children with a history of GI

problems (Song et al., 2004). Similarly, despite the overall abundance of Bacteroidetes in autistic subjects, lower counts of *Prevotella* are seen. Thus along with quantifying the relative increase or decrease in the populations of certain phyla, it is necessary to determine the populations of specific gut symbionts in order to understand the significance of certain physiological changes in the gut and/or the brain. One of the reasons why Clostridia are implicated in ASD is because autistic children subjected to oral Vancomycin treatment showed a regression of the characteristic symptoms of this disorder. Vancomycin is not absorbed in the intestine but can readily kill Gram-positive bacteria such as Clostridia. However, when the treatment was discontinued, the patients reverted back to their autistic behavior (Finegold, 2008). It is thought that clostridial spores, which are temperature-, pH- and antibiotic-resistant, also sporulate, further multiplying the mucosal populations of endotoxin-producing bacteria. Indeed, according to one current theory, the "leaky gut" syndrome, high counts of pathogenic bacteria in the gut impair the intestinal barrier by producing neuro- and endotoxins, which then expose the mucosa and sub-mucosa to bacteria. The bacterial invasion of this previously aseptic environment causes immune cell activation and infiltration as well as up-regulation of pro-inflammatory cytokines such as TNFα and Il-1β. This inflammatory response further increases barrier permeability thereby perpetuating an inflammatory cycle. Sandler et al. (2000) hypothesized that in a subgroup of children, disruption of indigenous gut microbiota might promote colonization by one or more neurotoxin-producing bacteria, contributing, at least in part, to eliciting autistic signs. These same investigators found that with broad-spectrum antimicrobial exposure followed by chronic persistent diarrhea, previously acquired skills deteriorated and autistic features emerged (Sandler et al., 2000). In a recent study of offspring exposed to maternal immune

activation (MIA), Hsaio et al. revealed that oral treatment with *Bacteroides fragillis* corrects gut permeability, alters microbial composition, and ameliorates defects in communicative, stereotypic, anxiety-like and sensorimotor behaviors mainly by altering the HPA axis response to stress. This experiment supports a microbiome-gut-brain connection in a mouse model of ASD and identifies a potential probiotic therapy for GI disorders and particular behavioral symptoms in human neurodevelopmental disorders (Hsiao et al., 2013).

Besides ASD, there has been considerable interest in understanding the role the gut microbiota plays in the development of ADHD and schizophrenia. In one study, infants were given either *Lactobacillus rhamnosus* GG or placebo during the first 6 months of life and gut microbiota was assessed over a period of 13 years. The study found a correlation between lower counts of *Bifidobacterium* species and development of ADHD or Asperger's Syndrome (Partty et al., 2015).

3.3.2 Neurodegenerative Disorders:

Parkinson's disease

The role of the gut microbiome in the pathogenesis of chronic neurodegenerative disorders such as Alzheimer's and Parkinson's diseases is beginning to emerge. In PD, GI dysregulation is often seen several years before the disease is even detected. Braak and colleagues hypothesized that the disease begins in the gut and spreads from gut to brain via the gut-brain axis, i.e., vagus nerve and spinal cord. Indeed, the parasympathetic fibers of the vagus nerve that innervate the intestine among other regions arise from the dorsal motor nucleus (DMVX). Lewy bodies (aggregated proteins, mainly alpha-synuclein and ubiquitin), which are the hallmark of PD, were found in the ENS in post-mortem cases of early PD (Braak et al., 2006). The presence of these protein aggregates correlated with the increasing

stages of PD and was subsequently found in the spinal cord, DMVX, prefrontal cortex and finally the mid-brain region of postmortem PD subjects. A recent study demonstrated that alpha-synuclein injected in the gut wall of rats migrated to the brain stem *via* the vagus nerve at a rate estimated to be 5-10 mm/day (Holmqvist et al., 2014). The idea that PD patients have a low-grade inflammation of the gut has been around for some time. Indeed, increased mRNA expression of pro-inflammatory cytokines has been observed in colonic biopsies of PD patients compared to control subjects (Devos et al., 2013). This chronic low-grade inflammation might be the trigger that leads to blood brain barrier leakiness, immune cell activation and infiltration and ultimately neuro-inflammation in the CNS.

Investigators are developing considerable interest in understanding the role of the gut microbiota in the context of PD. In one study, fecal microbiota collected from 72 PD subjects and age-matched controls showed higher counts of *Enterobacteriaceae* and reduced Prevotellaceae in PD patients. *Prevotella* is known to break down complex carbohydrates, providing short chain fatty acids (SCFA's) as well as thiamine and folate as byproducts that promote a healthy intestinal environment. Decreased *Prevotella* numbers are likely to result in reduced production of these important micronutrients. Unless compensated by dietary changes to supply these nutrients exogenously, decreased thiamine and folate might result in reduced production of essential vitamins and impaired secretions of gut hormones (Scheperjans et al., 2015). However, the study did not evaluate whether or not the patients had a history of GI disturbances or significant inflammation. Nevertheless, taken together, these results suggest that changes in the gut microbiome could have a direct effect on the CNS *via* the gut-brain axis with chronic mild systemic inflammation possibly driving the pathogenesis. Cyanobacteria present in small numbers in the GI tract are thought to produce

β-N-methylamino-L-alanine (BMAA), which is elevated in the brains of AD, PD and amyotrophic lateral sclerosis (ALS) patients. BMAA is an excitotoxin that activates metabotropic glutamate receptor 5, thereby inducing depletion of the major antioxidant glutathione. As a result, neurons and glial cells are unable to effectively control ROS and RNS production in the brain. The BMAA protein is also implicated in aiding protein misfolding and aggregation typically seen in AD, PD and ALS (Brenner, 2013). However, whether patients showing elevated levels of BMAA in their brain also show increased cyanobacteria populations in the gut is not clear and needs further study.

A majority of the clinically diagnosed PD cases are of the sporadic form, which is likely caused by a complex interplay of genetic and environmental factors. During the last few years, a number of epidemiological and clinical studies have suggested potential environmental risk factors for PD, including environmental exposure to certain pesticides and fungicides such as paraquat, rotenone and maneb, and some surrogate factors such as living in rural areas, drinking well water and farming. In addition, exposure to heavy metals such as iron, lead, mercury, cadmium, arsenic and manganese, as well as to metal-based nanoparticles, has also been shown to increase the risk of PD through the accumulation of metals in the mid brain and increased oxidative stress-mediated apoptosis (Aboud et al., 2014; Afeseh Ngwa et al., 2009; Afeseh Ngwa et al., 2011; Harischandra et al., 2015; Kanthasamy et al., 2012; Milatovic et al., 2009). Currently, the effect of environmental factors on the host gut microbiome is completely unknown.

Manganese is an essential trace element vital for normal bone development, fat and carbohydrate metabolism, blood sugar regulation, and the biological functions of a number of enzymes (Aschner and Aschner, 2005; Bowman et al., 2011). However, excessive

manganese is considered a neurotoxic pollutant in the environment and recently gained importance as a putative risk factor for environmentally-linked PD. Chronic exposure to occupational or environmental sources of manganese can cause a neurodegenerative disorder known as Manganism, characterized by severe neurological deficits that often resemble the involuntary extrapyramidal symptoms associated with PD. Manganism most frequently occurs from occupational manganese exposure during mining, welding metals, and dry battery manufacturing. Other manganese-containing products presenting a public exposure risk include fertilizers, varnish, fungicides, gasoline additives and livestock feeding supplements. The growing evidence indicates that manganese primarily causes damage to the basal ganglia in humans, where it affects dopamine release and causes GABA dysregulation (Brouillet et al., 1993; Erikson and Aschner, 2003; Fitsanakis et al., 2006; Roth et al., 2013). Yet, despite its prevalence and potential risk to human health, the mechanisms by which manganese exerts its toxic effects on the gut and gut microbiome have yet to be elucidated.

Preliminary experiments were conducted in our laboratory to assess the impact of manganese in altering gut physiology by exposing mice to 15 mg/kg/day $MnCl_2$ for 30 days *via* oral gavage. Manganese-exposed mice displayed increased whole gut transit time and an altered fecal metabolic profile. GC-MS studies carried out in stool samples showed that manganese exposure decreases butyrate production as well as α-tocopherol, which is involved in Vitamin-E synthesis, whereas it increases compounds such as cholic acid, which is known to saturate bile salts leading to the development of gall stones (Table 1). Thus, our results provide initial evidence that metal toxicity can influence gut motility and key gut microbial metabolites. Thus, it is likely that exposure to environmental toxins can influence the gut microbiome profile with potentially unfavorable physiological effects.

4. Factors Influencing Microbiome-Gut-Brain regulation

4.1 Environment

A recently described epigenetic model of disease development, called the LEARn model (Latent Early-Life Associated Regulation), predicts that early-life exposures to nutritional imbalances, metals, maternal care variations, or other environmental stressors can lead to modified expression of disorder-associated genes over the course of an individual's lifespan (Lahiri and Maloney, 2010). An early environmental influence is the maternal environment. The gut microbiota of mouse littermates are more similar than are those of pups born to different mothers despite being reared in adjacent boxes in the same animal room (Benson et al., 2010). Bacteria present in the mother's vaginal tract and on her skin serve as the first bacteria to colonize the neonate gut. Later, microbes present in the colostrum form a part of the gut microbiome, thus increasing the complexity of this environment. Our locality also plays an important role in determining individual gut microbiota profiles One study noted that ASD patients showed a gut microbiota profile similar to their healthy siblings, while unrelated healthy controls had significantly different profiles (Parracho et al., 2005).. Besides locality, additional environmental factors affecting the gut microbiome include ethnicity and culture (Annalisa et al., 2014; De Filippo et al., 2010; Holmes et al., 2008).

4.2 Diet, Microbes and Health

The relative abundance of gut microbiome is dependent upon the energy source available to them and their ability to utilize this source. In one study, switching from a low-fat, plant polysaccharide-rich diet to a high-fat, high-sugar diet shifted the community structure of the microbiome within a single day, changed the representation of metabolic pathways in the microbiome, and altered microbiome gene expression (Turnbaugh et al.,

2009). Firmicutes, especially Lactobacillaceae, Veillonellaceae, and Lachnospiraceae, were seen in greater proportions in obese individuals. Conversely, a high-fiber, low-fat diet decreased the population of Firmicutes (Parnell and Reimer, 2012).

While individual variations are seen, in general, diets high in animal fat and protein are associated with an abundance of *Bacteroides*, high-fiber diets with *Prevotella*, while plant-based diets are predominated by both *Bacteroides* and the Firmicutes (David et al., 2014; Wu et al., 2011). Furthermore, the gut microbiome composition is more complex in a host whose diet is primarily plant-based as opposed to animal-based (G. D. Wu, et al., 2011). Also, bacteria that can degrade complex carbohydrates are present in high-fiber diets in higher numbers, while bacteria that primarily break down proteins predominate in animal-based diets. However, the fact must be reiterated that while different studies state the overall change in bacterial phyla, it is important to understand which species show population changes. This is also necessary to know since commensal as well as pathogenic bacteria are present in each phylum. Summaries of the factors that potentially affect the host-gut microbiome relationship are shown in figure 4.

Changing one's diet towards complex carbohydrates such as less processed whole grain foods, fermented vegetables, and prebiotic-containing foods has been shown to induce weight loss, to reduce blood pressure, cholesterol and heart rate, and to decrease toxin-producing bacteria while increasing beneficial bacteria in the gut (Hvistendahl, 2012). Prebiotics are not digested by the host, but metabolized by the gut bacteria, thereby favoring specific changes in the activity and composition of the gut microbiome that benefit host health and wellness (Gibson et al., 2004). Preliminary research suggests that the risk of developing cardiovascular disease, T2D, obesity, and osteoporosis is reduced with the

addition of a prebiotic to the host's diet (Roberfroid, 2000). One of the first prebiotics an infant receives is oligosaccharides present in the mother's milk (Partty et al., 2015). Unlike the sugars found in infant formula, the oligosaccharides present in breast milk are only partially digested in the small intestine and so reach the colon where they provide an energy source for the development of bifidobacteria. A probiotic, on the other hand, is a microbe (bacterial or yeast) that is administered to the host to confer health benefits (Maslowski and Mackay, 2011). They are found in our food (yogurt, fermented vegetables) and have been implicated in alleviating lactose intolerance and boosting immune function. Common probiotics include *Propionibacterium*, lactic acid bacteria (LAB), bifidobacteria, and certain yeasts to name a few. Numerous studies have investigated the effects of probiotics on behavior and intestinal health (Bravo et al., 2011; D'Mello et al., 2015; Ostan et al., 2015; Savignac et al., 2014).

5. Biomarkers of interest

As mentioned before, gut microbiota produce various metabolites, some of which are involved in the host's metabolic processes while others help maintain a healthy gut environment. Although the gut residence times of these metabolites differ, they can be detected in the host's blood, urine, feces, or breath. Thus a useful and non-invasive way of diagnosing bacterial dysbiosis is by profiling biofluids for such compounds using metagenomics technology. For example, using ^{1}H NMR spectroscopy and targeted analysis, Schicho and colleagues were able to identify a number of urine, serum and plasma metabolites found in higher numbers in colitis patients verses healthy controls (Schicho et al., 2012). Another method employed to detect gut bacterial dysbiosis is by using selected ion

flow tube mass spectrometry [SIFT-MS] to measure volatile compounds in the breath, stool or urine of patients. Volatile organic compounds (VOC), such as ethane, methane, pentane, dimethyl sulfide, ammonia, dimethylamine, trimethylamine, are produced in part by bacteria. These can be measured in biofluids like urine, and saliva or breath and stool. Changes in the levels of these compounds could serve as a potential diagnostic tool. For example, elevated levels of pentane and ethane are found in individuals diagnosed with asthma and chronic obstructive pulmonary disorder (Van Berkel et al., 2010).

SCFAs are one of the most important gut microbial products. They affect a range of host processes, including energy utilization, host-microbe signaling, and colonic pH, with consequent effects on gut microbiome composition, gut motility, and epithelial cell proliferation (Musso et al., 2011). Butyrate, a common gut microbiome byproduct, and propionate can inhibit histone deacetylase (HDAC) enzymes and alter the expression of specific genes via conformational changes in the active site of HDAC leading to its inactivation (Aoyama et al., 2010; Dashwood et al., 2006). Microbe-derived butyrate can trigger cell cycle arrest and apoptosis in rapidly dividing colonocytes, and thus has proven effective at preventing colon cancer (Rooks and Garrett, 2011; Shenderov, 2012; Waby et al., 2010). *In vitro* studies have shown that butyrate amplifies the antioxidant properties of glutathione-S-transferase (Ebert et al., 2003). *Fecalibacterium prausnitzii*, *Roseburia intestinalis, Eubacteria hallii, E.coli* and *Butyricicoccus pullicaecorum* are some of the bacteria that produce butyrate in the gut. During ulcerative colitis, the populations of these bacteria decline (Kumari et al., 2013). Although gut microbial dysbiosis in T2D patients is moderate compared to the dramatic dysbiosis reported in obese patients, a study done by Qin et al. revealed that T2D patients exhibit fewer butyrate-producing bacteria and more

opportunistic pathogens. They also reported an enrichment of microbial functions conferring sulphate reduction and increased oxidative stress, which are indicative of pathogenicity (Qin et al., 2012). This promotes the idea that butyrate-producing bacteria protect the host against various diseases. Given that other intestinal diseases show a loss of butyrate-producing bacteria with a commensurate increase in opportunistic pathogens, it is worth considering butyrate as a potential biomarker for intestinal health.

Regarding the gut microbiome's influence on neurotransmitters, a recent study has shown that patients diagnosed with depression have increased volatile fatty acids such as isovaleric acid in their stool (Szczesniak et al., 2015). Isovaleric acid can cross the blood-brain barrier (BBB) and affect neurotransmitter release in the CNS, thus possibly worsening this disorder. This has diagnostic importance since a patient's stool can be screened for increased volatile fatty acids. Factor-S, a sleep promoting substance, accumulates in the brain and fluids of sleep-deprived individuals. It is in fact derived from the bacterial cell wall and thus released by gut bacteria (Collins and Bercik, 2009) and it provides yet another example of how bacterial products can influence brain activity and function. Rats given a strict antibiotic regimen exhibited greatly reduced slow-wave sleep and increased sleep onset latency (Brown et al., 1990).

6. Current model systems

Currently, 16s rRNA gene sequence analysis or shotgun sequencing for identifying bacteria is widely used. By applying these techniques, changes in the gut microbiome composition, from phyla to species level, can be ascertained. To analyze the gut microbial content in T2D patients, Qin et al. developed a novel metagenome-wide association study

(MGWAS) (Qin et al., 2012). Using deep shotgun sequencing of the gut microbiome of 345 Chinese individuals, they identified roughly 60,000 T2D markers, thus allowing them to establish a linkage group for bacterial species-level analysis. Larsen et al. examined fecal content to characterize the composition of the colonic microbiome in adults with T2D using qPCR and tag-encoded amplicon pyrosequencing of the V4 region of the 16s rRNA gene (Larsen et al., 2010). This hyper-variable V4 region is a bacterial gene segment used for distinguishing different bacteria, in this case phyla: Bacteroidetes, Firmicutes, Actinobacteria, Verrucomicrobia, and Proteobacteria. This study involved 36 males of varying BMIs, half with T2D and half serving as non-diabetic controls. Compared to controls, the diabetic group had elevated concentrations of plasma glucose and significantly reduced proportions of the phylum Firmicutes and class Clostridia.

One of the main obstacles in this area is the lack of an animal model system that successfully replicates a healthy or a diseased individual's gut microbiome. Since rodent diets differ substantially from the diet of humans, making comparisons between human and mouse gut microbiota studies inherently problematic (Flint, 2011; Ravussin et al., 2012). While studies have been done using conventional mice as the model organism, in some cases, the alterations seen in the intestinal bacterial population in mice are not validated by human data. For example, bacteria like *Prevotella* and *Ruminococcus* are dominant in the human gut but are under-represented in the mouse gut. Also, due to limited sequencing depth, many smaller microbial populations in both humans and mice may not be detected (Nguyen et al., 2015). However, while species differences exist between humans and rodents, the overall dominant families are more or less represented similarly between the two. Hence studies involving mouse models of different diseases/disorders can be used to understand certain

changes in human gut microbiome structure. However, these findings must be validated with human gut microbiome sequencing studies. An integrative approach, involving detailed epidemiological surveys (e.g., lifestyle, diet, health history), high-throughput sequencing as well as the use of advanced analytical tools, is needed to better understand the gut microbiome and its role in various biological systems in the body. Furthermore, another approach to bridging the translational gap posed by rodent model systems is by making "humanized mice" by adding specific bacterial strains common to the human GIT into germ-free mice (Martin et al., 2008; Turnbaugh et al., 2006; Turnbaugh et al., 2009).

7. Conclusions and Future directions

Understanding the complex transgenomic metabolic interactions within the gut microbiome perhaps poses the ultimate challenge in deciphering and learning how to optimize our gut microbiome to promote health and longevity. Understanding the gut microbiome has the potential to revolutionize the way human and animal diseases are treated. Novel antibiotics, prebiotics, probiotics, and even microbiome transplants could replace expensive surgeries or drug treatments. Actively managing the gut microbiome holds considerable potential in the realm of preventive medicine as well as the treatment of acquired diseases. The most difficult undertaking will be dissecting the complex metabolic, environmental, and genomic interactions between the host and its gut microbiome. Some of the pertinent areas to be studied are as follows:

1) The dynamics and impact of maternal gut microbiome transfer and the influence of infant nutrition on development of the gut microbiome in early childhood.
2) The influence of host genome variations and the fetal environment on the future gut microbiome and the influence of fetal development on the HMMA.

3) The effects of antibiotic use on the gut microbiome *in utero*, during childhood, and in the elderly population.
4) The influence of the gut microbiome on metabolism, pharmacokinetics, and the biotransformation of drugs and toxicants.
5) The effect of drugs and toxicants on gut microbiome population and gut metabolites.
6) The influence of the gut microbiome and the gut-brain axis on repair and remodeling in the CNS as well as on the development and progression of neurodegenerative diseases.
7) Developing a cost-effective technique to map an individual's complete gut microbiome at any point in time to better help physicians create a therapeutic regimen.

Along with advances in metabolomics and metagenomics, a greater understanding of the potential health benefits of our gut microbiome is within reach. Considering the complex and dynamic nature of the microbial population and its effect on the individual, collaboration in the fields of microbiology, neurobiology, biochemistry, immunology, gastroenterology, genetics, epidemiology, pharmacology, and toxicology is warranted to gain a better understanding of this important host-bacteria relationship.

Acknowledgements

The authors acknowledge Gary Zenitsky for his assistance in the preparation of this manuscript. This work was in part supported by National Institutes of Health (NIH) [Grants ES19267, NS 074443, and ES10586]. The W. Eugene and Linda Lloyd Endowed Chair to A.G.K. is also acknowledged.

8. References

Aboud, A. A., Tidball, A. M., Kumar, K. K., Neely, M. D., Han, B., Ess, K. C., Hong, C. C., Erikson, K. M., Hedera, P., & Bowman, A. B. (2014). PARK2 patient neuroprogenitors show increased mitochondrial sensitivity to copper. *Neurobiol Dis, 73C*, 204-212.

Afeseh Ngwa, H., Kanthasamy, A., Anantharam, V., Song, C., Witte, T., Houk, R., & Kanthasamy, A. G. (2009). Vanadium induces dopaminergic neurotoxicity via protein kinase Cdelta dependent oxidative signaling mechanisms: relevance to etiopathogenesis of Parkinson's disease. *Toxicol Appl Pharmacol, 240*, 273-285.

Afeseh Ngwa, H., Kanthasamy, A., Gu, Y., Fang, N., Anantharam, V., & Kanthasamy, A. G. (2011). Manganese nanoparticle activates mitochondrial dependent apoptotic signaling and autophagy in dopaminergic neuronal cells. *Toxicol Appl Pharmacol, 256*, 227-240.

Annalisa, N., Alessio, T., Claudette, T. D., Erald, V., Antonino de, L., & Nicola, D. D. (2014). Gut microbioma population: an indicator really sensible to any change in age, diet, metabolic syndrome, and life-style. *Mediators Inflamm, 2014*, 901308.

Aoyama, M., Kotani, J., & Usami, M. (2010). Butyrate and propionate induced activated or non-activated neutrophil apoptosis via HDAC inhibitor activity but without activating GPR-41/GPR-43 pathways. *Nutrition, 26*, 653-661.

Aschner, J. L., & Aschner, M. (2005). Nutritional aspects of manganese homeostasis. *Mol Aspects Med, 26*, 353-362.

Benson, A. K., Kelly, S. A., Legge, R., Ma, F., Low, S. J., Kim, J., Zhang, M., Oh, P. L., Nehrenberg, D., Hua, K., Kachman, S. D., Moriyama, E. N., Walter, J., Peterson, D.

A., & Pomp, D. (2010). Individuality in gut microbiota composition is a complex polygenic trait shaped by multiple environmental and host genetic factors. *Proc Natl Acad Sci U S A, 107*, 18933-18938.

Bergheim, I., Guo, L., Davis, M. A., Lambert, J. C., Beier, J. I., Duveau, I., Luyendyk, J. P., Roth, R. A., & Arteel, G. E. (2006). Metformin prevents alcohol-induced liver injury in the mouse: Critical role of plasminogen activator inhibitor-1. *Gastroenterology, 130*, 2099-2112.

Biagi, E., Nylund, L., Candela, M., Ostan, R., Bucci, L., Pini, E., Nikkila, J., Monti, D., Satokari, R., Franceschi, C., Brigidi, P., & De Vos, W. (2010). Through ageing, and beyond: gut microbiota and inflammatory status in seniors and centenarians. *PLoS One, 5*, e10667.

Bowman, A. B., Kwakye, G. F., Herrero Hernandez, E., & Aschner, M. (2011). Role of manganese in neurodegenerative diseases. *J Trace Elem Med Biol, 25*, 191-203.

Braak, H., de Vos, R. A., Bohl, J., & Del Tredici, K. (2006). Gastric alpha-synuclein immunoreactive inclusions in Meissner's and Auerbach's plexuses in cases staged for Parkinson's disease-related brain pathology. *Neurosci Lett, 396*, 67-72.

Bravo, J. A., Forsythe, P., Chew, M. V., Escaravage, E., Savignac, H. M., Dinan, T. G., Bienenstock, J., & Cryan, J. F. (2011). Ingestion of Lactobacillus strain regulates emotional behavior and central GABA receptor expression in a mouse via the vagus nerve. *Proc Natl Acad Sci U S A, 108*, 16050-16055.

Brenner, S. R. (2013). Blue-green algae or cyanobacteria in the intestinal micro-flora may produce neurotoxins such as Beta-N-Methylamino-L-Alanine (BMAA) which may be related to development of amyotrophic lateral sclerosis, Alzheimer's disease and

Parkinson-Dementia-Complex in humans and Equine Motor Neuron Disease in horses. *Med Hypotheses, 80*, 103.

Brouillet, E. P., Shinobu, L., McGarvey, U., Hochberg, F., & Beal, M. F. (1993). Manganese injection into the rat striatum produces excitotoxic lesions by impairing energy metabolism. *Exp Neurol, 120*, 89-94.

Brown, R., Price, R. J., King, M. G., & Husband, A. J. (1990). Are antibiotic effects on sleep behavior in the rat due to modulation of gut bacteria? *Physiol Behav, 48*, 561-565.

Collins, S. M., & Bercik, P. (2009). The relationship between intestinal microbiota and the central nervous system in normal gastrointestinal function and disease. *Gastroenterology, 136*, 2003-2014.

D'Mello, C., Ronaghan, N., Zaheer, R., Dicay, M., Le, T., MacNaughton, W. K., Surrette, M. G., & Swain, M. G. (2015). Probiotics Improve Inflammation-Associated Sickness Behavior by Altering Communication between the Peripheral Immune System and the Brain. *J Neurosci, 35*, 10821-10830.

Danielsson, H., & Gustafsson, B. (1959). On serum-cholesterol levels and neutral fecal sterols in germ-free rats; bile acids and steroids 59. *Arch Biochem Biophys, 83*, 482-485.

Dashwood, R. H., Myzak, M. C., & Ho, E. (2006). Dietary HDAC inhibitors: time to rethink weak ligands in cancer chemoprevention? *Carcinogenesis, 27*, 344-349.

David, L. A., Maurice, C. F., Carmody, R. N., Gootenberg, D. B., Button, J. E., Wolfe, B. E., Ling, A. V., Devlin, A. S., Varma, Y., Fischbach, M. A., Biddinger, S. B., Dutton, R. J., & Turnbaugh, P. J. (2014). Diet rapidly and reproducibly alters the human gut microbiome. *Nature, 505*, 559-563.

De Filippo, C., Cavalieri, D., Di Paola, M., Ramazzotti, M., Poullet, J. B., Massart, S., Collini, S., Pieraccini, G., & Lionetti, P. (2010). Impact of diet in shaping gut microbiota revealed by a comparative study in children from Europe and rural Africa. *Proceedings of the National Academy of Sciences of the United States of America, 107*, 14691-14696.

Devos, D., Lebouvier, T., Lardeux, B., Biraud, M., Rouaud, T., Pouclet, H., Coron, E., Bruley des Varannes, S., Naveilhan, P., Nguyen, J. M., Neunlist, M., & Derkinderen, P. (2013). Colonic inflammation in Parkinson's disease. *Neurobiol Dis, 50*, 42-48.

Diaz Heijtz, R., Wang, S., Anuar, F., Qian, Y., Bjorkholm, B., Samuelsson, A., Hibberd, M. L., Forssberg, H., & Pettersson, S. (2011). Normal gut microbiota modulates brain development and behavior. *Proceedings of the National Academy of Sciences of the United States of America, 108*, 3047-3052.

Dogra, S., Sakwinska, O., Soh, S. E., Ngom-Bru, C., Bruck, W. M., Berger, B., Brussow, H., Lee, Y. S., Yap, F., Chong, Y. S., Godfrey, K. M., Holbrook, J. D., & Group, G. S. (2015). Dynamics of infant gut microbiota are influenced by delivery mode and gestational duration and are associated with subsequent adiposity. *MBio, 6*.

Dupont, J. R., Jervis, H. R., & Sprinz, H. (1965). Auerbach's plexus of the rat cecum in relation to the germfree state. *J Comp Neurol, 125*, 11-18.

Ebert, M. N., Klinder, A., Peters, W. H., Schaferhenrich, A., Sendt, W., Scheele, J., & Pool-Zobel, B. L. (2003). Expression of glutathione S-transferases (GSTs) in human colon cells and inducibility of GSTM2 by butyrate. *Carcinogenesis, 24*, 1637-1644.

El-Mir, M. Y., Nogueira, V., Fontaine, E., Averet, N., Rigoulet, M., & Leverve, X. (2000). Dimethylbiguanide inhibits cell respiration via an indirect effect targeted on the respiratory chain complex I. *J Biol Chem, 275*, 223-228.

Erikson, K. M., & Aschner, M. (2003). Manganese neurotoxicity and glutamate-GABA interaction. *Neurochem Int, 43*, 475-480.

Everard, A., Belzer, C., Geurts, L., Ouwerkerk, J. P., Druart, C., Bindels, L. B., Guiot, Y., Derrien, M., Muccioli, G. G., Delzenne, N. M., de Vos, W. M., & Cani, P. D. (2013). Cross-talk between Akkermansia muciniphila and intestinal epithelium controls diet-induced obesity. *Proc Natl Acad Sci U S A, 110*, 9066-9071.

Falk, P. G., Hooper, L. V., Midtvedt, T., & Gordon, J. I. (1998). Creating and maintaining the gastrointestinal ecosystem: what we know and need to know from gnotobiology. *Microbiol Mol Biol Rev, 62*, 1157-1170.

Finegold, S. M. (2008). Therapy and epidemiology of autism--clostridial spores as key elements. *Med Hypotheses, 70*, 508-511.

Finegold, S. M., Dowd, S. E., Gontcharova, V., Liu, C., Henley, K. E., Wolcott, R. D., Youn, E., Summanen, P. H., Granpeesheh, D., Dixon, D., Liu, M., Molitoris, D. R., & Green, J. A., 3rd. (2010). Pyrosequencing study of fecal microflora of autistic and control children. *Anaerobe, 16*, 444-453.

Finegold, S. M., Downes, J., & Summanen, P. H. (2012). Microbiology of regressive autism. *Anaerobe, 18*, 260-262.

Fitsanakis, V. A., Au, C., Erikson, K. M., & Aschner, M. (2006). The effects of manganese on glutamate, dopamine and gamma-aminobutyric acid regulation. *Neurochem Int, 48*, 426-433.

Flint, H. J. (2011). Obesity and the gut microbiota. *J Clin Gastroenterol, 45 Suppl*, S128-132.

Gardiner, K. R., Erwin, P. J., Anderson, N. H., Barr, J. G., Halliday, M. I., & Rowlands, B. J. (1993). Colonic bacteria and bacterial translocation in experimental colitis. *Br J Surg, 80*, 512-516.

Gibson, G. R., Probert, H. M., Loo, J. V., Rastall, R. A., & Roberfroid, M. B. (2004). Dietary modulation of the human colonic microbiota: updating the concept of prebiotics. *Nutr Res Rev, 17*, 259-275.

Gustafsson, B. E. (1959). Vitamin K deficiency in germfree rats. *Ann N Y Acad Sci, 78*, 166-174.

Harischandra, D. S., Jin, H., Anantharam, V., Kanthasamy, A., & Kanthasamy, A. G. (2015). alpha-Synuclein protects against manganese neurotoxic insult during the early stages of exposure in a dopaminergic cell model of Parkinson's disease. *Toxicol Sci, 143*, 454-468.

Harmsen, H. J., Wildeboer-Veloo, A. C., Raangs, G. C., Wagendorp, A. A., Klijn, N., Bindels, J. G., & Welling, G. W. (2000). Analysis of intestinal flora development in breast-fed and formula-fed infants by using molecular identification and detection methods. *J Pediatr Gastroenterol Nutr, 30*, 61-67.

Holmes, E., Wilson, I. D., & Nicholson, J. K. (2008). Metabolic phenotyping in health and disease. *Cell, 134*, 714-717.

Holmqvist, S., Chutna, O., Bousset, L., Aldrin-Kirk, P., Li, W., Bjorklund, T., Wang, Z. Y., Roybon, L., Melki, R., & Li, J. Y. (2014). Direct evidence of Parkinson pathology spread from the gastrointestinal tract to the brain in rats. *Acta Neuropathol, 128*, 805-820.

Hooper, L. V., Midtvedt, T., & Gordon, J. I. (2002). How host-microbial interactions shape the nutrient environment of the mammalian intestine. *Annu Rev Nutr, 22*, 283-307.

Hsiao, E. Y., McBride, S. W., Hsien, S., Sharon, G., Hyde, E. R., McCue, T., Codelli, J. A., Chow, J., Reisman, S. E., Petrosino, J. F., Patterson, P. H., & Mazmanian, S. K. (2013). Microbiota modulate behavioral and physiological abnormalities associated with neurodevelopmental disorders. *Cell, 155*, 1451-1463.

Hu, G., Jousilahti, P., Bidel, S., Antikainen, R., & Tuomilehto, J. (2007). Type 2 diabetes and the risk of Parkinson's disease. *Diabetes Care, 30*, 842-847.

Hvistendahl, M. (2012). My microbiome and me. *Science, 336*, 1248-1250.

Kaneko, M., Hoshino, Y., Hashimoto, S., Okano, T., & Kumashiro, H. (1993). Hypothalamic-pituitary-adrenal axis function in children with attention-deficit hyperactivity disorder. *J Autism Dev Disord, 23*, 59-65.

Kanthasamy, A. G., Choi, C., Jin, H., Harischandra, D. S., Anantharam, V., & Kanthasamy, A. (2012). Effect of divalent metals on the neuronal proteasomal system, prion protein ubiquitination and aggregation. *Toxicol Lett, 214*, 288-295.

Kelly, D., King, T., & Aminov, R. (2007). Importance of microbial colonization of the gut in early life to the development of immunity. *Mutat Res, 622*, 58-69.

King, J. A., Barkley, R. A., & Barrett, S. (1998). Attention-deficit hyperactivity disorder and the stress response. *Biol Psychiatry, 44*, 72-74.

Knowler, W. C., Barrett-Connor, E., Fowler, S. E., Hamman, R. F., Lachin, J. M., Walker, E. A., Nathan, D. M., & Diabetes Prevention Program Research, G. (2002). Reduction in the incidence of type 2 diabetes with lifestyle intervention or metformin. *N Engl J Med, 346*, 393-403.

Knusel, B., Michel, P. P., Schwaber, J. S., & Hefti, F. (1990). Selective and nonselective stimulation of central cholinergic and dopaminergic development in vitro by nerve growth factor, basic fibroblast growth factor, epidermal growth factor, insulin and the insulin-like growth factors I and II. *J Neurosci, 10*, 558-570.

Koenig, J. E., Spor, A., Scalfone, N., Fricker, A. D., Stombaugh, J., Knight, R., Angenent, L. T., & Ley, R. E. (2011). Succession of microbial consortia in the developing infant gut microbiome. *Proceedings of the National Academy of Sciences of the United States of America, 108 Suppl 1*, 4578-4585.

Kumari, R., Ahuja, V., & Paul, J. (2013). Fluctuations in butyrate-producing bacteria in ulcerative colitis patients of North India. *World J Gastroenterol, 19*, 3404-3414.

Lahiri, D. K., & Maloney, B. (2010). The "LEARn" (Latent Early-life Associated Regulation) model integrates environmental risk factors and the developmental basis of Alzheimer's disease, and proposes remedial steps. *Exp Gerontol, 45*, 291-296.

Larsen, N., Vogensen, F. K., van den Berg, F. W., Nielsen, D. S., Andreasen, A. S., Pedersen, B. K., Al-Soud, W. A., Sorensen, S. J., Hansen, L. H., & Jakobsen, M. (2010). Gut microbiota in human adults with type 2 diabetes differs from non-diabetic adults. *PLoS ONE, 5*, e9085.

Lepage, P., Hasler, R., Spehlmann, M. E., Rehman, A., Zvirbliene, A., Begun, A., Ott, S., Kupcinskas, L., Dore, J., Raedler, A., & Schreiber, S. (2011). Twin study indicates loss of interaction between microbiota and mucosa of patients with ulcerative colitis. *Gastroenterology, 141*, 227-236.

Levine, R. L., Mosoni, L., Berlett, B. S., & Stadtman, E. R. (1996). Methionine residues as endogenous antioxidants in proteins. *Proceedings of the National Academy of Sciences of the United States of America, 93*, 15036-15040.

Littman, D. R., & Pamer, E. G. (2011). Role of the commensal microbiota in normal and pathogenic host immune responses. *Cell Host Microbe, 10*, 311-323.

Martin, F. P., Wang, Y., Sprenger, N., Yap, I. K., Lundstedt, T., Lek, P., Rezzi, S., Ramadan, Z., van Bladeren, P., Fay, L. B., Kochhar, S., Lindon, J. C., Holmes, E., & Nicholson, J. K. (2008). Probiotic modulation of symbiotic gut microbial-host metabolic interactions in a humanized microbiome mouse model. *Mol Syst Biol, 4*, 157.

Maslowski, K. M., & Mackay, C. R. (2011). Diet, gut microbiota and immune responses. *Nat Immunol, 12*, 5-9.

Mazmanian, S. K., Liu, C. H., Tzianabos, A. O., & Kasper, D. L. (2005). An immunomodulatory molecule of symbiotic bacteria directs maturation of the host immune system. *Cell, 122*, 107-118.

Mezzelani, A., Landini, M., Facchiano, F., Raggi, M. E., Villa, L., Molteni, M., De Santis, B., Brera, C., Caroli, A. M., Milanesi, L., & Marabotti, A. (2014). Environment, dysbiosis, immunity and sex-specific susceptibility: A translational hypothesis for regressive autism pathogenesis. *Nutr Neurosci*.

Milatovic, D., Zaja-Milatovic, S., Gupta, R. C., Yu, Y., & Aschner, M. (2009). Oxidative damage and neurodegeneration in manganese-induced neurotoxicity. *Toxicol Appl Pharmacol, 240*, 219-225.

Ming, X., Stein, T. P., Barnes, V., Rhodes, N., & Guo, L. (2012). Metabolic perturbance in autism spectrum disorders: a metabolomics study. *J Proteome Res, 11*, 5856-5862.

Mootha, V. K., Lindgren, C. M., Eriksson, K. F., Subramanian, A., Sihag, S., Lehar, J., Puigserver, P., Carlsson, E., Ridderstrale, M., Laurila, E., Houstis, N., Daly, M. J., Patterson, N., Mesirov, J. P., Golub, T. R., Tamayo, P., Spiegelman, B., Lander, E. S., Hirschhorn, J. N., Altshuler, D., & Groop, L. C. (2003). PGC-1alpha-responsive genes involved in oxidative phosphorylation are coordinately downregulated in human diabetes. *Nat Genet, 34*, 267-273.

Morelli, L. (2008). Postnatal development of intestinal microflora as influenced by infant nutrition. *J Nutr, 138*, 1791S-1795S.

Morgan, X. C., Tickle, T. L., Sokol, H., Gevers, D., Devaney, K. L., Ward, D. V., Reyes, J. A., Shah, S. A., LeLeiko, N., Snapper, S. B., Bousvaros, A., Korzenik, J., Sands, B. E., Xavier, R. J., & Huttenhower, C. (2012). Dysfunction of the intestinal microbiome in inflammatory bowel disease and treatment. *Genome Biol, 13*, R79.

Musso, G., Gambino, R., & Cassader, M. (2011). Interactions between gut microbiota and host metabolism predisposing to obesity and diabetes. *Annu Rev Med, 62*, 361-380.

Nguyen, T. L., Vieira-Silva, S., Liston, A., & Raes, J. (2015). How informative is the mouse for human gut microbiota research? *Dis Model Mech, 8*, 1-16.

Ostan, R., Bene, M. C., Spazzafumo, L., Pinto, A., Donini, L. M., Pryen, F., Charrouf, Z., Valentini, L., Lochs, H., Bourdel-Marchasson, I., Blanc-Bisson, C., Buccolini, F., Brigidi, P., Franceschi, C., & d'Alessio, P. A. (2015). Impact of diet and nutraceutical supplementation on inflammation in elderly people. Results from the RISTOMED study, an open-label randomized control trial. *Clin Nutr*.

Owen, M. R., Doran, E., & Halestrap, A. P. (2000). Evidence that metformin exerts its anti-diabetic effects through inhibition of complex 1 of the mitochondrial respiratory chain. *Biochem J, 348 Pt 3*, 607-614.

Parnell, J. A., & Reimer, R. A. (2012). Prebiotic fibres dose-dependently increase satiety hormones and alter *Bacteroidetes* and *Firmicutes* in lean and obese JCR:LA-cp rats. *Br J Nutr, 107*, 601-613.

Parracho, H. M., Bingham, M. O., Gibson, G. R., & McCartney, A. L. (2005). Differences between the gut microflora of children with autistic spectrum disorders and that of healthy children. *J Med Microbiol, 54*, 987-991.

Partty, A., Kalliomaki, M., Wacklin, P., Salminen, S., & Isolauri, E. (2015). A possible link between early probiotic intervention and the risk of neuropsychiatric disorders later in childhood: a randomized trial. *Pediatr Res, 77*, 823-828.

Penders, J., Thijs, C., Vink, C., Stelma, F. F., Snijders, B., Kummeling, I., van den Brandt, P. A., & Stobberingh, E. E. (2006). Factors influencing the composition of the intestinal microbiota in early infancy. *Pediatrics, 118*, 511-521.

Puigserver, P., & Spiegelman, B. M. (2003). Peroxisome proliferator-activated receptor-gamma coactivator 1 alpha (PGC-1 alpha): transcriptional coactivator and metabolic regulator. *Endocr Rev, 24*, 78-90.

Qin, J., Li, R., Raes, J., Arumugam, M., Burgdorf, K. S., Manichanh, C., Nielsen, T., Pons, N., Levenez, F., Yamada, T., Mende, D. R., Li, J., Xu, J., Li, S., Li, D., Cao, J., Wang, B., Liang, H., Zheng, H., Xie, Y., Tap, J., Lepage, P., Bertalan, M., Batto, J. M., Hansen, T., Le Paslier, D., Linneberg, A., Nielsen, H. B., Pelletier, E., Renault, P., Sicheritz-Ponten, T., Turner, K., Zhu, H., Yu, C., Li, S., Jian, M., Zhou, Y., Li, Y.,

Zhang, X., Li, S., Qin, N., Yang, H., Wang, J., Brunak, S., Dore, J., Guarner, F., Kristiansen, K., Pedersen, O., Parkhill, J., Weissenbach, J., Meta, H. I. T. C., Bork, P., Ehrlich, S. D., & Wang, J. (2010). A human gut microbial gene catalogue established by metagenomic sequencing. *Nature, 464*, 59-65.

Qin, J., Li, Y., Cai, Z., Li, S., Zhu, J., Zhang, F., Liang, S., Zhang, W., Guan, Y., Shen, D., Peng, Y., Zhang, D., Jie, Z., Wu, W., Qin, Y., Xue, W., Li, J., Han, L., Lu, D., Wu, P., Dai, Y., Sun, X., Li, Z., Tang, A., Zhong, S., Li, X., Chen, W., Xu, R., Wang, M., Feng, Q., Gong, M., Yu, J., Zhang, Y., Zhang, M., Hansen, T., Sanchez, G., Raes, J., Falony, G., Okuda, S., Almeida, M., LeChatelier, E., Renault, P., Pons, N., Batto, J. M., Zhang, Z., Chen, H., Yang, R., Zheng, W., Li, S., Yang, H., Wang, J., Ehrlich, S. D., Nielsen, R., Pedersen, O., Kristiansen, K., & Wang, J. (2012). A metagenome-wide association study of gut microbiota in type 2 diabetes. *Nature, 490*, 55-60.

Ravussin, Y., Koren, O., Spor, A., LeDuc, C., Gutman, R., Stombaugh, J., Knight, R., Ley, R. E., & Leibel, R. L. (2012). Responses of gut microbiota to diet composition and weight loss in lean and obese mice. *Obesity (Silver Spring), 20*, 738-747.

Resta, S. C. (2009). Effects of probiotics and commensals on intestinal epithelial physiology: implications for nutrient handling. *J Physiol, 587*, 4169-4174.

Roberfroid, M. B. (2000). Prebiotics and probiotics: are they functional foods? *Am J Clin Nutr, 71*, 1682S-1687S; discussion 1688S-1690S.

Roediger, W. E. (1980). Role of anaerobic bacteria in the metabolic welfare of the colonic mucosa in man. *Gut, 21*, 793-798.

Rooks, M. G., & Garrett, W. S. (2011). Bacteria, food, and cancer. *F1000 Biol Rep, 3*, 12.

Roth, J. A., Li, Z., Sridhar, S., & Khoshbouei, H. (2013). The effect of manganese on dopamine toxicity and dopamine transporter (DAT) in control and DAT transfected HEK cells. *Neurotoxicology, 35*, 121-128.

Sandler, R. H., Finegold, S. M., Bolte, E. R., Buchanan, C. P., Maxwell, A. P., Vaisanen, M. L., Nelson, M. N., & Wexler, H. M. (2000). Short-term benefit from oral vancomycin treatment of regressive-onset autism. *J Child Neurol, 15*, 429-435.

Santacruz, A., Collado, M. C., Garcia-Valdes, L., Segura, M. T., Martin-Lagos, J. A., Anjos, T., Marti-Romero, M., Lopez, R. M., Florido, J., Campoy, C., & Sanz, Y. (2010). Gut microbiota composition is associated with body weight, weight gain and biochemical parameters in pregnant women. *Br J Nutr, 104*, 83-92.

Savignac, H. M., Kiely, B., Dinan, T. G., & Cryan, J. F. (2014). Bifidobacteria exert strain-specific effects on stress-related behavior and physiology in BALB/c mice. *Neurogastroenterol Motil, 26*, 1615-1627.

Scheperjans, F., Aho, V., Pereira, P. A., Koskinen, K., Paulin, L., Pekkonen, E., Haapaniemi, E., Kaakkola, S., Eerola-Rautio, J., Pohja, M., Kinnunen, E., Murros, K., & Auvinen, P. (2015). Gut microbiota are related to Parkinson's disease and clinical phenotype. *Mov Disord, 30*, 350-358.

Scher, J. U., Ubeda, C., Artacho, A., Attur, M., Isaac, S., Reddy, S. M., Marmon, S., Neimann, A., Brusca, S., Patel, T., Manasson, J., Pamer, E. G., Littman, D. R., & Abramson, S. B. (2015). Decreased bacterial diversity characterizes the altered gut microbiota in patients with psoriatic arthritis, resembling dysbiosis in inflammatory bowel disease. *Arthritis Rheumatol, 67*, 128-139.

Schernhammer, E., Hansen, J., Rugbjerg, K., Wermuth, L., & Ritz, B. (2011). Diabetes and the risk of developing Parkinson's disease in Denmark. *Diabetes Care, 34*, 1102-1108.

Schicho, R., Shaykhutdinov, R., Ngo, J., Nazyrova, A., Schneider, C., Panaccione, R., Kaplan, G. G., Vogel, H. J., & Storr, M. (2012). Quantitative metabolomic profiling of serum, plasma, and urine by (1)H NMR spectroscopy discriminates between patients with inflammatory bowel disease and healthy individuals. *J Proteome Res, 11*, 3344-3357.

Schmidt, M. V., Oitzl, M. S., Levine, S., & de Kloet, E. R. (2002). The HPA system during the postnatal development of CD1 mice and the effects of maternal deprivation. *Brain Res Dev Brain Res, 139*, 39-49.

Serres, S., Anthony, D. C., Jiang, Y., Broom, K. A., Campbell, S. J., Tyler, D. J., van Kasteren, S. I., Davis, B. G., & Sibson, N. R. (2009). Systemic inflammatory response reactivates immune-mediated lesions in rat brain. *J Neurosci, 29*, 4820-4828.

Shenderov, B. A. (2012). Gut indigenous microbiota and epigenetics. *Microb Ecol Health Dis, 23*.

Shin, J. H., Ko, H. S., Kang, H., Lee, Y., Lee, Y. I., Pletinkova, O., Troconso, J. C., Dawson, V. L., & Dawson, T. M. (2011). PARIS (ZNF746) repression of PGC-1alpha contributes to neurodegeneration in Parkinson's disease. *Cell, 144*, 689-702.

Shin, N. R., Lee, J. C., Lee, H. Y., Kim, M. S., Whon, T. W., Lee, M. S., & Bae, J. W. (2014). An increase in the Akkermansia spp. population induced by metformin

treatment improves glucose homeostasis in diet-induced obese mice. *Gut, 63*, 727-735.

Sokol, H., Lepage, P., Seksik, P., Dore, J., & Marteau, P. (2007). Molecular comparison of dominant microbiota associated with injured versus healthy mucosa in ulcerative colitis. *Gut, 56*, 152-154.

Sokol, H., Seksik, P., Furet, J. P., Firmesse, O., Nion-Larmurier, I., Beaugerie, L., Cosnes, J., Corthier, G., Marteau, P., & Dore, J. (2009). Low counts of Faecalibacterium prausnitzii in colitis microbiota. *Inflamm Bowel Dis, 15*, 1183-1189.

Song, Y., Liu, C., & Finegold, S. M. (2004). Real-time PCR quantitation of clostridia in feces of autistic children. *Appl Environ Microbiol, 70*, 6459-6465.

Sudo, N., Chida, Y., Aiba, Y., Sonoda, J., Oyama, N., Yu, X. N., Kubo, C., & Koga, Y. (2004). Postnatal microbial colonization programs the hypothalamic-pituitary-adrenal system for stress response in mice. *J Physiol, 558*, 263-275.

Sumi, Y., Miyakawa, M., Kanzaki, M., & Kotake, Y. (1977). Vitamin B-6 deficiency in germfree rats. *J Nutr, 107*, 1707-1714.

Sun, Y., Chang, Y. H., Chen, H. F., Su, Y. H., Su, H. F., & Li, C. Y. (2012). Risk of Parkinson disease onset in patients with diabetes: a 9-year population-based cohort study with age and sex stratifications. *Diabetes Care, 35*, 1047-1049.

Szczesniak, O., Hestad, K., Hanssen, J. F., & Rudi, K. (2015). Isovaleric acid in stool correlates with human depression. *Nutr Neurosci*.

Szeri, I., Anderlik, P., Banos, Z., & Radnai, B. (1976). Decreased cellular immune response of germ-free mice. *Acta Microbiol Acad Sci Hung, 23*, 231-234.

Tilvis, R. S., Kahonen-Vare, M. H., Jolkkonen, J., Valvanne, J., Pitkala, K. H., & Strandberg, T. E. (2004). Predictors of cognitive decline and mortality of aged people over a 10-year period. *J Gerontol A Biol Sci Med Sci, 59*, 268-274.

Tsai, F., & Coyle, W. J. (2009). The microbiome and obesity: is obesity linked to our gut flora? *Curr Gastroenterol Rep, 11*, 307-313.

Turnbaugh, P. J., Ley, R. E., Mahowald, M. A., Magrini, V., Mardis, E. R., & Gordon, J. I. (2006). An obesity-associated gut microbiome with increased capacity for energy harvest. *Nature, 444*, 1027-1031.

Turnbaugh, P. J., Ridaura, V. K., Faith, J. J., Rey, F. E., Knight, R., & Gordon, J. I. (2009). The effect of diet on the human gut microbiome: a metagenomic analysis in humanized gnotobiotic mice. *Sci Transl Med, 1*, 6ra14.

Van Berkel, J. J., Dallinga, J. W., Moller, G. M., Godschalk, R. W., Moonen, E. J., Wouters, E. F., & Van Schooten, F. J. (2010). A profile of volatile organic compounds in breath discriminates COPD patients from controls. *Respir Med, 104*, 557-563.

Vasina, V., Barbara, G., Talamonti, L., Stanghellini, V., Corinaldesi, R., Tonini, M., De Ponti, F., & De Giorgio, R. (2006). Enteric neuroplasticity evoked by inflammation. *Auton Neurosci, 126-127*, 264-272.

Vieira, A. T., Macia, L., Galvao, I., Martins, F. S., Canesso, M. C., Amaral, F. A., Garcia, C. C., Maslowski, K. M., De Leon, E., Shim, D., Nicoli, J. R., Harper, J. L., Teixeira, M. M., & Mackay, C. R. (2015). A Role for Gut Microbiota and the Metabolite-Sensing Receptor GPR43 in a Murine Model of Gout. *Arthritis Rheumatol, 67*, 1646-1656.

Villaran, R. F., Espinosa-Oliva, A. M., Sarmiento, M., De Pablos, R. M., Arguelles, S., Delgado-Cortes, M. J., Sobrino, V., Van Rooijen, N., Venero, J. L., Herrera, A. J.,

Cano, J., & Machado, A. (2010). Ulcerative colitis exacerbates lipopolysaccharide-induced damage to the nigral dopaminergic system: potential risk factor in Parkinson`s disease. *J Neurochem, 114*, 1687-1700.

Waby, J. S., Chirakkal, H., Yu, C., Griffiths, G. J., Benson, R. S., Bingle, C. D., & Corfe, B. M. (2010). Sp1 acetylation is associated with loss of DNA binding at promoters associated with cell cycle arrest and cell death in a colon cell line. *Mol Cancer, 9*, 275.

Wahlqvist, M. L., Lee, M. S., Hsu, C. C., Chuang, S. Y., Lee, J. T., & Tsai, H. N. (2012). Metformin-inclusive sulfonylurea therapy reduces the risk of Parkinson's disease occurring with Type 2 diabetes in a Taiwanese population cohort. *Parkinsonism Relat Disord, 18*, 753-758.

Walker, A. W., & Lawley, T. D. (2013). Therapeutic modulation of intestinal dysbiosis. *Pharmacol Res, 69*, 75-86.

Wong, J. M., de Souza, R., Kendall, C. W., Emam, A., & Jenkins, D. J. (2006). Colonic health: fermentation and short chain fatty acids. *J Clin Gastroenterol, 40*, 235-243.

Wostmann, B. S. (1981). The germfree animal in nutritional studies. *Annu Rev Nutr, 1*, 257-279.

Wostmann, B. S., Wiech, N. L., & Kung, E. (1966). Catabolism and elimination of cholesterol in germfree rats. *J Lipid Res, 7*, 77-82.

Wu, G. D., Chen, J., Hoffmann, C., Bittinger, K., Chen, Y. Y., Keilbaugh, S. A., Bewtra, M., Knights, D., Walters, W. A., Knight, R., Sinha, R., Gilroy, E., Gupta, K., Baldassano, R., Nessel, L., Li, H., Bushman, F. D., & Lewis, J. D. (2011). Linking long-term dietary patterns with gut microbial enterotypes. *Science, 334*, 105-108.

Wu, Z., Puigserver, P., Andersson, U., Zhang, C., Adelmant, G., Mootha, V., Troy, A., Cinti, S., Lowell, B., Scarpulla, R. C., & Spiegelman, B. M. (1999). Mechanisms controlling mitochondrial biogenesis and respiration through the thermogenic coactivator PGC-1. *Cell, 98*, 115-124.

Yamashita, T., Kasahara, K., Emoto, T., Matsumoto, T., Mizoguchi, T., Kitano, N., Sasaki, N., & Hirata, K. (2015). Intestinal Immunity and Gut Microbiota as Therapeutic Targets for Preventing Atherosclerotic Cardiovascular Diseases. *Circ J, 79*, 1882-1890.

Yatsunenko, T., Rey, F. E., Manary, M. J., Trehan, I., Dominguez-Bello, M. G., Contreras, M., Magris, M., Hidalgo, G., Baldassano, R. N., Anokhin, A. P., Heath, A. C., Warner, B., Reeder, J., Kuczynski, J., Caporaso, J. G., Lozupone, C. A., Lauber, C., Clemente, J. C., Knights, D., Knight, R., & Gordon, J. I. (2012). Human gut microbiome viewed across age and geography. *Nature, 486*, 222-227.

Zhang, Y., & Zhang, H. (2013). Microbiota associated with type 2 diabetes and its related complications. *Food Science and Human Wellness, 2*, 167-172.

Zheng, B., Liao, Z., Locascio, J. J., Lesniak, K. A., Roderick, S. S., Watt, M. L., Eklund, A. C., Zhang-James, Y., Kim, P. D., Hauser, M. A., Grunblatt, E., Moran, L. B., Mandel, S. A., Riederer, P., Miller, R. M., Federoff, H. J., Wullner, U., Papapetropoulos, S., Youdim, M. B., Cantuti-Castelvetri, I., Young, A. B., Vance, J. M., Davis, R. L., Hedreen, J. C., Adler, C. H., Beach, T. G., Graeber, M. B., Middleton, F. A., Rochet, J. C., Scherzer, C. R., & Global, P. D. G. E. C. (2010). PGC-1alpha, a potential therapeutic target for early intervention in Parkinson's disease. *Sci Transl Med, 2*, 52ra73.

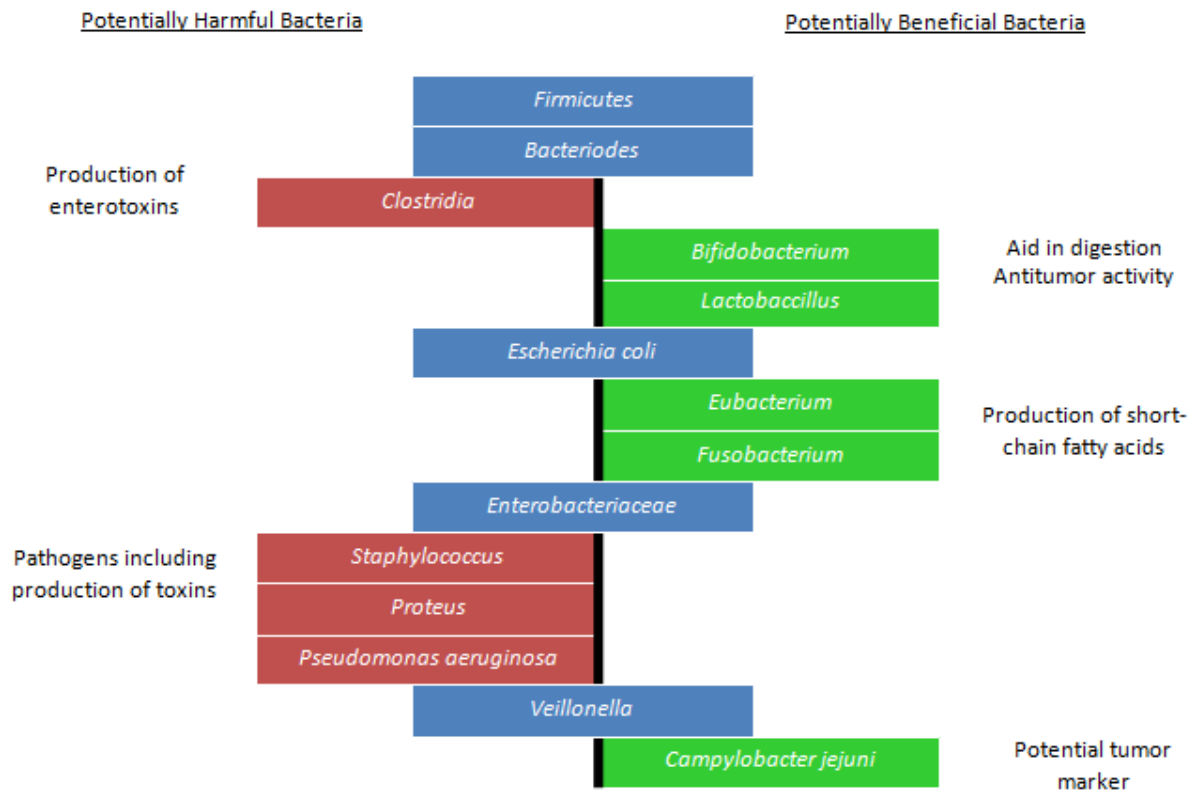

Figure 1: Schematic representation of potentially harmful and potentially beneficial bacteria present in the gut microbiome. Pro-biotic bacteria such as *Lactobacillus* and Bifidobacteria modulate the gut environment by releasing bioactive compounds that enhance enteric epithelial barrier function as well as by competitively binding to the epithelium thus outcompeting pathogenic bacteria. *Eubacterium rectale* and *Fusobacterium* produce fatty acids such as acetic acid, propionate and butyrate that are important as an energy source for intestinal epithelial cells as well as for modulating mucosal immune responses. In contrast, higher counts of bacteria such as *Staphylococcus* and *Pseudomonas* are seen in various metabolic disorders such as diabetes and obesity. *Clostridum tetani* spores are resistant to the acidic environment of the stomach and to regular antibiotic treatments. Production of the tetanus toxin by these bacteria is thought to contribute to the "leaky gut syndrome" prevalent in autistic children. *E.coli* is a common commensal of the gut microbiome. However, certain serotypes are pathogenic and are known to cause gastroenteritis and urinary tract infections.

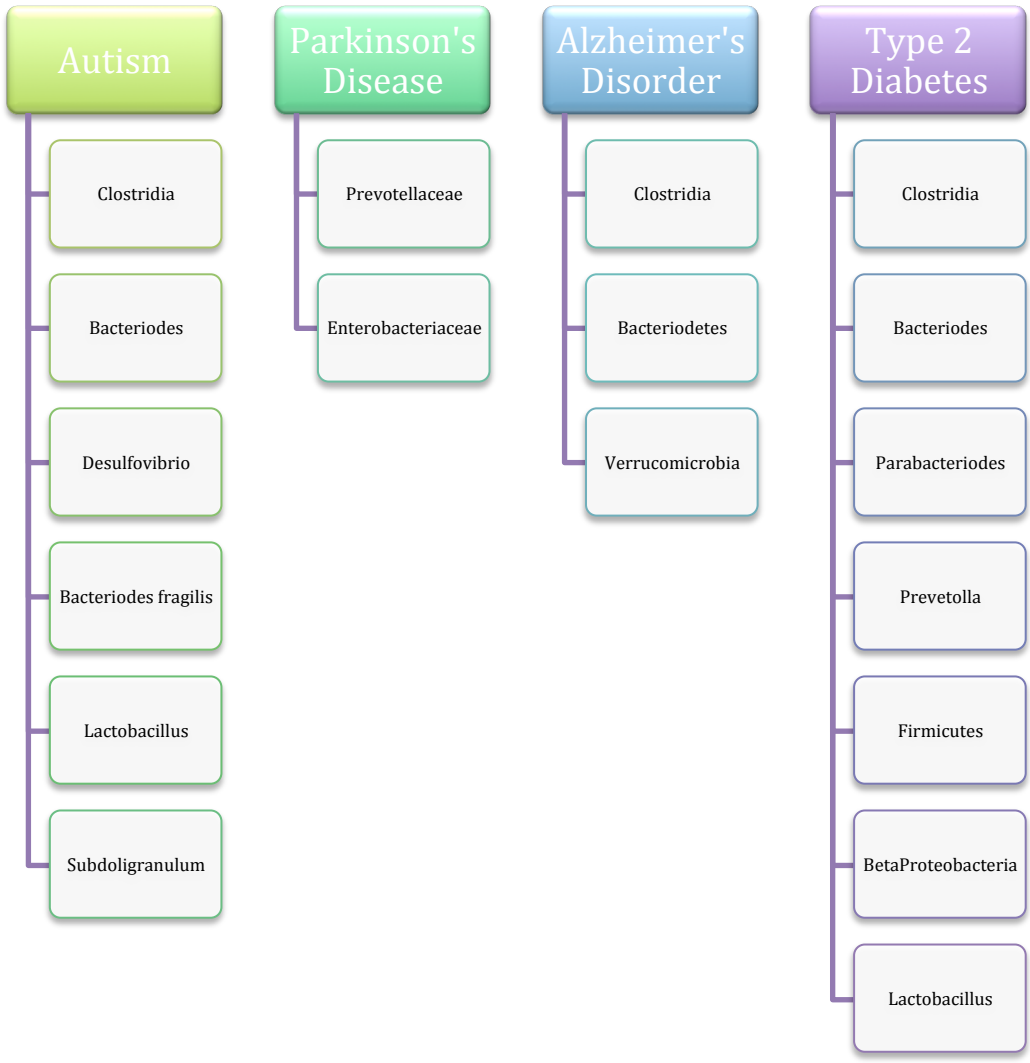

Figure 2: Bacterial species relevant to research on Autism, Parkinson's disease, Alzheimer's disorder, and Type-2 Diabetes. *Clostridia* are prevalent in many diseases and notably, presence of *C. tetani* in the gut microbiome of autistic children may contribute the "leaky gut" syndrome seen in these children. Lower counts of probiotic bacteria like *Lactobacillus* are also seen in many disorders. Understanding the differences in bacterial species seen in healthy and diseased states is crucial to understanding their importance to host health.

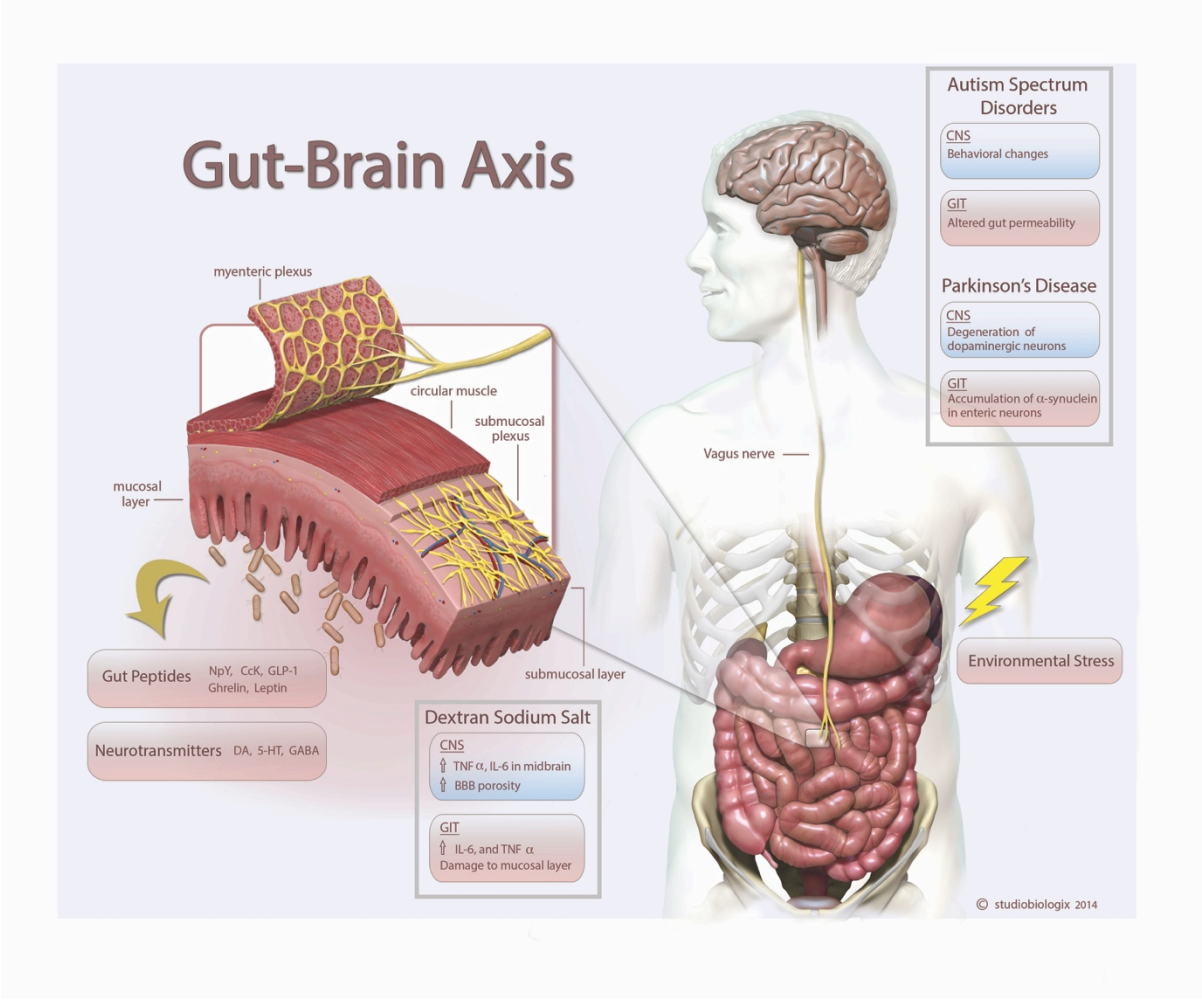

Figure 3: The Gut-Brain axis: Bidirectional signaling between the gastrointestinal tract (GIT) and central nervous system (CNS) occurs through spinal afferents and the vagus nerve. This mode of communication is thought to occur through peptides such as Neuropeptide Y (NpY), Cholecystokinin (CcK), ghrelin, leptin as well as by neurotransmitters like dopamine (DA), serotonin (5-HT), GABA, acetylcholine (Ach) and glutamate. Human and animal studies of various diseases demonstrate that these two systems are not exclusive of one another but do in fact show some parallels in terms of expression of pro-inflammatory cytokines and altered physiological functions.

Table 1: The fecal metabolic profile was altered by manganese treatment from day 10 until the completion of the study. The table above shows some key compounds that were different between treatment and control groups. Notably, decreased vitamin E and increased production of cholic acid were seen in manganese-exposed mice compared to healthy age-matched controls.

Compound	Manganese-treated mice	Physiological relevance
α-tocopherol	Decreased levels	Antioxidant, requires proper nerve conduction
Cholesterol	Decreased levels	Structural component of cell membranes and an important pre-cursor for production of steroids, bile acids, etc.
Cholestane	Decreased levels	Reduces number of synaptic vesicles, helps regulate neurotransmitter release
Palmitic acid	Higher levels	Induces anxiety-like behavior in mice. Can be a mild antioxidant.
Cholic acid	Higher levels	Downregulates bile acid synthesis increasing the tendency to develop gall stones.

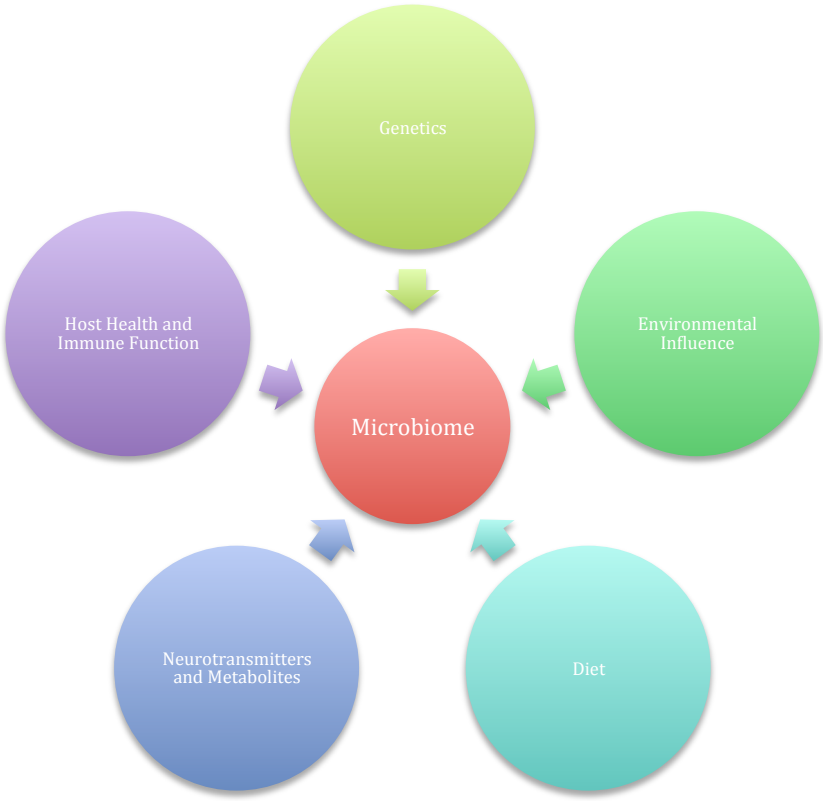

Figure 4: Factors affecting gut microbiota composition: The host-microbiota interaction is a complex and dynamic symbiosis. While diet and environment are well known factors affecting the populations of different phyla in the gut, some reports suggest that the host's genetic composition might pre-dispose the continued growth of certain microbiota

CHAPTER II

CHRONIC EXPOSURE TO MANGANESE CAUSES MITOCHONDRIAL DYSFUNCTION N THE ENTERIC NERVOUS SYSTEM LEADING TO ALTERED GASTROINTESTINAL PHYSIOLOGY

Manuscript to be submitted to Environment Health & Perspectives

Shivani Ghaisas[*], Dilshan S. Harischandra[*], Alexandra Proctor [†], Huajun Jin[*], Souvarish Sarkar[*], Monica Langley[*], Vellareddy Anantharam[*], Arthi Kanthasamy[*], Gregory J. Phillips[†], Anumantha Kanthasamy[*‡].

[*] Department of Biomedical Sciences, Iowa Center for Advanced Neurotoxicology, Iowa State University, Ames, Iowa 50011

[†] Department of Veterinary Microbiology & Preventive Medicine, College of Veterinary Medicine, Iowa State University, Ames, Iowa, 50011, United States of America.

[‡]Corresponding author:

Dr. Anumantha G. Kanthasamy, Distinguished Professor and Lloyd Chair,

Parkinson's Disorder Research Laboratory,

Iowa Center for Advanced Neurotoxicology,

Department of Biomedical Sciences,

2062 Veterinary Medicine Building,

Iowa State University,

Ames, IA 50011, U.S.A.

Phone: 1-515-294-2516;

Email: akanthas@iastate.edu

Abstract:

Occupational exposure to high level of manganese (Mn) causes debilitating damage to the central nervous system. However, its potential toxic effects on the enteric nervous system (ENS) have yet to be assessed. We therefore examined the effect of Mn on the ENS using both *in vitro* and *in vivo* approaches. After exposing a rat enteric glial cell line to Mn, we observed a dose-dependent mitochondrial toxicity as measured by decreased mitochondrial mass and activity as well as increased circular morphology indicating stressed and dying mitochondria. Interestingly, while small doses of Mn induced mitochondrial stress after 24 hours, only doses of 300 μM and above induced cell death. In a mouse primary enteric mixed culture model, Mn increased TNFα and iNOS causing concomitant enteric neuronal cell death as revealed by qRT-PCR and Western blot analysis, respectively. Using a mouse model of Mn toxicity, a non-toxic dose of Mn (15 mg/kg/day) given daily to mice for 30 days increased intestinal transit time compared to littermate controls. These mice also exhibited decreased mucopolysaccharide production in the colon as seen by Alcian Blue-Periodic Acid Schiff staining. Furthermore, increased production of TNFα and iNOS mRNA indicate augmented inflammation and consequently oxidative stress in the colon of these Mn-treated mice. Together, these results show Mn-induced mitochondrial dysfunction and subsequent inflammation in the ENS leading to altered gut physiology.

Keywords: Manganese, environmental toxicant, enteric glia, enteric nervous system, peristalsis, gastrointestinal physiology

Introduction:

Manganese (Mn) is an essential trace metal for many enzymatic reactions, taking part in protein, carbohydrate and lipid synthesis. It also plays a key role in bone formation, fat and carbohydrate metabolism, blood sugar regulation, and calcium absorption in the body (Bowman et al., 2011). Despite its nutritional benefits, chronic exposure to high levels of Mn affects functioning in the central nervous system (CNS), demonstrating the role of Mn as both an essential nutrient and a toxicant (Claus Henn et al., 2010; Zota et al., 2009). Chronic exposure to Mn via welding fumes, pesticides such as Maneb, or well water with high Mn content can lead to manganism, a neurological disorder sharing certain features with Parkinson's disease (PD) (Ferraz et al., 1988; Keen et al., 1999; Kondakis et al., 1989). Patients suffering from manganism report mild resting tremors, an inclination to fall backwards as well as facial and planar dystonia along with hallucinations and psychoses commonly referred to as "manganese madness" (Calne et al., 1994; Huang, 2007). Divalent and trivalent forms of Mn are widely used in industrial and agricultural products and high Mn exposure in early life is associated with poor cognitive performance, especially in the verbal domain of children (Menezes-Filho et al., 2011).

In the brain, Mn primarily accumulates in the globus pallidus. Upon Mn accretion in this region, mitochondrial impairment and loss of cellular functions can follow, resulting in neuroinflammation, neurotransmitter dysregulation and synaptic loss (Kraft and Harry, 2011). One of the early signs of neurological imbalance from chronic Mn exposure is

anosmia (Bowler et al., 2007). Curiously, loss of sense of smell, mood swings and sleep disturbances have been reported not only in patients suffering from manganism but also from PD, multiple system atrophy and dementia with Lewy bodies (Gagnon et al., 2006). These non-motor symptoms are thought to be early signs of neurological impairments in the CNS.

Another important non-motor symptom seen in many neurodegenerative disorders is altered gastrointestinal (GI) motility. Most PD patients have a history of GI problems – ranging from constipation to diarrhea and defecation dysfunction, many years before the disease is even detected (Pfeiffer, 2003). While the incidences reported are less, chronic Mn toxicity is also known to cause gastritis and peptic ulcers in both patients and experimental animals (Chandra and Imam, 1973; Huang and Lin, 2004). With an increased focus on the gut-brain axis, several theories regarding the development and progression of neurodegenerative diseases have focused on whether these neurological disorders begin in the enteric nervous system (ENS) (Pellegrini et al., 2015). If this is indeed the case, then changes in GI physiology are likely to occur before any CNS-controlled symptoms occur.

The ENS comprises of enteric neurons and glial cells present in two distinct layers in the GI tract and plays an important role governing nutrient absorption, peristalsis and maintaining bi-directional communication with peripheral immune cells and the CNS. Particularly, enteric glial cells (EGCs) are present not only in close contact with enteric neurons but are also present in the muscle layers and lamina propria (Gulbransen and Sharkey, 2012). EGCs play an important role in maintaining intestinal barrier and communicate with surveilling immune cells, smooth muscles cells as well as the epithelia lining the gut (Veiga-Fernandes and Pachnis, 2017; von Boyen and Steinkamp, 2010). The presence of EGCs in the lamina

propria indeed throughout the GI tract, leads to the assumption that these cells might play an important role not only in pathogen surveillance but also in sensing potential ingested toxins such as pesticides, heavy metals etc.

With much research devoted to understanding the mechanisms behind Mn toxicity in the brain, scant attention has been paid to its toxic effects in the gut. To our knowledge, no published data exist exploring Mn's potential toxic role in the ENS. Hence using both *in vitro* and *in vivo* models, we investigated the potential toxic effects of chronic Mn exposure in the ENS. Our results from these studies reveal that chronic Mn exposure affects the enteric neuronal and, in particular, the enteric glial functions and promotes an inflammatory response negatively affecting gastrointestinal transit. More importantly, with Mn found at higher than acceptable levels in a number of wells and underground water across USA (Ayotte et al., 2011), the effect of chronic exposure to this environmental neurotoxin on human health is of particular import.

Materials and methods

Chemicals and reagents

Manganese (II) chloride tetrahydrate ($MnCl_2$) and β-actin antibody were purchased from Sigma. Neurobasal medium and Dulbecco's modified Eagle's media (DMEM), B27 and N2 supplements, fetal bovine serum (FBS), Trypsin-EDTA (TE), L-glutamine, penicillin, and streptomycin were purchased from Invitrogen. Antibodies for PGP9.5 (Cat # AB1761-I) and GFAP (Cat # MAB3402) were purchased from Millipore while iNOS (Cat # sc-651) and Bax (Cat # sc-493) antibodies were purchased from Santa Cruz. Mouse recombinant GDNF (Cat # 450-44) and interferon-γ (Cat # 315-05) were purchased from Peprotech.

Cell cultures

The rat enteric glial cell line (Cat # CRL-2690) was purchased from ATCC. Cells were grown in DMEM media supplemented with 10% FBS, 1% L-glutamine, penicillin (100 units/mL) and streptomycin (100 units/mL), and maintained at 37°C in a humidified atmosphere of 5% CO_2.

To obtain a primary enteric mixed culture, intestines of E15; C57BL6 mice were obtained and minced in sterile ice-cold DMEM media containing antibiotics. The finely chopped pieces were enzymatically digested in serum-free media containing collagenase (0.2 mg/ml) and dispase (0.2 mg/ml) at 37°C for 30 minutes (min). The enzymatic digestion was stopped by adding 10% FBS and centrifuging the cells at 250 x g for 5 min. Supernatant was aspirated and the pellet was triturated in 10% DMEM/F-12 till a single cell suspension was obtained. Cells were filtered through a 40-μ cell strainer and plated on poly-D-lysine- (PDL-) and laminin pre-coated plates. After 24 h, media was changed to 1% DMEM/F-12 containing 50 ng/ml GDNF, N2 and B27 supplements and cultured for 3 weeks at 37°C and 5% CO_2. Half of the media was changed every 2 days.

MTS assay

Cell viability was measured by Cell Titer 96® aqueous non-radioactive cell proliferation assay (MTS assay, Promega) as previously described (Ay et al., 2015). MTS salt is reduced to purple-colored formazan in healthy cells so the amount of formazan produced is indicative of mitochondrial activity and in turn cell metabolic activity. Briefly, 25,000 enteric glial cells (EGCs) were seeded onto 96-well plates and treated with different doses of Mn (0-1000 μM)

for 24 h. Before completion of treatment, 20 μL of MTS solution was added to each well, and the plates were incubated at 37°C and 5% CO_2 for 1.5 h. Measurements were made at 490 nm and 670 nm (reference wavelength) using a fluorescence microplate reader (SpectraMax Gemini XS; Molecular Devices, Sunnyvale, CA, USA).

SYTOX green assay

Cell death was determined by the cell-impermeable dye SYTOX green (Song et al., 2010). EGCs were grown in 96-well plates and treated with different doses of Mn in 2% DMEM for 24 h. After treatment, 1 μM SYTOX green was added to each well for 20 min. Cell death was quantitatively measured with an excitation wavelength of 485 nm and an emission wavelength of 525 nm using a fluorescence microplate reader (SpectraMax Gemini). Nuclei were stained with Hoechst 3342 (5 μg/ml) for 15 min to determine total cell number in each well. Resulting green fluorescence readings were normalized to cell number. Photomicrographs showing cell death and cell morphology were also taken using an EVOS Floid cell imager (Invitrogen).

Caspase-3 activity

Following 24-hour exposure to different doses of Mn, EGCs were collected in individual tubes and 230 μl lysis buffer (10% sucrose, 5 mM dithiothreitol, 100mM HEPES, 0.1% CHAPS and 20 mM EDTA in dH_20, pH 7.4) was added to each sample and incubated for 20 minutes at 37°C to lyse the cells. Thereafter, 190 μl of lysate was added to individual wells of a 96 well black, clear bottom plate (catalog # Greiner 655079) containing 10 μl caspase-3 substrate (50 μM Ac-DEVD-AFC) at 37°C for 60 minutes. Formation of 7-amino-4-

methylcoumarin (AFC) resulting from caspase-3 activity was measured at Ex. 460 and Em. 510 nm using a fluorescence plate reader. The caspase-3 activity was normalized to protein concentration as determined by Bradford protein assay (Harischandra et al., 2015).

Determination of mitochondrial morphology and mass

40,000 EGCs were plated on PDL-coated coverslips and treated with different doses of Mn for 24 h. After treatment, cells were washed with HBSS containing Ca^{+2} and Mg^{+2} to remove any residual media. Next, 100 nM MitoTracker Red CMxRos probe (Invitrogen) was added to each well to stain the cells for 15 min. Cells were triple-washed with sterile HBSS to remove any dye and then fixed for 20 min in 4% paraformaldehyde (PFA). Alexa-488 phalloidin (Invitrogen) was used at a 1:100 dilution for 30 min to stain F-actin while nuclei were stained using Hoechst 3342 at a final concentration of 0.2 μg/ml for 7 min. The wells were washed three times with distilled water and coverslips were mounted onto pre-cleaned glass slides using Fluoromount (Sigma). Images were obtained using an inverted fluorescence Leica DMIRE2 confocal microscope with 63X magnification and image analysis was performed using ImageJ. Quantification of mitochondrial length and degree of circularity was accomplished using a macro text file plug-in for ImageJ (Dagda et al., 2009). For analyzing the images, eight images per group were quantified and two separate experiments were performed.

To determine mitochondrial mass, cells were stained with the MitoTracker Green FM probe. First, 25,000 EGCs were plated per well of a 96-well plate. Cells were treated with different doses of Mn (0-1000 μM) for 24 h. After treatment, the media was removed and 100 μl of

200 nM MitoTracker Green dye diluted in serum-free DMEM media was added to each well and incubated at 37 °C for 15 min. Following incubation, green fluorescence was measured at an excitation wavelength of 485 nm and an emission wavelength of 520 nm using a fluorescence microplate reader. Nuclei were stained with Hoechst (5 μg/ml) for 15 min to determine total cell number in each well. Resulting green fluorescence readings were normalized to cell number.

Aconitase assay

Mitochondrial aconitase (m-aconitase) levels in EGC's were measured using a commercial aconitase assay kit (Abcam, Cat.# ab83459) as described before with minor modifications (Langley et al., 2017). Briefly, 1×10^6 EGC's were grown in a T25 cell culture flask and exposed to 10 μM and 100 μM Mn for 24h. Cells were collected after treatment and resuspended in the supplied assay buffer on ice followed by centrifugation at 2000 × *g* for 5 min at 4 °C. The resulting supernatant was collected and further centrifuged at 20,000 × *g* for 15 min to collect the mitochondrial fraction. The pellet was thoroughly mixed with 100 μl of assay buffer and sonicated for 25 s at 4 °C. Citrate was added as a substrate to each well. Aconitase converts citrate to isocitrate that is further processed leading to the formation of a colored end product. The plate was then read at 450 nm using a microplate reader. The OD values were normalized to the protein concentration of each sample and the results were expressed as percentage control.

Mitochondrial oxygen consumption and extracellular flux analysis using Seahorse bioanalyzer

Mitochondrial oxygen consumption in EGCs treated with different doses of Mn was measured using the XF^e-24 Seahorse bioanalyzer (Seahorse Bioscience) and company recommended Mito Stress kit (Seahorse bioscience). One day before measurements, EGCs were seeded at 30,000 cells/well. The next day, cells were treated with 0, 10 or 100 μM Mn for 24 hours. Mitochondrial oxygen consumption rate (OCR) and ATP production was measured using Mito Stress kit. The experiment was repeated two times (n=2) in triplicate. No significant inter-assay differences were detected between the two repetitions regarding the appearance and viability of cells or the values of O_2 consumption that were obtained.

^{3}[H] Glutamate uptake assay

30,000 EGCs were plated per well of a 24-well plate. Cells were treated in triplicate with 0, 10 or 100 μM Mn for 24 hours. After treatment, cells were washed in Krebs solution (containing in mM: 32 NaCl, 4 KCl, 1.2 Na_2HPO_4, 1.4 $MgCl_2$, 6 glucose, 10 Hepes, 1 mM $CaCl_2$, pH 7.4) to remove any media. Cells were incubated with 2 μCi L-[3,4 ^{3}H] glutamic acid for 15 minutes at 37°C. Media was removed and cells were washed twice with ice-cold Krebs solution to stop the uptake. Cells were lysed in 0.5 ml 1N NaOH and the total radiolabeled glutamate uptake were measured via liquid scintillation counting. Experiments were repeated thrice, each time in triplicates.

Animal studies

We purchased 8 to 10 week old male C57BL/6 mice from Charles River Laboratories for all animal experiments. Mice were housed on a 12-h light cycle with *ad libitum* access to food and water. After 2 weeks of acclimatization, mice received either 15-mg/kg-body weight/day

Mn (as $MnCl_2 \cdot 2H_2O$) for 30 days or an equal volume of vehicle (water) via oral gavage. This dose regimen was chosen based on previous Mn neurotoxicity studies in humans and rodents (Crossgrove and Zheng, 2004; Li et al., 2006; Zheng et al., 2000). Animal care procedures strictly followed the NIH Guide for the Care and Use of Laboratory Animals and were approved by the Iowa State University IACUC. Body weight and whole gut transit time were measured every 10 days. At the end of the treatment regimen, animals were euthanized by CO_2, and then 3-cm strips of the duodenum, ileum and colon were collected and emptied of their contents by rinsing thoroughly in ice-cold PBS. Tissues were further excised into 1-cm pieces for various biochemical tests and stored at -80°C till further processing.

Behavioral analysis

Behavioral impairments resulting from Mn toxicity were assayed using the Versamax activity monitor and the Rotarod test, as described previously (Ghosh et al., 2016a). Briefly, exploratory locomotor activity was measured using the Versamax open-field apparatus (Accuscan Instruments, Columbus, OH) and the following indices were monitored for 10 min: rearing (labeled as vertical) activity and horizontal activity. Motor coordination was tested by measuring the latency to fall from a 3-cm diameter rod rotating at a constant 20-rpm till the mice fell or for 20 min. (Rotarod, *Accuscan* Instruments). Each mouse was subjected to 5 trials separated by 5- to 7-min intervals to eliminate stress and fatigue.

Gastrointestinal function testing

Whole gut transit time (WGTT)

WGTT was measured by ingestion of carmine red, a red dye that cannot be absorbed by the GI tract. Briefly, WGTT was measured by intragastric gavage of each mouse with 0.3 ml of 6% (w/v) carmine dye in 0.5% methylcellulose as previously described (Anderson et al., 2007). The time taken from administration of the dye until first appearance of a red stool pellet was recorded. Animals whose stool had no dye even after a maximum observation time of 8 h were recorded as >8 h.

Bead latency

Distal colonic motility was measured by the bead expulsion test (Vilz et al., 2012). Mice were anesthetized with isoflurane (1–2min) and a 2 mm-diameter lubricated glass bead is introduced into the distal colon (2cm from the anus margin) using a fire-polished glass rod. After insertion of the bead, mice were isolated in a plastic cage for observation. The time required for expulsion of the glass bead was recorded (bead latency) which is typically less than 15 min.

Fecal water content

30 days post Mn exposure, mice were kept in clear plastic cages and fecal pellets from individual cages were collected over the course of 1 hour. Pellets were transferred in 1.5 ml centrifuge tubes, capped and weighed to collect the wet weight of the pellets. Thereafter, with the caps opened, the tubes were placed in a 55C incubator and dried for 24 hours to dry out the pellets. The tubes were recapped and weighed after drying to obtain the dry weight of the pellets. Water content was calculated by calculating the difference between wet and dry weights.

Social discrimination and novel scent tests

To determine the olfactory function of control and Mn-exposed mice, we used a social discrimination test as previously described (Ngwa et al., 2014). However, this procedure was adapted to use AnyMaze tracking software (AMS, Stoelting Co., Wood Dale, IL) to determine time spent sniffing based on the animals head being within a defined zone (1-cm perimeter around dish) surrounding the bedding. Total time spent sniffing the opposite sex's bedding (from a group-housed cage) was recording during a 3-min trial. Similarly, AMS was used to determine time sniffing a novel scent. During a 3-min trial, time spent sniffing scented and non-scented zones was recorded using AMS. Vanilla was used as the novel scent whereas water served as the non-scent.

Quantitative real-time PCR (qRT-PCR)

Ten tissues of distal colon from control and Mn-treated groups were utilized for qRT-PCR. The samples were homogenized in a bullet blender (Next Advance) using DNAse- and RNAse-free stainless steel beads and RNA was extracted using RNeasy Plus Mini kit (Qiagen). 1 μg total RNA was converted to cDNA using the High-Capacity cDNA Reverse Transcription kit (Applied Biosystems Inc.) following manufacturer's instructions. Real-time PCR was performed in an Mx3000P QPCR system (Stratagene) using the Brilliant SYBR Green QPCR Master Mix kit (Stratagene), with cDNAs corresponding to 1 μg of total RNA, 10 μl of 2 × master mix and 0.2 μM of each primer in a 20-μl final reaction volume. All reactions were performed in triplicate. Mouse 18S rRNA was used as an internal standard for normalization. Validated QuantiTect primer sets for mouse 18S rRNA (Cat# QT02448075), TNFα (QT00104006), IL-1β (QT01048355) and iNOS (QT00100275, Qiagen) were also

used. The PCR cycling conditions contained an initial denaturation at 95°C for 10 min, followed by 40 cycles of denaturation at 95°C for 30 sec, annealing at 60°C for 30 sec, and extension at 72°C for 30 sec. Fluorescence was detected during the annealing step of each cycle. Dissociation curves were run to verify the singularity of the PCR product. Data were analyzed using the comparative threshold cycle (Ct) method (Livak and Schmittgen, 2001).

Western blots

Whole cell lysates or tissue lysates were prepared using modified radio immune precipitation assay (RIPA) buffer containing 20 mM Tris–HCl, pH 8.0, 2 mM EDTA, 10 mM EGTA, 2 mM dithiothreitol (DTT), 1 mM phenylmethylsulfonyl fluoride (PMSF), 20mM sodium orthovanadate, 1 mM sodium fluoride and protease and phosphatase inhibitor cocktail (Thermo Scientific, Waltham, MA), as described previously (Harischandra et al., 2015; Harischandra et al., 2014). The supernatants were obtained after centrifuging the homogenates at 15,000 rpm for 60 min. Protein concentration was measured using Bradford dye (Bio-Rad). Lysates containing equal amounts of protein were separated on a 12 or 15% SDS-polyacrylamide gel. After separation, proteins were electro-blotted onto a nitrocellulose membrane, and nonspecific binding sites were blocked with LICOR blocking buffer. PGP9.5 (1:1000), GFAP (1:1200), Bax (1:500), iNOS (1:500) and β-actin (1:10000) primary antibodies were used to blot the membranes for 16 h at 4°C. Thereafter, blots were washed in phosphate buffered saline (PBS) containing 0.01% Tween-20, incubated in respective secondary antibodies (Alexa Goat anti mouse 680 or Alexa Goat anti-rabbit 800) for 1 hour. Fluorescent bands corresponding to the protein of interest were observed by scanning membranes in a LICOR scanner.

Immunocytochemistry and Immunohistochemistry

For immunocytochemistry, primary enteric cells were grown on 12-mm coverslips previously coated with 50 μg/ml PDL for 3 hours followed by 10 μg/ml laminin for 12 hours. Two weeks post-plating, cells were treated with 100 μM $MnCl_2$ for 24 h. After treatment, cells were washed with PBS and incubated in 4% PFA for 30 min at RT. After fixing, cells were washed with PBS and incubated in blocking buffer (2% BSA, 0.05% Tween-20, and 0.5% Triton X-100 in PBS) for 1 h. Cells were then incubated with antibodies against PGP9.5 (1:1000) or GFAP (1:1000) and iNOS (1:1000) overnight at 4°C. After primary incubation, cells were washed and incubated in the dark for 90 min with Alexa-488 and -555 dye-conjugated secondary antibodies (Invitrogen, 1:1500). Nuclei were stained with 0.2 μg/ml Hoechst and the coverslips were then mounted on glass slides (Superfrost, Invitrogen) and viewed with 63× and 43× oil objectives using a Leica DMIRE2 confocal microscope.

For Immunohistochemistry, at the end of the treatment regime, animals were perfused first with PBS followed by 4% PFA. Guts were removed and post-fixed in 10% formalin for an additional 24 h. Tissues were embedded in paraffin and sectioned at 7 μm at Iowa State University's veterinary pathology lab. Paraffin-embedded sections of mouse tissues were deparaffinized in decreasing alcohol grades. Heat-mediated antigen retrieval was performed using 10 mM citrate buffer (pH 6.0) for 30 min. Sections were then incubated with blocking reagent (5% normal goat serum, 2% BSA and 0.5% Triton X-100 in PBS) for 60 min before being incubated with iNOS, PGP9.5 or GFAP primary antibodies for 24 h. Sections were then washed many times in PBS and incubated in the dark for 90 min with Alexa-488 and -555 dye-conjugated secondary antibodies (1:1500). Nuclei were stained with Hoechst

dye. Slides were viewed with 63× and 43× oil objectives using a Leica DMIRE2 confocal microscope.

Inductively coupled plasma mass spectroscopy (ICP-MS)

Colon samples were carefully excised and weighed prior to sample preparation. Samples were analyzed for Cd, Ca, Cr, Co, Cu, Fe, Mg, Mn, Mo, P, K, Se, Na, and Zn using Inductively coupled plasma mass spectrometry (ICP-MS, Analytik Jena Inc. Woburn, MA, USA) in CRI mode with hydrogen as the skimmer gas. Standards for elemental analyses were obtained from Inorganic Ventures (Christiansburg, VA) while digestion vessels; trace mineral grade nitric acid and hydrochloric acid were obtained from Fisher Scientific (Pittsburgh, PA). Briefly, samples were digested in 70 % nitric acid at 60˚C for ≥12 hours. Pre-weighed samples were transferred to 15mL tubes and 0.25 mL of 70% nitric acid was added. All samples were digested overnight at 60˚C. After digestion, all samples were diluted to 5 mL using 1% nitric acid with 0.5% hydrochloric acid and then analyzed by ICP-MS. For quality control, Bi, Sc, In, Li, Y, and Tb were used as internal standards for the ICP-MS.

Genomic DNA isolation

Immediately following sacrifice, the colon was removed and fecal pellets promptly collected, stored in an Eppendorf tube, and transferred into a -80°C freezer for long-term storage until analysis. Genomic DNA isolation was performed using the PowerSoil DNA Isolation kit (MoBio, Carlsbad, CA) on samples from 10 mice per group for each time point. The purified genomic DNA extracts were quantified using a Qubit 2.0 Fluorometer (Life Technologies, Carlsbad, CA) and stored at -20°C in 10 mM Tris buffer.

DNA sequencing and Analysis

PCR amplification of the V4 variable region of the 16S rRNA gene using V4 region-specific barcoded primers (515F-816R) and amplicon sequencing were performed by Institute for Genomics & Systems Biology at the Argonne National Laboratory (Argonne, IL) on the Illumina MiSeq Platform. The sequences were analyzed using QIIME (Quantitative Insights into Microbial Ecology) (Caporaso et al., 2010). Briefly, reads were first demultiplexed and quality filtered, then sequences with homopolymer runs or ambiguous bases greater than six, nonmatching barcodes, barcode errors, or quality scores less than 25 were removed. Operational taxonomic units (OTUs) were called using UCLUST and the closed reference OTU picking strategy in QIIME (Edgar, 2010). Sequences were aligned to the Greengenes (13_8) database using PyNAST at 97% similarity (DeSantis et al., 2006). Taxonomic assignments were made based on the Greengenes reference database using the RDP classifier 2.2 in QIIME (Wang et al., 2007). Alpha diversity, beta diversity, principal coordinate plots (PCoA), Analysis of similarity (ANOSIM), and Adonis tests were also generated using QIIME. Wilcoxon Rank Sum tests were performed on taxonomic summaries, obtained from the QIIME pipeline, using a custom R script (R Project) obtained from the Institute for Genome Sciences at the University of Maryland School of Medicine.

Gas chromatography and mass spectroscopy analysis (GC-MS)

To isolate the metabolites for the GC-MS analysis, we followed the methods described by Noutsos *et al* (Noutsos et al., 2015). Identification of fecal metabolites was done by comparing the mass spectral to NIST08 Library and using Retention Indices and were quantitated relative to internal standards. Prior to metabolite extraction, ~20 - 30 mg of fecal

matter was weighed, spiked with internal standards (20 μg of ribitol and 20 μg of nonadecanoic acid), and homogenized with 0.35 mL of hot methanol (60°C). The mixture was immediately incubated for 10 min at 60°C and sonicated for 10 min. 0.3 mL of chloroform and water respectively were added to this mixture and vortexed for 3 min. After centrifugation to separate phases, 0.2 mL of the upper polar phase and 0.2 mL of the lower non-polar phase were removed and transferred into 2-mL glass vials. Both fractions were dried in a SpeedVac concentrator. The extracts were subjected to methoximation with methoxyamine hydrochloride at 30°C for 90 min. Samples were silylated with BSTFA/TCMS at 60°C for 30 min, and then subjected to gas chromatography–mass spectrometry (GC-MS, Agilent Technologies) on an 6890N gas chromatograph in tandem with a 5973MSD detector equipped with a gas ionization detector (gas flow: UHP Helium, 1.0 ml/min.; ionization mode: El; polarity: positive; skimmer/focusing lens voltages: 70 eV). Samples were loaded onto the GC with a 7683B automatic liquid sampler. The mass range was set from 40–1000 m/z. The separation column was an HP5MSI (30 m long, 0.250 mm ID, 0.25 μm film thickness). The gas chromatography was operated by ChemStation software.

Data analysis

Data analysis was performed using Prism 4.0 Software (GraphPad Prism, San Diego, CA). Data were first analyzed using Student t-test or one-way ANOVA, and then Tukey's post-hoc test to compare all treatment groups. Differences with $p<0.05$ were considered significant.

Results

Manganese exposure induces mitochondrial stress in enteric glial cells

To determine response of the EGC cell line to Mn, we performed dose-response cytotoxicity and mitochondrial viability assays. MTS, otherwise known as 3-(4,5-dimethylthiazol-2-yl)-5-(3-carboxymethoxyphenyl)-2-(4-sulfophenyl)-2H-tetrazolium, is a compound that is reduced by viable cells with healthy and active mitochondria to a purple-colored formazan end product whose amount directly correlates with the metabolic capacity of the cells. When EGCs were treated with increasing doses of Mn (0 – 1000 μM) for 24 h, a dose-dependent decrease in formazan production was observed. The IC_{50} was calculated by a three-parameter non-linear regression curve and found to be about 5 μM (Fig. 1A). Since the metabolic activity assayed by MTS is in turn directly dependent on mitochondrial health, the results can be interpreted as a dose-dependent decrease in mitochondrial viability. Furthermore, EGCs treated with 0, 1, 3, 10 and 30 μM Mn for 24 h lost mitochondrial mass as evidenced by MitoTracker Green assay (Fig. 1B). Mitotracker Green FM is a dye that is fluorescent only upon accumulation in a mitochondrial lipid-rich environment (Agnello et al., 2008). Healthy mitochondria undergo multiplication by either the process of fission or fusion. If the mitochondria are stressed, they do not undergo further replication, consequently stressed cells could show less mitochondrial mass compared to untreated control cells. Corroborating with this point, the 3, 10 and 30 μM Mn doses decreased the mitochondrial mass by about 30, 32 and 60%, respectively, compared to untreated controls. To further strengthen our theory of Mn-induced mitochondrial damage, we observed mitochondrial morphology of treated and untreated EGC's using Mitotracker Red. As shown in Fig. 1C, untreated cells exhibited the characteristics of healthy mitochondria, such as long thread-like strands densely

surrounding the nucleus. However, when treated with Mn, these mitochondria become rounded and begin to disintegrate. Even at a low dose of 10 μM Mn, some mitochondria appeared rounded indicating their stressed status. At a high dose such as 100 μM Mn, mitochondria appeared to have coalesced into rounded structures surrounding the nucleus while at a very toxic dose of 1000 μM, fine punctate staining was observed indicating that the mitochondria have disintegrated. We quantified the degree of circularity (a measure of mitochondrial toxicity) using imageJ. The results show a 20 and 25% increase in circularity in cells treated with 10 and 100 μM Mn compared to untreated controls. As mentioned before, at 1000 μM, most of the mitochondria have disintegrated hence the degree of circularity could not be measured (Fig 1D). Similarly, mitochondrial aconitase (m-aconitase) activity was decreased in EGC's treated with 100 μM Mn (Fig 1E). m-aconitase activity is mainly hampered by superoxide production (Fig 1F) and consequently mitochondrial toxicity. We hypothesized that Mn exposure could impair basal mitochondrial respiration as well as spare respiratory capacity. Hence we measured the oxygen consumption rate (OCR) of 100 μM and untreated EGCs as an indicator of mitochondrial respiration (Figure 1G). There was significant reduction in basal respiration and ATP production (Figure 1H) in Mn treated EGCs compared to untreated controls indicating a decrease in mitochondrial respiration and hence mitochondrial (and cellular) stress following Mn exposure. These results convincingly prove that Mn causes mitochondrial damage in EGC's in a dose-dependent manner.

Cell death in enteric glia occurs only at higher concentrations of manganese

Interestingly, when the same Mn treatment paradigm was used to measure cytotoxicity in EGCs, we found that only EGCs treated with higher Mn doses of ≥300 μM stained positively for SYTOX green, a dye that can enter only dead cells with a compromised cell membrane (Fig. 2A-B). We further validated this observation by assessing caspase-3 activity of EGCs treated 24 h with different Mn doses. As shown in figure 2C, significant caspase-3 activity was observed mainly in cells exposed to ≥300 μM Mn for 24 hours. Would stressed enteric glia still manage to function as effectively as normal enteric glia? To answer this question, we analyzed glutamate uptake capacity of Mn exposed EGCs. Glutamate is one of the several neurotransmitters produced by the ENS and plays a role in the rhythmic intestinal contractions seen in the gut as well as in the bi-directional signaling of the gut-brain axis (Filpa et al., 2016). In the CNS, astrocytes play a major role in the glutamate uptake and regulating glutamatergic synapses. Since EGCs are similar to astrocytes (both share common surface markers GFAP and S100β) there is a strong possibility that these cells also regulate glutamate signaling in the gut much like astrocytes do in the brain. Hence we decided to assess glutamate uptake in these cells when treated with increasing concentrations of Mn. Cells treated with 5 or 10 μM Mn showed ~ 10% decreased uptake when compared to untreated cells. In comparison, EGCs treated with 100 μM Mn showed more than 50% decrease in glutamate uptake when compared to untreated controls (Fig 2D). As seen with our cytotoxicity assay and western blot, cells while stressed are not dead. Taken together, these results show that exposure to even small amounts of Mn can alter functioning of these cells, yet the actual dose required for cell death is quite high.

Manganese potentiates inflammation and cell death of neurons in a primary enteric culture

While EGCs might be particularly sensitive to Mn when observed as a pure culture, the kinetics of Mn-induced mitochondrial dysfunction would differ in the intestine since it is a complex network of various cell types including the EGCs and neurons, smooth muscle cells, surveilling peripheral immune cells and epithelial cells. As expected, when the primary enteric mixed culture was treated with increasing doses of Mn (0 – 1000 μM) for 24 h, the IC_{50} was calculated to be about 100 μM (Fig. 3A). At this dose, Mn triggered inflammation as evidenced by an upregulation in mRNA transcripts of TNFα and iNOS (Fig. 3B). There was a slight reduction ($n=6$, $p< 0.06$) in GFAP expression as evidenced by Western blot (Fig. 3C) indicating that 100 μM Mn was negatively affecting glial cell health. In the ENS, enteric glial cells are closely associated with the enteric neurons. Importantly, Western blot analysis showed that 100 μM Mn treatment decreased enteric neuronal PGP9.5 expression after 24 hours (Fig. 3D). Interestingly, expression of ferroportin, which is a Mn-responsive protein that can transport Mn out of the cell- was decreased while protein levels of DMT1 – a transporter involved in the influx of divalent metals (including Mn) – showed no change in the cultures exposed to Mn compared to controls (Figure 3D). These findings indicate that Mn treatment induces inflammation and neuronal cell death in primary enteric mixed cultures.

Our method of isolating and growing the mixed enteric culture is capable of generating spontaneous smooth-muscle contractions similar to the intestinal contractions seen *in vivo*. Primary enteric mixed cultures grown for approximately 3 weeks on PDL and laminin-coated plates show extensive neuronal networks (red arrows) growing over a bed of what appears to

be smooth muscle and epithelial cells (yellow arrow, S.figure 1A). Other cells types, possibly endothelial cells and fibroblasts are also present in the culture (S.figure 1B- 1C). At 3-4 weeks post-plating, isolated contractions were seen in different parts of the culture (Figure 3F). These spontaneous contractions gradually reduced in cultures treated with 100 μM Mn for 24 h (Figure 3G.). Western blot results and videographic evidence show loss of enteric neuronal cells. Since peristalsis occurs due to a concerted influence of the ENS, interstitial cells of Cajal and the smooth muscle cells, it is possible that the loss of enteric neurons disrupts this signaling thereby affecting muscle contraction (Huizinga, 1999).

Low-dose, chronic Mn administration in mice does not induce motor impairment

To assess gastro-intestinal changes following increased ingestion of Mn, mice were given a dose of 15 mg/kg/day for 30 days (Fig. 4A). While Mn-treated mice on an average, did not show any significant weight gain; the untreated group showed a trend of weight gain (Fig. 4B). Similarly, Rotarod (Fig. 4C) and Versamax open-field tests (Fig. 4D-E) did not show any significant differences between the two groups. The open-field test evaluates general locomotor activity in mice while Rotarod test evaluates motor co-ordination. Together, these two tests are routinely used to assess movement-associated neurological dysfunction in mice. Published reports have described significant reduction in motor behavior in mice treated with either 59 mg/kg Mn for 10 days or 100 mg/kg Mn for 8 weeks (Liu et al., 2006; Vezer et al., 2007). These mice also showed weight loss and other signs of sickness. However, as the aim of our study was to observe changes in gut physiology, the weight loss would be a compounding factor in any inference we derived from this study. Hence a non-toxic dose of

15 mg/kg/day for 30 days was chosen to observe any physiological changes in the gut intestinal physiology.

One of the consequences of enteric inflammation or ENS abnormalities is a change in gut physiology, especially peristalsis (Lee et al., 2014). Interestingly, increased WGTT was observed in the Mn-treated mice indicating decreased peristalsis. This group showed a trend ($p<0.06$) of altered intestinal transit time from day 20 onwards when compared to the control group (Fig. 4F). From day 20, these mice took an average of 350±10 min to expel the carmine red meal fed to them compared to the 320±10 min it took for mice in the control group to expel the same meal. Despite the longer transit time in both small and large intestine, there was no change in the fecal water content between groups (S. Figure 4). With regards to CTT, Mn-treated mice took on an average 7 minutes to expel the glass bead as opposed to control mice who took ~ 5.7 minutes (Fig. 4G). Taken together, the results point towards the presence of intestinal dysmotility despite a low-dose exposure to Mn and this intestinal de-regulation is seen before CNS-related symptoms are observed.

Low-dose, chronic Mn administration in mice causing enteric inflammation and increases gastrointestinal transit time

Microscopic analysis of tissue architecture in Mn-treated ileum and colon by hematoxylin and eosin (H&E) staining showed no signs of cell necrosis and immune cell infiltration (Fig. 5A). However, Alcian-blue-Periodic Acid Schiff (Ab-PAS) showed differential staining in the colons of control and treatment groups (Fig. 5B). Ab-PAS stains acidic and neutral mucopolysaccharides and glycoproteins, collectively known as mucins, that line the gastrointestinal tract (GIT) and protect the gut epithelium from mechanical shear stress as

well as from bacterial translocation into the deeper tissue of the intestine (Faure et al., 2003). These mucins are produced by goblet cells present in the villi. Mn-treated mice showed less intense staining as well as fewer goblet cells, indicating lower production of these mucopolysaccharides. An inadequate intestinal lining of mucin could slow the rate of movement of food. It might also affect the epithelial lining allowing for translocation of unwanted substances from the lumen to the sub-mucosa contributing to inflammation. Supporting this idea, we observed significant intestinal inflammation in the colon of Mn-treated mice. As shown in Fig. 5C, quantitative RT-PCR analysis showed 2.5- and 3.5-fold higher mRNA transcripts of TNFα and iNOS, respectively, in Mn-treated animals. Furthermore, Western blotting showed Mn increased the protein levels of iNOS (Fig. 5D). To ascertain if Mn-induced iNOS increase in part occurs in the ENS, whole mount sections containing the myenteric plexus were probed for GFAP and iNOS. Indeed, immunofluorescence images revealed more punctate presence of iNOS in the myenteric ganglia of Mn-treated animals (Fig. 5E). Protein analysis of full thickness colon (n=6) from both groups showed an increase in EGC marker GFAP as well as a decrease in mitochondrial protein DJ-1 (Fig. 5F). The receptor DMT1 is involved in the influx of divalent metal ions into cells while ferroportin (Fpn) removes iron and Mn from the cell. We found that while the protein levels of DMT1 remain unchanged, the levels of Fpn decreased in the Mn group suggesting a dysfunction in the export of metal from the cell. Indeed, as shown in figure 5G, q-RT-PCR analysis of common Mn transporters DMT1, Fpn and SLC30A10- a manganese efflux receptor- showed a decrease in SLC30A10 mRNA levels in the colon of Mn treated mice. Tissue levels of Mn were significantly increased (Figure 5H) in the colons of Mn-

treated group compared to control thus substantiating western blot and q-RT PCR results. No significant changes in tissue levels of other metals were found between the groups (S.Fig. 3).

Changes in taxonomic abundances between control and Mn-treated mice

The presence of increased intestinal transit time as well as upregulated iNOS and TNFα in the ENS pointed to some degree of colon inflammation. Since it is well known that a majority of the gut microbiota resides in the colon, we decided to analyze any potential changes in the gut bacterial population between age-matched untreated and Mn-treated mice. A total of 7,152,846 reads passed quality filtering with an average of 89,410.58±21,937.2 sequences per sample. DNA sequences representing fecal samples were submitted to comparisons at 97% similarity to the Greengenes database. Wilcoxon Rank Sum tests were used to compare taxonomic abundances from the control and Mn-treatment groups of the same day (i.e., day 0 control and day 0 Mn-treated groups). Figure 6A shows the taxonomic summary at the phylum level. For each group, *Bacteroidetes*, was the dominant phylum (control:63.75-73.83%, Mn:64.87-73.41%), followed by *Firmicutes* (control:24.42-34.41%; Mn:23.17-32.27%). Comparing taxonomic abundances at the phylum level, there were no significant differences between the control and Mn-treated groups at the same time point.

At the class level (Figure 6b), *Bacteroidia* was the dominant organism in each group (control: 63.75-73.83%; Mn: 64.87-73.41%). Within the phylum *Firmicutes*, the dominant classes were *Clostridia* (control: 21.54-29.90%; Mn: 20.10-28.80%) and *Bacilli* (control: 1.87-3.93%; Mn: 1.55-3.53%). While there were no significant changes in abundance

between the control and Mn-treated groups, on day 20 there appeared to be an enrichment of *Gammaproteobacteria* in the Mn treated mice (p=0.0819).

At the genus level (Figure 6C), the dominant genera were *Bacteroides*, *Parabacteroides*, and an unknown genus in the family S24-7, an environmental organism in the phylum *Bacteroidetes.* The two most dominant genera in the phylum *Firmicutes* were *Lactobacillus* and unknown genus in the order *Clostridiales*. In both groups, S24-7 increases over the 30-day period, while *Bacteroides* decreases. Statistical comparisons showed no differences between the control and Mn-treated mice at any time point.

Alpha diversity metrics were used to compare within sample diversity. Non-parametric two sample t-tests using Monte Carlo permutations were used to compare the observed OTUs (Figure 6d) and Faith's Phylogenetic Diversity (Figure 6e). Comparisons of alpha diversity values showed that control and Mn-treated mice did not differ significantly at any time point. Mn treatment had no effect on the diversity of the microbiota over the 30-day period. Inspection of the observed OTUs rarefaction plot showed the curves plateau, indicating the sequencing depth was sufficient as to exclude the discovery or new or rare OTUs.

Weighted (Figure 5f) Unifrac PCoA plots were generated using QIIME Groupings was compared using adonis and analysis of similarity (ANOSIM) tests. There appeared to be no obvious clustering based on treatment and sample date. Statistical test indicate no differences in groups at any time point. Adonis tests resulted in a p-value of 0.06 and R^2 value of 0.1293, meaning the clustering accounts for only 12.93% of the variation seen. ANOSIM tests resulted in a p-value of 0.19 and a test statistic of 0.0262, indicating weak grouping based on treatment and sample date.

Temporal and transient changes in fecal metabolites of mice treated with manganese

Abnormal peristalsis and changes in the gut microbial composition can have downstream effects on the bacterial population as well as the host's physiology. While there was no significant difference in the bacterial population changes in the host physiology, we wanted to confirm any changes in fecal metabolites that can indicate a change in the host physiology. We used GC-MS to screen fecal metabolites to determine any changes that might have occurred over the range of carbohydrates, amino acids, fatty acids etc. Log-scale transformation of data was used to provide better separation of samples and results are presented in a heat map with increasing color intensity corresponding to higher samples amount with respect to average control sample amounts (Figure 7A). A total of 1064 metabolites were identified using the NIST08 library and metabolites fell in 22 categories. GC-MS analysis of fecal samples collected at days 0, 10, 20 and 30 showed some significant differences as early as day 10 between Mn-treated and untreated mice. Notably decreased alanine production ($p<0.05$), α-linolenic acid acid ($p<0.03$) and oleic acid ($p<0.03$) production and increased and palmitic acid ($p<0.065$) production was seen at day 10 in the feces of Mn-treated mice when compared to day 10 control mice (Figure 7B-7D). α-linolenic acid is an omega-3 fatty acid that has been shown to reduce inflammation with reduced levels seen in many chronic diseases such as arthritis and high blood pressure (de Lorgeril et al., 1994). There appears to be a bi-directional relation between probiotic bacteria and omega-3 fatty acids since atopic infants given bifidobacterium over 7 months showed increased plasma α-linolenic acid levels (Logan and Katzman, 2005). Palmitic acid is the most common saturated fatty acid found in the body Increased palmitic acid can reduce

insulin production in pancreatic β-cells thus leading to type-2 diabetes (Solinas et al., 2006). Thus decreased alanine along with increased palmitic and stearic acid points towards intestinal dysregulation as early as 10 days post Mn exposure whereas the sugar glucopyranose was found to be lower in the fecal samples of Mn-treated mice at day 20 (Fig. 7E). The various classes of differentially expressed metabolites are summarized in figures 7F-7G in the form of pie charts. The pie charts illustrate the range of metabolites altered following Mn exposure at days 20 and 30. Amino acids, sugars, fatty acids as well as glycolytic intermediates reflected the largest percentage of compounds affected following Mn exposure. Thus transient changes in fecal metabolites, especially compounds that play a part in carbohydrate and fatty acid metabolism, are seen in the Mn treated mice.

Discussion

Since the discovery by Braak and colleagues that aggregated proteins - a hallmark of many neurodegenerative diseases including PD - are seen in the ENS of a number of early PD patients, scientific interest in the possibility of enteric dysfunction preceding CNS dysfunction has increased (Braak et al., 2006). Recent publications have shown a possible connection between ingestion/inhalation of environmental toxins and development of neurological disorders (Bhatt et al., 1999; Gomez-Mejiba et al., 2009). In the case of metal toxicity, Mn, aluminum, mercury and lead are known to be neurotoxic when present in high amounts in the body (Farina et al., 2013). While Mn toxicity in the brain has been studied extensively, scant attention has been paid to its possible toxic influence on enteric neurons despite cases of gastrointestinal disturbances having been reported following chronic Mn

exposure (Chandra and Imam, 1973; Huang and Lin, 2004). Hence we decided to investigate the possible toxic role of Mn exposure in the GI tract.

The GI tract is a complex composition of various cell types including enteric neurons and glia as well as resident immune cells. As mentioned before, EGCs are known to project into the mucosal villi, playing a crucial role in maintaining the intestinal barrier as well as cross-talking with immune cells and enteric neurons (Gulbransen and Sharkey, 2012; Neunlist et al., 2013; Savidge et al., 2007b). Recent evidence has suggested that a number of GI tract-related disorders occur partly due to a dysregulation of EGCs (von Boyen and Steinkamp, 2010; Yu and Li, 2014). Since EGCs can come into direct contact with Mn as it is absorbed via the enterocytes on the villi, we focused on the effect of Mn on EGCs. Similar to previous results showing astrocytes as being particularly sensitive to Mn toxicity (Wedler et al., 1982), EGCs are also affected by low doses of this metal. In particular, the mitochondria appear to be more sensitive as shown via various mitochondria-specific assays in this paper. Curiously enough, when exposed to similar doses of iron, copper and magnesium, the EGC's were resistant to mitochondrial stress and damage as shown in S.Figure 1. This shows that Mn selectively exerts toxic effect on the EGC's. While mitochondria show signs of damage induced by minute doses of Mn, the cells *per se* do not undergo apoptosis until the dose exceeds 300 μM for 24 h. This means that a window exists when cells, although stressed, do not die immediately (Fig. 2B-2C). However, stressed EGCs can increase iNOS production and release pro-inflammatory factors, which can affect surrounding non-glial cells, activating or suppressing immune cells or contributing to stressed enteric neurons (Bogdan, 2001; Capoccia et al., 2015). The ENS, in conjunction with different neuropeptides, Cajal cells and enteric smooth muscle cells, controls the peristaltic movement of ingested food through the

intestine. This is necessary for absorption of food and micronutrients (in the small intestine) as well as water and salt retention and fecal production (in the large intestine) (Huizinga, 1999). However in the long-term, the abnormal peristalsis exhibited by Mn-treated mice may have unfavorable consequences on health.

While enteric neurons are more resistant to Mn toxicity, they can be susceptible to stress induced by pro-inflammatory factors released by activated and stressed EGCs (Fig 3B) (Brown et al., 2016) that could potentiate enteric neuronal death (Fig 3D). Also, both primary enteric cultures and mice treated with a low dose of Mn for a prolonged period showed altered smooth muscle contractions. For instance, primary cultures treated with 100 μM Mn for 24 h showed decreased or no contractions along with apoptotic ganglia seen floating in the media (Figure 3F). Similarly, animals given 15 mg/kg/day Mn showed increased intestinal transit time compared to controls after day 20 (Figure 4F). These results have serious implications concerning the role of the ENS in regulating intestinal peristalsis and nutrient absorption. Slower peristalsis can result in small intestine bacterial overgrowth as well as constipation- two undesirable complications that can lead to poor digestion and nutrient imbalance thus affecting health in general. It is possible that interstitial cells of Cajal, called the pacemaker of the gut, might be sensitive to even small concentrations of Mn, similar to EGCs. These cells use changes in potassium and Ca^{+2} levels to communicate with smooth muscle cells and signal the timing and duration of each contraction (Parsons and Huizinga, 2010). Mn might compete with Ca^{+2} in entering the cell, limiting the generation of action potentials that cause surrounding smooth muscle cells to contract. However, more research is needed to understand this effect.

Following 30 days Mn exposure, mice had significantly more amount of Mn in the colon compared to vehicle (water) treated mice (Fig 5H). Indeed this impairment in Mn homeostasis was confirmed by probing for common Mn cellular transporters DMT1, ferroportin (Fpn) and SLC30A10. DMT1 is a receptor that transports most divalent ions- including Mn- inside a cell. DMT1 is expressed throughout the intestine especially on enterocytes present on intestinal villi and in the colon (Takeuchi et al., 2005). Similarly, Fpn and SLC30A10 are transporters present throughout the GI tract and are mainly involved in efflux of divalent metal ions. SLC30A10 is a Mn-specific efflux protein that removes Mn from the cell (Leyva-Illades et al., 2014). q-RT PCR analysis revealed decrease in SLC30A10 expression in the colon of Mn treated mice (Figure 5G) while Western blot analysis revealed decreased Fpn expression in the colon of Mn-exposed mice (Figure 5F). This could account for the increase in tissue Mn content in this group. Interestingly, no significant differences were observed between the groups with respect to other trace metals. Therefore, it is possible that presence of excess Mn in the intestinal tissue lead to oxidative stress and inflammation

H&E staining of the colon tissue of Mn-treated animals did not show any overt signs of immune cell infiltration indicative of large-scale inflammation or tissue damage (Fig. 5A). However, goblet cell numbers and consequently mucin production decreased in the treatment group (Fig. 5B). This shows that although cell death and tissue damage have not occurred following chronic Mn exposure, the function of certain cell types such as goblet cells was affected causing mild yet significant changes in the GI tract. Western blot and q-RT PCR quantification showed increased iNOS production, while immunofluorescence images showed a similar increase in iNOS in the myenteric plexus of the colon of Mn-treated mice.

Also, mRNA levels of TNFα were upregulated by low-dose, chronic Mn exposure. Collectively, these results indicate Mn-induced inflammation in the colon. Repeated toxin exposure has been thought to generate oxidative stress, intestinal inflammation and subsequently potentiate protein aggregation (House and Tansey, 2017). Hence we decided to probe for oligomeric protein expression using the A11 antibody. Slot blot analysis of colon lysates from Mn-exposed and unexposed mice (n=5) showed a trend of increased oligomeric protein expression in the colons from Mn-exposed group compared to controls (S. Figure 5).

In recent years, researchers have increasingly recognized the importance of gut microbiota in driving enteric inflammation as well as maintaining host health. In particular, there is considerable interest in the theory that the gut microbiome plays an important role in certain neurological disorders such as autism and PD (Ghaisas et al., 2016; Mulle et al., 2013; Scheperjans et al., 2015). While it is not known exactly how enteric microbiota initiate or aggravate neurological dysfunctions, it is thought that ingesting or inhaling environmental toxins affects the microbial population either by selectively enriching certain species of pathogenic bacteria or by reducing the number of beneficial bacteria, thus driving inflammation. Through the gut-brain axis, enteric inflammation is communicated to the CNS where neuroinflammation and later neurodegeneration progresses (Carabotti et al., 2015). The intestinal microbiota forms a regionally diverse and complex ecosystem, with a majority of the microorganisms residing in the large intestine (colon), while being sparsely present in the stomach and small intestine. Since we found inflammation in the colon, we characterized the gut bacteria of control and Mn-treated mice. Although we were unable to detect significant differences early during the treatment regime, a trend for increased *Gammaproteobacteria* was observed around 20 days post Mn exposure (Fig. 5B).

Interestingly, this class includes several pathogenic and opportunistic species (Li et al., 2012). It is also worth noting that this change in bacterial population coincided with increased intestinal transit time. Longer exposure to Mn could result in statistically significant changes in the composition of the gut microbiota.

Changes in fecal metabolite composition indicate either altered bacteria to host signaling or vice versa. Alanine, an amino acid that plays an important role in the biochemistry of a number of essential biological compounds was decreased within 10 days of Mn treatment. On the other hand, saturated fatty acids such as palmitic acid and stearic acid were present in significantly higher amounts in the treatment group compared to the control group. However, these changes were transient between the two groups as there were no significant differences by the end of the 30-day treatment. What is interesting though is the timeline of events that occur. 10 days post Mn treatment; changes in saturated fatty acid composition were observed. This was followed by an increase in *Gammproteobacteria* and in parallel, increased intestinal transit time.

To conclude, Mn overexposure affects the ENS even at low doses, impacting mainly the EGCs by causing mitochondrial damage. It also causes inflammation in the gut leading to decreased mucin production and slower peristalsis. These effects are observed despite exposure to non-toxic amounts of Mn, adding credence to the theory that environmental toxins influence ENS dysregulation and subsequently gastrointestinal dysfunction. Owing to the communication between the ENS and CNS via the gut-brain axis, this ENS dysregulation might ultimately contribute to irregularities in CNS functioning that precedes many neurological disorders.

Acknowledgments

This study was supported by grants from the National Institute of Health - ES19267, ES10586, and NS74443 to A.G.K. The W. Eugene and Linda Lloyd Endowed Chair to AGK and the Dean Endowed Professorship to A.K is also acknowledged. Our sincere thanks to Dwayne Schrunk and Olga T for the ICP-MS analysis and Lucas Showman and Dr. Ann Perera (W. M. Keck Lab) for help with the GC MS. We thank Gary Zenitsky for his assistance with manuscript preparation.

References

Agnello, M., G. Morici and A. M. Rinaldi (2008). "A method for measuring mitochondrial mass and activity." Cytotechnology **56**(3): 145-149.

Anderson, G., A. R. Noorian, G. Taylor, M. Anitha, D. Bernhard, S. Srinivasan and J. G. Greene (2007). "Loss of enteric dopaminergic neurons and associated changes in colon motility in an MPTP mouse model of Parkinson's disease." Exp Neurol **207**(1): 4-12.

Ay, M., H. Jin, D. S. Harischandra, A. Asaithambi, A. Kanthasamy, V. Anantharam and A. G. Kanthasamy (2015). "Molecular cloning, epigenetic regulation, and functional characterization of Prkd1 gene promoter in dopaminergic cell culture models of Parkinson's disease." J Neurochem **135**(2): 402-415.

Ayotte, J. D., J. A. M. Gronberg and L. E. Apodaca (2011). "Trace Elements National Synthesis Project." U.S. Geological Survey Scientific Investigations Report 115.

Bhatt, M. H., M. A. Elias and A. K. Mankodi (1999). "Acute and reversible parkinsonism due to organophosphate pesticide intoxication: five cases." Neurology **52**(7): 1467-1471.

Bogdan, C. (2001). "Nitric oxide and the immune response." Nat Immunol **2**(10): 907-916.

Bowler, R. M., H. A. Roels, S. Nakagawa, M. Drezgic, E. Diamond, R. Park, W. Koller, R. P. Bowler, D. Mergler, M. Bouchard, D. Smith, R. Gwiazda and R. L. Doty (2007). "Dose-effect relationships between manganese exposure and neurological, neuropsychological and pulmonary function in confined space bridge welders." Occup Environ Med **64**(3): 167-177.

Bowman, A. B., G. F. Kwakye, E. Herrero Hernandez and M. Aschner (2011). "Role of manganese in neurodegenerative diseases." J Trace Elem Med Biol **25**(4): 191-203.

Braak, H., R. A. de Vos, J. Bohl and K. Del Tredici (2006). "Gastric alpha-synuclein immunoreactive inclusions in Meissner's and Auerbach's plexuses in cases staged for Parkinson's disease-related brain pathology." Neurosci Lett **396**(1): 67-72.

Brown, I. A., J. L. McClain, R. E. Watson, B. A. Patel and B. D. Gulbransen (2016). "Enteric glia mediate neuron death in colitis through purinergic pathways that require connexin-43 and nitric oxide." Cell Mol Gastroenterol Hepatol **2**(1): 77-91.

Calne, D. B., N. S. Chu, C. C. Huang, C. S. Lu and W. Olanow (1994). "Manganism and idiopathic parkinsonism: similarities and differences." Neurology **44**(9): 1583-1586.

Capoccia, E., C. Cirillo, S. Gigli, M. Pesce, A. D'Alessandro, R. Cuomo, G. Sarnelli, L. Steardo and G. Esposito (2015). "Enteric glia: A new player in inflammatory bowel diseases." Int J Immunopathol Pharmacol **28**(4): 443-451.

Caporaso, J. G., J. Kuczynski, J. Stombaugh, K. Bittinger, F. D. Bushman, E. K. Costello, N. Fierer, A. G. Pena, J. K. Goodrich, J. I. Gordon, G. A. Huttley, S. T. Kelley, D. Knights, J. E. Koenig, R. E. Ley, C. A. Lozupone, D. McDonald, B. D. Muegge, M. Pirrung, J. Reeder, J. R. Sevinsky, P. J. Turnbaugh, W. A. Walters, J. Widmann, T. Yatsunenko, J. Zaneveld and R. Knight (2010). "QIIME allows analysis of high-throughput community sequencing data." Nat Methods **7**(5): 335-336.

Carabotti, M., A. Scirocco, M. A. Maselli and C. Severi (2015). "The gut-brain axis: interactions between enteric microbiota, central and enteric nervous systems." Ann Gastroenterol **28**(2): 203-209.

Chandra, S. V. and Z. Imam (1973). "Manganese induced histochemical and histological alterations in gastrointestinal mucosa of guinea pigs." Acta Pharmacol Toxicol (Copenh) **33**(5): 449-458.

Claus Henn, B., A. S. Ettinger, J. Schwartz, M. M. Tellez-Rojo, H. Lamadrid-Figueroa, M. Hernandez-Avila, L. Schnaas, C. Amarasiriwardena, D. C. Bellinger, H. Hu and R. O. Wright (2010). "Early postnatal blood manganese levels and children's neurodevelopment." Epidemiology **21**(4): 433-439.

Crossgrove, J. and W. Zheng (2004). "Manganese toxicity upon overexposure." NMR Biomed **17**(8): 544-553.

Dagda, R. K., S. J. Cherra, 3rd, S. M. Kulich, A. Tandon, D. Park and C. T. Chu (2009). "Loss of PINK1 function promotes mitophagy through effects on oxidative stress and mitochondrial fission." J Biol Chem **284**(20): 13843-13855.

de Lorgeril, M., S. Renaud, N. Mamelle, P. Salen, J. L. Martin, I. Monjaud, J. Guidollet, P. Touboul and J. Delaye (1994). "Mediterranean alpha-linolenic acid-rich diet in secondary prevention of coronary heart disease." Lancet **343**(8911): 1454-1459.

DeSantis, T. Z., P. Hugenholtz, N. Larsen, M. Rojas, E. L. Brodie, K. Keller, T. Huber, D. Dalevi, P. Hu and G. L. Andersen (2006). "Greengenes, a chimera-checked 16S rRNA gene database and workbench compatible with ARB." Appl Environ Microbiol **72**(7): 5069-5072.

Edgar, R. C. (2010). "Search and clustering orders of magnitude faster than BLAST." Bioinformatics **26**(19): 2460-2461.

Farina, M., D. S. Avila, J. B. da Rocha and M. Aschner (2013). "Metals, oxidative stress and neurodegeneration: a focus on iron, manganese and mercury." Neurochem Int **62**(5): 575-594.

Faure, M., D. Moennoz, F. Montigon, C. Mettraux, S. Mercier, E. J. Schiffrin, C. Obled, D. Breuille and J. Boza (2003). "Mucin production and composition is altered in dextran sulfate sodium-induced colitis in rats." Dig Dis Sci **48**(7): 1366-1373.

Ferraz, H. B., P. H. Bertolucci, J. S. Pereira, J. G. Lima and L. A. Andrade (1988). "Chronic exposure to the fungicide maneb may produce symptoms and signs of CNS manganese intoxication." Neurology **38**(4): 550-553.

Filpa, V., E. Moro, M. Protasoni, F. Crema, G. Frigo and C. Giaroni (2016). "Role of glutamatergic neurotransmission in the enteric nervous system and brain-gut axis in health and disease." Neuropharmacology **111**: 14-33.

Gagnon, J. F., R. B. Postuma, S. Mazza, J. Doyon and J. Montplaisir (2006). "Rapid-eye-movement sleep behaviour disorder and neurodegenerative diseases." Lancet Neurol **5**(5): 424-432.

Ghaisas, S., J. Maher and A. Kanthasamy (2016). "Gut microbiome in health and disease: Linking the microbiome-gut-brain axis and environmental factors in the pathogenesis of systemic and neurodegenerative diseases." Pharmacol Ther **158**: 52-62.

Ghosh, A., M. R. Langley, D. S. Harischandra, M. L. Neal, H. Jin, V. Anantharam, J. Joseph, T. Brenza, B. Narasimhan, A. Kanthasamy, B. Kalyanaraman and A. G. Kanthasamy (2016). "Mitoapocynin Treatment Protects Against Neuroinflammation and Dopaminergic Neurodegeneration in a Preclinical Animal Model of Parkinson's Disease." J Neuroimmune Pharmacol **11**(2): 259-278.

Gomez-Mejiba, S. E., Z. Zhai, H. Akram, Q. N. Pye, K. Hensley, B. T. Kurien, R. H. Scofield and D. C. Ramirez (2009). "Inhalation of environmental stressors & chronic inflammation: autoimmunity and neurodegeneration." Mutat Res **674**(1-2): 62-72.

Gulbransen, B. D. and K. A. Sharkey (2012). "Novel functional roles for enteric glia in the gastrointestinal tract." Nat Rev Gastroenterol Hepatol **9**(11): 625-632.

Harischandra, D. S., H. Jin, V. Anantharam, A. Kanthasamy and A. G. Kanthasamy (2015). "alpha-Synuclein protects against manganese neurotoxic insult during the early stages of exposure in a dopaminergic cell model of Parkinson's disease." Toxicol Sci **143**(2): 454-468.

Harischandra, D. S., N. Kondru, D. P. Martin, A. Kanthasamy, H. Jin, V. Anantharam and A. G. Kanthasamy (2014). "Role of proteolytic activation of protein kinase Cdelta in the pathogenesis of prion disease." Prion **8**(1): 143-153.

House, M. C. and M. G. Tansey (2017). "The gut-brain axis: is intestinal inflammation a silent driver of Parkinson's disease pathogenesis?" NPJ Parkinsons Dis. **3**(1).

Huang, C. C. (2007). "Parkinsonism induced by chronic manganese intoxication--an experience in Taiwan." Chang Gung Med J **30**(5): 385-395.

Huang, W. H. and J. L. Lin (2004). "Acute renal failure following ingestion of manganese-containing fertilizer." J Toxicol Clin Toxicol **42**(3): 305-307.

Huizinga, J. D. (1999). "Gastrointestinal peristalsis: joint action of enteric nerves, smooth muscle, and interstitial cells of Cajal." Microsc Res Tech **47**(4): 239-247.

Keen, C. L., J. L. Ensunsa, M. H. Watson, D. L. Baly, S. M. Donovan, M. H. Monaco and M. S. Clegg (1999). "Nutritional aspects of manganese from experimental studies." Neurotoxicology **20**(2-3): 213-223.

Kondakis, X. G., N. Makris, M. Leotsinidis, M. Prinou and T. Papapetropoulos (1989). "Possible health effects of high manganese concentration in drinking water." Arch Environ Health **44**(3): 175-178.

Kraft, A. D. and G. J. Harry (2011). "Features of microglia and neuroinflammation relevant to environmental exposure and neurotoxicity." Int J Environ Res Public Health **8**(7): 2980-3018.

Langley, M., A. Ghosh, A. Charli, S. Sarkar, M. Ay, J. Luo, J. Zielonka, T. Brenza, B. Bennett, H. Jin, S. Ghaisas, B. Schlichtmann, D. Kim, V. Anantharam, A. Kanthasamy, B. Narasimhan, B. Kalyanaraman and A. G. Kanthasamy (2017). "Mito-Apocynin Prevents Mitochondrial Dysfunction, Microglial Activation, Oxidative Damage, and Progressive Neurodegeneration in MitoPark Transgenic Mice." Antioxid Redox Signal.

Lee, Y. Y., A. Erdogan and S. S. Rao (2014). "How to assess regional and whole gut transit time with wireless motility capsule." J Neurogastroenterol Motil **20**(2): 265-270.

Leyva-Illades, D., P. Chen, C. E. Zogzas, S. Hutchens, J. M. Mercado, C. D. Swaim, R. A. Morrisett, A. B. Bowman, M. Aschner and S. Mukhopadhyay (2014). "SLC30A10 is a cell surface-localized manganese efflux transporter, and parkinsonism-causing mutations block its intracellular trafficking and efflux activity." J Neurosci **34**(42): 14079-14095.

Li, G. J., B. S. Choi, X. Wang, J. Liu, M. P. Waalkes and W. Zheng (2006). "Molecular mechanism of distorted iron regulation in the blood-CSF barrier and regional blood-brain barrier following in vivo subchronic manganese exposure." Neurotoxicology **27**(5): 737-744.

Li, Q., C. Wang, C. Tang, N. Li and J. Li (2012). "Molecular-phylogenetic characterization of the microbiota in ulcerated and non-ulcerated regions in the patients with Crohn's disease." PLoS One **7**(4): e34939.

Liu, X., K. A. Sullivan, J. E. Madl, M. Legare and R. B. Tjalkens (2006). "Manganese-induced neurotoxicity: the role of astroglial-derived nitric oxide in striatal interneuron degeneration." Toxicol Sci **91**(2): 521-531.

Livak, K. J. and T. D. Schmittgen (2001). "Analysis of relative gene expression data using real-time quantitative PCR and the 2(-Delta Delta C(T)) Method." Methods **25**(4): 402-408.

Logan, A. C. and M. Katzman (2005). "Major depressive disorder: probiotics may be an adjuvant therapy." Med Hypotheses **64**(3): 533-538.

Menezes-Filho, J. A., O. Novaes Cde, J. C. Moreira, P. N. Sarcinelli and D. Mergler (2011). "Elevated manganese and cognitive performance in school-aged children and their mothers." Environ Res **111**(1): 156-163.

Mulle, J. G., W. G. Sharp and J. F. Cubells (2013). "The gut microbiome: a new frontier in autism research." Curr Psychiatry Rep **15**(2): 337.

Neunlist, M., L. Van Landeghem, M. M. Mahe, P. Derkinderen, S. B. des Varannes and M. Rolli-Derkinderen (2013). "The digestive neuronal-glial-epithelial unit: a new actor in gut health and disease." Nat Rev Gastroenterol Hepatol **10**(2): 90-100.

Ngwa, H. A., A. Kanthasamy, H. Jin, V. Anantharam and A. G. Kanthasamy (2014). "Vanadium exposure induces olfactory dysfunction in an animal model of metal neurotoxicity." Neurotoxicology **43**: 73-81.

Noutsos, C., A. M. Perera, B. J. Nikolau, S. M. Seaver and D. H. Ware (2015). "Metabolomic Profiling of the Nectars of Aquilegia pubescens and A. Canadensis." PLoS One **10**(5): e0124501.

Parsons, S. P. and J. D. Huizinga (2010). "Transient outward potassium current in ICC." Am J Physiol Gastrointest Liver Physiol **298**(3): G456-466.

Pellegrini, C., L. Antonioli, R. Colucci, V. Ballabeni, E. Barocelli, N. Bernardini, C. Blandizzi and M. Fornai (2015). "Gastric motor dysfunctions in Parkinson's disease: Current pre-clinical evidence." Parkinsonism Relat Disord **21**(12): 1407-1414.

Pfeiffer, R. F. (2003). "Gastrointestinal dysfunction in Parkinson's disease." Lancet Neurol **2**(2): 107-116.

Savidge, T. C., M. V. Sofroniew and M. Neunlist (2007). "Starring roles for astroglia in barrier pathologies of gut and brain." Lab Invest **87**(8): 731-736.

Scheperjans, F., V. Aho, P. A. Pereira, K. Koskinen, L. Paulin, E. Pekkonen, E. Haapaniemi, S. Kaakkola, J. Eerola-Rautio, M. Pohja, E. Kinnunen, K. Murros and P. Auvinen (2015). "Gut microbiota are related to Parkinson's disease and clinical phenotype." Mov Disord **30**(3): 350-358.

Solinas, G., W. Naugler, F. Galimi, M. S. Lee and M. Karin (2006). "Saturated fatty acids inhibit induction of insulin gene transcription by JNK-mediated phosphorylation of insulin-receptor substrates." Proc Natl Acad Sci U S A **103**(44): 16454-16459.

Song, C., A. Kanthasamy, V. Anantharam, F. Sun and A. G. Kanthasamy (2010). "Environmental neurotoxic pesticide increases histone acetylation to promote apoptosis in dopaminergic neuronal cells: relevance to epigenetic mechanisms of neurodegeneration." Mol Pharmacol **77**(4): 621-632.

Takeuchi, K., I. Bjarnason, A. H. Laftah, G. O. Latunde-Dada, R. J. Simpson and A. T. McKie (2005). "Expression of iron absorption genes in mouse large intestine." Scand J Gastroenterol **40**(2): 169-177.

Veiga-Fernandes, H. and V. Pachnis (2017). "Neuroimmune regulation during intestinal development and homeostasis." Nat Immunol **18**(2): 116-122.

Vezer, T., A. Kurunczi, M. Naray, A. Papp and L. Nagymajtenyi (2007). "Behavioral effects of subchronic inorganic manganese exposure in rats." Am J Ind Med **50**(11): 841-852.

Vilz, T. O., M. Overhaus, B. Stoffels, M. Websky, J. C. Kalff and S. Wehner (2012). "Functional assessment of intestinal motility and gut wall inflammation in rodents: analyses in a standardized model of intestinal manipulation." J Vis Exp(67).

von Boyen, G. and M. Steinkamp (2010). "The role of enteric glia in gut inflammation." Neuron Glia Biol **6**(4): 231-236.

Wang, Q., G. M. Garrity, J. M. Tiedje and J. R. Cole (2007). "Naive Bayesian classifier for rapid assignment of rRNA sequences into the new bacterial taxonomy." Appl Environ Microbiol **73**(16): 5261-5267.

Wedler, F. C., R. B. Denman and W. G. Roby (1982). "Glutamine synthetase from ovine brain is a manganese(II) enzyme." Biochemistry **21**(25): 6389-6396.

Yu, Y. B. and Y. Q. Li (2014). "Enteric glial cells and their role in the intestinal epithelial barrier." World J Gastroenterol **20**(32): 11273-11280.

Zheng, W., H. Kim and Q. Zhao (2000). "Comparative toxicokinetics of manganese chloride and methylcyclopentadienyl manganese tricarbonyl (MMT) in Sprague-Dawley rats." Toxicol Sci **54**(2): 295-301.

Zota, A. R., A. S. Ettinger, M. Bouchard, C. J. Amarasiriwardena, J. Schwartz, H. Hu and R. O. Wright (2009). "Maternal blood manganese levels and infant birth weight." Epidemiology **20**(3): 367-373.

Figure legends

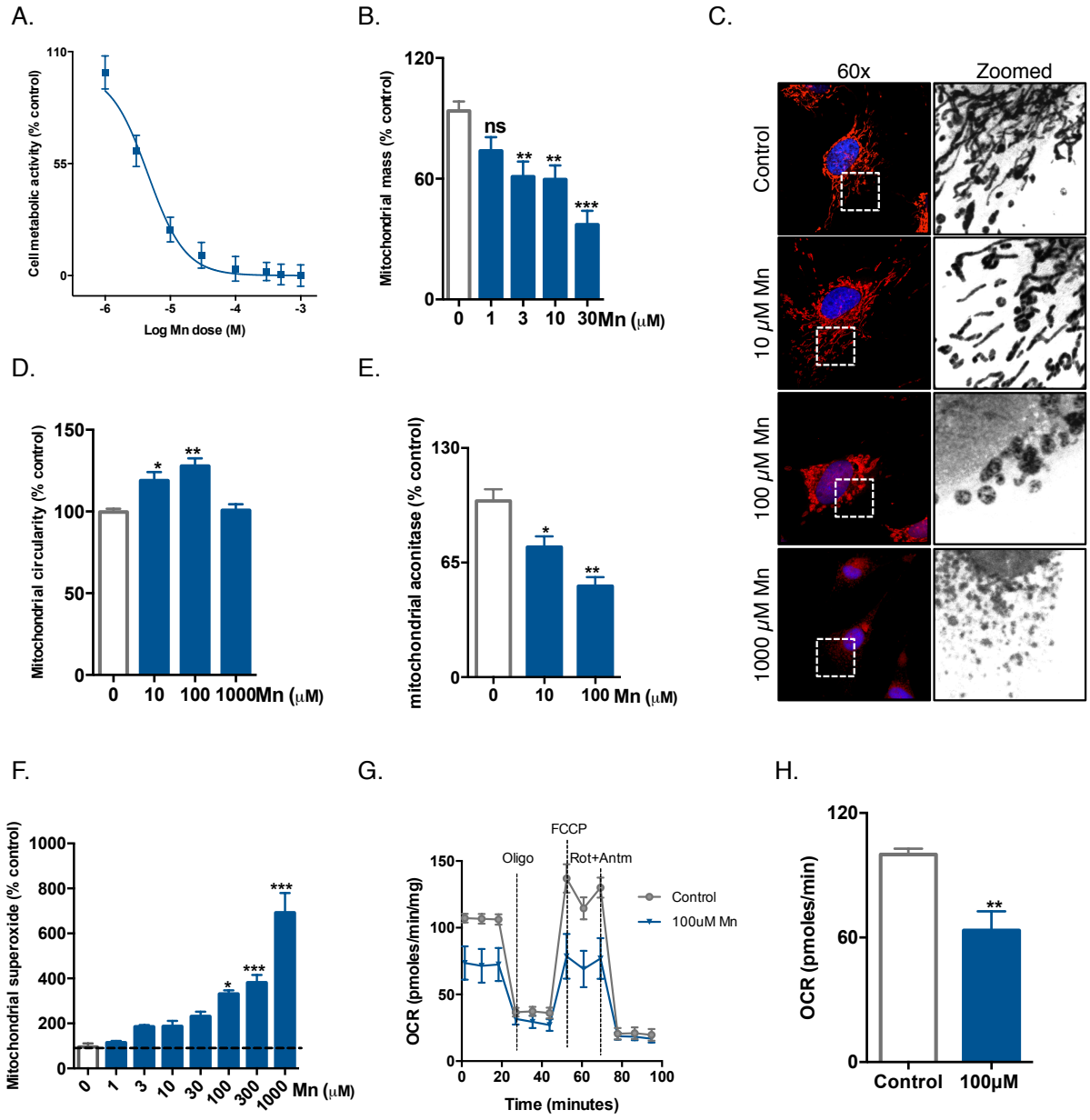

Figure 1. EGCs are highly sensitive to Mn. (A) EGCs were treated with increasing concentrations of Mn for 24 h. Cell viability was measured by MTS assay. Values are normalized to control and expressed as percent control. (B) EGCs treated with 1-30 μM Mn for 24 h were stained with 100 nM MitoTracker Green FM for 20 min. When this green fluorescence intensity is normalized to cell number (counted by Hoechst staining), it is

directly proportional to mitochondrial mass in each well. (C) Mitochondrial morphology was visualized by staining control and Mn-treated cells with 200 nM MitoTracker Red for 10 min. Scale bar = 10 μm. (D) Mitochondrial circularity expressed as percent control was determined by ImageJ analysis of mitochondria from seven different images/group. (E) EGC's were treated with 10 or 1000 μM Mn for 24 h then mitochondrial-aconitase activity was measured using a commercial kit as per manufacturer's instructions. (F) Dose dependent increase in mitochondrial superoxide upon Mn treatment was measured by MitoSox dye fluorescence. (G) Tracing showing oxygen consumption rate (OCR) of EGCs treated with 0, 5, 10 or 100 μM Mn for 24 h as measured by Seahorse XF24^{e}. (H) Dose dependent decrease in ATP production in EGCs treated with increasing concentration of Mn. (G) ATP production of untreated and Mn-treated EGCs after 24 hour exposure. Data represented as mean ± SEM (*$p<0.05$, **$p<0.01$, ***$p<0.001$, ns = non-significant) of four to six replicates.

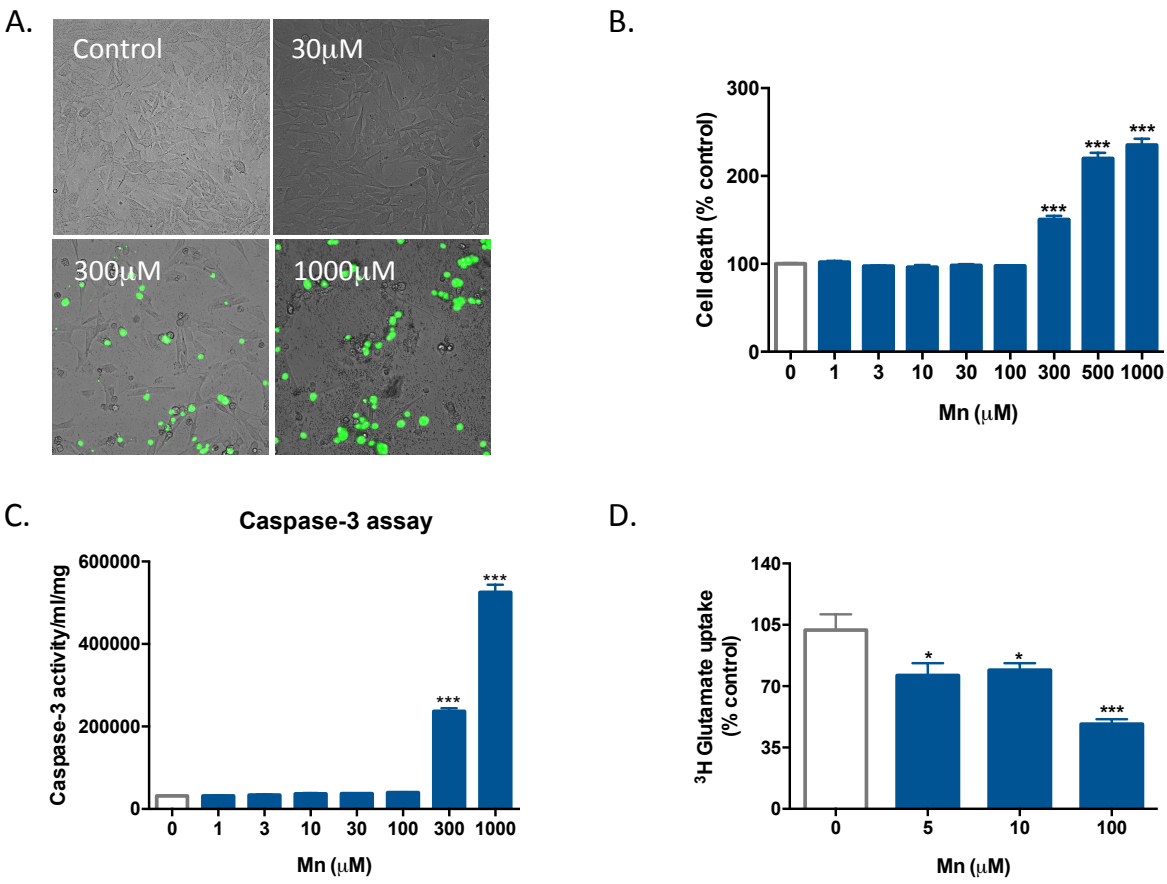

Figure 2. Enteric glial cytotoxicity occurs at higher concentrations of Mn. (A-B) Phase contrast and green fluorescence super-imposed images of EGCs treated with different doses of Mn (1-1000 μM) for 24 h. Cell death, which is expressed as % control and is directly proportional to green fluorescence intensity, was visible only at doses of 300 μM Mn and above. (C) Caspase-3 activity in EGCs treated with increasing dose of Mn for 24 hours. Significant caspase-3 activity was seen in 300 μM and 1000 μM Mn treatments. (D) Decreased ability of Mn treated EGCs to re-uptake L-[3,4 ^{3}H] glutamic acid. Data represented as the group mean ± SEM from at least 3 experiments. Asterisks (***$p<0.001$, **$p<0.01$ and *$p<0.05$) indicate significant differences between Mn-treated groups and control.

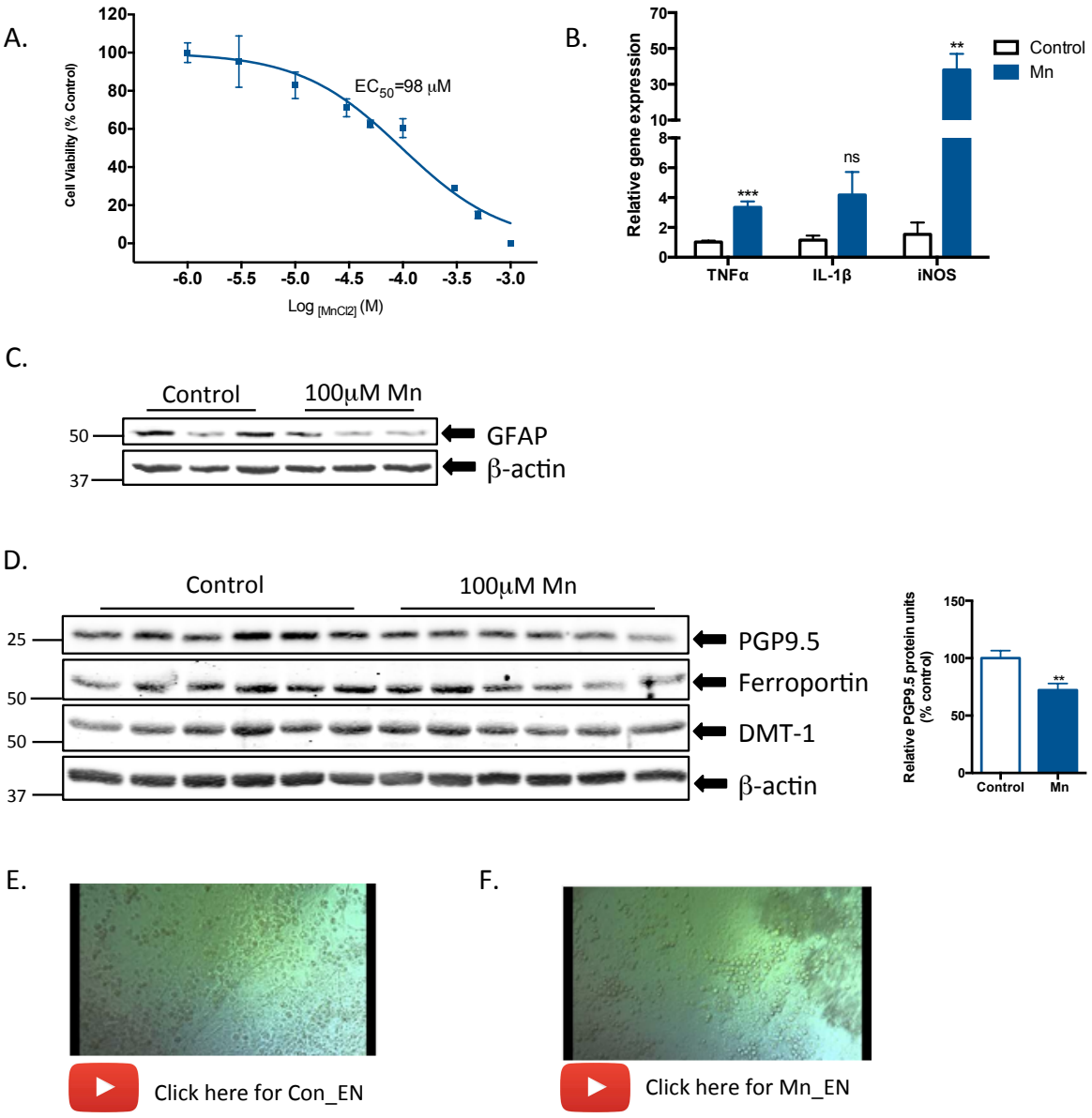

Figure 3. Mn treatment induces inflammation and enteric neuronal death in a primary enteric mixed culture. (A) Cell viability of the primary enteric mixed culture treated with increasing doses of Mn was measured by MTS assay, with values normalized to control and expressed as percent control (n=6). (B) qRT-PCR analysis of TNFα, IL-1β and iNOS mRNA transcripts, normalized to 18S rRNA expression. (C) Representative Western blot image showing decreased GFAP expression following 100 μM Mn exposure. (D) Western blot analysis of enteric neuron marker PGP9.5 and Mn transporters DMT1 and ferroportin

expression in untreated and 100 μM Mn-treated primary enteric mixed cultures (n=6). Quantification of bands revealed reduced PGP9.5 and ferroportin expression in Mn-treated samples. Expression of β−actin was used as a loading control. (E) Video showing spontaneous contractions in a 3-week old primary enteric culture. (F) Loss of spontaneous contractions in 3-week old primary enteric culture following 24 h treatment with 100 μM Mn. Data represented as the group mean ± SEM from at least 3 experiments. Asterisks (***p<0.001 and **p<0.01) indicate significant differences between Mn-treated groups and control.

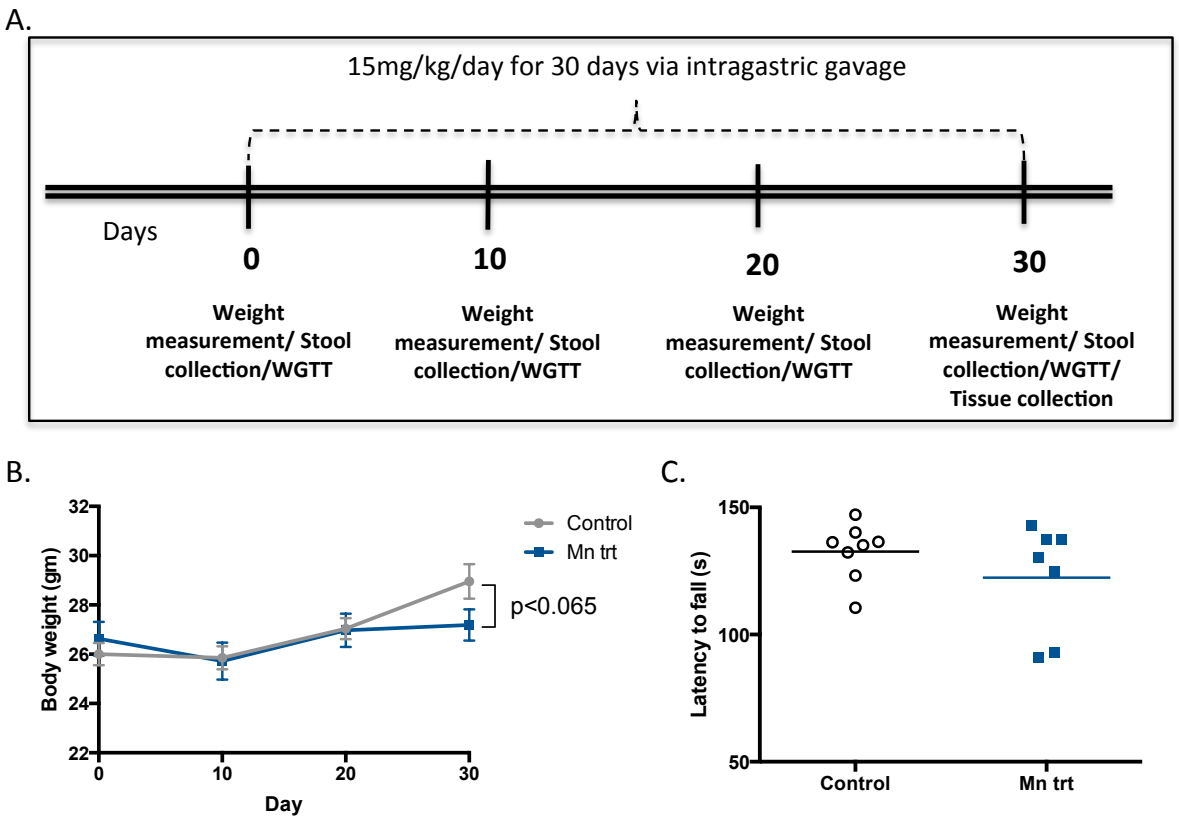

Figure 1 continued

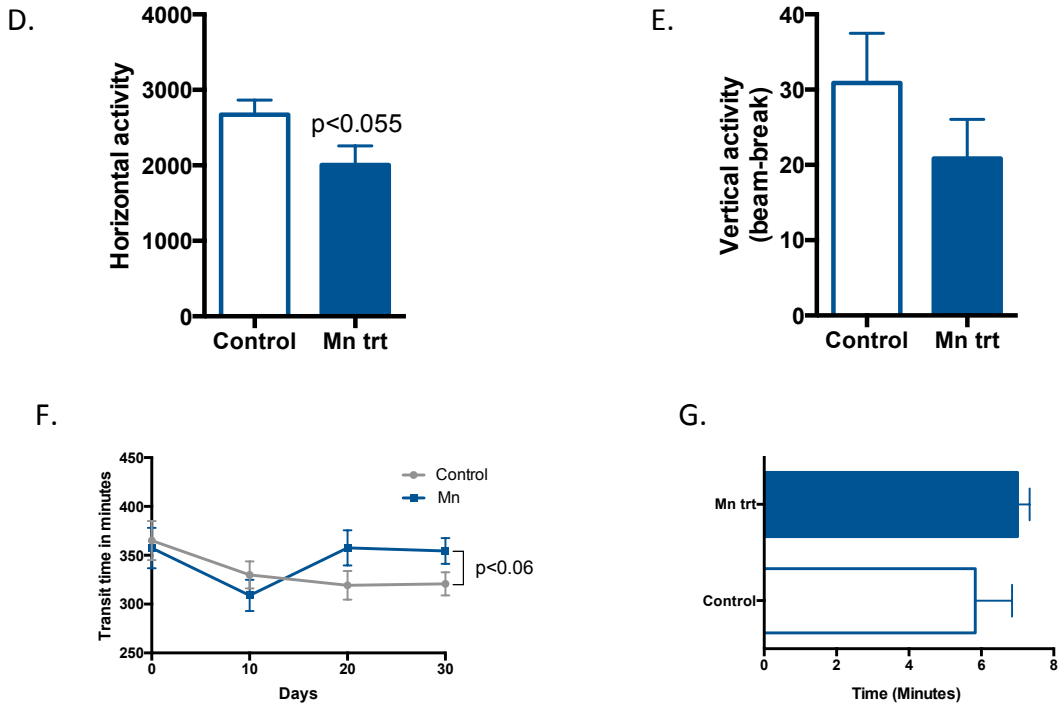

Figure 4. Altered gastrointestinal motility but no behavioral changes in mice treated with a low dose of Mn. (A) Schematic representation of the Mn treatment paradigm in C57 mice. (B) Mouse body weight development over the course of Mn study. (C) Rotarod test showing no statistical difference between control and Mn-treated mice with regards to balance and co-ordination. (D) Open-field test showing no difference in horizontal activity between the two groups. (E) No difference in vertical activity between the two groups as measured by open-field test. (F) Whole gut transit time (WGTT) as measured by carmine red meal over the course of the study. Increased WGTT was observed in the treatment group from day 20 onwards when compared to age-matched controls (n=13). (G) Bead latency test to determine distal colon transit time. No significant difference was observed between groups. Data represented as the group mean ± SEM from n=10 or n=13. Asterisks (***p<0.001 and **p<0.01) indicate significant differences between Mn-treated group and control.

A.

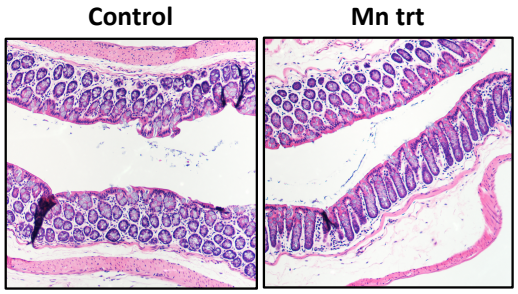
Control
Mn trt

B.

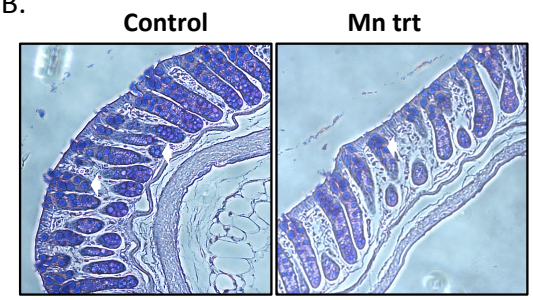
Control
Mn trt

C.

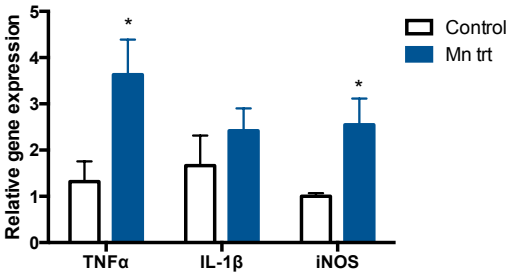
Relative gene expression
5
4
3
2
1
0
*
*
Control
Mn trt
TNFα
IL-1β
iNOS

D.

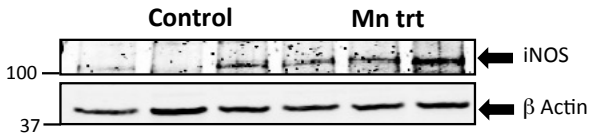
Control
Mn trt
100
37
iNOS
β Actin

E.

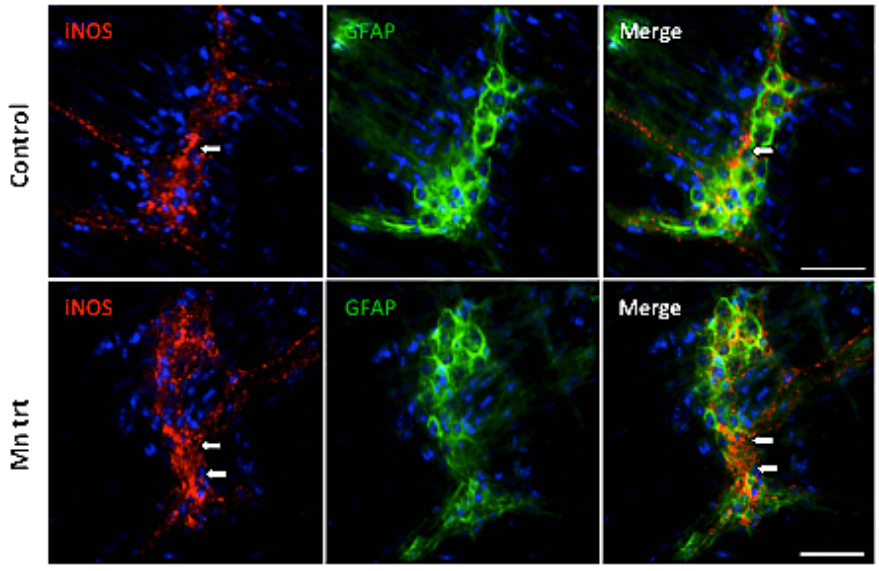
Control
Mn trt
iNOS
GFAP
Merge
iNOS
GFAP
Merge

Figure 5 continued

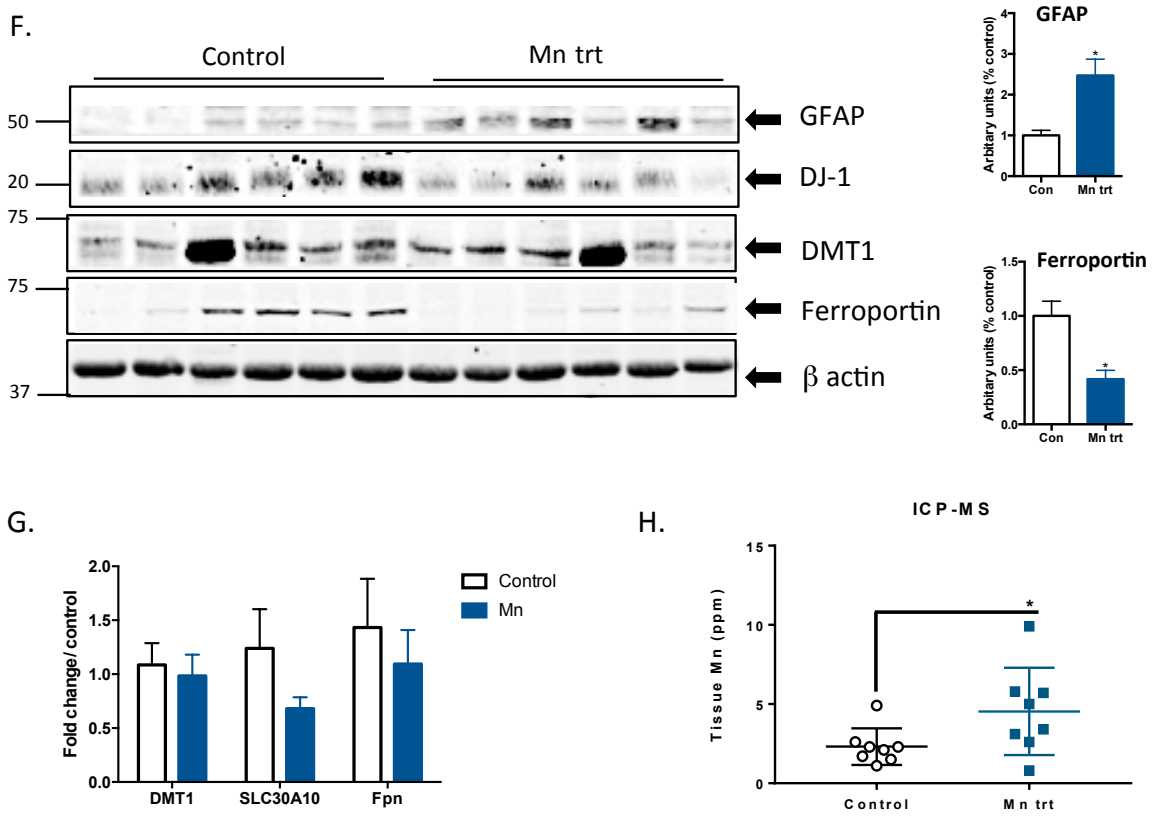

Figure 5. Evidence of colonic inflammation in mice treated with a low dose of Mn. (A) Representative 20x images of H&E-stained colon sections from untreated and Mn-treated groups (n=3). Scale bar = 100 µm. (B) Representative 20x images of Ab-PAS-stained colon sections. Mn-treated mice had fewer goblet cells and consequently less mucin production relative to controls as evidenced by decreased mucin staining in the colon sections of the treatment group. Scale bar = 100 µm. (C) qRT-PCR analysis of TNFα, IL-1β and iNOS mRNA transcripts, normalized to 18S rRNA expression (n=6). (D) Western blot analysis of iNOS production in colon samples from untreated and Mn-treated mice. (E) Representative 40x immunofluorescence images showing increased iNOS production in the myenteric plexus of Mn-treated mouse when compared to control. Scale bar = 100 µm. Arrows indicate

presence of punctate iNOS staining. (F) Western blot showing larger presence of EGCs, decreased mitochondrial protein DJ-1 expression along with decreased expression of ferroportin receptor indicates intestinal dysregulation in Mn treated mice. (G) Lower SLC30A10 transcripts in Mn-treated mice compared to control mice indicating dysreglation in Mn homeostasis in colon tissue. (H) ICP-MS data showing higher Mn^{+2} content in colon tissue. Asterisks (*p<0.05 and **p<0.01) indicate significant differences between Mn-treated group and control.

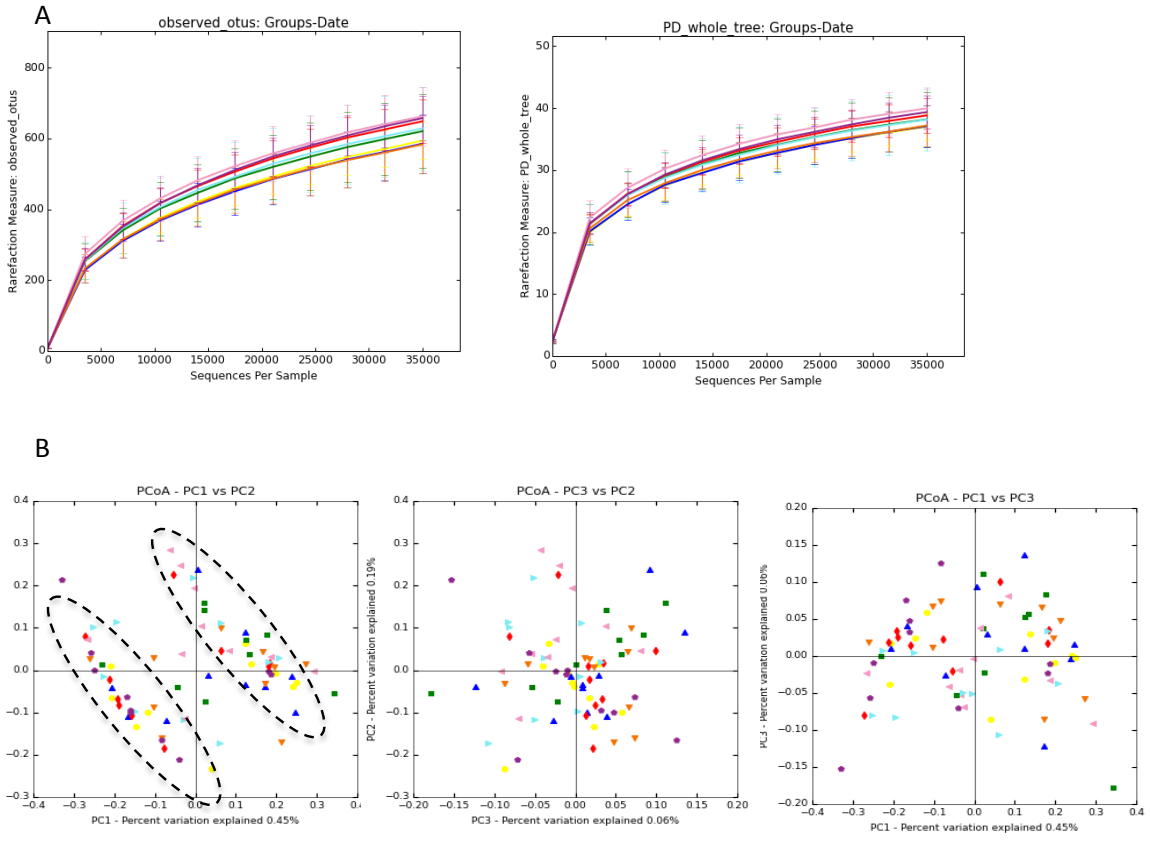

Figure 6 continued

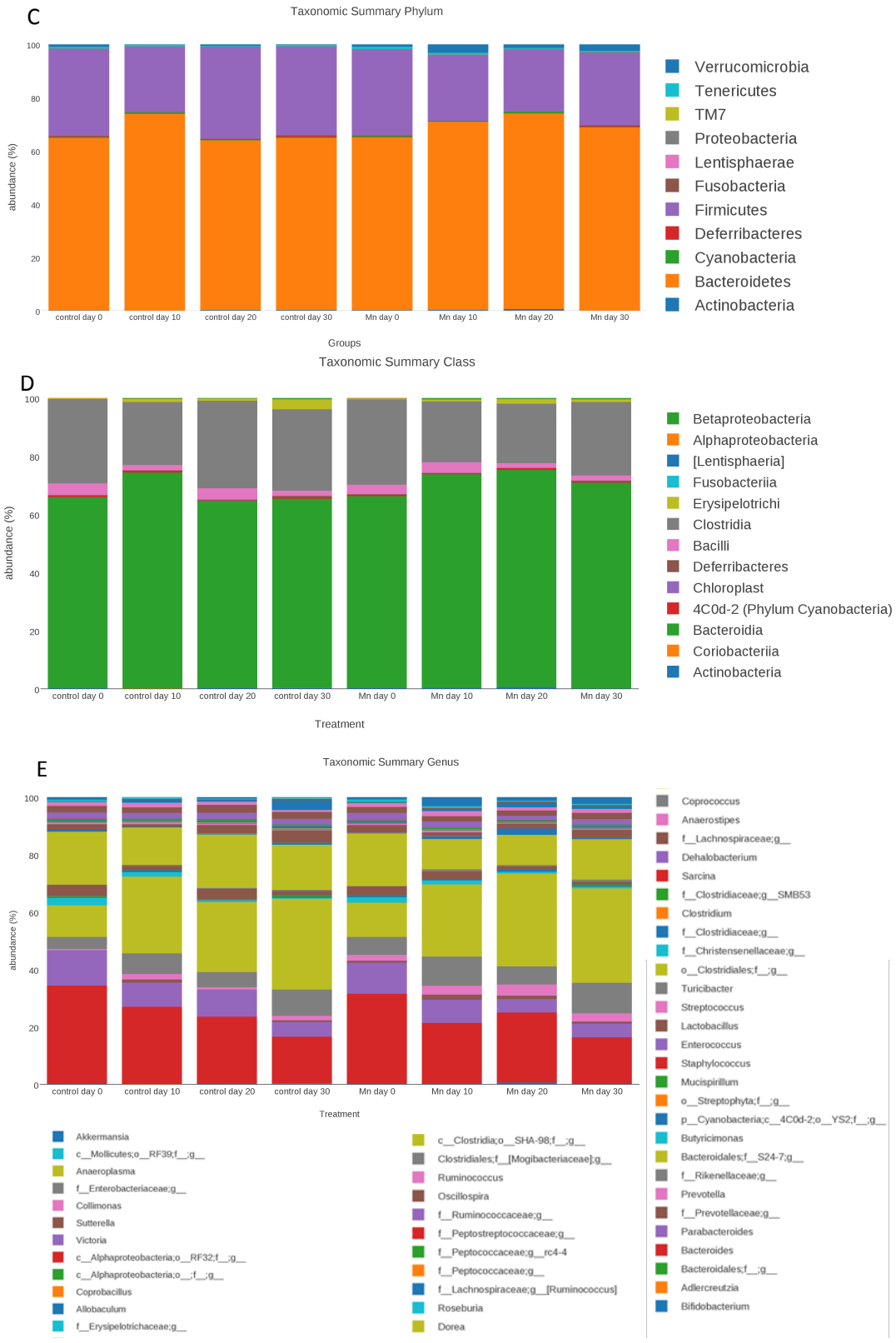

Figure 6. Changes in the gastrointestinal microbiota following manganese treatment. Taxonomic summaries at the phylum (A), class (B), and genus (C) levels. Rarefaction plots of observed species richness (D) and Faith's Phylogenetic Diveristy (E). Weighted Unifrac PCoA plots (F) where each point is a single sample and each color represents a group.

A.

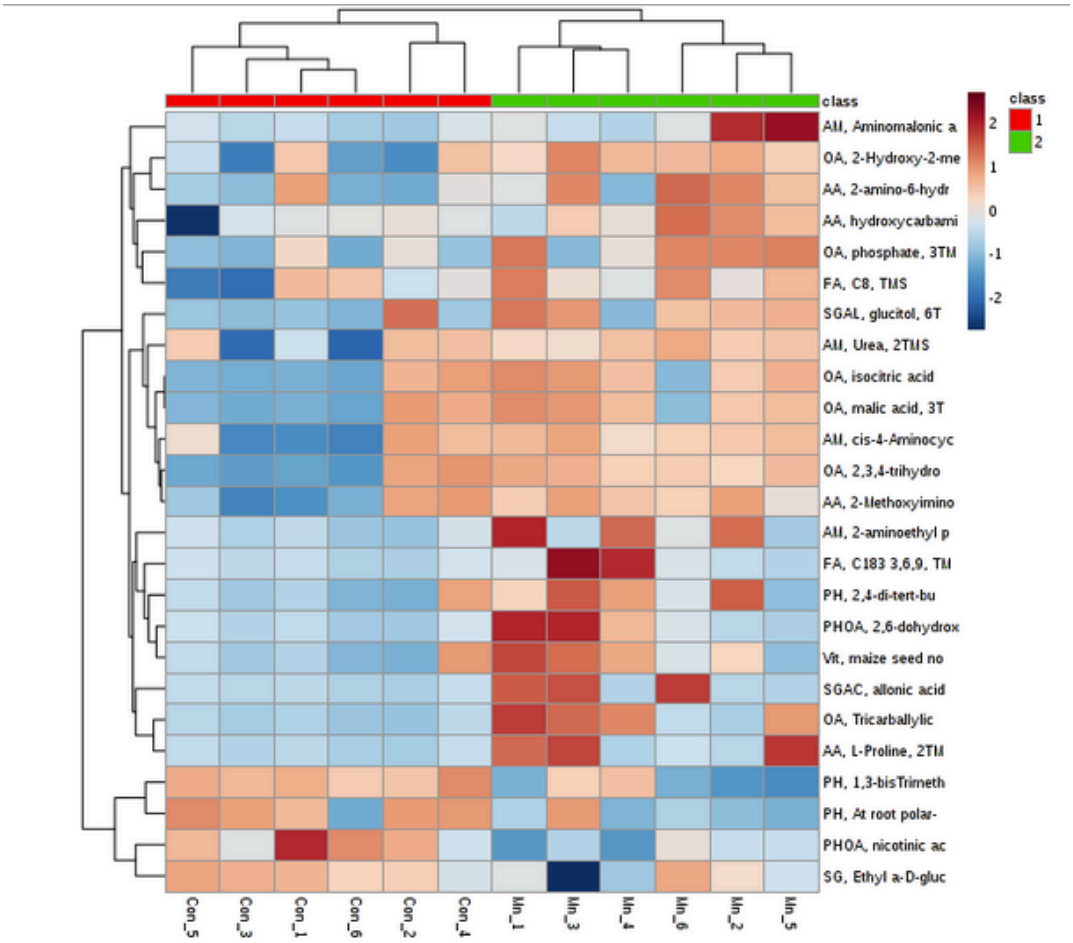

Figure 7 continued

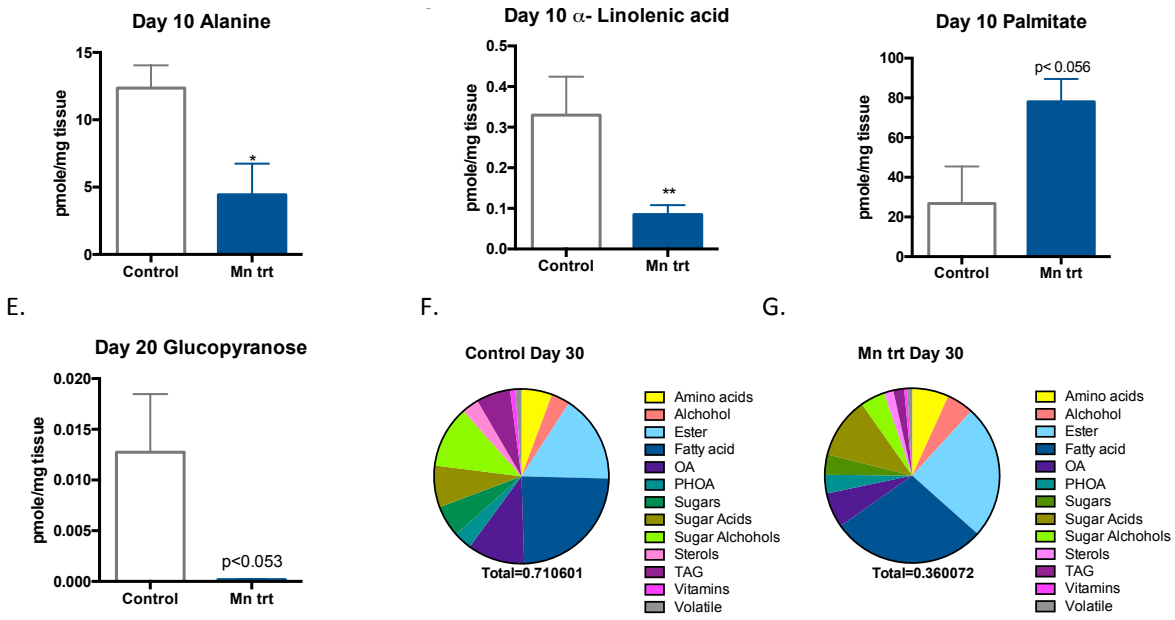

Figure 7: Changes in fecal metabolites following chronic manganese exposure. (A) Heat-map showing log-transformed GC-MS data (n=4-6). Color bar values correspond to log abundance of metabolites in individual samples measured in metabolomic analysis. (B) Alanine in pmoles per mg fecal sample in control and Mn-treated groups at day 10 (n=3-4). (C) Oleic acid in pmoles per mg fecal sample in control and Mn-treated groups at day 10 (n=3-4). (D) α-linolenic acid in pmoles per mg fecal sample in control and Mn-treated groups at day 10 (n=3-4). (E) Pie-chart denoting global changes in different classes of fecal metabolites in control samples at day 30. (F) Pie-chart denoting global changes in different classes of fecal metabolites in Mn exposed samples at day 30.

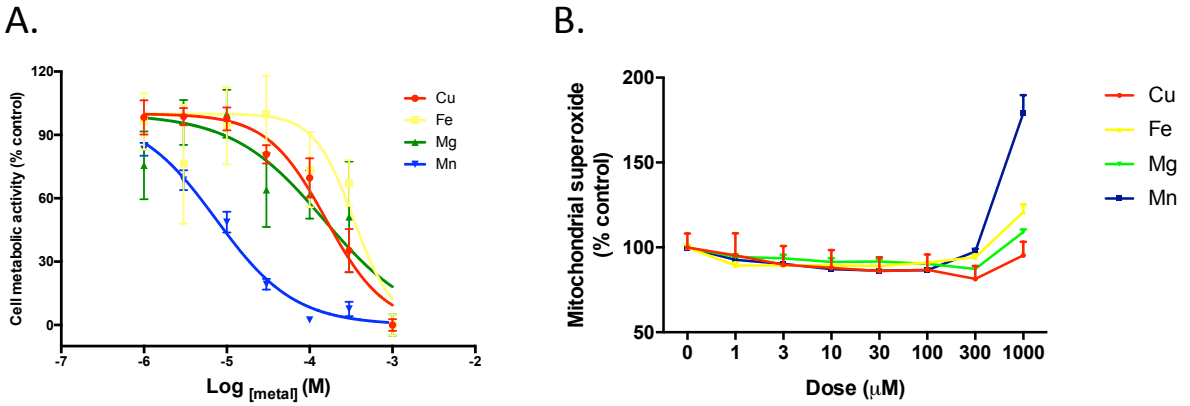

Supplementary Figure 1: Enteric glial cells are most susceptible to Mn-induced mitochondrial stress. (A) MTS assay of EGC's (n=6) treated with increasing doses of Copper (Cu), Iron (Fe), Magnesium (Mg) and Manganese (Mn). A potent decrease in metabolic activity was observed in cells treated with Mn compared to other metals. Values are normalized to control and expressed as percent control. (B) MitoSox assay showing significant increase in mitochondrial superoxide production mainly in EGC;s treated with Mn compared to other metals. Asterisks (*p<0.05 and **p<0.01) indicate significant differences between different treatments and control.

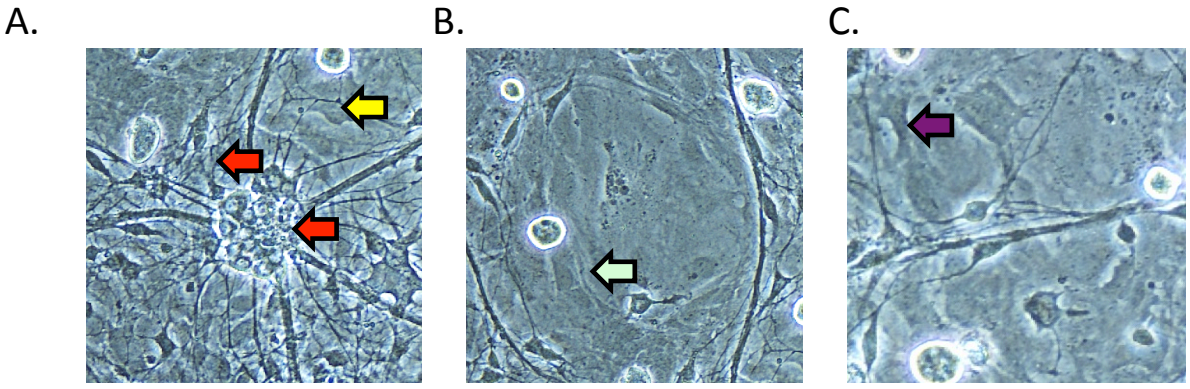

Supplementary Figure 2: Heterogeneous cell population in primary enteric mixed culture. (A) 40x image showing neurospheres (red arrow) as well as differentiated neurons growing in the culture after 14 days *in vitro*. (B-C). Fibroblasts (purple arrow) and

endothelial cells (green arrow) growing in confluent layers on the cell culture plate 10 days *in vitro*.

Plasma chemistry

	Albumin	Alk. Phosphatase	ALT	Amylase	Bilirubin	BUN	Calcium	Phosphorous	Creatinine	Glucose	Sodium	Potassium	Total Protein
Control	3.5	40	19	971	0.2	13	10.9	10.3	0.2	327	157	9	5.02
	4.2	44	33	1126	0.2	14	11.4	7.9	0.2	345	167	9	6
	3.63	51	26	897	0.2	13	10	8	0.2	182	175	9	5.5
	4.1	51	34	1108	0.2	13	11	7.7	0.2	336	160	9	5.9
	3.5	41	27	967	0.2	13	10.8	10.3	0.2	327	158	9	5.2
Manganese	4.1	49	39	1220	0.2	16	10.8	7.5	0.2	337	180	9	6
	4	44	24	1044	0.3	12	11	6.9	0.2	246	165	9	5.7
	3.3	50	25	1180	0.2	15	12.2	9.6	0.2	316	180	9	6.7
	3.8	66	23	945	0.3	18	10.8	5.7	0.2	195	180	8	5.8
	3.8	39	22	1162	0.2	14	10.7	8.1	0.2	198	180	7.5	5.9
	3.3	77	25	895	0.3	20	106	8.4	0.2	235	164	9	5.5
p value	0.74	0.23	0.71	0.43	0.074	0.074	0.38	0.2	0.073	0.24	0.039	0.2	0.14

Supplementary Figure 3: Trend of increase bile salt secretion in Mn-treated mice. Clinical pathology results of plasma samples showing mildly elevated bilirubin and blood urea nitrogen (BUN) levels in Mn treated mice compared to control mice ($p<0.07$).

ICP-MS of colon tissue

	Cd^{+2}	Ca^{+2}	Cr^{+2}	Co^{+2}	Cu^{+2}	Fe^{+2}	Mg^{+2}	Mb^{+2}	P^{+2}	K^{+2}	Se^{+2}	Na^{+2}	Zn^{+2}
Control	0.029	219	0.115	0.045	3	31	216	0.19	2387	3136	0.36	1665	38
	0.034	321	0.173	0.085	5	52	347	0.26	4069	5648	0.78	2332	66
	0.009	293	0.256	0.086	4	34	287	0.08	2960	3810	0.44	1318	57
	0.002	214	0.153	0.051	3	27	218	0.15	2703	3837	0.31	1339	59
	0.006	213	0.323	0.043	3	34	206	0.21	2321	2916	0.27	1838	39
	0.027	289	1.155	0.12	5	64	257	0.19	2706	3398	0.47	1439	68
	0.016	272	0.442	0.07	6	36	244	0.22	2804	3465	0.53	1493	44
	0.005	344	0.098	0.054	3	39	255	0.12	2866	3742	0.47	1080	36
Manganese	0.002	647	0.27	0.131	7	76	602	0.52	6203	8095	0.81	2924	98
	0.009	256	0.217	0.081	99	43	246	0.25	2778	3676	0.4	1528	60
	0.005	413	0.282	0.088	3	43	243	0.2	2641	3488	0.45	1271	38
	0.017	374	0.14	0.065	3	33	265	0.24	2539	3136	0.36	1350	42
	0.014	277	0.267	0.084	3	44	266	0.23	3134	3777	0.49	1591	48
	0.033	526	1.241	0.158	6	101	366	0.4	4878	5989	1.03	2463	197
	0.003	218	0.168	0.054	3	33	238	0.18	2422	2826	0.47	1443	40
	0.006	190	0.212	0.045	3	30	188	0.18	2397	3060	0.45	1377	35
p value	0.41	0.14	0.95	0.27	0.34	0.29	0.35	0.06	0.34	0.48	0.32	0.49	0.36

Supplementary Figure 4: ICP-MS data for trace metals. With the exception of Na^{+2}, no significant differences were seen between the two groups for the common tested trace metal as shown in the table.

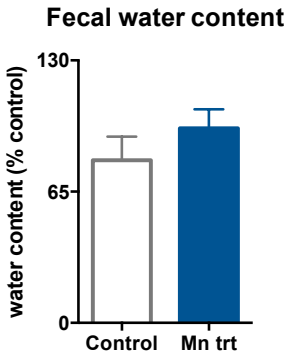

Supplementary Figure 5: Fecal water content. No change in fecal water content between control and Mn-exposed mice.

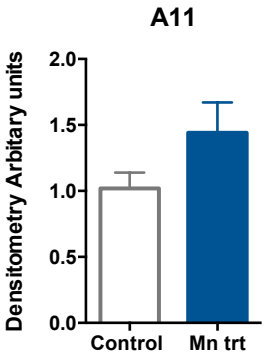

Supplementary Figure 5: No change in oligomeric protein expression between control and Mn-exposed mice. Dot Blot analysis of oligomeric protein in colon lysates from control and Mn-treated mice (n=5)

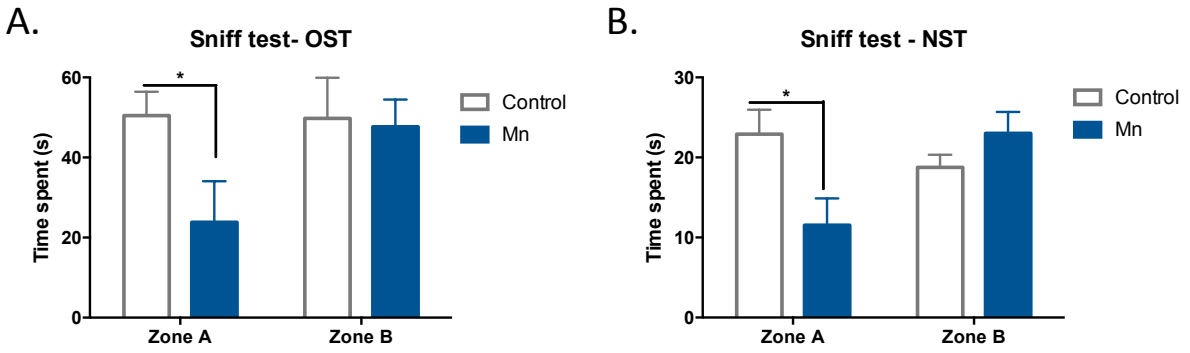

Supplementary Figure 6: Olfaction test. (A) Mn-treated mice showed lower ability to detect pheromones released from opposite sex bedding (OST). (B) Mn-treated mice showed lower ability to detect vanilla scent from non-scented (water) area (NST). Asterisks (*$p<0.05$) indicate significant differences between Mn-treated group and control.

CHAPTER III

SPATIAL DIFFERENCES IN GASTROINTESTINAL MOTILITY IN THE MITOPARK MOUSE MODEL OF PARKINSON'S DISEASE

Manuscript to be submitted to Neurotoxicology

Ghaisas, Shivani; Langley, Monica R; Palanisamy, Bharati; Jin, Huajun; Kanthasamy, Arthi; Anantharam, Vellareddy; Kanthasamy, Anumantha G

Parkinson Disorders Research Program, Iowa Center for Advanced Neurotoxicology, Department of Biomedical Sciences, Iowa State University, Ames, IA 50011.

‡**Address correspondence and proof requests to**

Dr. A.G. Kanthasamy,

Parkinson Disorders Research Laboratory,

Department of Biomedical Sciences, 2062 CVM Building,

Iowa State University, Ames, IA, 50011

Tel.: (515) 294-2516, Fax: (515) 294 2315,

E-mail: akanthas@iastate.edu

Keywords: Parkinson's disease, gastrointestinal motility, non-motor symptoms, intestinal inflammation

Abstract

Gastrointestinal (GI) disturbances are one of the earliest symptoms affecting most patients with Parkinson's disease (PD). In many cases these symptoms are observed years before motor impairments become apparent. Hence there is an increasing interest in understanding the molecular and cellular mechanisms that potentiate this early GI dysfunction. The MitoPark model is a chronic, progressive mouse model recapitulating several key pathophysiological aspects of PD. However GI dysfunction has not been categorized in this model. Here we show that GI motility was one of the first non-motor symptoms to develop, seen as early as 8 weeks with significantly different transit times from 12 weeks onwards. These symptoms are observed well before motor symptoms develop paralleling PD progression in humans. We also observed increased colon transit time and reduced fecal water content indicating constipation at 24 weeks of age compared to age matched littermate controls. Intestinal inflammation was observed with increased expression of iNOS and TNFα in the small and large intestine. Specifically, iNOS was observed mainly in the enteric plexi indicating enteric glial cell activation. At 24 weeks, there was pronounced loss of tyrosine hydroxylase positive neurons both in the mid-brain region as well as the gut leading to a corresponding decrease in dopamine production. However, despite loss of dopaminergic neurons, the total number of neurons did not significantly differ between the two groups. We also observed decreased DARPP-32 expression in the colon validating the loss of dopaminergic neurons in the gut. These mice also develop misfolded proteins as evidenced by positive oligomeric protein expression. Notably, exposure of young mice to an environmental toxin Mn, at a low dose of 10mg/ Kg body weight for 4 weeks lead to a dramatic increase in misfolded proteins when compared to unexposed MitoPark mice.

Together, the data sheds more light on the role of dopamine in maintaining intestinal health. Importantly, this model recapitulates the chronology and development of GI dysfunction along with other non-motor symptoms and can become an attractive model for pre-clinical assessment of the efficacy of new anti-parkinsonian drugs.

Introduction

Parkinson's disease (PD) is a chronic and progressive neurological disorder caused by loss of dopaminergic neurons present in the *substantia nigra* region of the brain. This disorder displays an array of symptoms, the most prominent being a sustained loss of motor control leading to bradykinesia, muscle rigidity, postural instability and poor coordination. Since publication of the medical essay "The Shaking Palsy" by Dr. James Parkinson, it has been known that PD is a multicentric disease affecting even the autonomic nerves and the enteric nervous system (ENS). Today, a number of retrospective studies and clinical observations of PD patients have shown the presence of many non-motor symptoms that may precede the disorder often decades before motor symptoms are diagnosed. The common non-motor symptoms include, dysphagia, constipation, hyposmia and sleep disturbances (Chen et al., 2013). An increasing number of studies have reported gastrointestinal problems especially constipation in 25-80% PD patients. Aside from constipation, PD patients also experience, dysphagia, excessive drooling, nausea and dyspepsia (Cersosimo and Benarroch, 2012; Pfeiffer, 2003).

Gastrointestinal motility is controlled by neural and hormonal signals arising from central and peripheral nervous systems. Notably, the enteric nervous system (ENS) plays an important role in maintaining a healthy gastrointestinal (GI) physiology by influencing

smooth muscle contraction and relaxation, absorption of nutrients and cross-talk with the immune cells patrolling the GI tract (Hansen, 2003). Of the many neurotransmitters that are produced in the GI tract, dopamine and serotonin are two important neurotransmitters involved in GI motility. Depending on the receptor subtype and location, both neurotransmitters modulate excitatory and inhibitory signals leading to location-specific contraction or relaxation of the GI tract. This complex signaling process results in coordinated peristalsis of the gut thus enabling nutrient absorption and proper waste removal. In the case of PD, an imbalance in dopamine secretion and/or reuptake has been speculated to induce irregular peristalsis (Greene et al., 2009; Zhang et al., 2007). This irregular peristalsis can lead to overgrowth of bacteria in the small bowel, sub optimal nutrient absorption and inadequate defecation. This irregularity in intestinal transit and hence absorption may also be an important reason why levodopa - despite being the therapeutic agent of choice given to PD patients- still shows inconsistent success in alleviating motor symptoms. Till date, several *ex vivo* studies on intestinal smooth muscles have been carried out, however the results differ from one another due to inconsistent sample preparation as well as the use of non-selective agonists or antagonists (Walker et al., 2000). Similarly, toxin-based rodent models of PD have also shown inconsistent results with regards to small and large intestinal motility(Anderson et al., 2007; Greene et al., 2009; Pellegrini et al., 2016). Hence there is a need to develop an in vivo model of PD that faithfully reproduces most of the GI symptoms seen in PD.

The MitoPark mouse model is generated by the *cre/lox* system wherein the mitochondrial transcription factor A (Tfam) is selectively removed from dopaminergic (DAT positive) neurons. This results in a progressive development of motor symptoms, notably loss of

coordination and muscle rigidity. Previously, other groups have shown development of non-motor symptoms in the MitoPark mouse model (Ekstrand et al., 2007; Galter et al., 2010). However, despite being an important non-motor symptom, GI disturbances in this model have not been described. Hence the aim of this study was to characterize GI motility and intestinal inflammation using a combination of motility and neurochemical tests.

Materials and Methods

Chemicals

Manganese (II) chloride tetrahydrate (MnCl2) and β-actin antibody were purchased from Sigma. Antibodies for PGP9.5 (Cat # AB1761-I) and GFAP (Cat # MAB3402) and Tyrosine hydroxylase (TH, Cat. # MAB318) were purchased from Millipore while iNOS (Cat # sc-651) and Bax (Cat # sc-493) antibodies were purchased from Santa Cruz. Hoechst 33342 nuclear stain was purchased from Invitrogen (H3570).

Experimental design

MitoPark mice were kindly provided by Dr. Nils-Goran Larson at the Karolinska Institue, Stockholm (Ekstrand et al., 2007). MitoPark mice (DAT $^{+/Cre}$: Tfam $^{LoxP/LoxP}$) and their littermate controls (DAT$^{+/+}$: Tfam $^{+/LoxP}$) were fed *ad libitum* and maintained at 22°C under a 12h light/dark cycle in standard conditions approved and supervised by the Institutional Animal Care and Use Committee (IACUC) at Iowa State University. Mice were weighed and subjected to behavioral tests every four weeks. At the age of 24-weeks, mice were euthanized via cervical dislocation and gastrointestinal tissue (colon, ileum and duodenum) as well as various microdissected brain tissues were collected and stored at -80°C until

further analysis. Neurochemical, biochemical, and histological studies were performed following sacrifice at age 24 wks.

In vivo GI motility assessment

Gastric emptying

Gastric emptying was performed on 24 week MitoPark and littermate controls. Prior to the experiment, mice were fasted for 12 hours with free access to water. At the time of the experiment, these mice were given access to standard laboratory diet for 1h. The amount of food consumed was calculated based on food weight before and after access. Two hours following food consumption, animals were sacrificed and the stomach was removed. Gastric emptying was calculated according to the following formula: gastric emptying (%) = [1 - (weight of food remaining in the stomach/weight of food intake)] * 100 (Tasselli et al., 2013).

Whole gut transit time (WGTT)

Carmine red is a red dye that is not absorbed by the gut during digestion but excreted with other waste products. Hence a solution of this dye was used to determine total gastrointestinal transit time in MitoPark and littermate control mice from 8 to 24 weeks of age. A solution of carmine red (60 mg/ml) in 0.5% (vol/vol) Carboxymethyl cellulose was administered by oral gavage using a 24 gauge round-tip feeding needle (Tasselli et al., 2013). The volume of carmine red solution used for each animal was calculated based on animal weight (0.3mg/g body weight). Based on pilot studies, we found that following gavage; animals did not show presence of red fecal pellets for one hour. Hence animals were monitored at 15 min intervals for the presence of carmine red one hour following oral

gavage. Again, prior pilot studies indicated that majority of the mice showed red fecal pellets by 8 hours and hence the experiment was terminated after 8 hours. Total gastrointestinal (GI) transit time is considered as the interval between the initiation of gavage and the time of first observance of carmine red in stool. Animals whose stool had no dye even after a maximum observation time of 8 h were recorded as >8 hours.

Bead latency

Distal colonic motility was measured by the bead latency test. Mice were anesthetized with isoflurane and a lubricated, 2 mm-diameter glass bead was introduced into the distal colon to a total depth of 2 cm from the anus margin using a fire-polished glass rod. After insertion of the bead, mice were isolated in clear plastic cages without food and water. The time required for expulsion of the glass bead was recorded which is typically less than 15 min.

One-hour stool collection

Each mouse will be placed in a separate clean cage without food and water and fecal pellets were collected over the course of one hour. The pellets were collected immediately after expulsion and placed in 1.5 ml microcentrifuge tubes to avoid drying. Tubes with the fresh pellets were weighed to obtain the wet weight of the stool. Following overnight drying at 65°C, the tubes were reweighed to obtain the dry weight. Total dry and wet stool weights as well as stool water content [(Wet weight – dry weight)/wet weight] *100 was calculated. Additionally, total number of fecal pellets and stool frequency was observed and recorded.

Western blot

Six tissues of colon from MitoPark and littermate control groups were e homogenized in a bullet blender (Next Advance) using 2mm diameter stainless steel beads. Tissue lysates were

prepared using modified radio immune precipitation assay (RIPA) buffer containing 20 mM Tris–HCl, pH 8.0, 2 mM EDTA, 10 mM EGTA, 2 mM dithiothreitol (DTT), 1 mM phenylmethylsulfonyl fluoride (PMSF), 20mM sodium orthovanadate, 1 mM sodium fluoride and protease and phosphatase inhibitor cocktail (Thermo Scientific, Waltham, MA), as described previously [30, 31]. The supernatants were obtained after centrifuging the homogenates at 15,000 rpm for 60 min. Protein concentration was measured using Bradford dye (Bio-Rad). Lysates containing equal amounts of protein were separated on a 12 or 15% SDS-polyacrylamide gel. After separation, proteins were electro- blotted onto a nitrocellulose membrane, and nonspecific binding sites were blocked with LICOR blocking buffer. TNFα (1:1000), iNOS (1:500) and β-actin (1:10000) primary antibodies were used to blot the membranes for 16 h at 4°C. Thereafter, blots were washed in phosphate buffered saline (PBS) containing 0.01% Tween-20, incubated in respective secondary antibodies (Alexa Goat anti mouse 680 or Alexa Goat anti-rabbit 790) for 1 hour. Fluorescent bands corresponding to the protein of interest were observed by scanning membranes in a LiCor scanner.

Quantitative real-time PCR (qRT-PCR)

Colons from MitoPark and littermate control groups were utilized for qRT-PCR (n=6). The samples were homogenized in a bullet blender (Next Advance) using DNAse- and RNAse-free stainless steel beads and RNA was extracted using RNeasy Plus Mini kit (Qiagen). 1 μg total RNA was converted to cDNA using the High-Capacity cDNA Reverse Transcription kit (Applied Biosystems Inc.) following manufacturer's instructions. Real-time PCR was performed in an Mx3000P QPCR system (Stratagene) using the Brilliant SYBR Green QPCR

Master Mix kit (Stratagene), with cDNAs corresponding to 1 μg of total RNA, 10 μl of 2 × master mix and 0.2 μM of each primer in a 20-μl final reaction volume. All reactions were performed in triplicate. Mouse 18S rRNA was used as an internal standard for normalization. Primers specific for NpY (NM_023456) were synthesized at the Iowa state University DNA facility while 18S rRNA (Cat# QT02448075) was obtained from Quantitect. The PCR cycling conditions contained an initial denaturation at 95°C for 10 min, followed by 40 cycles of denaturation at 95°C for 30 sec, annealing at 60°C for 30 sec, and extension at 72°C for 30 sec. Fluorescence was detected during the annealing step of each cycle. Dissociation curves were run to verify the singularity of the PCR product. Data were analyzed using the comparative threshold cycle (Ct) method.

Immunohistochemistry

For immunohistochemistry, at the end of the treatment, animals were perfused first with PBS followed by 4% PFA. Guts were removed and post-fixed in 10% formalin for an additional 24 h. Tissues were embedded in paraffin and sectioned at 7 μm at Iowa State University's veterinary pathology lab. Paraffin-embedded sections of mouse tissues were deparaffinized in decreasing alcohol grades. Heat-mediated antigen retrieval was performed using 10 mM citrate buffer (pH 6.0) for 30 min. Sections were then incubated with blocking reagent (5% normal goat serum, 2% BSA and 0.5% Triton X-100 in PBS) for 60 min before being incubated with TUJ (1:500), iNOS (1:500) or GFAP (1:300) primary antibodies for 24 h. Sections were then washed many times in PBS and incubated in the dark for 90 min with Alexa-488 and 555 dye-conjugated secondary antibodies (1:1500). Nuclei were stained with

Hoechst dye. Slides were viewed with 63× and 43× oil objectives using a Leica DMIRE2 confocal microscope.

Monoamine assessment via High performance liquid chromatography

Dissected colon and ileal segments were placed in buffer comprising 0.2 M perchloric acid, 0.05% Na_2EDTA, 0.1% $Na_2S_2O_5$ and isoproterenol (internal standard) and stored at -80°C until lysate preparation. To extract monoamine neurotransmitters, the samples were homogenized using bullet blender and 0.2 mm diameter stainless steel beads. Lysates were centrifuged and 300 μl of lysate was added to 30 mg alumina. The pH of the solution was quickly increased to 8.6 using 1M Tris buffer. The tubes were now rotated in a rotating shaker at 4°C for 15 minutes and then centrifuged at 10,000 rpm. The supernatant was aspirated and the monoamine neurotransmitters were eluted form the alumina with 0.2 M perchloric acid. Monoamine lysates were placed in a refrigerated automatic sampler (model WPS-3000TSL) until being separated isocratically by a reversed-phase C18 column with a flow rate of 0.6 ml/ min using a Dionex Ultimate 3000 HPLC system (pump ISO-3100SD, Thermo Scientific, Bannockburn, IL). Electrochemical detection was achieved using a CoulArray model 5600A coupled with an analytical cell (microdialysis cell 5014B) and a guard cell (model 5020) with cell potentials set at -350, 0, 150, and 220 mV. Data acquisition and analysis were performed using Chromeleon 7 and ESA CoulArray 3.10 HPLC Software and quantified data were normalized to wet tissue weight.

Statistical evaluation

Data are expressed as the mean ± SEM. Unpaired t-test or two-way ANOVA followed by post hoc analysis using the Bonferroni method were performed using GraphPad Prism 6 (GraphPad Software Company). Results were considered statistically significant at $P < 0.05$.

Results

MitoPark mice demonstrate age-dependent decrease in body weight but normal food intake compared to age-matched littermate controls

For this study, mice were weighed once a month for 6 months to determine change in body weights (Figure 1A). Compared to age-matched littermate controls (LCs), MitoPark mice begin to display significantly lower body weights from 20 weeks of age (Figure 1B). There onwards, these mice steadily loose weight with the average weight of the LCs being 37 grams compared to the MitoPark group with an average body weight of 24 grams just before conclusion of the study.

To account for the weight loss and any intestinal dysmotility, we also measured food intake of both groups prior to conclusion of the study. Intriguingly, we found no difference in food intake between MitoPark and LCs even at 24 weeks of age when the MitoPark mice showed extensive weight loss (Figure 1C).

Spatial differences in gastrointestinal motility in MitoPark mice compared to age-matched controls

In the MitoPark mouse model, these mice gradually loose dopaminergic neurons and show age-dependent progression of motor and non-motor symptoms when compared to age-

matched healthy mice (Galter et al., 2010; Li et al., 2013). Till date, various groups have studied the motor deficits in this model that mirror the adult-onset and age-dependent progressive motor symptoms seen in patients with PD. However, an important non-motor symptom – gastrointestinal dysfunction- that is seen in almost 80% PD patients has not been characterized in this model.

Curiously, from 8 weeks of age MitoPark mice showed lower Whole gut transit time (WGTT) indicating more GI motility in these mice compared to LCs (Figure 2A). WGTT as the name suggests, measures GI motility from the time food enters the stomach till it is removed from the body as waste matter. With different regions of the GI tract uniquely involved in processes of digestion, absorption and waste production it is necessary to understand precisely which part of the gut is affected. Hence we evaluated regional motility by measuring gastric emptying and colon transit time. As gastric emptying involves euthanizing the mice, collecting and weighing stomach contents, this study was carried out only once at the culmination of the study.

At 24 weeks of age, there was no difference in the gastric emptying between both groups (Figure 2B). However the MitoPark mice had increased colon transit time (CTT) compared to age-matched LCs (Figure 2C). On an average, MitoPark mice took about 20 minutes to expel the glass bead inserted in the distal colon compared to LC mice that took about 4 minutes to expel a similar bead. To determine the rate of bead propulsion (an indirect measurement of propulsive action of the colon) we divided the time required for bead expulsion with the colon length. The rate of bead movement in the distal colon was significantly decreased in the MitoPark group compared to the LC group (Figure 2D). Similarly MitoPark mice showed reduced fecal pellet output at 24 weeks of age further

suggesting loss of colonic motility in these mice when equated with LCs (Figure 2E). A trend of lower fecal water content was observed from 16 weeks in MitoPark mice when compared to age-matched LCs (Figure 2F). By 24-weeks of age, these mice now have significantly lower amount of fecal water content compared to age-matched LCs. Unusually, colon lengths in these mice were smaller when compared to that of the LCs despite no gross observation of inflammation (Figure 2G).

Altered gastrointestinal monoamine neurotransmitter levels but no changes in dopamine receptor expression in the MitoPark mice

Since dopamine plays an important role in modulating GI motility, we decided to assess intestinal dopamine content via HPLC.

Following 12 weeks of age, MitoPark mice begin to show a reduction in striatal dopamine with significantly increased dopamine turnover from 12 week onwards (Galter et al., 2010). We observed reduced dopamine levels in 24-week old MitoPark mice compared to age matched LCs (Figure 3A). Curiously, the levels of 3,4-Dihydroxyphenylacetic acid (DOPAC) and homovanillic acid (HVA) were unchanged in these mice compared to LCs (Figure 3A). We also measured the mRNA levels of prominent dopamine receptors present in the colon. We found no significant differences in D1R and D2R transcript levels between groups (Figure 3B).

24 week-old MitoPark mice show low-grade intestinal inflammation

Intestinal or systemic inflammation can cause alterations in GI motility. Given the perplexing spatial differences in motility in this transgenic model, we investigated the presence or

absence of inflammation in the GI tract. In the ileum, a trend of increased expression of tumor necrosis factor alpha (TNFα) and inducible nitric oxide synthase (iNOS) were observed in the MitoPark mice compared to age-matched LCs (Figure 4A). Enteric glial cells (EGCs) along with neurons form the enteric nervous system (ENS). EGCs are required for maintaining optimum gut epithelial barrier thus preventing translocation of intestinal bacteria and other harmful compounds from entering into the deeper layers of the GI tissue (Yu and Li, 2014). EGCs can also sense pathogenic and commensal or probiotic bacteria and hence are important in maintaining intestinal health (Turco et al., 2014). Various studies investigating the role of EGCs in diverse diseases have shown that EGCs increase in numbers in response to inflammation yet ablation or cell death of EGCs in healthy mice results in development of intestinal inflammation (Sharkey, 2015). At the age of 24 weeks, MitoPark mice showed increased glial fibrillary acidic protein (GFAP)- a marker of EGCs – by western blot analysis of full thickness colon samples (Figure 5A). However, EGCs are present not only in association with the neurons in the myenteric and submucosal plexus but are also present in the muscle layers and extend into the mucosal villi (S.Figure 1) Surprisingly, immunohistochemical analysis of GFAP expression presented significantly lower numbers of EGCs in the villi (Figure 4B) while higher expression of GFAP was observed in the myenteric plexus (Figure 4C).

In the colon we observed significantly higher expression of TNFα and a trend of increased iNOS was observed (Figure 5A). Specifically, we found increased iNOS expression in the myenteric (LMMP) and sub-mucosal plexi (SMP) in the colon of MitoPark mice over LC colon (Figure 5E). Together the data points towards increased intestinal inflammation in these mice compared to age-matched LCs. In a rat model of PD, the toxin 6-hydroxy

dopamine (6-OHDA) caused a decrease in DARPP-32^{+} (Dopamine and cAMP regulated phosphoprotein-32) neurons in the substantia nigra. The consequence of reduced DARPP-32 was reflected in muscle rigidity in these rats similar to that seen in PD patients. DARPP-32 is regulated in part by dopamine. Indeed 24-week MitoPark mice colon showed significantly lower expression of DARPP-32. Together the results suggest that at 24 weeks of age MitoPark mice have low-grade intestinal inflammation We also found higher expression of oligomeric proteins were observed in the 24 week MitoPark colon samples compared to LCs suggesting increased aggregated protein in the MitoPark gut (Figure 5B). However, based on published literature regarding this model, we speculate that the components of the aggregates may primarily be mitochondrial proteins rather than α-synuclein as no significant changes in aggregated α-synuclein levels were observed between groups (Figure 5C).

Reduced number of dopaminergic neurons but no significant changes in total number of enteric neurons in the GI tract.

Since the MitoPark mouse model utilizes the *cre/lox* system to specifically induce dopaminergic neuronal loss in the transgenic mice, this means that there is a progressive reduction in the number of dopaminergic neurons both in the mid-brain as well as the gut (S. Figure 2 and Figure 6A). As shown in Figure 5B, whole-mounts of the myenteric plexus present on longitudinal muscle shows reduction in tyrosine hydroxylase positive (TH^{+}) dopaminergic neurons in the colon compared to age-matched LCs.

However, colon and ileum sections stained for pan enteric neuronal marker - protein gene product 9.5 (PGP9.5) showed no significant differences between 24-week old MitoPark mice compared to LCs (Figure 6B).

Environmental toxin manganese exacerbates intestinal inflammation and oligomeric protein formation in the MitoPark colon

Chronic exposure to manganese (Mn) is a known occupational and environmental hazard leading to neurological symptoms similar to PD (Rokad et al., 2016). Various labs including ours have investigated the role of Mn in the development of neuromotor and neurocognitive deficits (Afeseh Ngwa et al., 2011; Bouchard et al., 2007; Latchoumycandane et al., 2005). However, the effect of this toxin on the GI system in the context of PD has not been explored.

8-week old MitoPark mice were given 10mg Mn/Kg body weight for 4 weeks via intragastric gavage while animals in the control group received vehicle (water) during this time period. After 4 weeks of Mn exposure, mice showed increased Bax expression in the colon compared to vehicle-treated controls (Figure 7A). Bax is a pro-apoptotic protein and its expression indicates increased cellular apoptosis when compared to control colon samples. Interestingly, a mere 4 weeks of low-dose Mn lead to a trend of increased oligomeric protein expression in the colon compared to the unexposed group (Figure 7B). Mn exposure also exacerbates motor dysfunction; for instance, between the ages 8-12 weeks movement coordination is similar between LCs and MitoPark mice, yet Mn exposed mice of the same age have coordination and motor deficits following exposure to Mn. Together the results – while preliminary- suggest that even a sub-acute exposure to Mn for 4 weeks can exacerbate protein aggregation in a living system with genetically disrupted protein quality control.

Discussion

GI problems have been known to develop in PD patients sometimes decades before clinical diagnosis of the disease (Mukherjee et al., 2016). More importantly, the continued presence of altered intestinal transit can hamper optimal absorption of anti-parkinsonian medications thus decreasing the efficacy of these drugs (Bestetti et al., 2017; Mukherjee et al., 2016). Hence it is necessary to understand the role of dopaminergic neurons in gastrointestinal motility. The MitoPark transgenic mouse model recapitulates many characteristic symptoms of PD including a progressive loss of dopaminergic neurons as well as associated behavioral and motor deficits (Galter et al., 2010). Previously, we have observed the development of non-motor symptoms of reduced spatial memory retention as well anosmia early on in these mice compared to age-matched LCs (data not shown). In the present study, we show that GI dysfunction is one of the earliest non-motor symptoms observed in this model, a trait similarly seen in PD patients.

From 20 weeks of age, MitoPark mice begin to show weight loss compared to age-matched LCs (figure 1B). This weight loss occurred despite the fact that animals from both groups ate similar amounts of food (Figure 1C). Knowing that the gut-brain axis modulates appetite and hence feeding behavior, we decided to probe the hypothalamus of 24 week MitoPark and LC for the known appetite modulator- neuropeptide Y (NpY). In the hypothalamus, NpY is increased following fasting/food deprivation with the levels falling following food consumption (Hanson and Dallman, 1995; Schwartz et al., 1998). We observed increased mRNA expression of NpY in the hypothalamus of 24-week MitoPark mice when compared to LCs (S. Figure 2). This increased NpY is possibly in response to poor nutrient absorption and subsequent weight loss in these mice.

Since 8 weeks of age, MitoPark mice take less time to remove waste matter following intragastric gavage of a known volume of meal (Figure 2A). The GI tract includes the, stomach, the small intestine that is further divided into duodenum, jejunum and ileum, the large intestine or colon, appendix/cecum and the rectum. Each part of this GI tract play an important role in food breakdown, nutrient or electrolyte absorption and finally waste formation and removal. As a result, the motility pattern varies from one intestinal segment to another. Since WGTT measures the time required for the carmine red dye to pass through the entire tract, despite an altered motility time when compared to controls, it cannot confirm the exact region of dysfunction. Hence a combination of tests was performed to solve this problem. Subsequently, it was revealed that in MitoPark mice a normal gastric emptying rate (Figure 2B) but lower colon motility (Figure 2D-2E). Together, these results pointed towards increased peristalsis (constriction and relaxation of intestinal smooth muscles) in the small intestine but reduced peristalsis in the colon. Increased colon transit time has also been demonstrated in GI studies on PD cohorts. However, reports on gastric emptying and small intestinal transit time are conflicting with some studies reporting increased gastric emptying and small intestinal transit while others report no significant differences between younger PD ($\leq$ 65 years) and healthy volunteers (Goetze et al., 2006; Hardoff et al., 2001; Heetun and Quigley, 2012). In most of the studies conducted, patients were already on l-DOPA replacement therapies. Long-term l-DOPA medication has been proven to increase intestinal transit time (Pfeiffer et al., 2012). Therefore such a major confounding factor must be taken into account when reporting intestinal dysmotility in patients with PD.

In the GI tract and CNS, various dopamine receptors (D_1R-D_5R) are present and fall in two classes. D1 and D5 receptors fall in the D1R category that are mainly post-synaptic receptors

present on intestinal smooth muscle cells and blood vessels where as D2, D3 and D4 (D2R family of receptors) are present on enteric neurons. Dopamine plays a dual role in the GI tract based on the target receptors and cell type. For instance, dopamine can act on DA1 receptors on smooth muscles and cause muscle relaxation while the same neurotransmitter on DA2 receptors present on post-ganglionic sympathetic nerves counteracts the effect of norepinephrine induced muscle relaxation thus inducing contraction (Kirschstein et al., 2009; Zizzo et al., 2010). Since our data shows spatial differences in GI motility, differential expression of these DA receptor subtypes might be the key to understanding this peculiar phenomenon. While there was a trend of increased D2 and D1 receptor transcript levels in the colon of MitoPark mice, these values were not significantly different from LCs. More studies need to be conducted to understand how loss of dopamine amounts to opposing motility behavior in the small and large intestine.

Since this transgenic mouse model is based on progressive dopaminergic neuronal loss, as expected, we observed lower levels of dopamine (Figure 2A) and very few TH^+ neurons (Figures 6A and 6B) in the GI tract compared to LCs. However no significant differences were observed in total neuronal population as stained by the pan enteric neuronal marker PGP9.5 (Figure 6C).

Interestingly, Kirschstein *et al* showed that the dopamine exerts differential effects on intestinal smooth muscle contraction, showing increased contraction in the proximal but gradually relaxation in the distal parts of the gut (Kirschstein et al., 2009). This observation holds true for the MitoPark mouse model too.

Another cause for disruption in normal GI motility is the presence of intestinal inflammation. Increased pro-inflammatory factors can disrupt normal cellular signaling leading to altered

intestinal transit times. When we probed ileum and colon samples for TNFα and iNOS, we observed increased protein expression of these pro-inflammatory factors especially in the colon (Figures 4A, 5A and 5D). Curiously, while western blot showed a mildly elevated expression of the enteric glial cell marker GFAP in the ileum, we observed reduced GFAP expression in the villi in this region compared to LCs. Despite expressing the same cell markers, nonetheless enteric glia differ in morphology and possibly cellular communication based on their location in the different layers of the gut (Boesmans et al., 2015; Rao et al., 2015). It is possible that the loss of dopamine might have an effect on glial health and the presence of inflammation leading to a reduced glial cell expression in the villi and an increased presence of enteric glial cells to protect neurons from cell death. Future studies should focus on understanding the effect of dopamine on enteric glial cell health and functioning.

Previous publications have reported presence of cytoplasmic inclusions constituting cellular fragments and aggregate proteins in the dopaminergic neurons of MitoPark mice (Ekstrand et al., 2007). Similarly, we have observed higher oligomeric protein expression in the colon of 24-week old MitoPark mice compared to age-matched LCs (Figure 5B). Interestingly in the presence of an environmental toxicant such as Mn, these mice show higher incidence of protein aggregation as seen in Figure 7B. Notably, despite a low-dose Mn exposure regime, these mice had increased Bax expression in the colon (Figure 7A). Bax is a pro-apoptotic protein therefore increased Bax protein levels correspond to higher cell apoptotic incidences. Since the gut is made up of various cell types arranged in specific layers, the cell type particularly affected by Mn exposure would need to be determined. Still, increased Bax and protein aggregation upon low-dose Mn exposure demonstrates that a complex interaction

between genetic predisposition and environmental toxin exposure is what leads to protein aggregation and neurological dysfunctioning in most cases.

To conclude, we have characterized GI dysfunction in the MitoPark mouse model of PD. Specifically, we show a progressive loss of normal GI motility with increased transit time in the colon and reduced transit time in the small intestine. At 24-weeks, MitoPark mice also developed mild intestinal inflammation and protein aggregation presumably due to loss of dopamine and deregulation in enteric glial cell numbers. Thus we demonstrate that the MitoPark mouse model recapitulates early GI dysfunction and constipation similar to PD patients and is an ideal pre-clinical candidate to determine the efficacy and action of new anti-parkisonian drugs.

Acknowledgements

We would like to thank Gary Zenitsky for his help in preparing the manuscript.

Funding

Supported by NIH grants ES10586 and NS074443 and NS039958.

References

Afeseh Ngwa, H., A. Kanthasamy, Y. Gu, N. Fang, V. Anantharam and A. G. Kanthasamy (2011). "Manganese nanoparticle activates mitochondrial dependent apoptotic signaling and autophagy in dopaminergic neuronal cells." Toxicol Appl Pharmacol **256**(3): 227-240.

Anderson, G., A. R. Noorian, G. Taylor, M. Anitha, D. Bernhard, S. Srinivasan and J. G. Greene (2007). "Loss of enteric dopaminergic neurons and associated changes in colon motility in an MPTP mouse model of Parkinson's disease." Exp Neurol **207**(1): 4-12.

Bestetti, A., A. Capozza, M. Lacerenza, L. Manfredi and F. Mancini (2017). "Delayed Gastric Emptying in Advanced Parkinson Disease: Correlation With Therapeutic Doses." Clin Nucl Med **42**(2): 83-87.

Boesmans, W., R. Lasrado, P. Vanden Berghe and V. Pachnis (2015). "Heterogeneity and phenotypic plasticity of glial cells in the mammalian enteric nervous system." Glia **63**(2): 229-241.

Bouchard, M., F. Laforest, L. Vandelac, D. Bellinger and D. Mergler (2007). "Hair manganese and hyperactive behaviors: pilot study of school-age children exposed through tap water." Environ Health Perspect **115**(1): 122-127.

Cersosimo, M. G. and E. E. Benarroch (2012). "Autonomic involvement in Parkinson's disease: pathology, pathophysiology, clinical features and possible peripheral biomarkers." J Neurol Sci **313**(1-2): 57-63.

Chen, H., E. A. Burton, G. W. Ross, X. Huang, R. Savica, R. D. Abbott, A. Ascherio, J. N. Caviness, X. Gao, K. A. Gray, J. S. Hong, F. Kamel, D. Jennings, A. Kirshner, C. Lawler, R. Liu, G. W. Miller, R. Nussbaum, S. D. Peddada, A. C. Rick, B. Ritz, A. D. Siderowf, C. M. Tanner, A. I. Troster and J. Zhang (2013). "Research on the premotor symptoms of Parkinson's disease: clinical and etiological implications." Environ Health Perspect **121**(11-12): 1245-1252.

Ekstrand, M. I., M. Terzioglu, D. Galter, S. Zhu, C. Hofstetter, E. Lindqvist, S. Thams, A. Bergstrand, F. S. Hansson, A. Trifunovic, B. Hoffer, S. Cullheim, A. H. Mohammed, L.

Olson and N. G. Larsson (2007). "Progressive parkinsonism in mice with respiratory-chain-deficient dopamine neurons." Proc Natl Acad Sci U S A **104**(4): 1325-1330.

Galter, D., K. Pernold, T. Yoshitake, E. Lindqvist, B. Hoffer, J. Kehr, N. G. Larsson and L. Olson (2010). "MitoPark mice mirror the slow progression of key symptoms and L-DOPA response in Parkinson's disease." Genes Brain Behav **9**(2): 173-181.

Goetze, O., A. B. Nikodem, J. Wiezcorek, M. Banasch, H. Przuntek, T. Mueller, W. E. Schmidt and D. Woitalla (2006). "Predictors of gastric emptying in Parkinson's disease." Neurogastroenterol Motil **18**(5): 369-375.

Greene, J. G., A. R. Noorian and S. Srinivasan (2009). "Delayed gastric emptying and enteric nervous system dysfunction in the rotenone model of Parkinson's disease." Exp Neurol **218**(1): 154-161.

Hansen, M. B. (2003). "The enteric nervous system II: gastrointestinal functions." Pharmacol Toxicol **92**(6): 249-257.

Hanson, E. S. and M. F. Dallman (1995). "Neuropeptide Y (NPY) may integrate responses of hypothalamic feeding systems and the hypothalamo-pituitary-adrenal axis." J Neuroendocrinol **7**(4): 273-279.

Hardoff, R., M. Sula, A. Tamir, A. Soil, A. Front, S. Badarna, S. Honigman and N. Giladi (2001). "Gastric emptying time and gastric motility in patients with Parkinson's disease." Mov Disord **16**(6): 1041-1047.

Heetun, Z. S. and E. M. Quigley (2012). "Gastroparesis and Parkinson's disease: a systematic review." Parkinsonism Relat Disord **18**(5): 433-440.

Kirschstein, T., F. Dammann, J. Klostermann, M. Rehberg, T. Tokay, R. Schubert and R. Kohling (2009). "Dopamine induces contraction in the proximal, but relaxation in the distal rat isolated small intestine." Neurosci Lett **465**(1): 21-26.

Latchoumycandane, C., V. Anantharam, M. Kitazawa, Y. Yang, A. Kanthasamy and A. G. Kanthasamy (2005). "Protein kinase Cdelta is a key downstream mediator of manganese-induced apoptosis in dopaminergic neuronal cells." J Pharmacol Exp Ther **313**(1): 46-55.

Li, X., L. Redus, C. Chen, P. A. Martinez, R. Strong, S. Li and J. C. O'Connor (2013). "Cognitive dysfunction precedes the onset of motor symptoms in the MitoPark mouse model of Parkinson's disease." PLoS One **8**(8): e71341.

Mukherjee, A., A. Biswas and S. K. Das (2016). "Gut dysfunction in Parkinson's disease." World J Gastroenterol **22**(25): 5742-5752.

Pellegrini, C., M. Fornai, R. Colucci, E. Tirotta, F. Blandini, G. Levandis, S. Cerri, C. Segnani, C. Ippolito, N. Bernardini, K. Cseri, C. Blandizzi, G. Hasko and L. Antonioli (2016). "Alteration of colonic excitatory tachykininergic motility and enteric inflammation following dopaminergic nigrostriatal neurodegeneration." J Neuroinflammation **13**(1): 146.

Pfeiffer, R. F. (2003). "Gastrointestinal dysfunction in Parkinson's disease." Lancet Neurol **2**(2): 107-116.

Pfeiffer, R. F., Z. K. Wszolek and M. Ebadi (2012). "Parkinson's Disease, Second Edition." CRC Press, Taylor & Francis Group: 1308.

Rao, M., B. D. Nelms, L. Dong, V. Salinas-Rios, M. Rutlin, M. D. Gershon and G. Corfas (2015). "Enteric glia express proteolipid protein 1 and are a transcriptionally unique population of glia in the mammalian nervous system." Glia.

Rokad, D., S. Ghaisas, D. S. Harischandra, H. Jin, V. Anantharam, A. Kanthasamy and A. G. Kanthasamy (2016). "Role of neurotoxicants and traumatic brain injury in alpha-synuclein protein misfolding and aggregation." Brain Res Bull.

Schwartz, M. W., J. C. Erickson, D. G. Baskin and R. D. Palmiter (1998). "Effect of fasting and leptin deficiency on hypothalamic neuropeptide Y gene transcription in vivo revealed by expression of a lacZ reporter gene." Endocrinology **139**(5): 2629-2635.

Sharkey, K. A. (2015). "Emerging roles for enteric glia in gastrointestinal disorders." J Clin Invest **125**(3): 918-925.

Tasselli, M., T. Chaumette, S. Paillusson, Y. Monnet, A. Lafoux, C. Huchet-Cadiou, P. Aubert, S. Hunot, P. Derkinderen and M. Neunlist (2013). "Effects of oral administration of rotenone on gastrointestinal functions in mice." Neurogastroenterol Motil **25**(3): e183-193.

Turco, F., G. Sarnelli, C. Cirillo, I. Palumbo, F. De Giorgi, A. D'Alessandro, M. Cammarota, M. Giuliano and R. Cuomo (2014). "Enteroglial-derived S100B protein integrates bacteria-induced Toll-like receptor signalling in human enteric glial cells." Gut **63**(1): 105-115.

Walker, J. K., R. R. Gainetdinov, A. W. Mangel, M. G. Caron and M. A. Shetzline (2000). "Mice lacking the dopamine transporter display altered regulation of distal colonic motility." Am J Physiol Gastrointest Liver Physiol **279**(2): G311-318.

Yu, Y. B. and Y. Q. Li (2014). "Enteric glial cells and their role in the intestinal epithelial barrier." World J Gastroenterol **20**(32): 11273-11280.

Zizzo, M. G., F. Mule, M. Mastropaolo and R. Serio (2010). "D1 receptors play a major role in the dopamine modulation of mouse ileum contractility." Pharmacol Res **61**(5): 371-378.

Figures

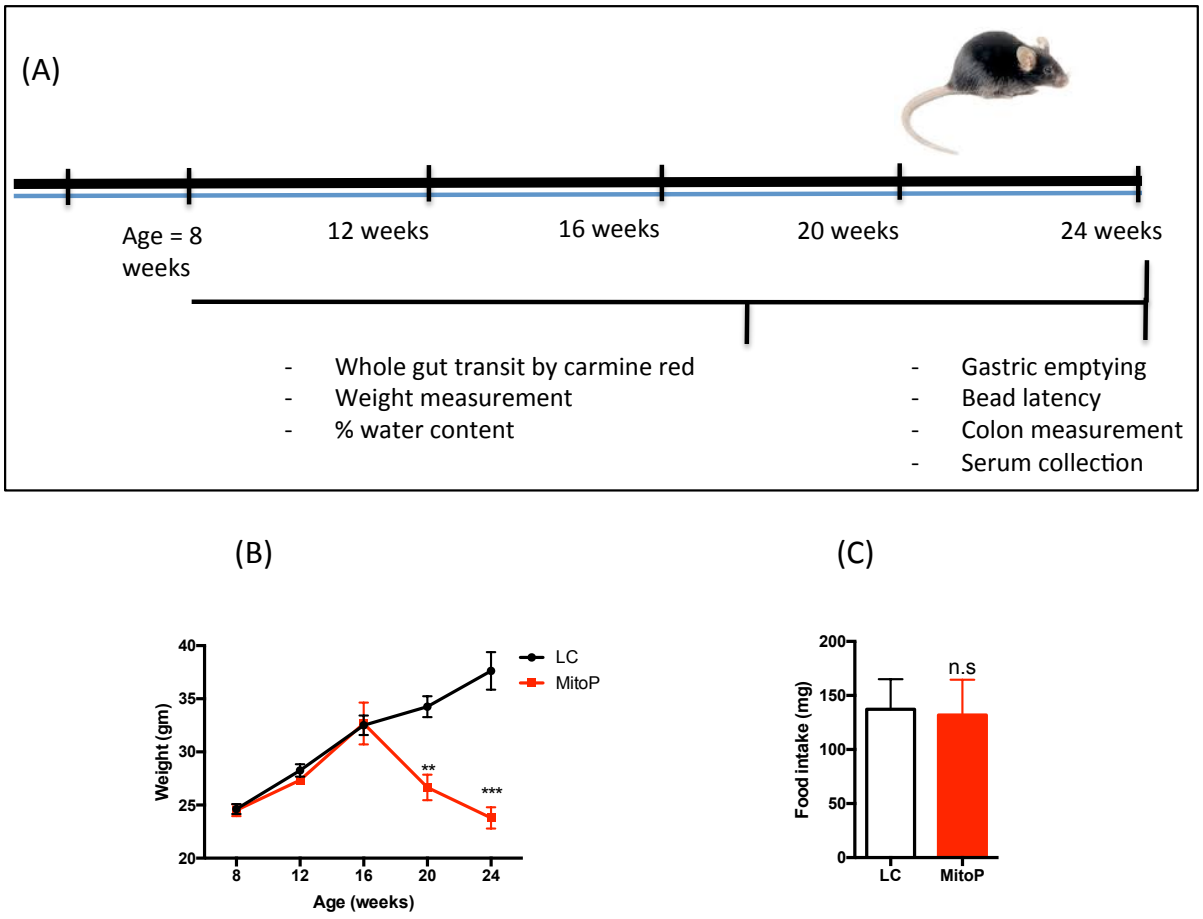

Figure 1: Weight loss observed in MitoPark mice despite regular food intake

(A) Treatment paradigm. (B) Body weights measured over the duartion of the study showing progressive weight loss in MitoPark mice. (C) Food intake of both groups at 24 weeks of age. Food intake was measured by weighing food pellets before and after a 1 hour feeding time. The difference in pellet weight in miligrams was accounted as food consumed in that 1 hour. No difference was observed between groups. Data represented as the group mean ± SEM from n=10. Asterisks (**p<0.01 and ***p<0.001) indicate significant differences between MitoPark and LC. n.s = no statistical significance.

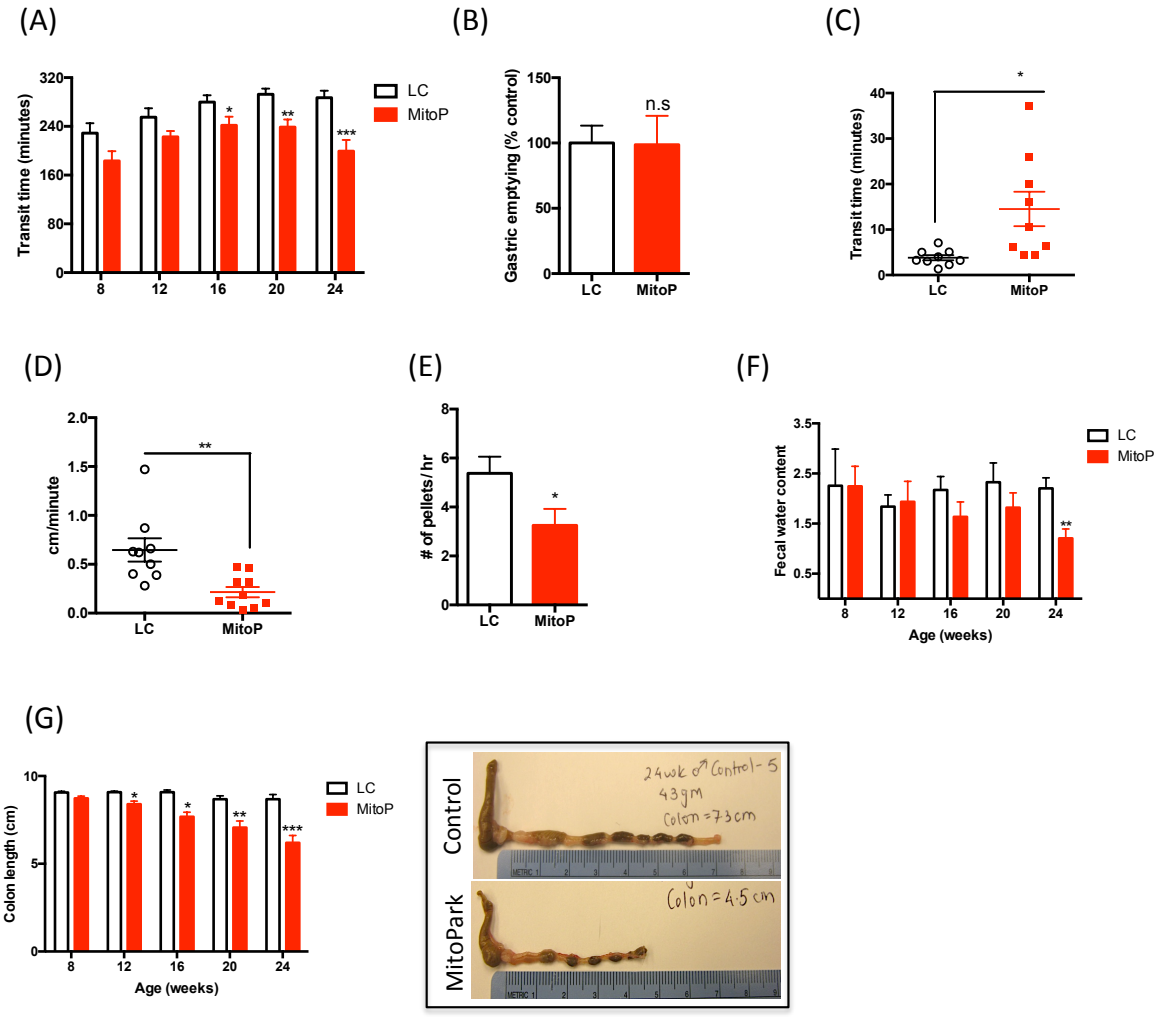

Figure 2: Gastrointestinal motility assessment showing faster small intestinal motility and slower large intestinal motility in MitoPark mice.

(A) Whole gut transit time. Significant time difference was observed from 12 weeks of age onwards with MitoPark mice taking significantly lesser time to expel carmine red that was administered via intragastric gavage. (B) Gastric emptying. 24-week old MitoPark and LC mice took similar times for ingested food to leave the stomach into the small intestine. (C) Colon transit time. 24-week old MitoPark mice took significantly more time in expeling the glass bead inserted 2 cm into the distal colon. (D) Rate of colonic motility- time required for

the glass bead to traverse the 2 cm distance before being expelled by the animal. 24-week old MitoPark mice lower rate of motility compared to age matched LCs displaying a constipated behavior. (E) Stool frequency. 24-week old MitoPark mice expelled significantly fewer fecal pellets compared to LCs. (F) Fecal water content. MitoPark mice progressively show lower water content in their fecal pellets indicating constipation. (G) Colon length in centimeters. Representative photographs showing smaller colon length in 24-week old MitoPark mice compared to LCs. Data represented as the group mean ± SEM from n=10. Asterisks (*p<0.05, **p<0.01 and ***p<0.001) indicate significant differences between MitoPark and LC.

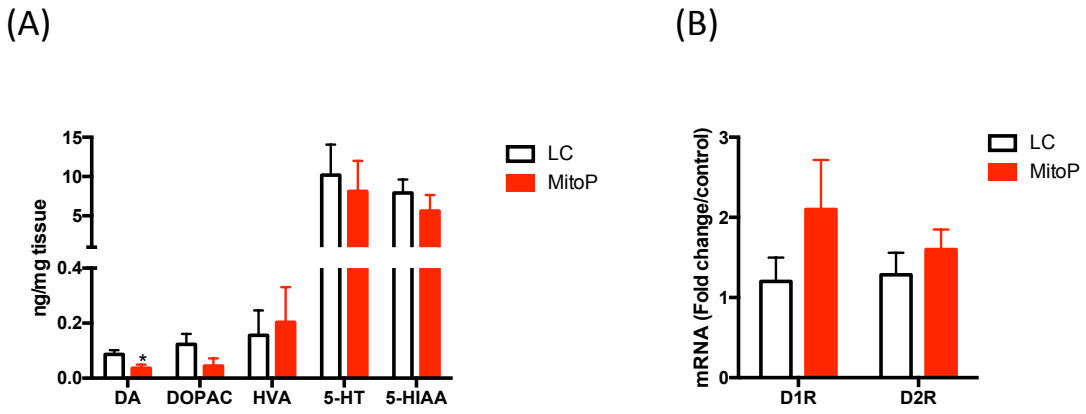

Figure 3: Lower dopamine levels in the colon of 24 week old MitoPark mice compared to age-matched LCs.

(A) HPLC analysis of manoamine neurotransmitter levels in the colon in nanograms per miligram tissue. Dopamine levels were decreased in the colon of 24-week old MitoPark mice compared to LCs. (B) Dopamine receptor mRNA transcript levels. No significant difference between D1R and D2R levels in the colon between groups. Data represented as the group mean ± SEM from n=10 or n=6. Asterisks (*p<0.05) indicate significant differences between MitoPark and LC.

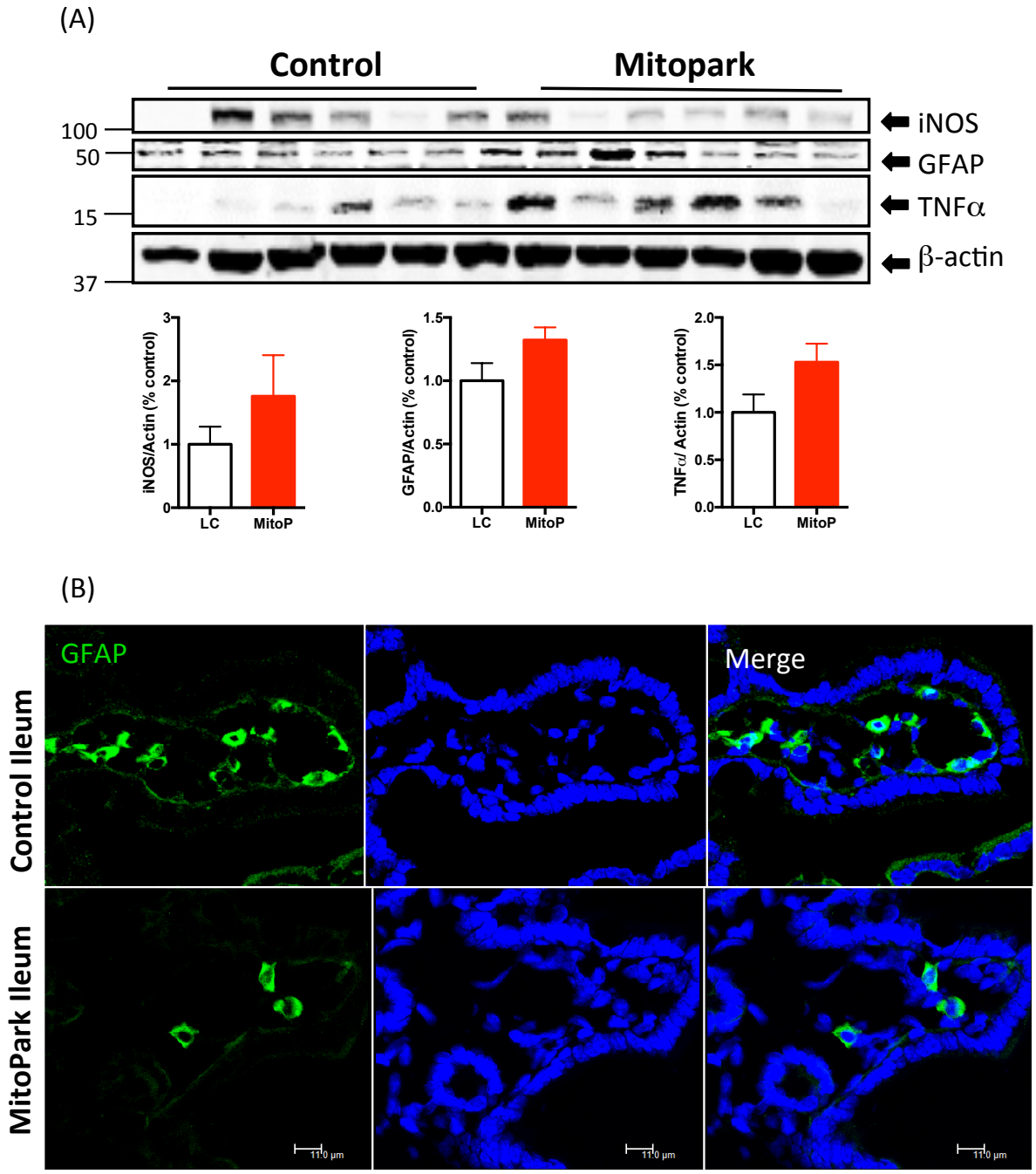

Figure 4: Mild ileitis in older MitoPark mice compared to age-matched LCs.

(A) Western blot of ileum samples (n=6) showing a trend of higher iNOS and TNFα expression in MitoPark mice compared to LCs. Blot intensities normalized to β-actin and expressed as arbitary units. (B) Representative 60x images of ileum sections stained with

GFAP showing decreased enteric glial numbers in the villi. Scale bar = 11 μm Data represented as the group mean ± SEM from n=10 or n=6.

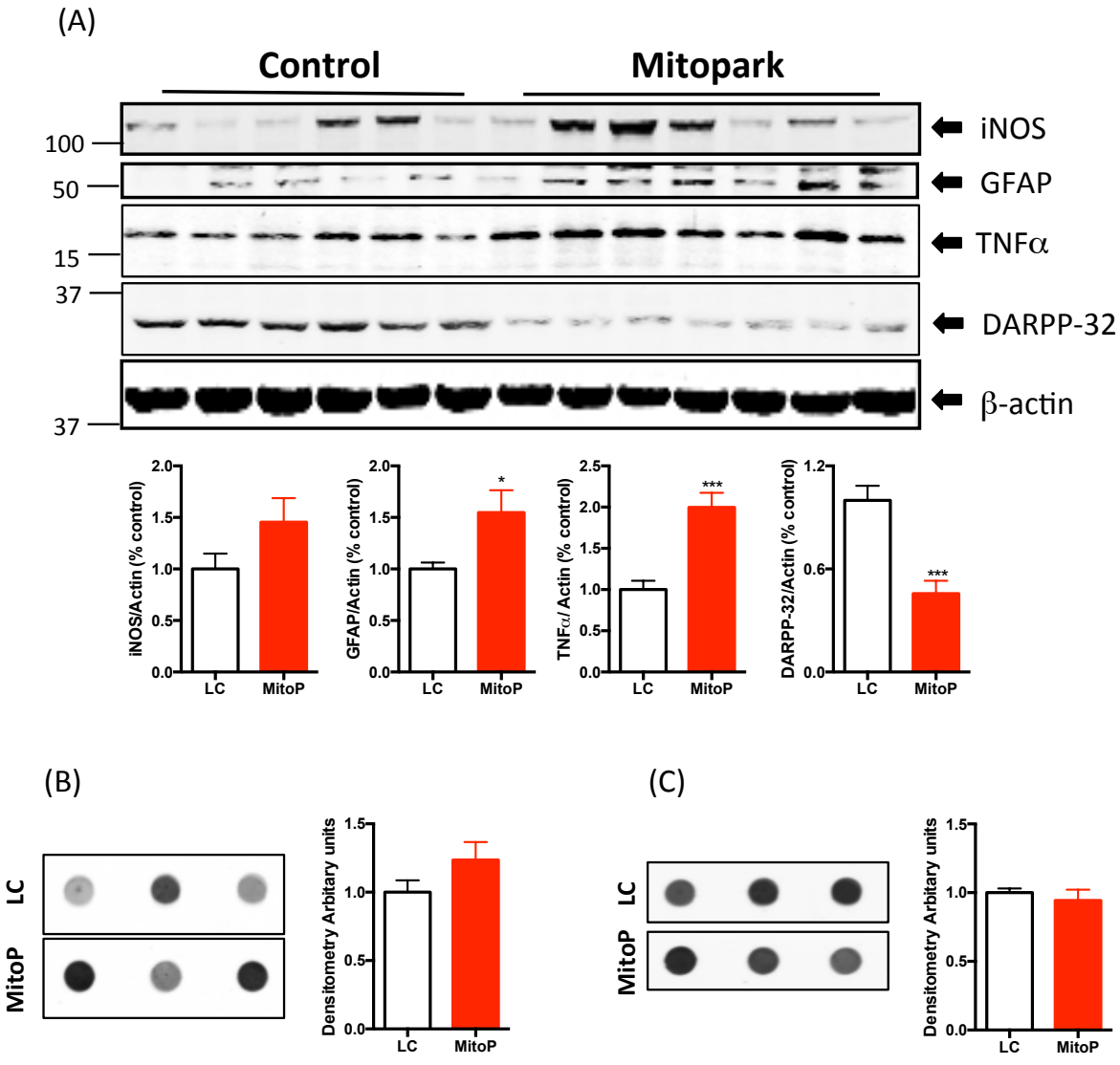

Figure 5 continued

(D)

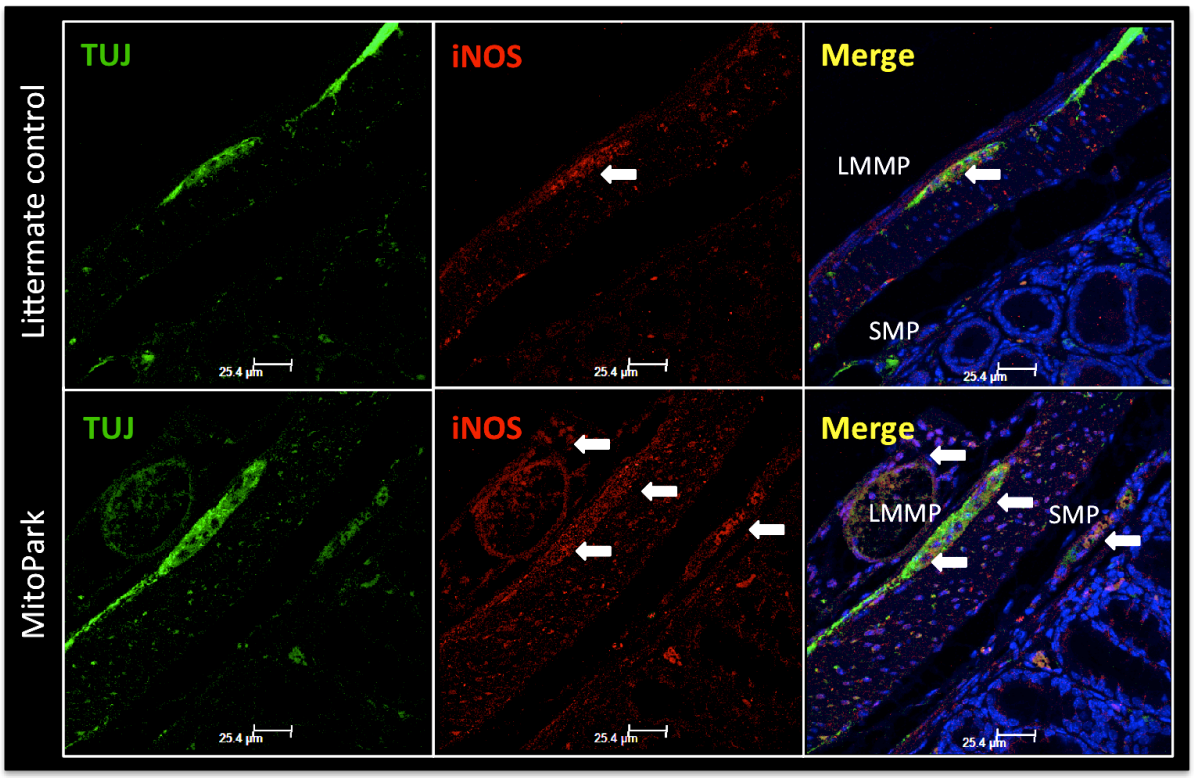

Figure 5: Colonic inflammation observed in 24-week MitoPark mice (A) Western blot of colon samples (n=6) showing increased GFAP and TNFα and a decrease in DARPP-32 expression in 24-week MitoPark mice compared to LCs. No significant differences in iNOS expressed was observed between groups. (B) Oligomeric protein detection. Dot blot analysis of oligomeric protein content in the colon of 24-week MitoPark and LCs. A trend though not significant increase in oligomeric protein expression was observed. (C) Dot blot analysis of aggregated α-synuclein expression in the colon showed no significant difference between groups. (D) Representative 60x image showing increased expression of iNOS in the myenteric (LMMP) and submucosal plexus (SMP) in 24-week MitoPark mice compared to LC. Data represented as the group mean ± SEM from n=6. Asterisks (*p<0.05, **p<0.01 and ***p<0.001) indicate significant differences between MitoPark and LC.

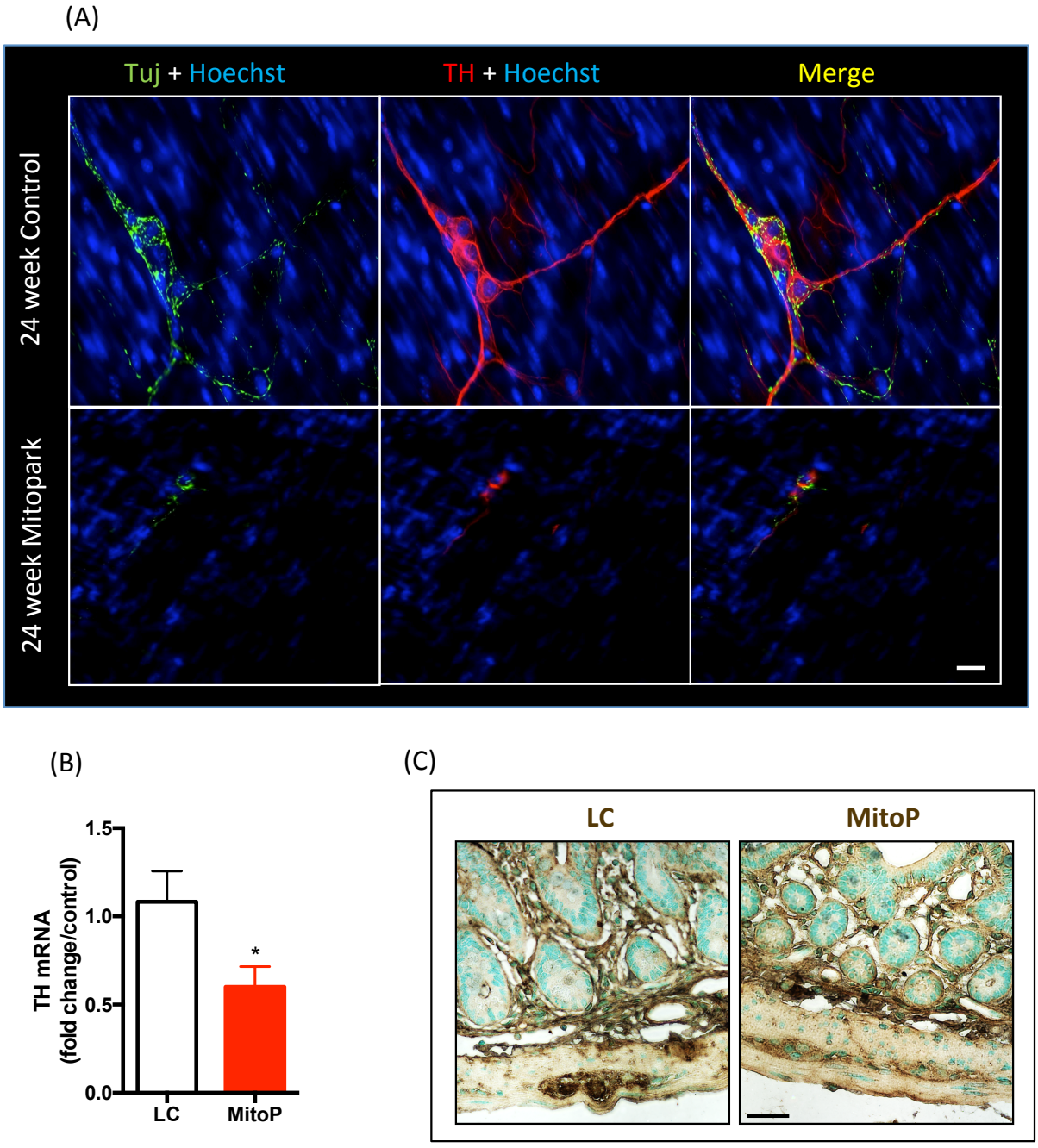

Figure 6: Decreased expression of dopaminergic neurons but no significant difference in total neuronal population between MitoPark and LCs: (A) Representative 60x image showing decreaed number of tyrosine hydroxylae (TH) positive neurons in the myenteric plexus of the colon in MitoPark mice. Scale bar = 7 μm (B) qRT-PCR analysis of TH mRNA transcript, normalized to 18S rRNA expression (n=6). (C) Representative 40x images of

PGP9.5 positive enteric neurons in the colon of LC and MitoPark mice. No significant differences were observed between groups. Scale bar = 35 μm. Data represented as the group mean ± SEM from n=6. Asterisks (*p<0.05) indicate significant differences between MitoPark and LC.

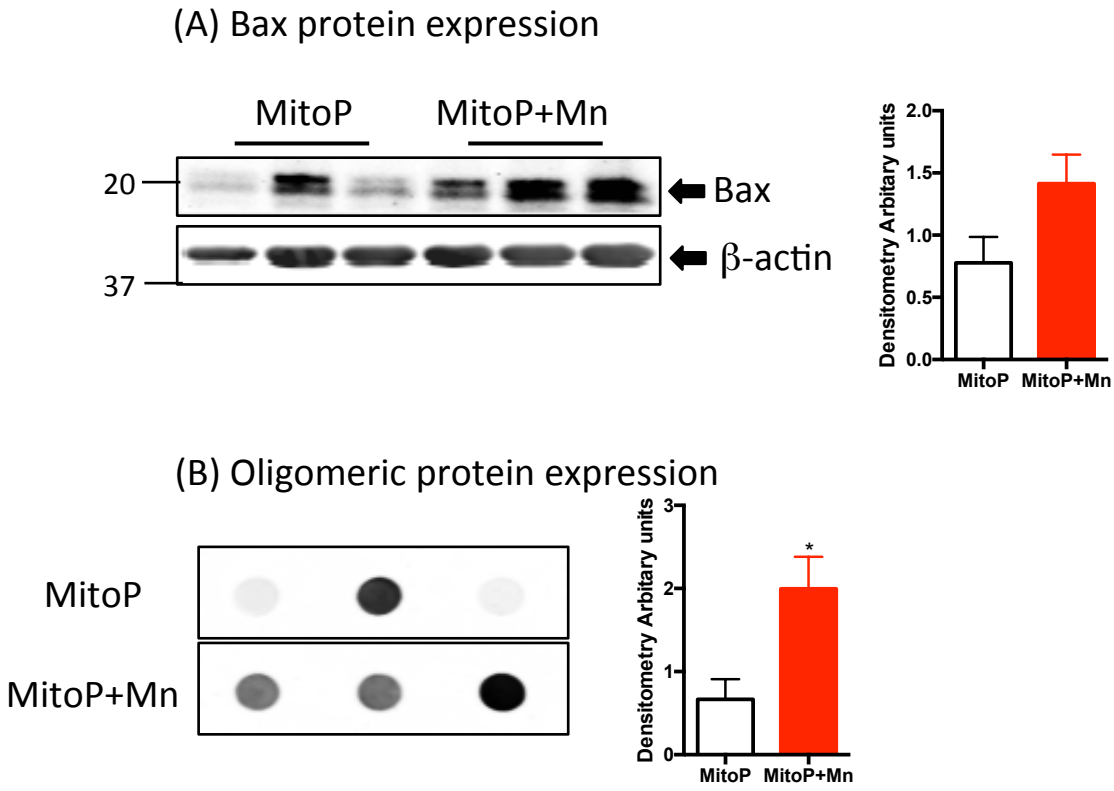

Figure 7: Exposure to environmental manganese potentiates cell death in the colon of MitoPark mice. (A) Western blot of colon lysates showing increased bax protein expression in MitoPark mice given Mn compared to untreated transgenic mice. (B) Dot blot analysis showing increased oligomeric protein expression in the colon of MitoPark mice exposed to Mn compared to unexposed mice. Data represented as the group mean ± SEM from n=3. Asterisks (*p<0.05) indicate significant differences between MitoPark and LC

Supplemental Figures

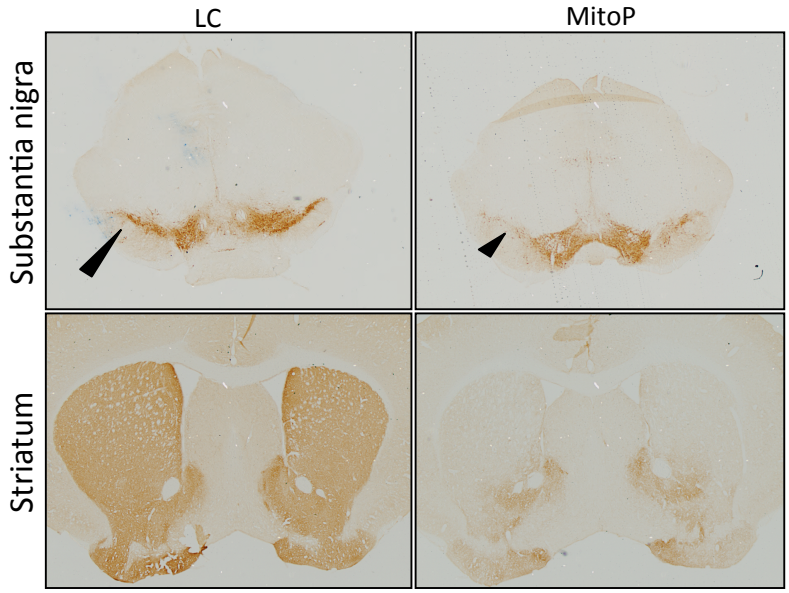

S. Figure 1: 24-week MitoPark mice have significantly fewer number of dopaminergic neurons compared to age-matched LCs. DAB staining showing reduced TH positive dopaminergic neurons in the striatum and substantia nigra of MitoPark mice (left panels) compared to LCs (right panels).

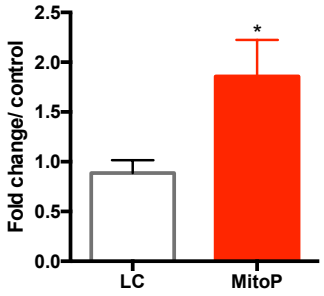

S. Figure 2: Increased neuropeptide Y expression in the hypothalamus of MitoPark mice. qRT-PCR analysis of NpY mRNA transcript, normalized to 18S rRNA expression (n=6). Data represented as the group mean ± SEM from n=3. Asterisks (*p<0.05) indicate significant differences between MitoPark and LC

CHAPTER III

ULCERATIVE COLITIS INDUCES INFLAMMATION AND PERIPHERAL IMMUNE INFILTRATION IN THE MIDBRAIN: IMPLICATIONS OF INTESTINAL INFLAMMATION AND THE GUT-BRAIN AXIS IN DRIVINF NEUROINFLAMMATION IN THE BRAIN

Manuscript to be submitted to Journal of Neuroinflammation

Shivani Ghaisas[*], Souvarish Sarkar[*], Meghan Wymore-Brand[†], Huajun Jin[*], Vellareddy Anantharam[*], Michael Wannemuehler[†], Anumantha Kanthasamy[*‡].

[*] Department of Biomedical Sciences, Iowa Center for Advanced Neurotoxicology, Iowa State University, Ames, Iowa 50011

[†] Department of Veterinary Microbiology & Preventive Medicine, College of Veterinary Medicine, Iowa State University, Ames, Iowa, 50011, United States of America.

[‡]Corresponding author:

Dr. Anumantha G. Kanthasamy, Distinguished Professor and Lloyd Chair,

Parkinson's Disorder Research Laboratory,

Iowa Center for Advanced Neurotoxicology,

Department of Biomedical Sciences,

2062 Veterinary Medicine Building,

Iowa State University,

Ames, IA 50011, U.S.A.

Phone: 1-515-294-2516;

Email: akanthas@iastate.edu

Abstract

Recent post-mortem studies on patients with Parkinson's disease or autism spectrum disorders have found increased peripheral or intestinal inflammation. On the other hand, patients with chronic intestinal inflammation such as Crohn's disease or ulcerative colitis are more susceptible to neurological complications as the disease chronicity increases. To determine the possibility that intestinal inflammation can potentiate neuroinflammation in the central nervous system (CNS), we assessed presence of pro-inflammatory cytokine expression and microglial activation in the CNS of mice given acute colitis. DSS induced acute colitis resulted in expected colonic inflammation and damage to the mucosa and sub-mucosa. We observed immune cell influx at the sight of these lesions with increased iNOS production. The inflamed colons had lower levels of the neurotransmitter serotonin with increased metabolite turnover possibly due to decreased expression of 5-HT_4 receptors. DSS-treated animals also expressed high levels of prokineticin-2 in the distal colon to possibly counteract the loss of contractility due to lower serotonin and 5-HT4 levels. Interestingly, we also observed increased pro-inflammatory transcripts of TNFα, IL-1β and iNOS in the lumbosacral region of the spinal cord and in the *substantia nigra* with a slightly elevated microglial density in the ventromedial hypothalamus. Together, the data points to priming of the mid-brain region towards neuroinflammation following intestinal inflammation.

Introduction

Ulcerative colitis (UC) is a chronic condition of intestinal inflammation of the colon. Along with Crohn's disease, UC falls under the umbrella of inflammatory bowel diseases (IBD) and affects 1-1.3 million people in the United States and 2.5 million in Europe (Kaplan, 2015). A rapidly emerging disease in developed countries, it constitutes about 0.5% of the diseases commonly seen in the general population (Molodecky et al., 2012). The disease is characterized by continued irregular recurrence of inflammation in the colon and especially the rectum. Unlike Crohn's disease where inflammation can occur throughout the gastrointestinal (GI) tract, UC is mainly restricted to the mucosa and submucosa of the affected region. Histologically, severe crypt architecture distortion, decreased crypt density, reduced mucous production and massive immune cell infiltration (basal plasmacytosis) along with erythema and edema (DeRoche et al., 2014). The precise etiology of the disease is unknown hence there is no cure for colitis; the disease recurrences are managed by a combination of anti-inflammatory or immunosuppressive drugs, steroids, analgesics and modifications in personal diet.

Understanding extraintestinal manifestations of IBD has steadily gained more importance due to new theories hypothesizing intestinal or peripheral inflammation as a trigger for neuroinflammation in the central nervous system (CNS) (Bonaz, 2013; Ghaisas et al., 2016). The idea that the GI and olfactory tract are (other than our skin) constantly exposed to pollutants, xenobiotics and potential toxic substances thus acting as a passageway for developing oxidative stress in the body has steadily gained credence following reports of intestinal inflammation or GI associated problems occurring in patients with Parkinson's

disease and autism spectrum disorders (ASD) (Lin et al., 2016; Walker et al., 2013; Welch et al., 2005).

The gut-brain axis is now recognized as an important conduit linking CNS signaling with GI functioning and vice versa. The autonomic nervous system including the sympathetic (visceral efferent neurons) and parasympathetic (including the splanchic and vagus nerves) nerves conveys signals bidirectionally thus integrating the functioning of the CNS and the GI tract. Following induction of UC or Crohn's disease, patients report increased visceral pain indicating heightened pain perception (Taylor and Keely, 2007). Interestingly, nerve hyperplasia and an increase in neuronal cell number in the myenteric plexus have been noted in a number of reports (Dvorak and Silen, 1985; Steinhoff et al., 1988). Vagal and spinal sensory neurons arise from different regions in the brain stem and terminate along the gut wall either in the large or small intestine and stomach. Due to nerve hyperplasia following intestinal inflammation, there is altered neuronal signaling in the hypothalamus-pituitary axis (HPA) (Bonaz and Bernstein, 2013). Interestingly, the *substantia nigra* (SN) region is presented immediately caudal to the hypothalamus. Dopaminergic neurons are present in the SN and these neurons pass through the hypothalamus as they extend rostral, to the striatum. The SN region plays an important role in reward and movement and loss of dopaminergic neurons in the *substantia nigra pars compacta* results in development of Parkinson's disease (PD). Notably, about 25-80% PD patients suffer from chronic GI problems including dyspepsia, dysphagia, excessive drooling or constipation and are thought to suffer from chronic intestinal inflammation compared to healthy individuals (Mishima et al., 2017; Shannon et al., 2012). Taking these facts into consideration, we hypothesize that peripheral

inflammation resulting from UC could be the trigger to develop neuroinflammation in the SN.

Materials and Methods

Chemicals

Dextran sodium sulfate (DSS) was obtained from MP Biomedicals (Cat. # 02160110). Antibodies CD68 (Cat. # MABF216) and glial fibrillary acidic protein (GFAP, Cat. # MAB360) were obtained from Millipore. Tumor necrosis factor- alpha antibody (TNFα, Cat. # AF-410-NA) was purchased from R&D signaling while inducible nitric oxide synthase (iNOS, Cat. #D6B6S) was bought from cell signaling technologies and prokineticin-2 (PK-2, Cat. #sc-67176) was obtained from Santa Cruz. β-actin was purchased from Sigma (Cat. # A2228). Hoechst 33342 nuclear stain was purchased from Invitrogen (H3570).

Animal studies

We purchased 10-12 week old C3H mice from Harlan laboratory for all animal experiments. Mice were housed on a 12-h light cycle with ad libitum access to food and water. After 3 days of acclimatization, mice received 3% DSS in drinking water for 7 days followed by regular tap water for 3 days or tap water for the entire duration of the study. This dose regimen was chosen based on previous rodent studies (Chaluvadi et al., 2009; Lange et al., 1996; Sanders et al., 2006). Animal care procedures strictly followed the NIH Guide for the Care and Use of Laboratory Animals and were approved by the Iowa State University IACUC. Body weight and whole gut transit time were measured every 10 days. At the end of the treatment regimen, animals were euthanized by CO_2, and then 3-cm strips of the colon

were collected and emptied of their contents by rinsing thoroughly in ice-cold PBS. Tissues were further excised into 1-cm pieces for various biochemical tests and stored at -80°C till further processing.

Tissue collection

Following euthanasia, the colon and cecum were removed and washed in phosphate-buffered saline (PBS). Colons were placed on filter papers to measure colonic lengths, score macroscopic cecal lesions, and obtain photographs of each tissue. Gross cecal lesions were scored using published criteria (Ye et al., 2009). Macroscopic cecal lesions were scored 0–4 as follows: no gross lesions (grade 0, normal); evidence of atrophy (grade 1, mild); excess intraluminal mucus with atrophy localized to the cecal apex (grade 2, moderate); generalized cecal atrophy with increased intraluminal mucus and no cecal contents (grade 3, severe); and score 3 plus bloody cecal content (grade 4, most severe.

Multiplex cytokine Luminex immunoassays

Blood was collected following terminal cardiac puncture and placed in serum collection tubes and frozen at −80°C. The levels of cytokines and chemokines in the supernatants were determined using the Luminex bead-based immunoassay platform (Panicker et al., 2015; Vignali, 2000) and prevalidated multiplex kits (Milliplex mouse cytokine panel, Millipore) according to the manufacturer's instructions.

Quantitative real-time PCR (qRT-PCR)

Ten tissues of distal colon from control and DSS-treated groups were utilized for qRT-PCR. The samples were homogenized in a bullet blender (Next Advance) using DNAse- and RNAse-free stainless steel beads and RNA was extracted using RNeasy Plus Mini kit (Qiagen). 1 μg total RNA was converted to cDNA using the High-Capacity cDNA Reverse Transcription kit (Applied Biosystems Inc.) following manufacturer's instructions. Real-time PCR was performed in an Mx3000P QPCR system (Stratagene) using the Brilliant SYBR Green QPCR Master Mix kit (Stratagene), with cDNAs corresponding to 0.5 μg of total RNA, 10 μl of 2 × master mix and 0.2 μM of each primer in a 20-μl final reaction volume. All reactions were performed in triplicate. Mouse 18S rRNA was used as an internal standard for normalization. Validated QuantiTect primer sets for mouse 18S rRNA (Cat# QT02448075), TNFα (QT00104006), IL-1β (QT01048355) and iNOS (QT00100275, Qiagen) were also used. The PCR cycling conditions contained an initial denaturation at 95°C for 10 min, followed by 40 cycles of denaturation at 95°C for 30 sec, annealing at 60°C for 30 sec, and extension at 72°C for 30 sec. Fluorescence was detected during the annealing step of each cycle. Dissociation curves were run to verify the singularity of the PCR product. Data were analyzed using the comparative threshold cycle (Ct) method (Schmittgen and Livak, 2008).

Western blots

Whole cell lysates or tissue lysates were prepared using modified radio immune precipitation assay (RIPA) buffer containing 20 mM Tris–HCl, pH 8.0, 2 mM EDTA, 10 mM EGTA, 2 mM dithiothreitol (DTT), 1 mM phenylmethylsulfonyl fluoride (PMSF), 20mM sodium

orthovanadate, 1 mM sodium fluoride and protease and phosphatase inhibitor cocktail (Thermo Scientific, Waltham, MA), as described previously (Harischandra, Kondru et al. 2014, Harischandra, Jin et al. 2015). The supernatants were obtained after centrifuging the homogenates at 15,000 rpm for 60 min. Protein concentration was measured using Bradford dye (Bio-Rad). Lysates containing equal amounts of protein were separated on a 12 or 15% SDS-polyacrylamide gel. After separation, proteins were electro-blotted onto a nitrocellulose membrane, and nonspecific binding sites were blocked with LICOR blocking buffer. PGP9.5 (1:1000), GFAP (1:1200), Bax (1:500), iNOS (1:500) and β-actin (1:10000) primary antibodies were used to blot the membranes for 16 h at 4°C. Thereafter, blots were washed in phosphate buffered saline (PBS) containing 0.01% Tween-20, incubated in respective secondary antibodies (Alexa Goat anti mouse 680 or Alexa Goat anti-rabbit 800) for 1 hour. Fluorescent bands corresponding to the protein of interest were observed by scanning membranes in a LICOR scanner.

Monoamine assessment via High performance liquid chromatography

Dissected colon segments were placed in buffer comprising 0.2 M perchloric acid, 0.05% Na_2EDTA, 0.1% $Na_2S_2O_5$ and isoproterenol (internal standard) and stored at -80°C until lysate preparation. To extract monoamine neurotransmitters, the samples were homogenized using bullet blender and 0.2 mm diameter stainless steel beads. Lysates were centrifuged and 300 µl of lysate was added to 30 mg alumina. The pH of the solution was quickly increased to 8.6 using 1M Tris buffer. The tubes were now rotated in a rotating shaker at 4°C for 15 minutes and then centrifuged at 10,000 rpm. The supernatant was aspirated and the monoamine neurotransmitters were eluted form the alumina with 0.2 M perchloric acid.

Monoamine lysates were placed in a refrigerated automatic sampler (model WPS-3000TSL) until being separated isocratically by a reversed-phase C18 column with a flow rate of 0.6 ml/ min using a Dionex Ultimate 3000 HPLC system (pump ISO-3100SD, Thermo Scientific, Bannockburn, IL). Electrochemical detection was achieved using a CoulArray model 5600A coupled with an analytical cell (microdialysis cell 5014B) and a guard cell (model 5020) with cell potentials set at -350, 0, 150, and 220 mV. Data acquisition and analysis were performed using Chromeleon 7 and ESA CoulArray 3.10 HPLC Software and quantified data were normalized to wet tissue weight.

Immunocytochemistry and Immunohistochemistry

For Immunohistochemistry, at the end of the treatment regime, animals were perfused first with PBS followed by 4% PFA. Guts were removed and post-fixed in 10% formalin for an additional 24 h. Tissues were embedded in paraffin and sectioned at 7 μm at Iowa State University's veterinary pathology lab. Paraffin-embedded sections of mouse tissues were deparaffinized in decreasing alcohol grades. Heat-mediated antigen retrieval was performed using 10 mM citrate buffer (pH 6.0) for 30 min. Sections were then incubated with blocking reagent (5% normal goat serum, 2% BSA and 0.5% Triton X-100 in PBS) for 60 min before being incubated with iNOS, CD68, PGP9.5 or GFAP primary antibodies for 24 h at 4°C. Sections were then washed many times in PBS and incubated in the dark for 90 min with Alexa-488 and 555 dye-conjugated secondary antibodies (1:1500). Nuclei were stained with Hoechst dye (1:5000) for 10 minutes at room temperature. Slides were viewed with 63× and 43× oil objectives using a Leica DMIRE2 confocal microscope.

Following perfusion, the rodent brains were removed and post fixed in 4% PFA for an additional 24 hours. To ensure cryopreservation of tissue architecture, the fixed brains were suspended in 30% sucrose for 3 days. The fixed brains were then embedded in OCT blocks and cryosectioned at 30 μm to obtain free-floating sections. The sections were washed in 1X PBS followed by heat mediated antigen retrieval using citrate buffer (pH 8.0) for 30 minutes. After blocking for 1 hour (5% normal goat serum, 2% BSA and 0.5% Triton X-100 in PBS) the sections were incubated in primary antibodies CD68 (mouse monoclonal, 1:300) and iNOS (rabbit monoclonal, 1:350) for 14 hours at 4°C followed by washing and secondary antibody application as mentioned above. Nuclei were stained with Hoechst dye (1:5000) for 10 minutes at room temperature. Slides were viewed with 63× and 43× oil objectives using a Leica DMIRE2 confocal microscope

Statistical analysis

All data are means ± standard error (SE). Unpaired t-test was used for statistical analysis using Graphpad Prism v.6.01. P-values less than 0.05 were considered to indicate statistical significance.

Results

Acute DSS-induced ulcerative colitis results in intestinal mucosal and sub-mucosal damage as well as systemic inflammation

We have used a known and validated DSS regime to induce acute colitis in these mice (Figure 1A). Thus mice given 3% DSS in drinking water for 7 days begin to show a steady decline in body weight (Figure 1B), movement and food consumption with some rectal

bleeding. Even after the mice receive regular drinking water without DSS, they do not regain their body weight by the end of the study. Following completion of the study, the colon was excised and gross observations were made. DSS treated (n=11) mice had shortened colons having cecal atrophy, enlarged cecal tonsil with thickening of the cecal and colon muscle wall (S. Table 1). A few mice (~50%) showed absence of formed fecal pellets indicating loss of colonic contractility in these mice. Such observation was not seen in any colon from the control group (n=10). There was considerable shortening of the colon with the average length in the DSS group being 6.9 cm compared to 9.3 cm seen in the control group (Figure 1C). Importantly, based on the high scores obtained by our scoring system (Figure 1E) as well as photographic evidence (Figure 1D), DSS treated mice showed much tissue damage compared to the control group. With pronounced weight loss and sickness behavior observed, we also assessed cytokine levels in the serum from both groups. As expected, DSS treated mice showed higher levels of IL-6 and IL-12 (Figure 1F) compared to control animals indicating peripheral inflammation following induction of UC.

Intestinal inflammation induces enteric neuronal and glial cell expression affecting monoamine neurotransmitter signaling.

Histological observation of hematoxylin and eosin stained sections showed alteration of the epithelia, massive immune cell infiltration in the mucosa and sub-mucosa and loss of crypts (Figure 2A). Distal colons from the DSS group had pronounced increase in pro-inflammatory factors such as TNFα, IL-1β and iNOS compared to the untreated group (Figure 2B). Loss of colonic epithelia leads to increased translocation of intestinal bacteria into the mucosa and deeper muscle layers exacerbating inflammation. The resulting intestinal damage and

inflammation results in pronounced immune cell migration with lymphocytes and neutrophils prominently seen at the sight of lesion (Campaniello et al., 2017). Indeed, colon sections from DSS treated mice showed increased iNOS and $CD68^+$ immune cell influx at the sight of lesion compared to the few patrolling cells usually observed in healthy GI tissue (Figure 2C).

Interestingly, we observed a decrease in dopamine (DA) and serotonin (5-HT) levels with no significant differences in their metabolites DOPAC and 5-HIAA respectively (Figure 3A). We also observed an increase in metabolite turnover (Figure 3B) indicating either a reduction in DA and 5-HT synthesis or reduced re-uptake by corresponding receptors. We then analyzed common DA and 5-HT receptor levels in the colon and found that the receptor 5-HT_4 had lower mRNA transcripts in the inflamed colon in comparison to the control group (Figure 3C). 5-HT_4 is mainly expressed in the colonic epithelium and mediates mucus secretion from and degranulation of goblet cells, chloride secretion from enterocytes and 5-HT production from enterochromaffin cells (Hoffman et al., 2012). Importantly, agonists of this receptor promote GI motility and reduce visceral pain (Kim, 2009; Sengupta et al., 2014). Thus reduced expression of this receptor can be linked to the sickness behavior and loose feces observed in the DSS treated mice. Acute DSS treatment increased the transcription of prokineticin-2 (PK-2, Figure 3D), a secreted protein that can potently induce GI contractions (Li et al., 2001). Immune cells also mainly secrete it during intestinal tissue damage. The presence of increased iNOS and PK-2 proteins were also quantified by Western blot. A 3-fold increase in iNOS and 3.5-fold increase in PK-2 was observed in DSS exposed colons compared to colons from untreated group (n=3-4, Figure 3F) Increased inflammation and corresponding intestinal damage has been linked to increased neurogenesis in the gut to

counteract the loss of enteric neurons and glial cells from the mucosal and sub-mucosal regions that are primarily affected in UC (Belkind-Gerson et al., 2015). Surprisingly, in this model of acute colitis we did not see increased expression of neurons (PGP9.5) or enteric glia (GFAP, Figure 3F) Rather, there was a decrease in glial derived neurotrophic factor (GDNF, Figure 3E), a protein involved in neurogenesis. Together, the data points towards acute colitis altering monoamine neurotransmitter production and signaling by downregulating their specific receptors. The immune influx and intestinal damage leads to high production of inflammatory factors that further exacerbate the inflammation leading not only to epithelial sloughing but also enteric neuronal and glial death.

Intestinal inflammation leads to increased pro-inflammatory cytokine production in the lumbosacral region of the spinal cord

While much research has focused on the role of the vagus nerve as an important conduit for signaling along the gut-brain axis, limited research has been conducted with regards to the spinal cord (Van Der Zanden et al., 2009). The spinal cord is divided into 4 regions with the lumbar and sacral spinal afferents projecting in the ileum and colon. Following induction of UC, 2-3 fold increase in the mRNA of pro-inflammatory cytokines TNFα and IL-1β as well as iNOS was observed in the lumbosacral region of the spinal cord (Figure 4A). Despite presence of increase inflammatory transcripts, we did not observe an increase in the resident immune cells- the microglia or in astrocytes as there was no significant increase in Iba-1 or GFAP protein expression (Figure 4B).

Neuroinflammation and peripheral immune infiltration is observed in the midbrain following induction of DSS-induced ulcerative colitis

Enteric inflammation is commonly observed in PD, autism and schizophrenia (Devos et al., 2013; Schieve et al., 2012; Severance et al., 2012). However, it is not known whether intestinal inflammation precedes and drives neurological dysfunction or is a consequence of it (Engelender and Isacson, 2017). Hence we analyzed the *substantia nigra pars compacta* (SNpc)- an important region that regulates fine motor control and reward behavior and is the primarily affected in PD. SNpc from the DSS treated group showed increased mRNA transcripts of iNOS and IL-1β (Figure 5A). Both pro-inflammatory factors were increased about 2-fold when compared to SNpc samples from the untreated group. Interestingly, while we did not observe any gliosis or microglial activation in the SNpc (Figure 5B), we did observe more Iba-1^{+} microglia in the ventral hypothalamic nuclei (Figure 5C). Together, the data suggests that acute DSS-induced colitis potentially primes the SNpc where there is an increased transcript level of pro-inflammatory factors.

Discussion

Ulcerative colitis is a chronic intestinal inflammatory condition with intermittent recurrences despite proper medications. The disease is characterized by loss of colonic epithelia and inflammation in the mucosa and sub-mucosa. In most cases, the body is unable to regulate the sustained mucosal immune response resulting in greater production of inflammatory cytokines and chemokines leading to tissue damage (Parray et al., 2012). In most cases, the chronicity of intestinal inflammation leads to alterations in the autonomic nervous system (ANS) with nerve hyperplasia in the affected tissue and fluctuations in neurotransmitter

signaling (Neunlist et al., 2003). However, do the effects on the ANS lead to changes in the CNS? To answer this pertinent question, we used a known mouse model of UC. C3H mice given 3% DSS for 7 days followed by 3 days of normal drinking water mimics the acute phase of UC with distal colonic inflammation (Figures 1D and 1E), damage to the mucosa and sub-mucosa (Figure 2A) and shortening of the colon (Figures 1C and 1D). Influx of macrophages was evident in DSS treated colons (Figure 2C) and high production of iNOS and other pro-inflammatory factors (Figure 2B and 3F). Notably despite removal of DSS from drinking water in the last 3 days before completion of the study, the mice continued to loose weight (Figure 1B) and had peripheral inflammation as evidenced by high levels of IL-6 and IL-12 in the serum of DSS exposed mice compared to untreated mice (Figure 1F). IL-6 plays an important role in differentiation of Th17 cells and is vital in preventing intestinal epithelial apoptosis during inflammation. Hence elevated IL-6 levels in the serum might be a counteractive measure against loss of colonic epithelia. However, IL-6 is also involved in propagating inflammation and its continued presence is considered harmful in many chronic diseases such as rheumatoid arthritis, ischemia and PD (Chao et al., 2014; Liang et al., 2009; Zhang et al., 2015).

Acute colitis also resulted in a decrease in serotonin (Figure 3A) and increased turnover in dopamine and serotonin metabolites (Figure 3B). Loss of enteric neuronal or glial terminals in the sub-mucosa and mucosa as well as loss of enterochromaffin cells present in this region might lead to a decrease altered neurotransmitter production. The increased monoamine neurotransmitter turnover might be due to loss of DA or 5-HT receptors. Hence we screened various neurotransmitter receptors present in the gut (data not known). We observed a down-regulation of 5-HT_4 receptor transcript in the distal colon (Figure 3C). This was an

interesting observation as we had also found a lack of formed fecal pellets in many colons from the DSS group (Figures 1D). 5-HT_4 receptors are present mainly in the mucosa while a subset (5-HT_{4e} and 5-HT_{4f}) are mainly present on pre-synaptic terminals (Liu et al., 2005). The main function of these presynaptic 5-HT_4 receptors is to increase excitatory neurotransmission thus inducing prokinetic effect on the smooth muscles. This initiates intestinal smooth muscle contraction. Even the 5-HT_4 receptors present in the mucosa initiate motility and reduce visceral hypersensitivity (Hoffman et al., 2012). Thus a loss of 5-HT_4 in the affected portion of the colon can reduce the propulsive action and contractility required for proper fecal pellet formation. However following loss of 5-HT_4 receptor expression, the body might produce prokinetics that would directly act on smooth muscles leading to contraction. This might be the reason why increased PK-2 was observed in the same regions that had lower transcript level of 5-HT_4 receptors. PK-2 is predominantly expressed by infiltrating macrophages and neutrophils at the site of intestinal lesion and can enhance GI motility (Watson et al., 2012). Increased production of PK2 might potentiate contraction allowing the non-inflamed regions the colon to come closer minimizing intestinal permeability. However, more work needs to be conducted with PK-2 knockout mice to validate this theory.

Perhaps the most interesting observation made was the presence of increased inflammatory transcripts in the spinal cord and SNpc region in the brain following acute colitis. A modest increase of iNOS, IL-1β and even TNFα was observed in both regions despite these areas not being the primary site of inflammation (Figures 4A and 5A). We did not observe such increase in pro-inflammatory transcripts in other parts of the brain (data not shown). Hence

intestinal inflammation possibly influenced neuroinflammation in the mid-brain possibly through the pelvic and sacral nerves that innervate the colon and rectum- incidentally the two regions most affected by UC. It is possible that the HPA axis is activated leading to stress and sickness behavior observed in other studies of DSS induced colitis (Melgar et al., 2008; Reichmann et al., 2015).

The presence of peripheral inflammation might condition the host's immune system to a pro-inflammatory profile. Initially thought to be an immune privileged site, we now know that peripheral immune cells routinely patrol the CNS sampling antigens and surveilling the CNS much like the brains own resident immune cells- the microglia. While increased inflammation in the SNpc did not correspond to activation of the astrocytes, microglia or peripheral immune cells infiltration, we did observe a modestly elevated microglial density in DSS- treated ventromedial hypothalamus (Figure 5C). Villarán *et al* have shown that ulcerative colitis in mice exacerbated lipopolysaccharide induced SN damage (Villaran et al., 2010). It is possible that the acute phase of this disorder primes the microglia to hyper vigilant state with exaggerated immune response that would be observed as the disease progresses. Serum IL-6 can increase the porosity of the blood brain barrier leading to influx of not only peripheral immune cells but also potential toxic substances and other pro-inflammatory factors thus generating neuroinflammation in the CNS. Together the data points towards neuroinflammation in the mid-brain region brought on by intestinal inflammation that can lead to development of exaggerated microglial activation if the peripheral inflammation continues unabated.

Future studies aimed at validating these findings in UC patients post-mortem is needed.

Acknowledgements

We would like to thank Gary Zenitsky for his help in preparing the manuscript.

Funding

Supported by NIH grants ES10586 and NS074443 and NS039958.

References

Belkind-Gerson, J., R. Hotta, N. Nagy, A. R. Thomas, H. Graham, L. Cheng, J. Solorzano, D. Nguyen, M. Kamionek, J. Dietrich, B. J. Cherayil and A. M. Goldstein (2015). "Colitis induces enteric neurogenesis through a 5-HT4-dependent mechanism." Inflamm Bowel Dis **21**(4): 870-878.

Bonaz, B. (2013). "Inflammatory bowel diseases: a dysfunction of brain-gut interactions?" Minerva Gastroenterol Dietol **59**(3): 241-259.

Bonaz, B. L. and C. N. Bernstein (2013). "Brain-gut interactions in inflammatory bowel disease." Gastroenterology **144**(1): 36-49.

Campaniello, M. A., C. Mavrangelos, S. Eade, A. M. Harrington, L. A. Blackshaw, S. M. Brierley, S. D. Smid and P. A. Hughes (2017). "Acute colitis chronically alters immune infiltration mechanisms and sensory neuro-immune interactions." Brain Behav Immun **60**: 319-332.

Chaluvadi, M. R., B. A. Nyagode, R. D. Kinloch and E. T. Morgan (2009). "TLR4-dependent and -independent regulation of hepatic cytochrome P450 in mice with chemically induced inflammatory bowel disease." Biochem Pharmacol **77**(3): 464-471.

Chao, Y., S. C. Wong and E. K. Tan (2014). "Evidence of inflammatory system involvement in Parkinson's disease." Biomed Res Int **2014**: 308654.

DeRoche, T. C., S. Y. Xiao and X. Liu (2014). "Histological evaluation in ulcerative colitis." Gastroenterol Rep (Oxf) **2**(3): 178-192.

Devos, D., T. Lebouvier, B. Lardeux, M. Biraud, T. Rouaud, H. Pouclet, E. Coron, S. Bruley des Varannes, P. Naveilhan, J. M. Nguyen, M. Neunlist and P. Derkinderen (2013). "Colonic inflammation in Parkinson's disease." Neurobiol Dis **50**: 42-48.

Dvorak, A. M. and W. Silen (1985). "Differentiation between Crohn's disease and other inflammatory conditions by electron microscopy." Ann Surg **201**(1): 53-63.

Engelender, S. and O. Isacson (2017). "The Threshold Theory for Parkinson's Disease." Trends Neurosci **40**(1): 4-14.

Ghaisas, S., J. Maher and A. Kanthasamy (2016). "Gut microbiome in health and disease: Linking the microbiome-gut-brain axis and environmental factors in the pathogenesis of systemic and neurodegenerative diseases." Pharmacol Ther **158**: 52-62.

Hoffman, J. M., K. Tyler, S. J. MacEachern, O. B. Balemba, A. C. Johnson, E. M. Brooks, H. Zhao, G. M. Swain, P. L. Moses, J. J. Galligan, K. A. Sharkey, B. Greenwood-Van Meerveld and G. M. Mawe (2012). "Activation of colonic mucosal 5-HT(4) receptors accelerates propulsive motility and inhibits visceral hypersensitivity." Gastroenterology **142**(4): 844-854 e844.

Kaplan, G. G. (2015). "The global burden of IBD: from 2015 to 2025." Nat Rev Gastroenterol Hepatol **12**(12): 720-727.

Kim, H. S. (2009). "5-Hydroxytryptamine4 receptor agonists and colonic motility." J Smooth Muscle Res **45**(1): 25-29.

Lange, S., D. S. Delbro, E. Jennische and I. Mattsby-Baltzer (1996). "The role of the Lps gene in experimental ulcerative colitis in mice." APMIS **104**(11): 823-833.

Li, M., C. M. Bullock, D. J. Knauer, F. J. Ehlert and Q. Y. Zhou (2001). "Identification of two prokineticin cDNAs: recombinant proteins potently contract gastrointestinal smooth muscle." Mol Pharmacol **59**(4): 692-698.

Liang, B., Z. Song, B. Wu, D. Gardner, D. Shealy, X. Y. Song and P. H. Wooley (2009). "Evaluation of anti-IL-6 monoclonal antibody therapy using murine type II collagen-induced arthritis." J Inflamm (Lond) **6**: 10.

Lin, J. C., C. S. Lin, C. W. Hsu, C. L. Lin and C. H. Kao (2016). "Association Between Parkinson's Disease and Inflammatory Bowel Disease: a Nationwide Taiwanese Retrospective Cohort Study." Inflamm Bowel Dis **22**(5): 1049-1055.

Liu, M., M. S. Geddis, Y. Wen, W. Setlik and M. D. Gershon (2005). "Expression and function of 5-HT4 receptors in the mouse enteric nervous system." Am J Physiol Gastrointest Liver Physiol **289**(6): G1148-1163.

Melgar, S., K. Engstrom, A. Jagervall and V. Martinez (2008). "Psychological stress reactivates dextran sulfate sodium-induced chronic colitis in mice." Stress **11**(5): 348-362.

Mishima, T., J. Fukae, S. Fujioka, K. Inoue and Y. Tsuboi (2017). "The Prevalence of Constipation and Irritable Bowel Syndrome in Parkinson's Disease Patients According to Rome III Diagnostic Criteria." J Parkinsons Dis.

Molodecky, N. A., I. S. Soon, D. M. Rabi, W. A. Ghali, M. Ferris, G. Chernoff, E. I. Benchimol, R. Panaccione, S. Ghosh, H. W. Barkema and G. G. Kaplan (2012). "Increasing incidence and prevalence of the inflammatory bowel diseases with time, based on systematic review." Gastroenterology **142**(1): 46-54 e42; quiz e30.

Neunlist, M., P. Aubert, C. Toquet, T. Oreshkova, J. Barouk, P. A. Lehur, M. Schemann and J. P. Galmiche (2003). "Changes in chemical coding of myenteric neurones in ulcerative colitis." Gut **52**(1): 84-90.

Panicker, N., H. Saminathan, H. Jin, M. Neal, D. S. Harischandra, R. Gordon, K. Kanthasamy, V. Lawana, S. Sarkar, J. Luo, V. Anantharam, A. G. Kanthasamy and A. Kanthasamy (2015). "Fyn Kinase Regulates Microglial Neuroinflammatory Responses in Cell Culture and Animal Models of Parkinson's Disease." J Neurosci **35**(27): 10058-10077.

Parray, F. Q., M. L. Wani, A. A. Malik, S. N. Wani, A. H. Bijli, I. Irshad and H. Nayeem Ul (2012). "Ulcerative colitis: a challenge to surgeons." Int J Prev Med **3**(11): 749-763.

Reichmann, F., A. M. Hassan, A. Farzi, P. Jain, R. Schuligoi and P. Holzer (2015). "Dextran sulfate sodium-induced colitis alters stress-associated behaviour and neuropeptide gene expression in the amygdala-hippocampus network of mice." Sci Rep **5**: 9970.

Sanders, C. J., Y. Yu, D. A. Moore, 3rd, I. R. Williams and A. T. Gewirtz (2006). "Humoral immune response to flagellin requires T cells and activation of innate immunity." J Immunol **177**(5): 2810-2818.

Schieve, L. A., V. Gonzalez, S. L. Boulet, S. N. Visser, C. E. Rice, K. Van Naarden Braun and C. A. Boyle (2012). "Concurrent medical conditions and health care use and needs among children with learning and behavioral developmental disabilities, National Health Interview Survey, 2006-2010." Res Dev Disabil **33**(2): 467-476.

Schmittgen, T. D. and K. J. Livak (2008). "Analyzing real-time PCR data by the comparative C(T) method." Nat Protoc **3**(6): 1101-1108.

Sengupta, J. N., A. Mickle, P. Kannampalli, R. Spruell, J. McRorie, R. Shaker and A. Miranda (2014). "Visceral analgesic effect of 5-HT(4) receptor agonist in rats involves the rostroventral medulla (RVM)." Neuropharmacology **79**: 345-358.

Severance, E. G., A. Alaedini, S. Yang, M. Halling, K. L. Gressitt, C. R. Stallings, A. E. Origoni, C. Vaughan, S. Khushalani, F. M. Leweke, F. B. Dickerson and R. H. Yolken (2012). "Gastrointestinal inflammation and associated immune activation in schizophrenia." Schizophr Res **138**(1): 48-53.

Shannon, K. M., A. Keshavarzian, E. Mutlu, H. B. Dodiya, D. Daian, J. A. Jaglin and J. H. Kordower (2012). "Alpha-synuclein in colonic submucosa in early untreated Parkinson's disease." Mov Disord **27**(6): 709-715.

Steinhoff, M. M., I. J. Kodner and K. DeSchryver-Kecskemeti (1988). "Axonal degeneration/necrosis: a possible ultrastructural marker for Crohn's disease." Mod Pathol **1**(3): 182-187.

Taylor, C. T. and S. J. Keely (2007). "The autonomic nervous system and inflammatory bowel disease." Auton Neurosci **133**(1): 104-114.

Van Der Zanden, E. P., G. E. Boeckxstaens and W. J. de Jonge (2009). "The vagus nerve as a modulator of intestinal inflammation." Neurogastroenterol Motil **21**(1): 6-17.

Vignali, D. A. (2000). "Multiplexed particle-based flow cytometric assays." J Immunol Methods **243**(1-2): 243-255.

Villaran, R. F., A. M. Espinosa-Oliva, M. Sarmiento, R. M. De Pablos, S. Arguelles, M. J. Delgado-Cortes, V. Sobrino, N. Van Rooijen, J. L. Venero, A. J. Herrera, J. Cano and A. Machado (2010). "Ulcerative colitis exacerbates lipopolysaccharide-induced damage to the

nigral dopaminergic system: potential risk factor in Parkinson`s disease." J Neurochem **114**(6): 1687-1700.

Walker, S. J., J. Fortunato, L. G. Gonzalez and A. Krigsman (2013). "Identification of unique gene expression profile in children with regressive autism spectrum disorder (ASD) and ileocolitis." PLoS One **8**(3): e58058.

Watson, R. P., E. Lilley, M. Panesar, G. Bhalay, S. Langridge, S. S. Tian, C. McClenaghan, A. Ropenga, F. Zeng and M. S. Nash (2012). "Increased prokineticin 2 expression in gut inflammation: role in visceral pain and intestinal ion transport." Neurogastroenterol Motil **24**(1): 65-75, e12.

Welch, M. G., T. B. Welch-Horan, M. Anwar, N. Anwar, R. J. Ludwig and D. A. Ruggiero (2005). "Brain effects of chronic IBD in areas abnormal in autism and treatment by single neuropeptides secretin and oxytocin." J Mol Neurosci **25**(3): 259-274.

Ye, Z., Z. Liu, A. Henderson, K. Lee, J. Hostetter, M. Wannemuehler and S. Hendrich (2009). "Increased CYP4B1 mRNA is associated with the inhibition of dextran sulfate sodium-induced colitis by caffeic acid in mice." Exp Biol Med (Maywood) **234**(6): 605-616.

Zhang, J., G. B. Sadowska, X. Chen, S. Y. Park, J. E. Kim, C. A. Bodge, E. Cummings, Y. P. Lim, O. Makeyev, W. G. Besio, J. Gaitanis, W. A. Banks and B. S. Stonestreet (2015). "Anti-IL-6 neutralizing antibody modulates blood-brain barrier function in the ovine fetus." FASEB J **29**(5): 1739-1753.

Figures

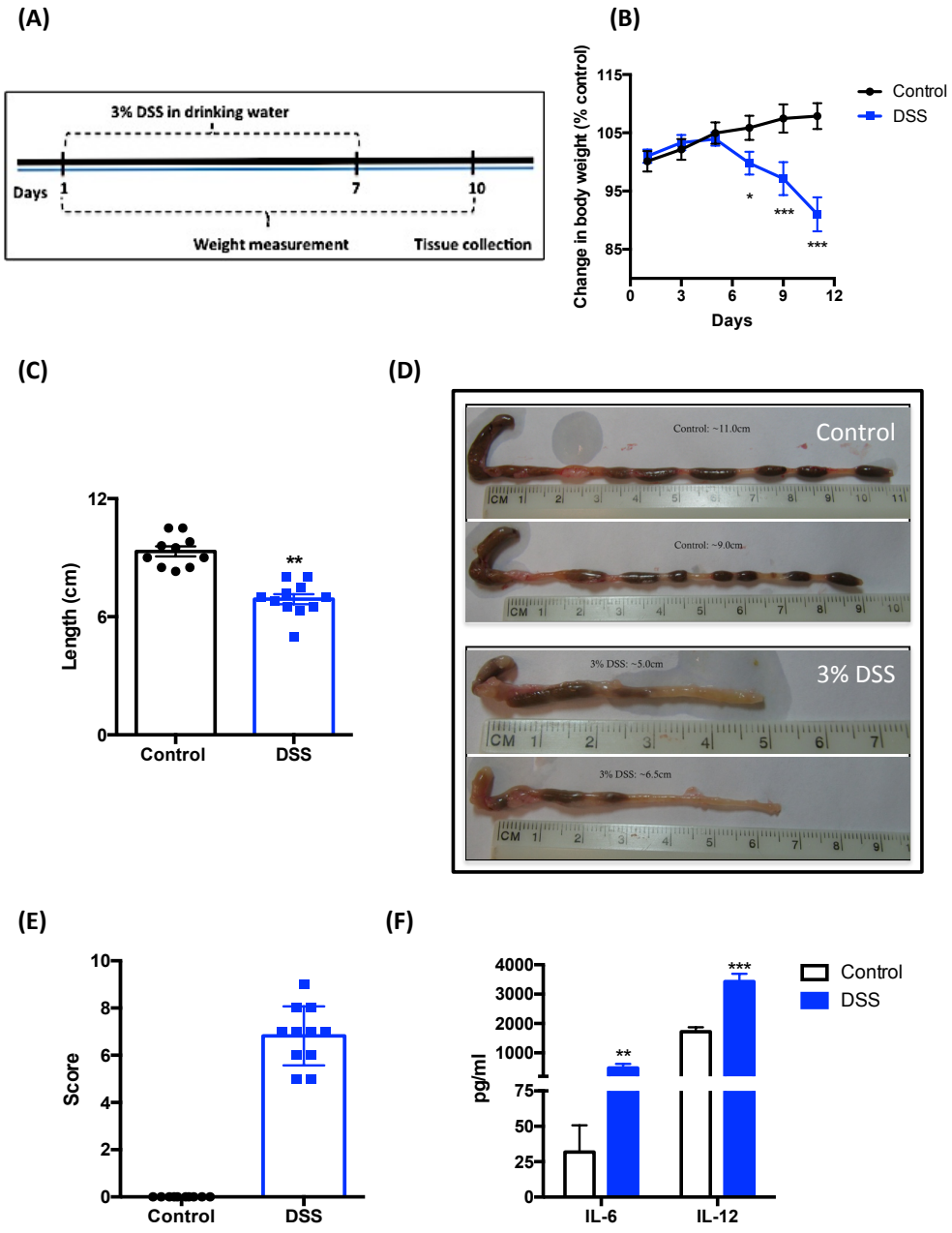

Figure 1: Acute DSS-induced ulcerative colitis induces tissue damage to the colon

(A) Treatment paradigm. (B) Body weight change. Body weight change was calculated for each mouse by dividing its body weight on the specified day by its weight at day 0 (C) Colon length in centimeters. (D) Representative photos of colon from control (upper panel) and DSS group (lower panel) at day 10. (E) Inflammation scoring based on gross observation of

the cecum and colon from each animal in both groups. (F) Analysis of serum IL-6 and IL-12 levels from mice in each group in pictograms per milliliter serum. Data represented as the group mean ± SEM from n=10 or n=11. Asterisks (*p<0.05, **p<0.01 and ***p<0.001) indicate significant differences between DSS-treated group and control.

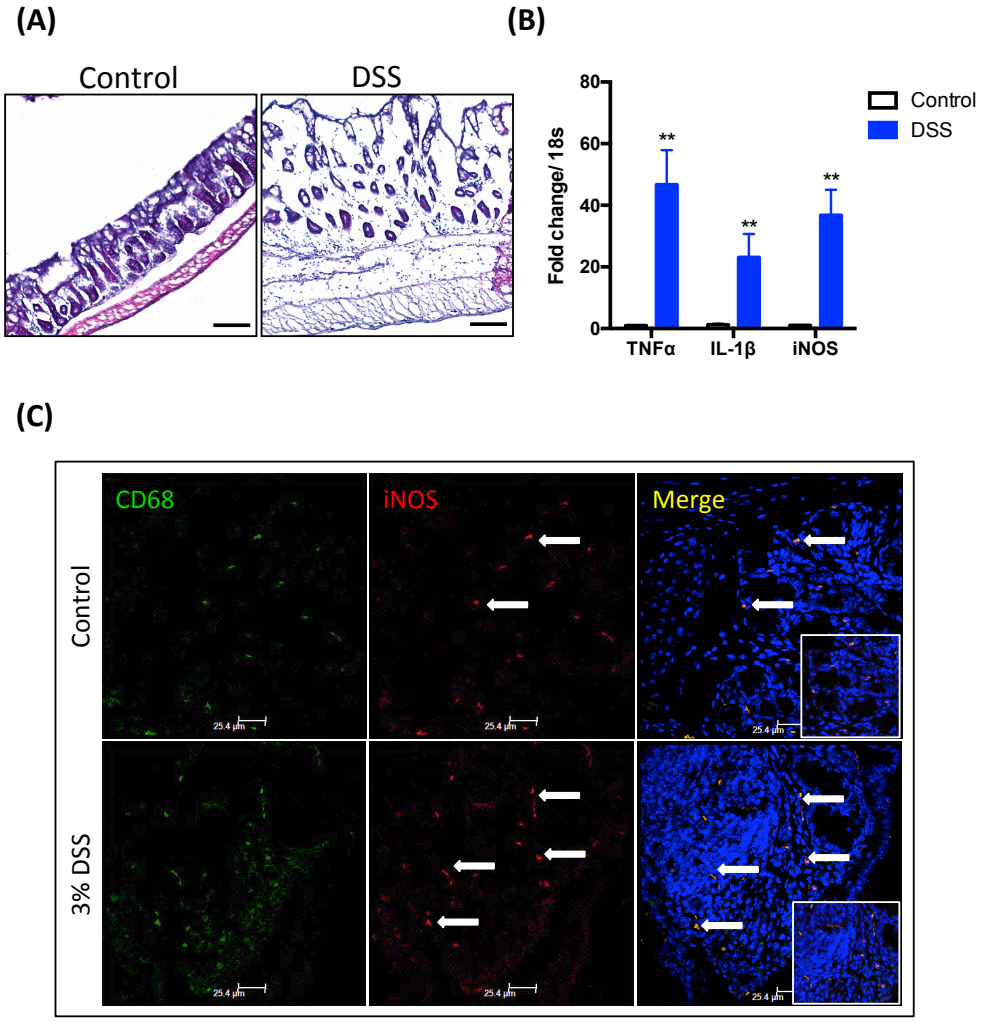

Figure 2: Immune cell infiltration at site of inflammation in the colon

(A) Representative 10x images of hematoxylin and eosin-stained colon sections from untreated and DSS-treated groups (n=3). Scale bar = 50 µm. (B) qRT-PCR analysis of TNFα, IL-1β and iNOS mRNA transcripts, normalized to 18S rRNA expression (n=7). (C)

Representative 60x immunofluorescence images showing increased iNOS production in the distal colon of DSS-treated mouse when compared to control. Scale bar = 25.4 µm. Arrows indicate presence of iNOS staining. Data represented as the group mean ± SEM. Asterisks (***p<0.001) indicate significant differences between DSS-treated group and control.

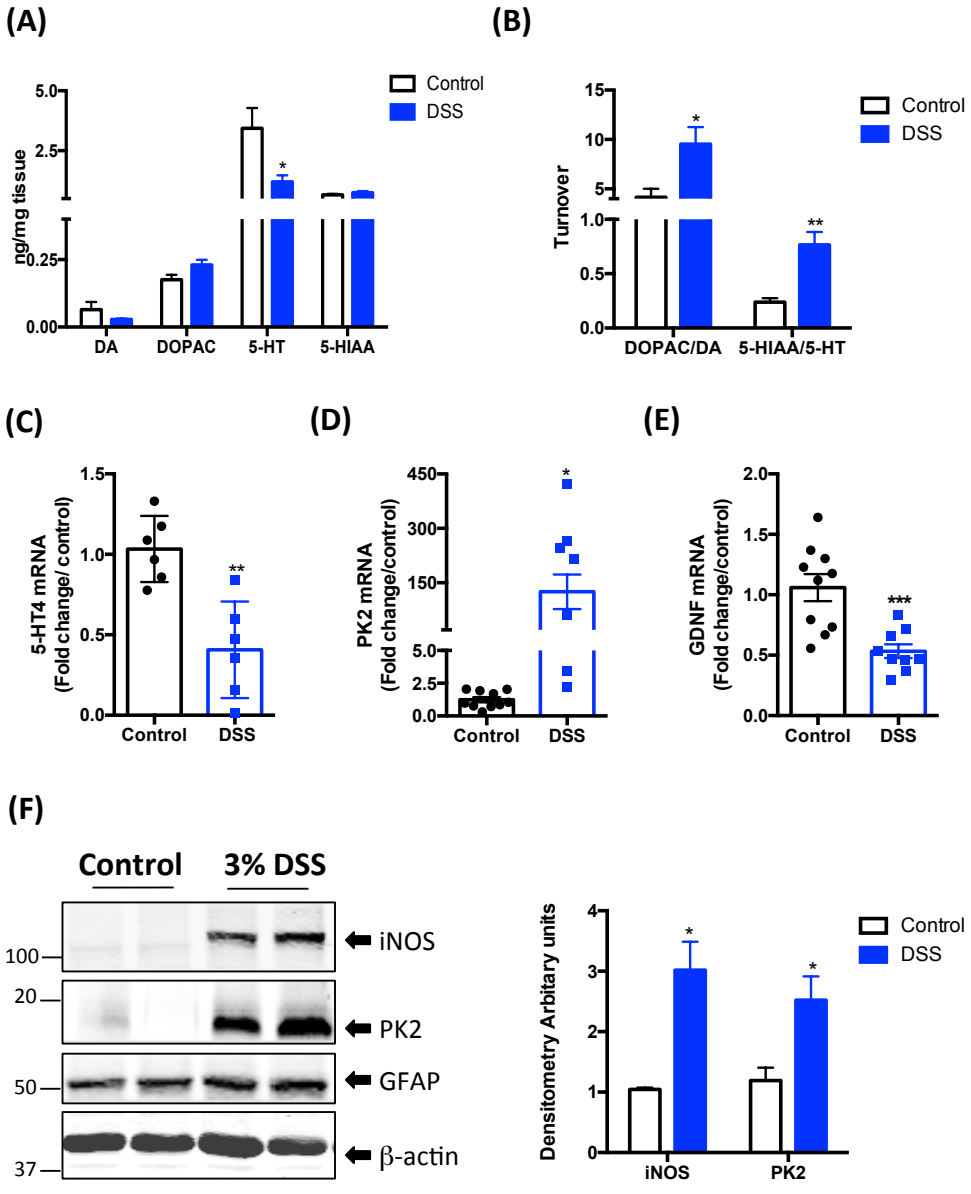

Figure 3: Acute colitis leads to altered neurotransmitter and their receptor levels and increased prokineticin-2. (A) HPLC analysis of monoamine neurotransmitter levels in the

distal colon in nanograms per miligram tissue. (B) Turnover ratio of metabolite to its neurotransmitter. (C) q-RT PCR analysis of 5-HT_4 receptor transcripts normalized to 18s rRNA expression (n=6) (D) q-RT PCR analysis of PK-2 transcripts normalized to 18s rRNA expression (n=7) (E) q-RT PCR analysis of GDNF receptor transcripts normalized to 18s rRNA expression (n=10) (F) Representative Western blots showing increased iNOS and PK-2 expression in DSS treated colons compared to the untreated group. No significant change in GFAP expression is observed between the two groups. Data represented as the group mean ± SEM. Asterisks (*p<0.05, **p<0.01 and ***p<0.001) indicate significant differences between DSS-treated group and control.

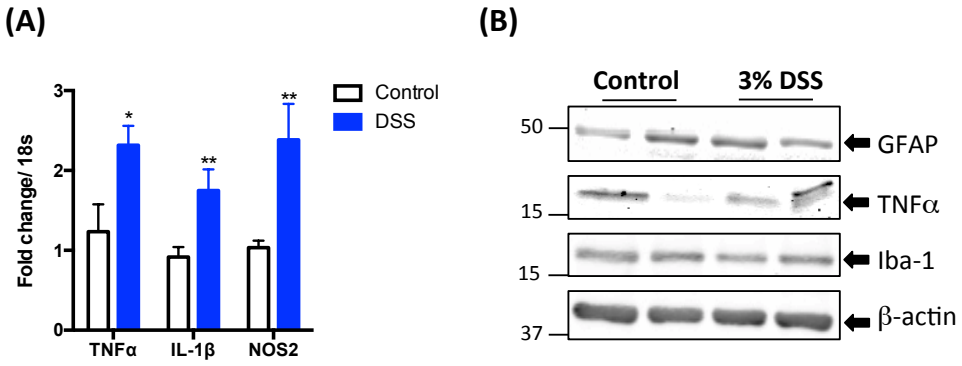

Figure 4: DSS induced colitis potentiates inflammation in the spinal cord

(A) qRT-PCR analysis of TNFα, IL-1β and iNOS mRNA transcripts, normalized to 18S rRNA expression (n=6). (B) Representative Western blots showing no significant difference in GFAP, TNFα or IBA-1 expression in the spinal cord between control and DSS groups. Data represented as the group mean ± SEM. Asterisks (*p<0.05, **p<0.01 and ***p<0.001) indicate significant differences between DSS-treated group and control.

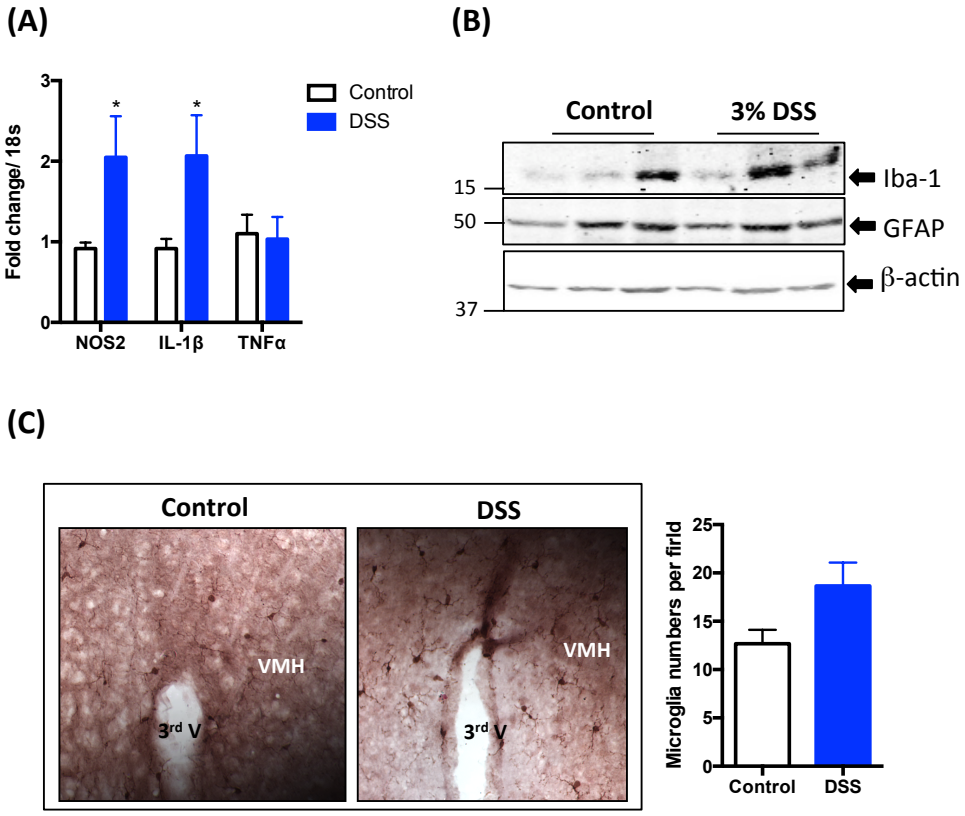

Figure 5: Acute colitis potentiates inflammation in the mid-brain

(A) qRT-PCR analysis of TNFα, IL-1β and iNOS mRNA transcripts, normalized to 18S rRNA expression (n=6). (B) Representative Western blots showing no significant difference in GFAP or IBA-1 expression in the substantia nigra between control and DSS groups. (C) Representative 30x images of microglia in the ventromedial hypothalamus. Modest increase in IBA-1 positive microglia present around the 3rd ventricle in the ventromedial hypothalamic region of DSS group compared to control. Data represented as the group mean ± SEM. Asterisks (*$p<0.05$) indicate significant differences between DSS-treated group and control.

S. Table 1: Inflammation scoring based on gross observations

	Cecal atrophy	Enlarged cecal tonsil/ lymph node aggregate	Cecal empyting	Abnormally watery/ mucoid intraluminal cecal contents	Abnormally watery/ mucoid intraluminal colon contents	Luminal blood in cecum	Luminal blood in colon	Thickening / rigidity cecum	Thickening / rigidity colon	Absence formed fecal pellets in colon	Colon Length
Control											10.5
											9
											9.5
											8.3
											9.6
											9
											8.5
											9.8
											10.5
											8.5
3% DSS	1	1		1		1		1	1	1	7
	1	1		1	1	1		1	1	1	5
	1	1	1	1	1			1	1	1	6.5
	1	1	1	1	1	1		1	1	1	6.3
	1	1	1	1		1		1	1		8
	1	1		1		1		1	1		8
	1	1		1		1		1	1	1	6.8
	1	1		1		1		1	1		7.5
	1	1		1				1	1		7.2
	1	1		1		1		1	1	1	7
	1	1	1					1	1		6.5

GENERAL CONCLUSIONS AND FUTURE DIRECTIONS

This section presents an overview of the results and findings of this dissertation, with special emphasis on their overall implications for the role of intestinal inflammation in priming the CNS to develop neuroinflammation. The major findings of each research chapter included in this dissertation are covered in the discussion section of the relevant chapter.

CHRONIC EXPOSURE TO ENVIRONMENTAL TOXIN MANGANESE (Mn) LEADS TO INTESTINAL INFLAMMATION AND SUBSEQUENT ALTERATIONS IN GASTROINTESTINAL PHYSIOLOGY

The enteric nervous system, which plays an important role in maintaining gut physiology, consists of enteric neurons and glia. Enteric glia cells (EGCs) share similar features with astrocytes present in the CNS, namely, presence of glial fibrillary acidic protein (GFAP) as well as S-100β as cell markers (Jessen and Mirsky, 1983). EGCs play an important role in supporting intestinal health by regulating the intestinal-epithelial barrier and acting as a bridge between neuronal and immune signaling circuits (Gulbransen and Sharkey, 2012). Hence, maintaining a healthy population of EGCs is necessary to maintain proper intestinal function. Manganese (Mn) is a an important divalent metal that is required in trace amounts for our normal body functioning (Avila et al., 2013), but chronic exposure to excessive Mn induces a Parkinsonian-like neurotoxic response. The effect of low-dose Mn on EGCs has not been well characterized.

In this chapter, we demonstrated that low nanomolar doses of Mn affect EGCs by compromising mitochondrial health. Notably, the low doses caused only cell stress rather than cell death, a point of particular importance because human exposure to Mn occurs

mainly in low doses rather than a single high dose. Typically, at higher doses of Mn exposure we found both caspase-3-mediated apoptosis as well as necrotic cell death.

However, the gut is made up of different cell types present in distinct layers. Hence, to get a better sense of how Mn affects GI tissues, we developed methods for a new primary enteric culture representing all major cell types in the GI tract. The kinetics of Mn-induced toxicity changed considerably in this mixed culture with a 100-μM Mn exposure inducing metabolic stress in the cell population as a whole. Specifically, it caused production of inflammatory factors such as TNFα, IL-1β and iNOS, culminating in neuronal cell death.

In an *in vivo* model of chronic exposure, we observed that even a low dose of Mn causes modest but definite changes in the GI tract. Specifically, 15 mg/kg/day Mn for 30 days induced mild colonic inflammation without causing any overt tissue damage. Chronic exposure to this metal down regulated expression of the Mn exporters ferroportin and SLC30A10 with no change in the Mn importer DMT1. This indicates that Mn was accumulating in the gut tissue during chronic low-dose exposure. ICP-MS of colonic tissue further confirmed that Mn-exposed animals had significantly higher Mn content in the intestine compared to unexposed controls. Importantly, Mn-exposed mice required more time for food to be absorbed and removed as waste compared to control mice, suggesting that normal intestinal peristalsis was affected following Mn treatment. Finally we showed that Mn exposure alters intestinal physiology affecting carbohydrate and especially fatty acid and amino acid synthesis with more pro-inflammatory-provoking short chain fatty acids produced in the presence of elevated Mn. While gut microbial populations did not differ significantly between groups, we did observe an increase in *Gammaproteobacteria* at Day 20, incidentally at the same time we observed increases in whole gut transit time. It is important to note that

the concentration of Mn that we administered to mice was comparable to the elevated levels found in groundwater (Bouchard et al., 2011).

Future studies will be aimed at decoding the molecular and biochemical signaling pathways that stressed EGCs employ and how the presence of Mn skews the host's physiology. Utilization of cell culture models for mechanistic studies will provide new insights into the Mn-induced neurotoxicity response of the ENS.

SPATIAL DIFFERENCES IN GUT MOTILITY IN THE MITOPARK MOUSE MODEL OF PARKINSON'S DISEASE

In Chapter 2, we demonstrated for the first time how chronic exposure to even low doses of Mn affect intestinal physiology. Occupational exposure to Mn can lead to "manganism", a neurological condition showing motor symptoms similar to Parkinson's disease (PD) (Gunnarsson and Bodin, 2017). PD is thought to be a complex interplay of genetic and environmental factors (Warner and Schapira, 2003). While PD is defined by the presence of motor deficits such as muscle rigidity and a slow shuffling gait, incoordination, resting tremor and postural instability, recent studies have shown that sleep disturbances, constipation and anosmia are seen in most patients decades before actual disease diagnosis. Hence, it is important to understand whether these non-motor symptoms potentiate neurological dysfunction or are an early consequence, affected even by slight changes in neurological signaling.

The MitoPark mouse model of PD mimics the adult onset and age-dependent dopaminergic neuron loss typically seen in PD patients (Ekstrand and Galter, 2009). Much emphasis has been given to this model's use as a tool to study the progressive motor symptoms associated

with PD. However, characterization of its non-motor symptoms, especially GI dysfunction, has yet to be systematically carried out. In our study, we systematically observed CNS-related behavior and GI motility in mice ranging in age from 8-24 weeks of age. MitoPark mice began to exhibit significant loss of dopaminergic neurons from 12-16 weeks of age, during which time we also observed lower reserves of dopamine in the colon. MitoPark mice showed increased colon transit time at 24 weeks compared to age-matched littermate controls (LCs), thus displaying a constipated phenotype similarly seen in PD patients. Paradoxically, the small intestine's transit time seemed to be faster than that in LC mice, leading us to speculate that the effect of dopamine (dopamine signaling) on smooth muscle contraction differed between the small and large intestines. For instance, dopamine acting on DA1 receptors on smooth muscles causes muscle relaxation, while the same neurotransmitter acting on DA2 receptors present on post-ganglionic sympathetic nerves counteracts the effect of norepinephrine-induced muscle relaxation, thereby inducing contraction (Kirschstein et al., 2009; Zizzo et al., 2010). We found no significant difference between D1 and D2 receptor expression in the colon. We speculate that alpha- and beta-adrenergic receptors might play a more important role in dopamine-induced muscle contraction or relaxation as they are known to be part of the dopamine circuitry (Bech et al., 1982; Seiler et al., 2005). More studies need to be conducted to understand how PD-related dopamine loss contributes to opposing motility behavior in the small and large intestine. Despite the loss of dopaminergic neurons, we did not observe significant differences in the enteric neuronal population, suggesting that other neuronal sub-types might be altered in response to reduced dopamine to counteract the effects brought upon by dopamine loss. An interesting observation that needs further investigation is the role of the hypothalamus-pituitary axis

(HPA) in the context of PD. We observed increased levels of neuropeptide Y, a peptide that plays an important role in regulating hunger. We observed increased NpY in the hypothalamus of MitoPark mice displaying normal feeding behavior despite prominent weight loss. Such weight loss in animals with an otherwise normal appetite relative to LCs brings us back to the motility deficits in these animals. Small intestine motility affects digestion and absorption of nutrients, while colonic peristalsis is required for water and electrolyte absorption. Hence, faster motility in the small intestine means that nutrients are not optimally absorbed despite a healthy diet. These results have implications for PD treatment and diet and hence future studies will focus on understanding the neurochemical differences between the small and large intestines and how dopamine possibly plays dual roles in these regions.

ULCERATIVE COLITIS INDUCES INFLAMMATION IN THE MID-BRAIN: IMPLICATIONS OF INTESTINAL INFLAMMATION AND THE GUT-BRAIN AXIS IN DRIVING NEUROINFLAMMATION IN THE CNS

Intestinal inflammation has been observed in many neurological disorders, while neurological complications are found in patients with chronic intestinal inflammation. In chapter 4, we explore the role of intestinal inflammation in driving neuroinflammation in the CNS. DSS-induced acute colitis resulted in the expected colonic inflammation and damage to the mucosa and sub-mucosa. Consistent with other studies, we observed immune cell influx at the sight of these lesions together with increased iNOS production (Camuesco et al., 2004). The inflamed colons had lower levels of the neurotransmitter serotonin with increased metabolite turnover possibly due to decreased expression of 5-HT_4 receptors. Serotonin and

5-HT_4 are involved in contraction of smooth muscle cells (Spiller, 2001). This could explain why we observed fewer formed fecal pellets in the colons of DSS mice. DSS-treated animals also expressed high levels of prokineticin-2 (PK2) in the distal colon. Increased production of PK2 might potentiate contraction of GI tissue allowing the non-inflamed regions of the colon to develop toward ulcerative colitis (UC) (Catalano et al., 2010). Interestingly, we also observed more pro-inflammatory transcripts of TNFα, IL-1β and iNOS in the lumbosacral region of the spinal cord and in the *substantia nigra* with a slightly elevated microglial density in the ventromedial hypothalamus. Hence, intestinal inflammation may have influenced neuroinflammation in the mid-brain possibly through the pelvic and sacral nerves that innervate the colon and rectum. It is possible that the HPA is activated leading to the stress and sickness behavior observed in other studies of DSS-induced colitis. Together, our data suggest a possible priming of the mid-brain region towards neuroinflammation following intestinal inflammation.

Since it is difficult to differentiate peripheral immune infiltration from resident microglial populations in the brain due to overlapping cellular markers, peripheral cell influx following induction of UC needs to be studied using flow cytometry. Future studies should focus on the possible priming of the mid-brain to produce more inflammatory cytokines as well as on changes in blood-brain barrier porosity and peripheral immune infiltration. These three pathological changes are consistent with observations from post-mortem PD cases.

REFERENCES

Avila, D. S., R. L. Puntel and M. Aschner (2013). "Manganese in health and disease." Met Ions Life Sci **13**: 199-227.

Bech, K., C. P. Hovendal and D. Andersen (1982). "Effect of dopamine on pentagastrin-stimulated gastric antral motility in dogs with gastric fistula." Scand J Gastroenterol **17**(1): 103-107.

Bouchard, M. F., S. Sauve, B. Barbeau, M. Legrand, M. E. Brodeur, T. Bouffard, E. Limoges, D. C. Bellinger and D. Mergler (2011). "Intellectual impairment in school-age children exposed to manganese from drinking water." Environ Health Perspect **119**(1): 138-143.

Camuesco, D., M. Comalada, M. E. Rodriguez-Cabezas, A. Nieto, M. D. Lorente, A. Concha, A. Zarzuelo and J. Galvez (2004). "The intestinal anti-inflammatory effect of quercitrin is associated with an inhibition in iNOS expression." Br J Pharmacol **143**(7): 908-918.

Catalano, R. D., T. R. Lannagan, M. Gorowiec, F. C. Denison, J. E. Norman and H. N. Jabbour (2010). "Prokineticins: novel mediators of inflammatory and contractile pathways at parturition?" Mol Hum Reprod **16**(5): 311-319.

Ekstrand, M. I. and D. Galter (2009). "The MitoPark Mouse - an animal model of Parkinson's disease with impaired respiratory chain function in dopamine neurons." Parkinsonism Relat Disord **15 Suppl 3**: S185-188.

Gulbransen, B. D. and K. A. Sharkey (2012). "Novel functional roles for enteric glia in the gastrointestinal tract." Nat Rev Gastroenterol Hepatol **9**(11): 625-632.

Gunnarsson, L. G. and L. Bodin (2017). "Parkinson's disease and occupational exposures: a systematic literature review and meta-analyses." Scand J Work Environ Health.

Jessen, K. R. and R. Mirsky (1983). "Astrocyte-like glia in the peripheral nervous system: an immunohistochemical study of enteric glia." J Neurosci **3**(11): 2206-2218.

Kirschstein, T., F. Dammann, J. Klostermann, M. Rehberg, T. Tokay, R. Schubert and R. Kohling (2009). "Dopamine induces contraction in the proximal, but relaxation in the distal rat isolated small intestine." Neurosci Lett **465**(1): 21-26.

Seiler, R., A. Rickenbacher, S. Shaw and B. M. Balsiger (2005). "alpha- and beta-adrenergic receptor mechanisms in spontaneous contractile activity of rat ileal longitudinal smooth muscle." J Gastrointest Surg **9**(2): 227-235.

Spiller, R. C. (2001). "Effects of serotonin on intestinal secretion and motility." Curr Opin Gastroenterol **17**(2): 99-103.

Warner, T. T. and A. H. Schapira (2003). "Genetic and environmental factors in the cause of Parkinson's disease." Ann Neurol **53 Suppl 3**: S16-23; discussion S23-15.

Zizzo, M. G., F. Mule, M. Mastropaolo and R. Serio (2010). "D1 receptors play a major role in the dopamine modulation of mouse ileum contractility." Pharmacol Res **61**(5): 371-378.

APPENDIX I

NEURONAL PROTECTION AGAINST OXIDATIVE INSULT BY POLYANHYDRIDE NANOPARTICLE-BASED MITOCHONDRIA-TARGETED ANTIOXIDANT THERAPY

Manuscript published in Nanomedicine: Nanotechnology, Biology and Medicine

Timothy M. Brenza, PhD [a, 1], Shivani Ghaisas, MS [b, 1], Julia E. Vela Ramirez, PhD [a], Dilshan Harischandra, BS[b], Vellareddy Anantharam, PhD [b], Balaraman Kalyanaraman, PhD [c], Anumantha G. Kanthasamy, PhD [b, *], and Balaji Narasimhan, PhD [a, **]

[1] These authors contributed equally to this work

[a] Department of Chemical and Biological Engineering, Iowa State University, Ames, IA, USA

[b] Department of Biomedical Sciences, Iowa State University, Ames, IA, USA

[c] Department of Biophysics, Medical College of Wisconsin, Milwaukee, WI, USA

Corresponding authors:

** B. Narasimhan, Department of Chemical and Biological Engineering, Iowa State University, 2035 Sweeney Hall, Ames, IA 50011, USA. Tel: +1 515 294 8019; e-mail: nbalaji@iastate.edu

* A. G. Kanthasamy, Biomedical Sciences Department, Iowa State University, 2062 Vet Med, Ames IA 50011, USA. Tel: +1 515 294 2516; e-mail: akanthas@iastate.edu

ABSTRACT

A progressive loss of neuronal structure and function is a signature of many neurodegenerative conditions including chronic traumatic encephalopathy, Parkinson's, Huntington's and Alzheimer's diseases. Mitochondrial dysfunction and oxidative and nitrative stress have been implicated as key pathological mechanisms underlying the neurodegenerative processes. However, current therapeutic approaches targeting oxidative damage are ineffective in preventing the progression of neurodegeneration. Mitochondria-targeted antioxidants were recently shown to alleviate oxidative damage. In this work, we investigated the delivery of biodegradable polyanhydride nanoparticles containing the mitochondria-targeted antioxidant Mito-Apocynin (Mito-Apo) to neuronal cells and the ability of the nano-formulation to protect cells against oxidative stress. The nano-formulated Mito-Apo provided excellent protection against oxidative stress-induced mitochondrial dysfunction and neuronal damage in a dopaminergic neuronal cell line, mouse primary cortical neurons, and a human mesencephalic cell line. Collectively, our results demonstrate that nano-formulated Mito-Apo may offer improved efficacy of mitochondria-targeted antioxidants to treat neurodegenerative disease.

Key words: Neurodegeneration; Oxidative stress; Polyanhydride nanoparticles; Mito-Apocynin

Introduction

Neurodegenerative diseases such as chronic traumatic encephalopathy (CTE), Alzheimer's Disease (AD), Parkinson's Disease (PD) and stroke are becoming more prominent as the world population ages (Tofaris and Schapira, 2015). These diseases typically manifest mid- to late-life and progressively worsen with increased morbidity. Chronic exposure to environmental toxins such as manganese in fertilizers and welding fumes (Harischandra et al., 2015), pesticides such as paraquat and rotenone, and brain trauma caused by a single or successive concussive blows to the head increase the risk of developing neurodegenerative disease (Goldstein et al., 2012). In terms of head trauma, Lehman *et al.* (Lehman et al., 2012) conducted a post-mortem review of the brains of ex-National Football League athletes, which revealed signs of protein misfolding and tauopathy seen in AD patients. Peskind *et al.* (Peskind et al., 2011) reported that soldiers exposed to improvised explosive devices showed cognitive impairment and deficits in speech and attention span. The economic burden associated with the increased medical management of neurodegenerative diseases and decreased individual productivity is projected to escalate steeply, making it increasingly urgent to develop effective medications. Currently, drugs are available on the market that manage the symptoms of CTE, AD, and PD. However, they do not slow disease progression.

One of the major disease mechanisms of neurodegeneration is mitochondrial dysfunction, which contributes to oxidative stress through the build-up of reactive oxygen species and reactive nitrogen species. While anti-inflammatory and antioxidant drugs have been developed, the major factors compromising efficacy include reduced drug diffusion through the blood-brain barrier (BBB), limited availability due to drug metabolism, and undesirable

side effects. In this context, the non-toxic plant-derived molecule apocynin (4-hydroxy-3-methoxyacetophenone) has been used as an antioxidant and an inhibitor of NADPH oxidase in pre-clinical models of PD (Anantharam et al., 2007; Cristovao et al., 2009; Gao et al., 2003). At a high dose of 300 mg/kg, its dimer diapocynin is neuroprotective and anti-neuroinflammatory in the MPTP and the progressively degenerative LRRK2R1441G transgenic (tg) mouse models (Dranka et al., 2014; Ghosh et al., 2012). To enhance efficacy at lower doses, we recently synthesized several more potent mitochondria-targeted apocynins with different carbon-chain lengths by conjugating with triphenylphosphonium cation moiety. The lipophilic chain and delocalized cationic moiety in the mitochondria-targeted apocynin (Mito-Apo) increases its cell permeability and sequestration into mitochondria (Dranka et al., 2014). We recently demonstrated that a low oral Mito-Apo dose (3 mg/kg) prevented hyposmia and loss of motor function in the LRRK2R1441G tg mouse model (11). The compound also showed moderate efficacy against dopaminergic neurodegeneration in the MPTP mouse model (Ghosh et al., 2016b). The next logical step is to enhance Mito-Apo bioavailability by using nano-carriers to facilitate transport and delivery to the central nervous system (CNS).

By combining the ability to cross highly selective biological barriers with intracellular targeting, nano-carriers can deliver diverse payloads to organelles with reduced toxicity and increased bioavailability (Ross et al.). Biodegradable nanomaterials have been extensively evaluated for drug delivery across the BBB (Mallapragada et al., 2015). In particular, biodegradable polyanhydride-based nano-carriers have been utilized to provide sustained delivery of diverse payloads (Binnebose et al., 2015; Brenza et al., 2015; Carino et al., 2000;

Carrillo-Conde et al., 2015; Determan et al., 2004; Determan et al., 2006; Haughney et al., 2013; Masters et al., 1993; Park et al., 1998; Ross et al., 2015; Storm et al., 2002; Torres et al., 2007; Vela Ramirez et al., 2014; Weiner et al., 2008). Polyanhydride nanoparticles possess excellent biocompatibility and erodible surfaces, both of which are central to their utilization as delivery vehicles (Burkersroda et al., 2002). Polyanhydride-based carriers have been translated to the clinic as evidenced by the FDA-approved Gliadel® wafer, which is composed of sebacic acid (SA) and 1,3 bis(*p*-carboxyphenoxy)propane (CPP), and carries the anti-cancer drug, carmustine (Westphal et al., 2006). Copolymers based on SA, CPP, 1,6 bis(*p*-carboxyphenoxy)hexane (CPH), and 1,8 bis(*p*-carboxyphenoxy)-3,6-dioxaoctane (CPTEG) have been used for sustained delivery. A major advantage of polyanhydrides is that by chemically altering their copolymer composition, their degradation rates can be varied from days to months, offering exceptional control of the release rate of encapsulated payloads (Jain et al., 2008; Shieh et al., 1994; Tabata and Langer, 1993). Moreover, these particles can be functionalized with ligands to enable targeted delivery to specific types of cells and/or tissues (Chavez-Santoscoy et al., 2012; Narasimhan et al., 2015; Phanse et al., 2014). However, little information exists on the interaction of these nanomaterials with neuronal cells. In this work, we demonstrate that polyanhydride nanoparticles can efficiently deliver Mito-Apo to a mesencephalic neuronal cell line and to primary cortical neurons. For these studies, 20:80 CPH:SA nanoparticles were utilized because of their dual capabilities to rapidly deliver payloads (Petersen et al., 2010; Shen et al., 2002) and to be internalized efficiently by phagocytic cells (Petersen et al., 2009).

Methods

Materials

Synthesis of 20:80 CPH:SA copolymer was performed as described previously (Kipper et al., 2002; Shen et al., 2002). Proton NMR (VXR-300, Varian) was used to measure polymer molecular weight and purity. Quantum dots (QDs, λ_{ex} = 554 nm, λ_{em} = 627 nm) were purchased from Sigma-Aldrich. Neurobasal medium, RPMI 1640 and Dulbecco's modified Eagle's media (DMEM), B27 supplement, fetal bovine serum (FBS), Trypsin-EDTA (TE), L-glutamine, penicillin, and streptomycin were purchased from Invitrogen. The MTS cell viability kit (Catalog# G3580) was acquired from Promega. Primary antibodies against cleaved caspase-3 (Catalog# 9661) and β-III tubulin (Catalog# 14545) were purchased from Cell Signaling and Millipore, respectively.

Mito-apo synthesis

Mito-Apo was synthesized by modifying a previous protocol for Mito-Q and long-chain Mito-Apo-C11 synthesis (Dranka et al., 2014; Ghosh et al., 2010; Kelso et al., 2002). Briefly, acetylvanillic acid chloride was synthesized by first mixing acetylvanillic acid with thionyl chloride, and then dissolving the mixture in methylene chloride, aminoethyltriphenylphosphonium bromide, and pyridine. The acetylated Mito-Apo was purified on a silica gel column followed by removal of the acetyl protective group. The final product was purified and characterized by HPLC and LC-MS (Dranka et al., 2014; Ghosh et al., 2010; Kelso et al., 2002).

Nanoparticle synthesis

Either 0.5 wt% QD or 5 wt% Mito-Apo were incorporated into polyanhydride nanoparticles by a modified anti-solvent nano-encapsulation method (Ulery et al., 2009). Briefly, the synthesized polymer (100 mg), QD, or Mito-Apo (0.1 or 0.2 mg) were dispersed in 4 mL of methylene chloride (Fisher Scientific) and sonicated for 60 s with a sonication probe (Sonics and Materials) (Gendelman et al., 2015). The solution was poured into 1 L of pentane (Fisher Scientific) and the particles were recovered by vacuum filtration. The particle morphology and particle size were determined using scanning electron microscopy (Quanta 250 FE-SEM, FEI). ImageJ 1.43u (National Institutes of Health) was utilized to quantify primary particle sizes for construction of the particle size distribution.

Folic acid surface functionalization

Functionalization of polyanhydride nanoparticles with folic acid (FA) was performed using a two-step amine-carboxylic acid coupling reaction. We performed studies using this reaction with other molecules to functionalize polyanhydride nanoparticle surfaces (Carrillo-Conde et al., 2011; Chavez-Santoscoy et al., 2012), and the optimized conditions were used in the FA functionalization as described below.

The coupling reaction was performed by incubating a nanoparticle suspension (33 mg/mL) in ultrapure water with 10 equivalents of 1-ethyl-3-(3-dimethylaminopropyl)-carbodiimide hydrochloride (EDC), 12 equivalents of *N*-hydroxysuccinimide (NHS), and 10 equivalents of ethylenediamine. The first incubation was carried out for 1 h at 4°C and a constant agitation of 350 rpm. Next, the nanoparticle suspension was centrifuged at 10,000 rpm for 10 min.

After removing the supernatant, an equal amount of ultrapure water was added to the nanoparticles, vortexed, centrifuged again to remove excess reactants, and the new supernatant was removed. The second step was performed by mixing 10 equivalents of EDC, 12 equivalents of NHS, and corresponding equivalents of FA in ultrapure water under constant agitation of 350 rpm for 1 h at 4°C. Particles were centrifuged and the washing step was performed as previously described. Next, nanoparticles were vacuum-dried for 1 h. During the functionalization process, probe sonication was used before and after incubation to break agglomerated particles.

Experiments with varying amounts of FA were performed to optimize the amount of FA needed to functionalize the nanoparticles. Surface-functionalized nanoparticles were characterized by measuring the zeta potential using quasi-elastic light scattering (QELS, Zetasizer Nano, Malvern Instruments Ltd.) and XPS analysis (PHI 5500 MultiTechnique system, Physical Electronics, Inc.). Binding energies were referenced to the aliphatic hydrocarbon peak (285.0 eV). High-resolution C1s peaks were collected and fitted using CasaXPS software (RBS Instruments).

Mito-Apo release

Quantification of Mito-Apo encapsulation efficiency and release kinetics was carried out. For these studies, the Mito-Apo-containing nanoparticles were suspended in phosphate buffered saline (PBS, pH 7.4) at 37°C on a shaking incubator. At specific time points, the particles were separated from the aqueous media by centrifugation, and after collecting each supernatant, the remaining nanoparticles were resuspended in fresh PBS. The supernatants

were analyzed by HPLC (Agilent Technologies 1200). 20 µL samples were injected and separation was performed with a Kinetex C18 column (Phenomenex) using a gradient elution comprising of solvent A (90% water and 10% acetonitrile) and solvent B (100% acetonitrile) for seven min at a flow rate of 1.5 mL/min at 40°C. Mito-Apo was quantified by UV absorbance at a wavelength of 262nm.

For clarity, henceforth NP will refer to non-functionalized nanoparticles, while particles functionalized with 0.25 eq. of FA will be designated as FA-NP and particles functionalized with 2 eq. of FA will be designated as 2FA-NP. Mito-Apo-encapsulated particles will be designated as M:(NP) or M:(FA-NP) depending on the absence or presence of FA functionalization.

Cell culture

Immortalized rat mesencephalic cells (N27) were grown in RPMI media supplemented with 10% FBS, 1% L-glutamine, penicillin (100 units/mL) and streptomycin (100 units/mL), and maintained at 37°C in a humidified atmosphere of 5% CO_2 as described elsewhere (Harischandra et al., 2015; Song et al., 2011).

Primary cortical neurons were isolated and prepared as described previously (Ghosh et al., 2013). Briefly, cortical neurons were isolated from mouse embryos on gestational days 14-15 and maintained in ice-cold DMEM followed by dissociation using 0.25% TE at 37°C for 15 min. The action of TE was stopped by DMEM containing 10% FBS. Single cell suspension was achieved by triturating the neurons several times through a 10 mL pipette. Neurons were

plated at 0.1 x 10^6 cells per well on 96-well plates (Costar) coated with poly-D-lysine (PDL, 50 μg/mL). Cultures were grown in neurobasal media with B27 neuronal supplement, 500 mM L-glutamine, 50 U/mL penicillin, and 50 mg/mL streptomycin. Primary neurons were maintained in a humidified atmosphere with 5% CO_2 at 37°C for seven days with half the media changed every two days.

The Lund human mesencephalic (LUHMES) cell line, derived from female human embryonic ventral mesencephalic cells by conditional immortalization (tetracycline-controlled v-myc-overexpression) and subsequent clonal selection, was obtained from the American Type Culture Collection. This cell line can be differentiated into post-mitotic neurons with a dopaminergic phenotype (Ay et al., 2015; Jin et al., 2014). Undifferentiated LUHMES cells were propagated in Advanced DMEM/F12 supplemented with 1× N-2 supplement, 2 mM L-glutamine, and 40 ng/mL recombinant bFGF on multi-well plates pre-coated with 50 μg/mL poly-L-ornithine and 1 μg/mL fibronectin. Differentiation of LUHMES cells was initiated by the addition of differentiation medium containing Advanced DMEM/F12, 1× N-2 supplement, 2 mM L-glutamine, 1 mM dibutyryl cAMP, 1 μg/mL tetracycline and 2 ng/mL recombinant human GDNF. After two days, cells were trypsinized and seeded onto multi-well plates at a density of 1.5 × 10^5 cells/cm^2. LUHMES cells differentiate into a dopaminergic phenotype after being cultured an additional three days in differentiation medium. For 6-hydroxydopamine (6-OHDA) treatment studies, at day five differentiated LUHMES cells were pre-treated in the presence or absence of the respective treatments for 12 h and co-incubated with 30 μM of 6-OHDA for another 12 h.

Cell viability

To evaluate if the nanoparticles are toxic to neurons, N27 cells and primary cortical neurons were incubated for 24 h with 100 μg/mL of NP, FA-NP and 2FA-NP. Cell viability was measured by Cell Titer 96® AQueous Non-radioactive Cell Proliferation Assay (MTS assay, Promega G5430) as described previously (Jin et al., 2014). Briefly, 20 μL of MTS reagent was added to each well 1.5 h prior to incubation. Next, 25 μL of 1% SDS was added to each well to dissolve the formazan crystals. Absorbance was measured at 490nm using a 96-well plate reader (SpectraMax 190, Molecular Devices). A reference wavelength of 670nm was used to eliminate background.

Treatment with Mito-Apo-encapsulated NPs

We seeded 0.1 x 10^6 primary cortical neurons onto a PDL-coated 96-well plate. Seven days post-seeding, cells were pre-treated with either 10 μM Mito-Apo alone or 100 μg/mL of M:(NP) or M:(FA-NP) for 24 h. The cells were challenged with 50 μM H_2O_2 for 1.5 h. Cell viability was evaluated by the MTS assay.

Mitochondrial superoxide production

LUHMES cells (~250,000 per well) were grown in glass bottom dishes 16-18 h prior to treatments and exposed to 100 μg/mL of the nano-formulations for 12 h. We added 30 μg/mL 6-OHDA to all the wells except control wells for another 12 h. Mitochondrial superoxide production in the cells was measured using MitoSOX fluorescence probe in Hank's buffered salt solution (HBSS) containing calcium and magnesium, according to the manufacturer's protocol. MitoSOX was added to a final concentration of 5 μM in HBSS.

Cells were incubated with MitoSOX for 30 min and washed twice with HBSS. Absorbance was measured at 580nm using a 96-well plate reader.

Nanoparticle internalization

Flow cytometry was used to quantify cellular internalization of QD-containing nanoparticles. Briefly, 1.0 x 10^6 N27 cells seeded in T25 flasks (Corning) were treated with 100 μg/ml of CdSeS/ZnS-alloyed QD (λ_{em} 490 nm) containing particles (NP, FA-NP or 2FA-NP) suspended in 2% RPMI. After 24 h, media was removed and the cells were washed twice with sterile PBS (Invitrogen) to remove excess QDs. Cells harvested by trypsinization were collected in 2-mL centrifuge tubes and fixed with 2% paraformaldehyde (PFA) for 20 min. Internalization of QD-containing nanoparticles was analyzed using a FACScanto™ flow cytometer (BD Biosciences, excitation - UV spectrum, emission - 490nm). Results are reported as percentage of total cell population normalized to control (cells without QDs).

Confocal microscopy

N27 cells (15,000/well) were plated on PDL-coated coverslips and particles were added. After 24 h, cells were washed several times with sterile PBS and fixed in 4% PFA. Non-specific binding was blocked using 2% bovine serum albumin (BSA, (Sigma) in PBS with 0.1% Triton-X (Sigma) and 0.01% Tween-20 (Bio-Rad) for 30 min. Cells were stained for 20 min with 10 μM phalloidin (Invitrogen). Nuclei were stained with 2 μg/mL Hoechst 33342. Images were taken using an inverted Leica TCS NT confocal microscope.

Transmission electron microscopy (TEM) imaging of nanoparticles

Primary cortical neurons were incubated for 24 h with 100 μg/mL QD-containing NP, FA-NP and 2FA-NP. After treatment, cells were washed several times with sterile PBS and fixed with 2% glutaraldehyde (w/v) and 2% PFA (w/v) in PBS (pH 7.4) for 24 h at 4°C. The samples were washed in buffer and subsequently fixed in 1% osmium tetroxide in 0.1 M cacodylate buffer for 1 h at RT. Following fixation, the samples were dehydrated in a graded ethanol series and infiltrated and embedded using a modified EPON epoxy resin (Embed 812). Resin blocks were polymerized for 48 h at 70°C. Thick and ultrathin sections were prepared using a Leica UC6 ultramicrotome (Leeds Precision Instruments). The ultrathin sections were collected onto copper grids and images were collected using a JEM 2100 200 kV scanning and transmission electron microscope (Japan Electron Optic Laboratories).

Immunocytochemistry

Primary cortical neurons were seeded on PDL-coated coverslips at 0.2 x 10^6 neurons/well. After pre-treatment for 24 h with 100 μg/mL of M:(NP) or M:(FA-NP), neurons were challenged with 50 μM H_2O_2. After 1.5 h, media was aspirated and cultures were washed twice with sterile PBS. Cells were fixed in 4% PFA for 20 min followed by blocking with 3% BSA containing 0.1% triton-X and 0.01% Tween-20 for 1 h. Primary antibodies to cleaved caspase-3 (rabbit monoclonal at 1:1500) and β-III tubulin (mouse monoclonal at 1:2000) were added to each well and incubated overnight at 4°C. The next day, each well was washed five times with PBS and incubated at RT for 1.5 h with the secondary antibodies Alexa-488 conjugated (1:10,000) donkey-anti mouse and Alexa-555 conjugated donkey anti-rabbit (1:10,000). Nuclei were counterstained for 7 min with Hoechst (1:5000, Invitrogen).

Cells were mounted and coverslipped on clean slides (Colorfrost, Fisher) with Fluoromount. Neurons were imaged with a SPOT digital camera (Diagnostic Instruments) attached to a TE-2000U inverted fluorescence microscope (Nikon).

High affinity [^{3}H] dopamine uptake assay

Dopamine uptake measurements were measured as described previously (Ay et al., 2015; Harischandra et al., 2014) with modifications. Briefly, differentiated LUHMES cells grown in 6-well plates were washed twice with Krebs-Ringer buffer (16 mM NaH_2PO_4, 120 mM NaCl, 4.7 mM KCl, 1.8 mM $CaCl_2$, 1.2 mM $MgSO_4$, 1.3 mM EDTA, and 5.6 mM glucose, pH 7.4), followed by incubation with 10 nM [^{3}H] dopamine for 30 min at 37°C. Next, the cultures were triple-washed with fresh ice-cold Krebs-Ringer buffer and lysed with 1N NaOH. Radioactivity was measured with a liquid scintillation counter (Tri-Crab 4000, Packard) after adding a 5-mL scintillation cocktail to each vial. Specific dopamine uptake was expressed as mean values of counts.

Statistical analysis

Data analysis was performed using Prism 4.0 (GraphPad). One-way ANOVA was applied to compare control and treatment groups. Differences with $p<0.05$ were considered significant from three or more independent experiments, which were performed in triplicate.

Results

Nanoparticle synthesis and characterization

The anti-solvent nano-encapsulation method resulted in polydisperse spherical particles (Table 1). The surface functionalization of the nanoparticles with FA was performed with a low and high FA surface concentration. The functionalized particles were characterized by QELS and XPS (Table 1). All three formulations (with or without functionalization) resulted in negatively charged particles. The degree of FA attachment increased with percent nitrogen, which was quantified using XPS.

The nanoparticles were formulated with QDs for imaging purposes or Mito-Apo for evaluating therapeutic efficacy (electron microscopy images in Table 1). These particles were subsequently functionalized with FA, and no statistically significant primary particle size differences were observed between the various formulations (Table 2). The Mito-Apo-containing particles were subjected to complete degradation to determine the encapsulation efficiency. The encapsulation efficiency (Table 2) indicated a loss of Mito-Apo during functionalization, from 57% for NP to 43% for FA-NP to 37% for 2FA-NP.

The cumulative release profile of Mito-Apo from the particles over the first three days is shown in Fig. 1. After two hours of degradation, a greater amount of Mito-Apo was released as a burst from the non-functionalized particles. This initial burst could account for the lower encapsulation efficiency of the surface-functionalized particles since this would occur during the functionalization process. After 24 h of degradation, approximately 35% of the Mito-Apo

was released from the functionalized particles. A near linear release of drug was observed from all the nano-formulations.

Nanoparticle toxicity and internalization

Prior to encapsulation of Mito-Apo into the nano-formulations, their toxicity was assessed using the N27 dopaminergic neuronal cell line. None of the nano-formulations synthesized had any effect on cell viability at any of the doses tested (Fig. 2a). Next we determined if N27 cells differentially internalized the various nano-formulations using QD-loaded particles. Cellular uptake was determined by two independent methods: flow cytometry and confocal microscopy. Flow cytometric analysis revealed uptake of both NP and FA-NP. Functionalization with FA improved nanoparticle internalization, with 32% of N27 cells internalizing FA-NP compared to only 25% of cells internalizing NP (Fig. 2b). However, the amount of FA on the particle surface may have affected the internalization, because only 10-15% of N27 cells internalized 2FA-NP.

We further confirmed nanoparticle internalization in N27 cells by confocal microscopy, with consecutive z-stack images revealing that most of the particles were internalized and not attached to the surface of cells (Fig. 2c). Consistent with the flow cytometry results, N27 cells internalized a significantly higher number of FA-NP compared to NP or 2FA-NP. Together, these results indicate that FA-NP were internalized more efficiently by neuronal cells than NP.

Next, we evaluated the potential toxicity of the nano-formulations in primary cortical cells. As a positive control for cell death, some cells were treated with 50 μM of H_2O_2. Treatment

of primary cortical neurons with the oxidative stress inducer H_2O_2 alone reduced cell viability by more than 30%. Similar to the results obtained with N27 cells, none of the treatments had any effect on the viability of primary cortical cultures (Fig. 3a). Treating the cells with Mito-Apo alone also did not reduce cell viability.

Intracellular localization of QD-loaded NP and FA-NP in primary cortical neurons was evaluated using TEM. Both NP and FA-NP were internalized by neurons (Fig. 3b). The images (Fig. 3b) indicate that both nano-formulations were located within the cytosol (shown by black arrows) and not associated with mitochondria (indicated by black stars).

Mito-Apo-encapsulated particles protect neurons against oxidative stress-induced death

Since FA-NP was internalized more efficiently compared to 2FA-NP, FA-NP was evaluated for its therapeutic efficacy and NP was used as a control. In these experiments, we tested the neuroprotective effect of M:(NP) and M:(FA-NP) in primary cortical neurons. While H_2O_2 treatment reduced cell viability by >50%, pre-treating cells with either Mito-Apo alone, M:(NP), or M:(FA-NP) significantly protected against H_2O_2-induced toxicity (Fig 4a). However, M:(FA-NP) was more efficacious than M:(NP) or Mito-Apo alone. Together, these results indicate that encapsulation of Mito-Apo into FA-NP facilitates Mito-Apo internalization by neurons and increases its efficacy.

Next, we evaluated caspase-3 activation using immunofluorescence since the proteolytic activation of caspase-3 is widely used as a marker of apoptotic cell death (Kaul et al., 2003; Porter and Janicke, 1999; Tadokoro et al., 2010). Primary cortical neurons were incubated with the nano-formulations and treated with 50 μM H_2O_2 as described previously. Very

strongly cleaved caspase-3 immunostaining (red) was evident in the H_2O_2-treated primary cortical neurons (Fig. 4b). However, neurons co-treated with M:(NP), M:(FA-NP) or Mito-Apo alone showed less cleaved caspase-3 immunostaining. The cleaved caspase-3 immunostaining in the H_2O_2-treated neurons increased three-fold compared to untreated controls (Fig. 4b), whereas treating the cells with Mito-Apo-encapsulated nano-formulations (with or without FA) and Mito-Apo alone limited the H_2O_2-induced increase in cleaved caspase-3 immunostaining to 1.5-, 2.0- and 2.5-fold, respectively. Together these results indicate that M:(FA-NP) effectively inhibited H_2O_2-induced cell death, especially compared to M:(NP) or Mito-Apo alone.

Neuroprotective effect of M:(FA-NP) against 6-OHDA-induced superoxide production, caspase-3 activation, and dopaminergic cell loss

For these studies, we used human mesencephalon-derived neuronal LUHMES cells, which are used to model human dopaminergic degeneration (Zhang et al., 2014). With the addition of cAMP and GDNF, LUHMES cells differentiate by forming long axons with relatively dense interconnections typically seen in the mesencephalic region in the brain (Scholz et al., 2011). One of the early responses of stressed neurons is the retraction of their axons followed by loss of membrane integrity as the neurons undergo apoptosis. Superoxide production, caspase-3 cleavage, and dopamine uptake are markers of mitochondrial dysfunction, apoptosis and tyrosine hydroxylase (TH) neuronal loss respectively. Pre-treatment with Mito-Apo alone or M:(NP) failed to reduce superoxide production in LUHMES cells challenged with 6-OHDA (Fig. 5a). In contrast, LUHMES cells pre-treated with M:(FA-NP) had

significantly lower production of superoxide following 6-OHDA treatment, similar to the untreated controls.

Next, we counted TH-positive neurons by a [^{3}H] dopamine uptake assay. Healthy dopaminergic neurons can re-uptake dopamine while stressed neurons have reduced dopamine uptake. As expected, 30 μM 6-OHDA caused a significant loss of dopaminergic neurons compared to untreated controls. However, pre-treatment with M:(FA-NP) significantly attenuated the 6-OHDA-induced loss of dopaminergic neurons. In contrast, pre-treatment with M:(NP) or Mito-Apo alone did not significantly protect dopaminergic neurons (Fig. 5b).

Finally, we determined proteolytic activation of caspase-3 using cleaved caspase-3 antibody in immunofluorescence experiments. Significantly more cleaved caspase-3 stained cells were observed in 6-OHDA-treated LUHMES cells compared to untreated controls (Fig. 5c). Similar to the results observed with cortical neurons, pre-treatment with M:(FA-NP) significantly protected LUHMES cells incubated with 6-OHDA compared to cells exposed to 6-OHDA alone ($p<0.001$). Cells pre-treated with M:(NP) and Mito-Apo alone also showed fewer cleaved caspase-3-positive neurons compared to the 6-OHDA-alone group ($p<0.05$). However, the neuroprotection provided by pre-treatment with M:(FA-NP) was more effective at preventing dopaminergic neuronal degeneration compared to the other treatments. Together, these results demonstrate that M:(FA-NP) is more efficacious in protecting human mesencephalic neurons against mitochondrial damage and apoptotic cell death.

Discussion

New drugs are urgently needed to slow the progression of debilitating brain disorders, such as CTE, AD, and PD. We previously demonstrated the effectiveness of Mito-Apo against oxidative stress (11). In this work, we demonstrate that Mito-Apo efficacy can be further enhanced with its incorporation into targeted biodegradable nano-carriers. Nano-formulated Mito-Apo provided excellent protection against oxidative stress-induced mitochondrial dysfunction and neuronal damage in a rat dopaminergic neuronal cell line, mouse primary cortical neurons, and a human mesencephalic cell line.

A significant advantage provided by the polyanhydride nanoparticles is the slow and controlled erosion of the particles, enabling a sustained release of the encapsulated cargo (Binnebose et al., 2015). The FA functionalization of Mito-Apo-containing nano-formulations lowered the encapsulation efficiency as expected because of exposure to aqueous conditions. However, a near-linear Mito-Apo release profile was observed from the nano-formulations (Fig. 1). This is important because it indicates that the drug release rate over time to neurons will be constant, potentially leading to increased bioavailability. Adding to the vast literature on the biocompatibility of polyanhydride particles, functionalized or otherwise (Adler et al., 2009; Huntimer et al., 2013a; Vela-Ramirez et al., 2015), our work shows that these nanoparticles were non-toxic to dopaminergic or primary cortical neurons (Figs. 2a and 3a).

Unlike other cells, neuronal uptake of exogenously added compounds such as xenobiotics or drugs is very limited (Sun et al., 2013). However, treating neuronal cell lines with FA-

functionalized polyanhydride particles significantly increased the percentage of neurons internalizing these particles in comparison to cells internalizing non-functionalized particles (Fig. 2c). This is likely due to the uptake of the functionalized nanoparticles by receptor-mediated endocytosis via folate receptors present on neurons and is consistent with previous studies on folate-modified nano-carriers (Kanmogne et al., 2012; Li et al., 2015; Puligujja et al., 2015; Puligujja et al., 2013). It was observed (Fig. 2c) that particles functionalized with 2 eq. FA were internalized by fewer cells compared to particles functionalized with 0.25 eq. FA or even non-functionalized particles. While not specifically investigated herein, this could be attributed to oversaturation of the folate receptors by excess FA, which might reduce that receptor's ability to carry out endocytosis (Saul et al., 2003). Thereafter, we investigated nano-formulations functionalized with 0.25 eq. of FA (FA-NP), using non-functionalized particles (NP) as an internal control.

Even with 43% encapsulation efficiency and 35% of the Mito-Apo being released over the first 24 hours, M:(FA-NP) provided equivalent if not better protection than Mito-Apo alone against apoptosis (Fig. 4) and dopaminergic neuronal degeneration (Fig. 5). The amount of Mito-Apo required to confer protection to neurons might be much less than the 10 μM of Mito-Apo used in the *in vitro* protection studies. Our hypothesis is that a steady supply of the antioxidant in small (but appropriate) quantities – enabled by the nanoparticles – is more beneficial than delivering a large bolus of Mito-Apo alone. This may explain why M:(FA-NP) is more efficacious in neuroprotection over Mito-Apo alone. The encapsulation efficiency coupled with the equivalent protection as compared to Mito-Apo alone also

indicates that the nano-formulations provide dose-sparing, which has been observed previously (Binnebose et al., 2015; Huntimer et al., 2013b).

While encapsulating Mito-Apo within nanoparticles, it is possible that a fraction of the Mito-Apo segregated to the nanoparticle surface, which may guide the particles to the mitochondria. However, TEM images (Fig. 3b) showed very few internalized particles (regardless of functionalization) inside the mitochondria, which suggests that the enhanced cellular internalization compensates for the lower amount of Mito-Apo released within the cells. Consequently, M:(NP) and M:(FA-NP) were more effective at preventing H_2O_2-induced cell death when compared to Mito-Apo alone in both N27 cells and primary cortical neurons (Figs. 3 and 4). Similarly, cells pre-treated with M:(FA-NP) were protected against 6-OHDA-induced superoxide production, caspase-3 activation, and TH neuronal loss (Fig. 5). These observations support the hypothesis that the actual amount of Mito-Apo required for neuroprotection is small. Thus, to protect neurons from oxidative stress, the sustained release of small amounts of Mito-Apo over a period of 24 hours is more effective than delivering a single bolus of a larger amount of the antioxidant.

Conclusions

Our studies demonstrate that intracellular delivery of the mitochondria-targeted antioxidant, Mito-Apo, using FA-modified polyanhydride nanoparticles effectively protected against oxidative stress-induced neuronal damage in neuronal cell types across three species, including humans. While nanoparticle-mediated delivery of antioxidants for treatment of neurodegenerative disorders is promising, the ability of these particles to transverse the BBB

and deliver this cargo needs to be evaluated in animal models. Recent work demonstrated that monocyte-internalized FA-functionalized particles efficiently traversed the BBB (Kanmogne et al., 2012). Ongoing studies are focused on delivery of Mito-Apo-encapsulated FA-functionalized polyanhydride nanoparticles to the CNS.

Acknowledgments

The authors thank the U.S. Army Medical Research and Materiel Command (Grant No. W81XWH-11-1-0700) for financial support. The authors acknowledge Tracey Pepper for her assistance in sample preparation and TEM image acquisition. The Iowa State University Materials Analysis and Research Laboratory assisted in collection and analysis of XPS data. We also thank Gary Zenitsky for assistance with manuscript preparation.

The authors declare no competing financial interests.

References

1. Tofaris GK, Schapira AH. Neurodegenerative diseases in the era of targeted therapeutics: how to handle a tangled issue. Mol Cell Neurosci. 2015;66:1-2.

2. Harischandra DS, Jin H, Anantharam V, Kanthasamy A, Kanthasamy AG. alpha-Synuclein protects against manganese neurotoxic insult during the early stages of exposure in a dopaminergic cell model of Parkinson's disease. Toxicol Sci. 2015;143(2):454-68.

3. Goldstein LE, Fisher AM, Tagge CA, Zhang XL, Velisek L, Sullivan JA, et al. Chronic traumatic encephalopathy in blast-exposed military veterans and a blast neurotrauma mouse model. Science Transl Med. 2012;4(134):1 34ra60.

4. Kamel F, Engel LS, Gladen BC, Hoppin JA, Alavanja MC, Sandler DP. Neurologic symptoms in licensed private pesticide applicators in the agricultural health study. Environ Health Persp. 2005;113(7):877-82.

5. Lehman EJ, Hein MJ, Baron SL, Gersic CM. Neurodegenerative causes of death among retired National Football League players. Neurology. 2012;79(19):1970-4.

6. Peskind ER, Petrie EC, Cross DJ, Pagulayan K, McCraw K, Hoff D, et al. Cerebrocerebellar hypometabolism associated with repetitive blast exposure mild traumatic brain injury in 12 Iraq war Veterans with persistent post-concussive symptoms. NeuroImage. 2011;54 Suppl 1:S76-82.

7. Gao H-M, Liu B, Zhang W, Hong J-S. Critical role of microglial NADPH oxidase-derived free radicals in the in vitro MPTP model of Parkinson's disease. FASEB J. 2003;17(13):1954-6.

8. Cristovao AC, Choi D-H, Baltazar G, Beal MF, Kim Y-S. The role of NADPH Oxidase 1-derived reactive oxygen species in paraquat-mediated dopaminergic cell death. Antiox Redox Signal. 2009;11(9):2105-18.

9. Anantharam V, Kaul S, Song C, Kanthasamy A, Kanthasamy AG. Pharmacological inhibition of neuronal NADPH oxidase protects against 1-methyl-4-phenylpyridinium (MPP+)-induced oxidative stress and apoptosis in mesencephalic dopaminergic neuronal cells. NeuroToxicol. 2007;28(5):988-97.

10. Dranka BP, Gifford A, McAllister D, Zielonka J, Joseph J, O'Hara CL, et al. A novel mitochondrially-targeted apocynin derivative prevents hyposmia and loss of motor function in the leucine-rich repeat kinase 2 (LRRK2R1441G) transgenic mouse model of Parkinson's disease. Neurosci Lett. 2014;583:159-64.

11. Ghosh A, Kanthasamy A, Joseph J, Anantharam V, Srivastava P, Dranka BP, et al. Anti-inflammatory and neuroprotective effects of an orally active apocynin derivative in pre-clinical models of Parkinson's disease. J Neuroinflam. 2012;9:241.

12. Ghosh A, Langley MR, Harischandra DS, Neal ML, Jin H, Anantharam V, et al. Mitoapocynin Treatment Protects Against Neuroinflammation and Dopaminergic Neurodegeneration in a Preclinical Animal Model of Parkinson's Disease. J Neuroimmune Pharmacol. 2016;11(2):259-78.

13. Ross KA, Brenza TM, Binnebose AM, Phanse Y, Kanthasamy AG, Gendelman HE, et al. Nano-enabled delivery of diverse payloads across complex biological barriers. J Contr Rel. 2015;219:548-59.

14. Mallapragada SK, Brenza TM, McMillan JM, Narasimhan B, Sakaguchi DS, Sharma AD, et al. Enabling nanomaterial, nanofabrication and cellular technologies for nanoneuromedicines. Nanomedicine: Nanotechnol Biol Med. 2015;11(3):715-29.

15. Binnebose AM, Haughney SL, Martin R, Imerman PM, Narasimhan B, Bellaire BH. Polyanhydride Nanoparticle Delivery Platform Dramatically Enhances Killing of Filarial Worms. PLoS Negl Trop Dis. 2015;9(10):e0004173.

16. Carrillo-Conde BR, Darling RJ, Seiler SJ, Ramer-Tait AE, Wannemuehler MJ, Narasimhan B. Sustained release and stabilization of therapeutic antibodies using amphiphilic polyanhydride nanoparticles. Chem Eng Sci. 2015;125:98-107.

17. Ross KA, Loyd H, Wu W, Huntimer L, Ahmed S, Sambol A, et al. Polyanhydride-based H5 hemagglutinin influenza nanovaccines elicit protective virus neutralizing titers and cell-mediated immunity. Int J Nanomed. 2015;10:229-43.

18. Brenza TM, Petersen LK, Zhang Y, Huntimer LM, Ramer-Tait AE, Hostetter JM, et al. Pulmonary biodistribution and cellular uptake of intranasally administered monodisperse particles. Pharm Res. 2015;32(4):1368-82.

19. Torres MP, Determan AS, Anderson GL, Mallapragada SK, Narasimhan B. Amphiphilic polyanhydrides for protein stabilization and release. Biomaterials. 2007;28(1):108-16.

20. Determan AS, Trewyn BG, Lin VSY, Nilsen-Hamilton M, Narasimhan B. Encapsulation, Stabilization, and Release of BSA-FITC from Polyanhydride Microspheres. J Contr Rel. 2004;100(1):97-109.

21. Determan AS, Wilson JH, Kipper MJ, Wannemuehler MJ, Narasimhan B. Protein stability in the presence of polymer degradation products: consequences for controlled release formulations. Biomaterials. 2006;27(17):3312-20.

22. Haughney SL, Petersen LK, Schoofs AD, Ramer-Tait AE, King JD, Briles DE, et al. Retention of structure, antigenicity, and biological function of pneumococcal surface protein A (PspA) released from polyanhydride nanoparticles. Acta Biomater. 2013;9(9):8262-71.

23. Vela Ramirez JE, Roychoudhury R, Habte HH, Cho MW, Pohl NLB, Narasimhan B. Carbohydrate-functionalized nanovaccines preserve HIV-1 antigen stability and activate antigen presenting cells. J Biomater Sci Polym Ed. 2014;25(13):1387-406.

24. Burkersroda F, Schedl L, Göpferich A. Why Degradable Polymers Undergo Surface Erosion or Bulk Erosion. Biomaterials. 2002;23(21):4221-31.

25. Westphal M, Ram Z, Riddle V, Hilt D, Bortey E. Gliadel (R) wafer in initial surgery for malignant glioma: long-term follow-up of a multicenter controlled trial. Acta Neurochirurgica. 2006;148(3):269-75.

26. Tabata Y, Langer R. Polyanhydride microspheres that display near-constant release of water-soluble model drug compounds. Pharm Res. 1993;10(3):391-9.

27. Jain JP, Modi S, Kumar N. Hydroxy fatty acid based polyanhydride as drug delivery system: synthesis, characterization, *in vitro* degradation, drug release, and biocompatibility. J Biomed Mater Res A. 2008;84:740-52.

28. Shieh L, Tamada J, Chen I, Pang J, Domb A, Langer R. Erosion of a new family of biodegradable polyanhydrides. J Biomed Mater Res. 1994;28:1465-75.

29. Chavez-Santoscoy AV, Roychoudhury R, Pohl NLB, Wannemuehler MJ, Narasimhan B, Ramer-Tait AE. Tailoring the immune response by targeting C-type lectin receptors on alveolar macrophages using "pathogen-like" amphiphilic polyanhydride nanoparticles. Biomaterials. 2012;33(18):4762-72.

30. Phanse Y, Carrillo-Conde BR, Ramer-Tait AE, Broderick S, Kong CS, Rajan K, et al. A systems approach to designing next generation vaccines: combining α-galactose modified antigens with nanoparticle platforms. Sci Rep. 2014;4:3775.

31. Narasimhan B, Goodman JT, Vela Ramirez JE. Rational Design of Targeted Next-Generation Carriers for Drug and Vaccine Delivery. Ann Rev Biomed Eng. 2016;18:25-49.

32. Shen E, Kipper MJ, Dziadul B, Lim M-K, Narasimhan B. Mechanistic Relationships between Polymer Microstructure and Drug Release Kinetics in Bioerodible Polyanhydrides. J Contr Rel. 2002;82(1):115-25.

33. Petersen LK, Sackett CK, Narasimhan B. Novel, High Throughput Method to Study in Vitro Protein Release from Polymer Nanospheres. J Comb Chem. 2010;12(1):51-6.

34. Petersen LK, Xue L, Wannemuehler MJ, Rajan K, Narasimhan B. The Simultaneous Effect of Polymer Chemistry and Device Geometry on the In Vitro Activation of Murine Dendritic Cells. Biomaterials. 2009;30(28):5131-42.

35. Kipper MJ, Shen E, Determan A, Narasimhan B. Design of an Injectable System Based on Bioerodible Polyanhydride Microspheres for Sustained Drug Delivery. Biomaterials. 2002;23(22):4405-12.

36. Kelso GF, Porteous CM, Hughes G, Ledgerwood EC, Gane AM, Smith RAJ, et al. Prevention of Mitochondrial Oxidative Damage Using Targeted Antioxidants. Ann New York Acad Sci. 2002;959(1):263-74.

37. Ghosh A, Chandran K, Kalivendi SV, Joseph J, Antholine WE, Hillard CJ, et al. Neuroprotection by a mitochondria-targeted drug in a Parkinson's disease model. Free Radical Biol Med. 2010;49:1674-84.

38. Ulery BD, Phanse Y, Sinha A, Wannemuehler MJ, Narasimhan B, Bellaire BH. Polymer Chemistry Influences Monocytic Uptake of Polyanhydride Nanospheres. Pharm Res. 2009;26(3):683-90.

39. Gendelman HE, Anantharam V, Bronich T, Ghaisas S, Jin H, Kanthasamy AG, et al. Nanoneuromedicines for degenerative, inflammatory, and infectious nervous system diseases. Nanomedicine Nanotechnol Biol Med. 2015;11(3):751-67.

40. Carrillo-Conde B, Song E-H, Chavez-Santoscoy A, Phanse Y, Ramer-Tait AE, Pohl NLB, et al. Mannose-Functionalized “Pathogen-like” Polyanhydride Nanoparticles Target C-Type Lectin Receptors on Dendritic Cells. Mol Pharm. 2011;8(5):1877-86.

41. Song C, Kanthasamy A, Jin H, Anantharam V, Kanthasamy AG. Paraquat induces epigenetic changes by promoting histone acetylation in cell culture models of dopaminergic degeneration. Neurotoxicol. 2011;32(5):586-95.

42. Ghosh A, Saminathan H, Kanthasamy A, Anantharam V, Jin H, Sondarva G, et al. The peptidyl-prolyl isomerase Pin1 up-regulation and proapoptotic function in dopaminergic neurons: relevance to the pathogenesis of Parkinson disease. J Biol Chem. 2013;288(30):21955-71.

43. Ay M, Jin H, Harischandra DS, Asaithambi A, Kanthasamy A, Anantharam V, et al. Molecular cloning, epigenetic regulation, and functional characterization of Prkd1 gene promoter in dopaminergic cell culture models of Parkinson's disease. J Neurochem. 2015;135(2):402-15.

44. Jin H, Kanthasamy A, Harischandra DS, Kondru N, Ghosh A, Panicker N, et al. Histone hyperacetylation up-regulates protein kinase Cdelta in dopaminergic neurons to induce cell death: relevance to epigenetic mechanisms of neurodegeneration in Parkinson disease. J Biol Chem. 2014;289(50):34743-67.

45. Harischandra DS, Kondru N, Martin DP, Kanthasamy A, Jin H, Anantharam V, et al. Role of proteolytic activation of protein kinase Cdelta in the pathogenesis of prion disease. Prion. 2014;8(1):143-53.

46. Kaul S, Kanthasamy A, Kitazawa M, Anantharam V, Kanthasamy AG. Caspase-3 dependent proteolytic activation of protein kinase Cδ mediates and regulates 1-methyl-4-phenylpyridinium (MPP+)-induced apoptotic cell death in dopaminergic cells: relevance to oxidative stress in dopaminergic degeneration. Eur J Neurosci. 2003;18(6):1387-401.

47. Porter AG, Janicke RU. Emerging roles of caspase-3 in apoptosis. Cell Death Diff. 1999;6:99-104.

48. Tadokoro D, Takahama S, Shimizu K, Hayashi S, Endo Y, Sawasaki T. Characterization of a caspase-3-substrate kinome using an N- and C-terminally tagged protein kinase library produced by a cell-free system. Cell Death Dis. 2010;1:e89.

49. Zhang X-m, Yin M, Zhang M-h. Cell-based assays for Parkinson's disease using differentiated human LUHMES cells. Acta Pharmacol Sin. 2014;35(7):945-56.

50. Scholz D, Pöltl D, Genewsky A, Weng M, Waldmann T, Schildknecht S, et al. Rapid, complete and large-scale generation of post-mitotic neurons from the human LUHMES cell line. J Neurochem. 2011;119(5):957-71.

51. Huntimer L, Ramer-Tait AE, Petersen LK, Ross KA, Walz KA, Wang C, et al. Evaluation of biocompatibility and administration site reactogenicity of polyanhydride-particle-based platform for vaccine delivery. Adv Healthcare Mater. 2013;2(2):369-78.

52. Vela-Ramirez J, Goodman J, Boggiatto P, Roychoudhury R, Pohl NB, Hostetter J, et al. Safety and Biocompatibility of Carbohydrate-Functionalized Polyanhydride Nanoparticles. The AAPS J. 2015;17(1):256-67.

53. Adler AF, Petersen LK, Wilson JH, Torres MP, Thorstenson JB, Gardner SW, et al. High Throughput Cell-Based Screening of Biodegradable Polyanhydride Libraries. Comb Chem High Through Screen. 2009;12(7):634-45.

54. Sun Z, Yathindranath V, Worden M, Thliveris JA, Chu S, Parkinson FE, et al. Characterization of cellular uptake and toxicity of aminosilane-coated iron oxide nanoparticles with different charges in central nervous system-relevant cell culture models. Int J Nanomed. 2013;8:961-70.

55. Kanmogne GD, Singh S, Roy U, Liu X, McMillan J, Gorantla S, et al. Mononuclear phagocyte intercellular crosstalk facilitates transmission of cell-targeted nanoformulated antiretroviral drugs to human brain endothelial cells. Int J Nanomed. 2012;7:2373-88.

56. Puligujja P, McMillan J, Kendrick L, Li T, Balkundi S, Smith N, et al. Macrophage folate receptor-targeted antiretroviral therapy facilitates drug entry, retention, antiretroviral activities and biodistribution for reduction of human immunodeficiency virus infections. Nanomedicine: Nanotechnol Biol Med. 2013;9(8):1263-73.

57. Li T, Gendelman HE, Zhang G, Puligujja P, McMillan JM, Bronich TK, et al. Magnetic resonance imaging of folic acid-coated magnetite nanoparticles reflects tissue biodistribution of long-acting antiretroviral therapy. Int J Nanomed. 2015;10:3779-90.

58. Puligujja P, Balkundi SS, Kendrick LM, Baldridge HM, Hilaire JR, Bade AN, et al. Pharmacodynamics of long-acting folic acid-receptor targeted ritonavir-boosted atazanavir nanoformulations. Biomaterials. 2015;41:141-50.

59. Saul JM, Annapragada A, Natarajan JV, Bellamkonda RV. Controlled targeting of liposomal doxorubicin via the folate receptor in vitro. J Contr Rel. 2003;92(1–2):49-67.

60. Huntimer L, Wilson Welder JH, Ross K, Carrillo-Conde B, Pruisner L, Wang C, et al. Single immunization with a suboptimal antigen dose encapsulated into polyanhydride microparticles promotes high titer and avid antibody responses. J Biomed Mater Res B Appl Biomater. 2013;101B(1):91-8.

Figures

Table 1. Characterization of non-functionalized and folic acid functionalized 20:80 CPH:SA nanoparticles.

Nano-formulation	*SEM Photomicrographs*	*ζ potential (mV)*	*Carbon (%)*	*Oxygen (%)*	*Nitrogen (%)*
20:80 CPH:SA nanoparticles (NP)	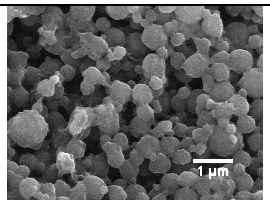	-25.7 ± 4.7	74.5 ± 0.1	25.5 ± 0.1	0.0 ± 0.0
0.25 eq. FA-NPs (FA-NP)	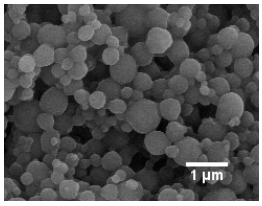	-12.5 ± 4.7	71.8 ± 2.0	21.6 ± 0.4	6.5 ± 1.7
2.0 eq. FA-NPs (2FA-NP)	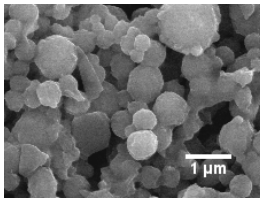	-25.4 ± 7.1	64.7 ± 1.2	21.6 ± 0.1	13.7 ± 1.2

Fig. 1. Mito-Apo release kinetics from 20:80 CPH:SA nanoparticles. The amount of Mito-Apo released at each time point was normalized by the total amount of Mito-Apo encapsulated within the particles. The experiments were performed in triplicate and are reported as means ± SEM.

Table 2. Characterization of QD- and Mito-Apo-loaded 20:80 CPH:SA nanoparticles.

Payload	Formulation	Geometric Mean (nm)	Geometric SD	Encapsulation Efficiency (%)
QD	NP	254	1.33	N/A
	FA-NP	315	1.21	N/A
	2FA-NP	346	1.21	N/A
Mito-Apo	M:(NP)	324	1.26	56.5 ± 3.8
	M:(FA-NP)	385	1.17	42.7 ± 1.8
	M:(2FA-NP)	346	1.21	36.6 ± 3.7

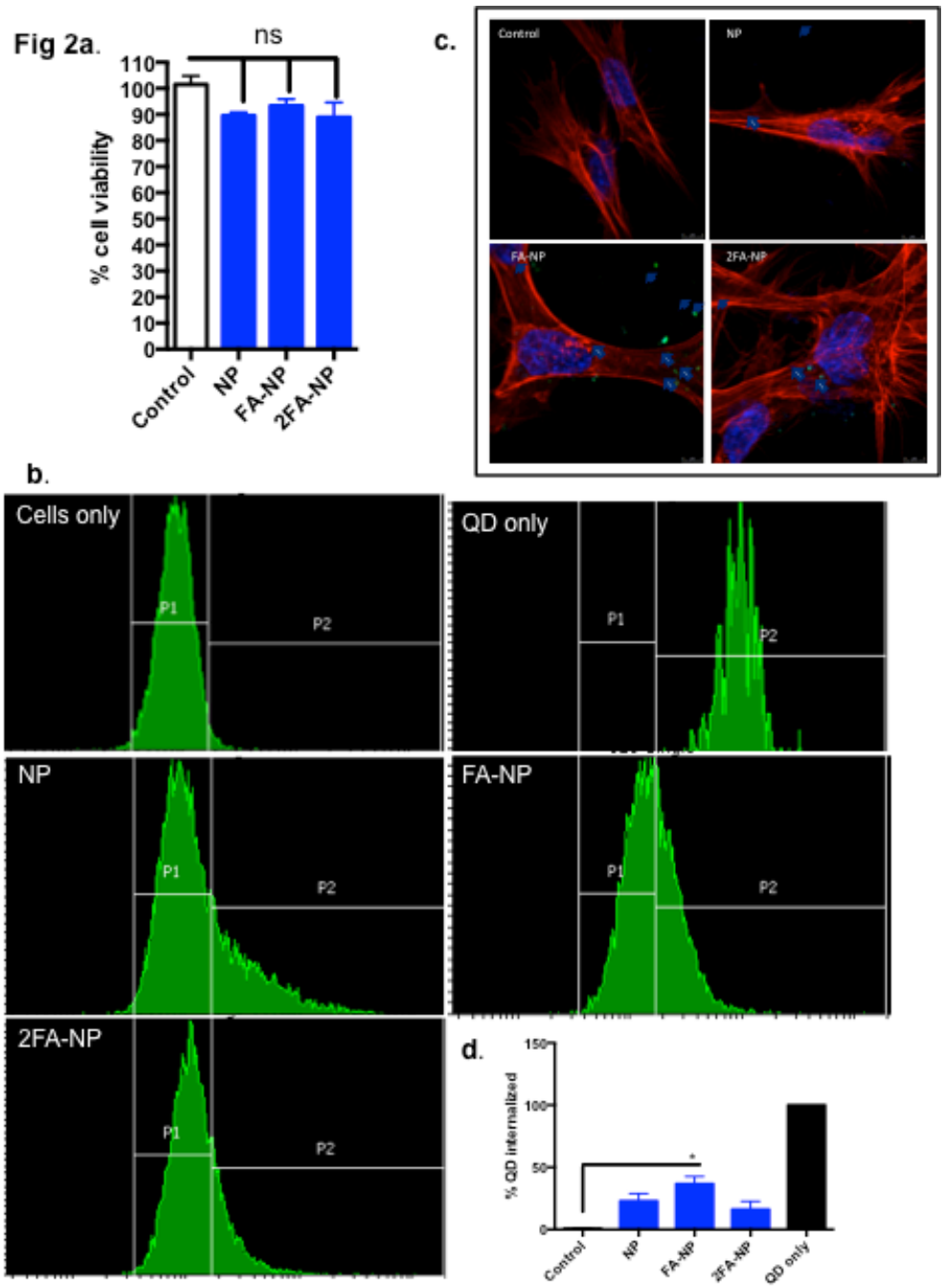

Fig. 2. Nanoparticle interactions with N27 neuronal cells. Cells were treated with 20:80 CPH:SA particles for 24 h. a) Cell viability was measured by using the MTS reagent. Data is expressed as percent viability compared to H_2O_2-treated controls. QD-loaded NPs were added separately to N27 cells for 24 h. Internalization was measured by flow cytometry (b)

and confocal microscopy (c). 40% of the cells internalized QD-loaded FA-NP as compared to only 25% of the cells that internalized QD-loaded NP.

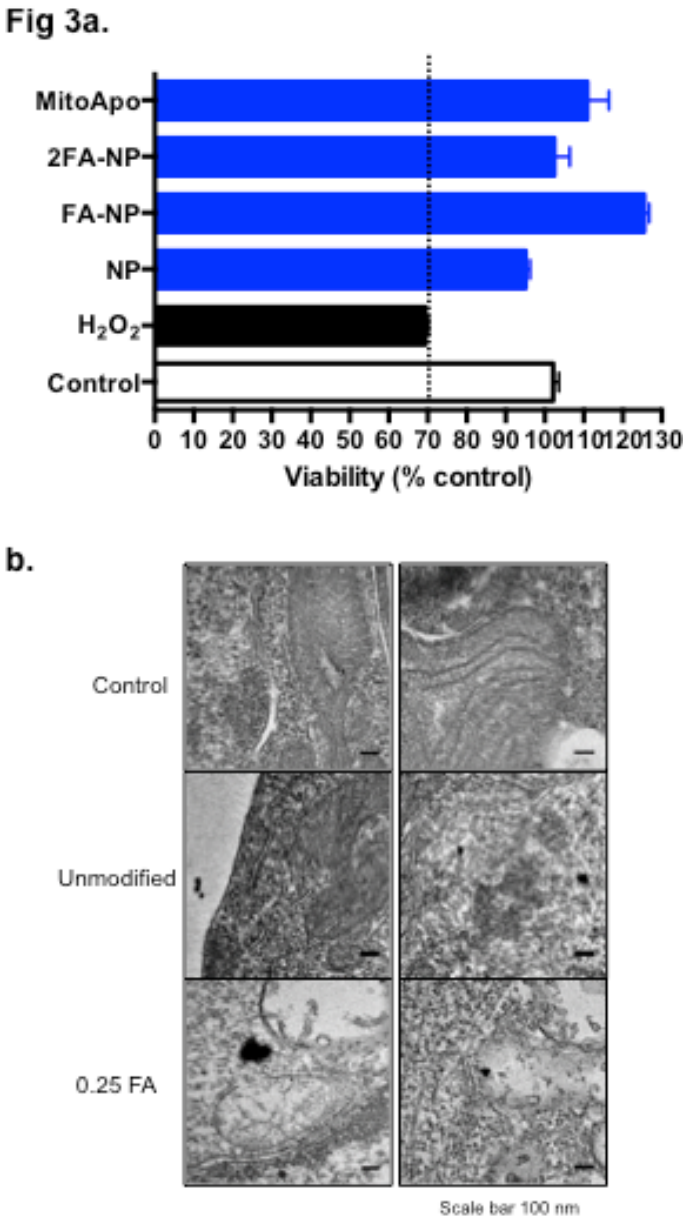

Fig. 3. Assessment of neuronal viability and nanoparticle internalization. Primary cortical cells were pre-treated for 24 h with NP, FA-NP, and 2FA-NP. a) MTS assay was used to measure the mitochondrial conversion of the tetrazolium salt to a water-soluble

formazan salt. Neurons treated with H_2O_2 for 1.5 h were used as a control for oxidative stress-induced cell death. b) TEM photomicrographs show presence of QD-loaded NP and FA-NP in the cytosol of cortical cells. Scale bar: 100 nm.

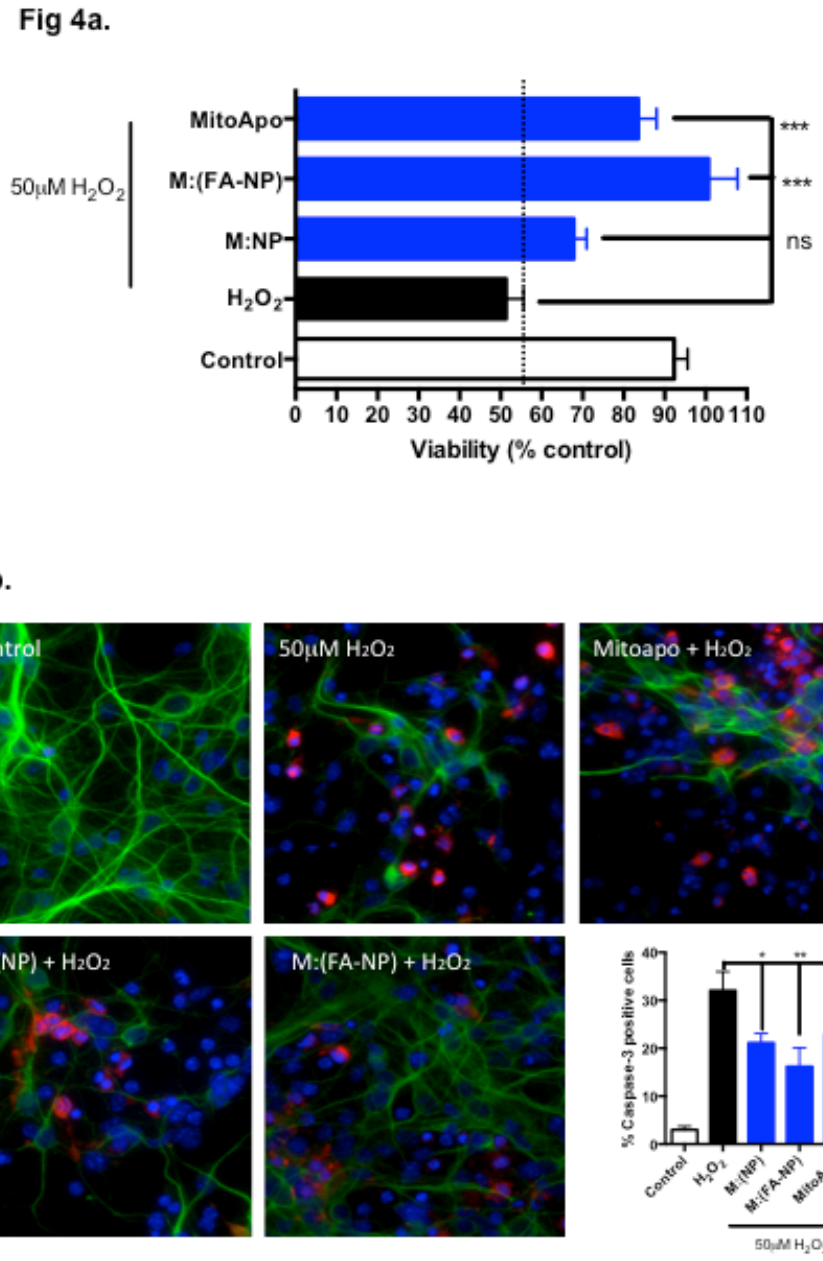

Fig. 4. Efficacy of Mito-Apo-encapsulated nano-formulations on primary cortical neurons. Neurons were pre-treated with the various nano-formulations for 24 h and challenged with H_2O_2 for 1.5 h. a) Cell viability was measured by MTS reagent. Data is

expressed as percent viability compared to untreated controls. b) Neurons were stained for β-III tubulin (green) and cleaved caspase-3 (red). Cell death was quantified by the presence of cleaved caspase-3 and by the reduction in neurite length. Caspase-3-positive cells were quantified as shown in the graph.

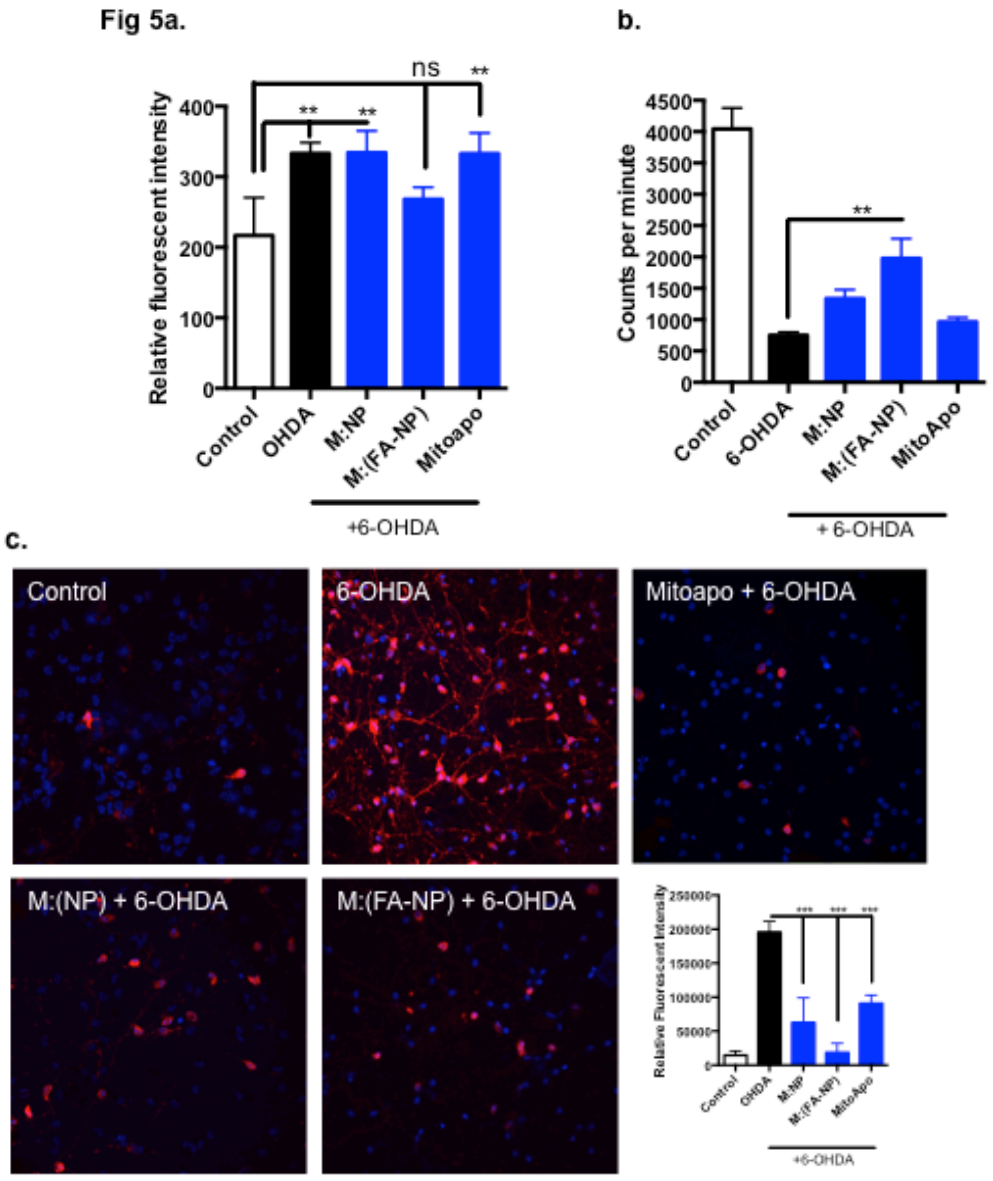

Fig. 5. Neuroprotective role of M:(FA-NP) against 6-OHDA-induced dopaminergic neuronal degeneration. a) LUHMES cells were treated with 6-OHDA and superoxide levels were measured as fluorescence intensity. b) Neuronal function was assessed by dopamine

uptake. Cells were pre-treated with various formulations and exposed to 6-OHDA. Dopamine uptake was measured using a high affinity [^{3}H] assay and expressed as mean values of counts. c) Cell death was quantified by the presence of cleaved caspase-3 in cells exposed to various treatments. Caspase-3-positive cells were quantified as shown in the graph.

ACKNOWLEDGMENTS

I would like to thank Dr. Anumantha Kanthasamy for giving me the opportunity to be a part of this exciting research lab for my PhD work and for all his guidance and support along the way. I would also like to acknowledge my committee members for their support and helpful suggestions over the years. I would like to thank all of my lab members, past and present, for helping keep the work environment friendly, encouraging, and productive. In particular, I would like to recognize Drs. Dilshan Harischandra and Monica Langley and my lab mates Souvarish Sarkar, Dharmin Rokad and Bharathi Palanisamy for their help in my projects as well as Gary Zenitsky for proofreading my manuscripts. Most importantly, I would like to thank my parents Sulabha and Vishwas and my brother Siddharth for their unmitigated love, support and encouragement.